UNIVERSITA' DEGLI STUDI DI PISA

RESEARCH DOCTORATE SCHOOL IN BIOLOGICAL AND MOLECULAR SCIENCE

PhD COURSE IN BIOMATERIALS

SYNTHESIS AND DESIGN OF POLY(AMIDOAMINE)S WITH TAILORED PROPERTIES FOR BIOMEDICAL APPLICATIONS

PhD Student: **Nicolò MAURO**

Matricola: 461650

Tutor: Chiar.mo Prof. Elisabetta Ranucci

UNIVERSITA' DEGLI STUDI DI MILANO - DIPARTIMENTO DI CHIMICA

XXV CYCLE 2010 - 2012

“Theory is when we know all there is to know about something but nothing works. Practice is when everything works, but nobody can tell why and how. But, here, today, we combine theory and practice: nothing works and nobody can tell why.”

Albert Einstein

TABLE OF CONTENT

CHAPTER 1

INTRODUCTION

1.1 BIOMATERIALS

The field of biomaterials encompass distinct disciplines including life sciences, medicine, materials science and engineering. This dates from egyptian history, where gold-filled teeth and glass eyes were commonly used. Although the necessity of replacing tissue and organs is quite old and known, new development of well-defined and effective biomaterials is needed to ensure that the appropriate parameters are being addressed. The most popular definition of biomaterial, proposed in 1983 during the Consensus Development Conference on Clinical Application of Biomaterial, describes these as "any material (other than a drug) or combination of material, synthetic or natural in origin, which can be used for any period of time, as a whole or as a part of a system which treats, augments, or replaces any tissue, organ, or function of the body".[1] Although this definition paved the way for the development of many interesting biomaterials, making quite clear the concept of biocompatibility, it did not include any reference about the interactions between biomaterial and living organism. Indeed, researchers in the field of biomaterials are aware of the potential benefits that can be obtained by fully understanding all events that occur at the biological environment/ material interface (Figure 1.1 A).

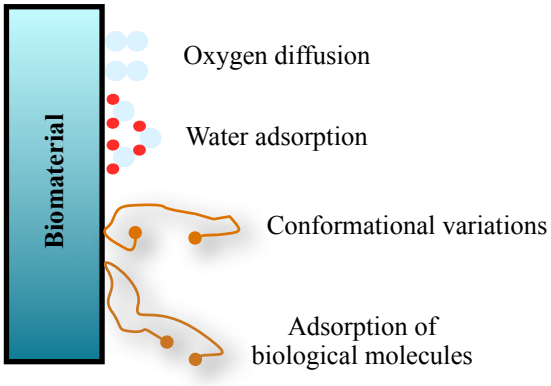

Figure 1.1 A Illustration of interactions at interface between biological environment and a biomaterial: adsorbed proteins can undergo conformational changes that lead to loss of biological functions and consequently inflammation.

Hence the definition of biomaterial was extended during the Consensus Conference on Biomaterials in 1991, in which they was defined as " materials designed to interface with biological system to evaluate, support or replace any tissue, organ or body function".[2] This definition fits very well with

[1] Galletti, P., M.; Beretos, J., W., J. Biomed. Mater. Res., 1983, 17, 539-555.

[2] 2nd Consensus Conference on Biomaterials, J. Mater. Sci., 1991, 2 (1), 62.

the modern research because provide a basic principle to synthesize new and better biomaterials, able to favorably interact with cells and a whole tissue. This is mostly due to the necessity of producing materials able to evoke either minimal host response, according to the most common definition of biocompatibility,[3] or specific biological response of tissues, depending on the purpose. For instance, all devices for blood preservation, e.g. filters, pocket and tubes for emodialysis, should be designed to minimize the coagulation; whereas, bone implants should be projected to appropriately interact with the surrounding tissue to allow and help tissue regeneration and eventually the integration of the biomaterial. Overall, in order to successfully produce biomaterials, they should perform several expectations: biocompatibility, proper physical characteristics (in terms of hydrophobicity, hydrophilicity, mechanical properties, stability, biodegradability, etc) and appropriate biological activity (tailored interactions at biological environment/material interface).[4]

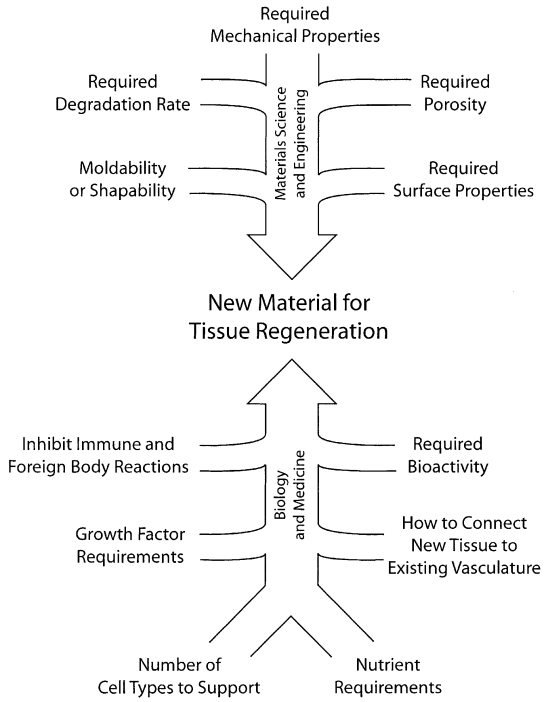

Figure 1.1 C. Illustration of the factors that must be integrated to achieve successful biomaterials for tissue regeneration. (Image from reference [5]).

Figure 1.1 C depicts all these factors in the case of tissue engineering, even if it can be almost considered for all biomedical applications, suggesting that biological and medical criteria should fully meet physico-chemical properties of the material.

---

[3] **Williams, D., F., Consensus and definitions in biomaterials. In: de Putter, C.; de Lange, K.; de Groot, K.: Lee, A., J., C., eds., Advanced in Biomaterials, Elsevier Sci., Amsterdam, 1988.**

[4] **Lloyd, A., W., Med. Device Technol., 2002, 13, 18-22.**

[5] **Seal, B., L.; Otero, T., C.; Panitch, A.,Materials Sci. Eng. Rev., 2001, 34, 147-230.**

Today a large number of biomaterials have been introduced in medical practice, such as bone inset, ligaments grafts, vascular grafts, heart valves, intraocular lenses, dental implants, pacemakers, biosensors, plates implant, joint replacement, drug and gene delivery systems, etc (Figure 1.1 B).

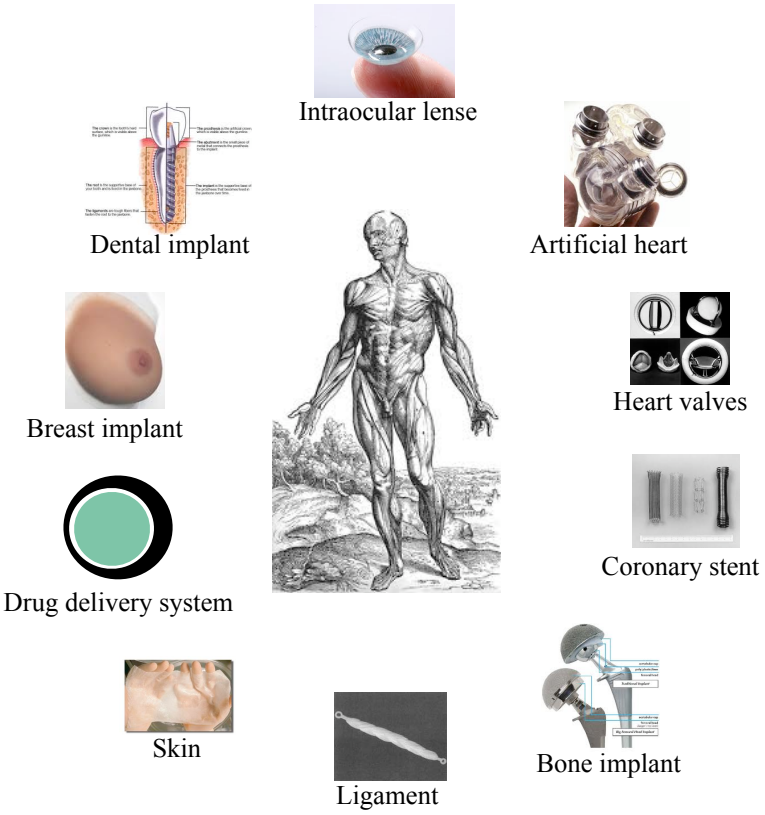

Figure 1.1 B. Some example of biomedical applications of biomaterials in human body.

Biomaterials can be classified on the basis of their medical applications, biological interactions with living organism or physico-chemical properties.[6] [7] According with their chemical nature, they can be classified in: ceramics, metals, polymers and composites.[8] For now ceramic biomaterials consist of alumina, zirconia, bioglass, carbon and hydroxyapatite, which are useful for producing orthopedic and dental implants.

They are highly bioinert materials and are endowed with good mechanical properties that make them suitable for hard tissue substitution.

Metals biomaterials are usually made of iron (Fe), chromium (Cr), cobalt (Co), nickel (Ni), titanium (Ti), tantalum (Ta), niobium (Nb), molybdenum (Mo), gold (Au), tungsten (W) and their alloys. Having outstanding mechanical, electrical and thermal properties, metals have been extensively

[6] Hench, L., L.; Polak, J., M., Science, 2002, 295 (5557) 1014-1017.

[7] Ratner, B., D.; Hoffman, A., S.; Choen, F., J.; Lemon, J., E., Biomaterials Sci., 2nd ed.: An introduction to materials in medicine, Elsevier Academic Press, New York, 2004.

[8] Black, J.; Hasting, G., W., Handbook of Biomaterials Properties, Chapman and Hall, London, UK, 1998.

used as biomaterials for cardiovascular, dental and orthopedic applications; especially as pacemakers, coronary stent, heart valves and dental prosthesis. In spite of this they do not fulfill biocompatibility requirements due to corrosion and ions release phenomena.[9]

Polymeric biomaterials are the most versatile class of material and show very heterogeneous properties in function of the polymeric architecture employed, thus they have been used in a wide range of biomedical applications. They are largely biocompatible if compared with metals and can be designed in order to degrade after the therapeutic effect is accomplished. Along the latter line biodegradable polymeric material can be used as temporary prostheses, three-dimensional porous scaffolds for tissue engineering applications and as drug/gene and protein delivery systems (DDS).[10] Polymeric biomaterials have several important uses in addition to tissue reconstruction and DDS. Examples include poly(methyl methacrylate) bone cement, poly(glycolic acid) degradable sutures, poly(glycolic-co-lactic acid) bone screws and poly(vinyl siloxaene) dental impression materials.[11] Polymers such as poly(ethylene glycol), are currently used to extend the bioavailability of some drugs and proteins. Poly(hydroxyethyl methacrylate) is used to produce soft contact lenses and silicon rubber is basically the main material to make implantable drug delivery devices. Poly(urethane), poly(tetrafluoroethylene), poly(methylmetacrylate), poly (ethyleneterephtalate), poly(lactic acid) and poly(glycolic-co-lactic acid) are other examples of polymeric material usefull as implants or scaffolds for tissue regeneration. Finally, dextran and poly (hydroxyethylaspartamide) are few examples of plasma expander.[12] [13] Generally, polymers can be easly designed and prepared in order to specifically tune their chemical, physical and biological properties, leading us to foresee their behavior in the biological environment, and then to fit the requests for specific applications.

Composite biomaterials are combinations of two or more materials (e.g., polymers-ceramics, metals-ceramics, or other combinations of materials), that if properly designed may show peculiar chemical and physical properties which cannot be achieved by using a single material. For instance, more stable and hard materials can be made by combining nano/micro-fibers with polymeric matrices.

---

[9] **Variola, F.; Veltrone, F.; Richert, L.; Jedrzejowski, P.; Yi, J., H.; Zalzal, S.; Sarkissian, A.; Perepichka, D., F.; Wuest, J., D.; Rosei, F.; Nanci, A., Small, 2009, 5 (9), 996-1006.**

[10] **Mallapragda, K.; Narasimha, B.; Handbook of Biodegradable Polymeric Materials, American Scientific Publishers, Stevenson Ranch, California, 2006.**

[11] **Seal, B., L.; Otero, T., C.; Panitch, A.,Materials Sci. Eng. Rev., 2001, 34, 147-230.**

[12] **Jorgensen, P., S.; Rasmussen, S., W.; Rornoim, C., Clin. Appl. Thromb. Hemost., 1997, 3, 267-269.**

[13] **Neri, P.; Antoni, G.; Benvenuti, F.; Cocola, F.; Gazzei, G., J. Medicinal Chem., 1973, 16, 893-897.**

1.1.1 DRUG DELIVERY SYSTEMS

Today, pharmacotherapy is mostly based upon the administration of very known low-molecular-weight drugs, which therapeutic effect arises from their quasi-specific binding with receptors. Very few pharmaceuticals exhibit unique specificity for their pharmacological target, and the pharmacokinetic-pharmacodynamic profile is often suboptimal. For instance, although β2-agonists prevailingly interact with β2 receptors they can bind the others β-adrenergic receptors affording undesired side effects. In addition it can be unaware of others synergic interactions, that cause iatrogenic effects. So, improving the therapeutic index of drugs is a main goal in many therapeutic areas, in which iatrogenic and side effects are very considerable, such as cancer, inflammatory, infective and heart diseases. Two distinct approaches can be taken in the quest for improvement (Figure 1.1.1 A).

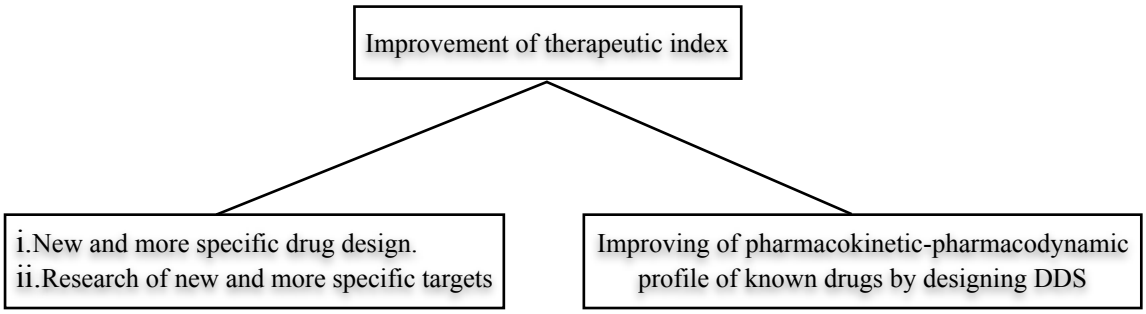

Figure 1.1.1 A. Schematic representation of new pharmacological approaches.

First the search for unique pharmacological cell targets and new drug design.[14] Along this line, in the face of the progresses obtained though genomics, target-oriented drugs and target-oriented macromolecular therapeutics have been developed, including antibody,[15] proteins, peptides and oligonucleotides[16] (siRNA). Unfortunately, results have shown that, overall, the clinical benefit has been much more modest than was predicted by theory.[17] The alternative to new drug design is the development of a drug delivery system (DDS) able to address a known drug to its site of action (targeting) and/or to control the release to ensure that an optimal concentration of drug is maintained at the therapeutic target over a desired time frame. Among these requests, the control of the drug release and consequently their bioavailability is achievable and represents already reality today. Sustained, prolonged, protracted, extended and retarded release can be indeed obtained by

[14] **Duncan, R.; Gaspar, R., Mol. Pharmaceutics, 2011, 8, 2101-2141.**

[15] **Nelson, A., L.; Dhimolea, E.; Reichert, J., M., Nat. Rev. Drug Discovery, 2010, 9, 767-774.**

[16] **Tiemann, K.; Rossi, J., J., EMBO Mol. Med., 2009, 1 (3), 142-151.**

[17] **Jarvis, L., M.; Chem. Eng. News, 2010, 88 (28) p28.**

using different technologies, which differ from the conventional one in a fundamental aspect (Figure 1.1.1 B). For the conventional systems, namely compresses, solutions, capsules, etc., drug is rapidly released once the site of absorption is reached and, after absorption, it can go to the site of action to get eliminated. Since in this systems the velocity of release is greater than the velocity of absorption ($K_r >>> K_a$) the process is limited by the letter parameter and strongly depends on the way of administration. Generally drugs diffuse rapidly into healthy tissue and are distributed evenly within the body, reaching small amount of the drug at the site of action for few time. In contrast, prolonged release systems show the inverse behavior ($K_r <<< K_a$) and hence the amount of drug in blood can essentially be modulated by controlling the value of the K_r.

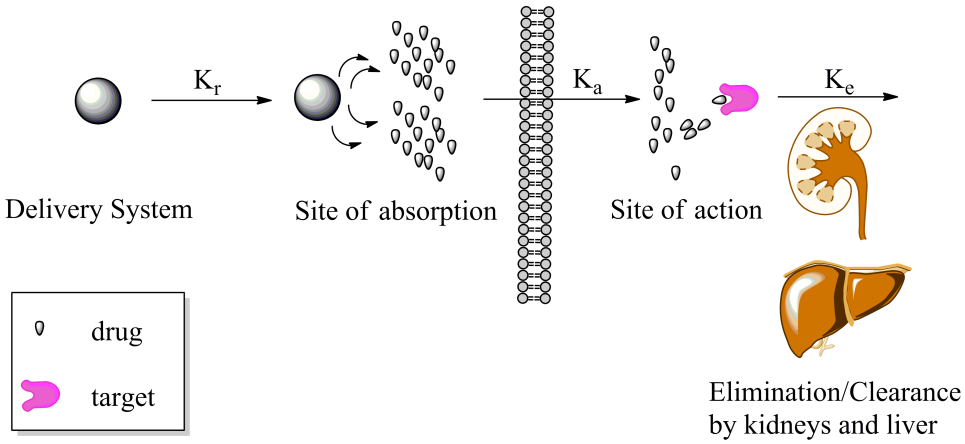

Figure 1.1.1 B. Illustration of biopharmaceutics mechanisms and pharmacokinetics after administration of a delivery system: the drug is released, absorbed across biological membranes, and eliminated following complexes equilibria.

In order to maintain a sufficient and constant plasmatic concentration of drug, the velocity of release should fulfill some necessities, i.e (i) to equal the velocity of bioelimination of drug and (ii) to be constant (kinetic of zero order). Different early micro- and macro-technologies make full use of this strategy to guarantee a better performance of several drugs, including silicon-based implantable device , osmotically controlled oral drug delivery technology (OROS), biodegradable polymeric implants and microparticles.[18] [19] They were useful for sustaining the release of orally administered low-molecular-weight drugs and to improve the bioavailability of drugs/peptides administered by the nasal, transdermal and pulmonary routes.[20]

[18] Croxatto, H., B.; NORPLANT, Ann. Med., 1993, 25 (2), 155-160

[19] Conley, R.; Gupta, S., K.; Sathyan, G., OROS, Curr. Med. Res. Opin., 2006, 22 (10), 1879-1892

[20] Duncan, R.; Gaspar, R., Mol. Pharmaceutics, 2011, 8, 2101-2141.

On the other hand, although drug targeting was object of several studies, except for rare cases, it has not been yet achieved.[20] A number of nano-sized delivery systems are under investigation to circumvent this issue, whose drug is physically or chemically bound into the polymeric system, encompassing liposomes, nanocapsules, nanoparticles, DNA-drug complexes, non-covalent polymeric nanocarriers and macromolecular pro-drugs (i.e., polymer-drug conjugates and protein-drug conjugates).[21] [22] [23] [24][25] The concept of targeting, that points out the cell-specific drug release, was kicked off by Ringsdorf.[26] In Ringsdorf's model (Figure 1.1.1 C) the drug is bound to a macromolecule by means of a spacer molecule, which should bear specific cleavage point to provide release of the drug at the site of action by appropriate stimuli (changing of pH, specific enzymatic reaction, etc.).

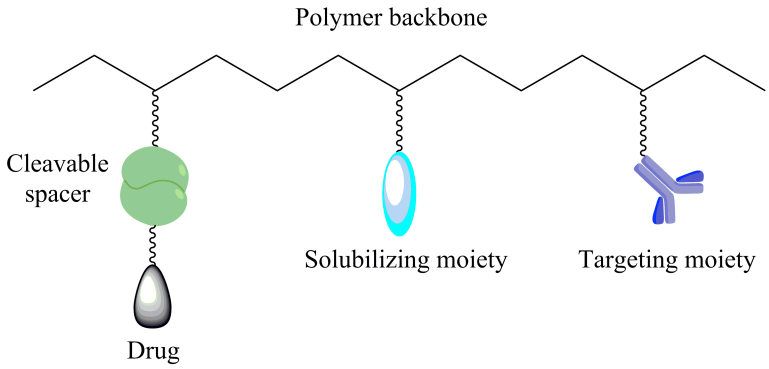

Figure 1.1.1 C. Schematic representation of Ringsdorf's model.

The drug-polymer conjugate must also contain targeting molecules, e.g. sugar or antibody moieties, which guarantee the cell-specific delivery of the drug by interacting with their antigen or receptor. Finally, in the case of poorly soluble polymers, a solubilizing moiety can be conjugate to the polymer backbone to taylor the bioavailability of the drug-polymer conjugate. The design of effective macromolecular pro-drugs should fulfill many requests. Obviously, the chosen macromolecule should ideally be water soluble, nontoxic, and non immunogenic, as well as degraded and/or eliminated from the organism.[27] [28] From the polymer chemistry standpoint, the

[21] Haag, R.; Kratz, F., Angew. Chem. Int. Ed., 2006, 45, 1198-1215.

[22] Cornu, G.; Michaux, J., L.; Sokal, G.; Trouet, A., Eur. J. Cancer, 1974, 10, 695-700.

[23] Speiser, P., P.; Front. Biol., 1979, 48, 653-668.

[24] Couvreur, P.; Tulkens, P.; Roland, M.; Trouet, A.; Speiser, P., FEBS, Lett., 1977, 84 (2), 323-326.

[25] Moreno-Aspitia, A.; Perez, E., A., Fut. Oncol., 2005, 1 (6), 755-762.

[26] Ringsdorf, H., J. Polym. Sci. Polym. Symp., 1975, 51, 135-153.

[27] Haag, R.; Kratz, F., Angew. Chem. Int. Ed., 2006, 45, 1198-1215.

[28] Godwin, A.; Bolina, K.; Clochard, M.; Dinand, E.; Rankin, S.; Simic, S.; Brocchim, S., 2001, 53, 1175-1184.

macromolecule should carry functional groups that are liable to react with the respective moieties. N-(2-hydroxypropyl)methacrylamides (HPMA)s copolymers were intensively studied according with this model, and some of these were transferred into clinical trials for cancer therapy. [29] [30] [31] Unfortunately most of these have shown not enough efficacy and unclear results. However HPMAs copolymers provided the thrust for the synthesis of other promising polyvalent ad well-defined polymers with both structural and architectural variations, such as monofunctional linear, polyfunctional linear and dendritic polymers, that have paved the way for designing tailor-made supramolecolar complexes which are able to vehicle many drug and/or bioactive macromolecules. These include (i) nanoparticles, nanocapsules and interpolyelectrolytic complexes (IPEC) (ii) nanogels (iii) drug-loaded polymeric micelles with core-shell architectures and (iv) polymer as drug (e.g, PAMAM) (Figure 1.1.1 D).[32] [33] [34] [35]

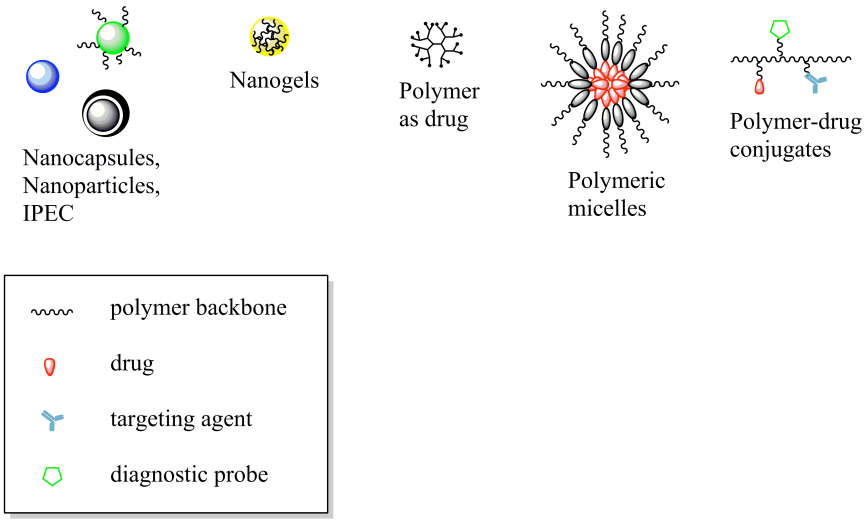

Figure 1.1.1 D. Main classes of nano-sized DDS for cell-specific drug release. The inset gives an idea of the type of system that ca be used to vehicle a drug in a specific body district (targeting).

These DDS apart from some structural variation fit the requirements of Ringsdorf's model above listed, since they are endowed with targeting moiety (EPR effect[36] due to the nano-sized dimension

[29] Vasey, P.; Kaye, S., B.; Morrison, R.; Twelves, C.; Wilson, P.; Duncan, R.; Thomson, A., H.; Murray, L., S.; Hilditch, T., E.; Murray, T.; Burtless, S.; Fraier, D.; Frigerio, E.; Cassidy, J., Clin. Cancer, Res., 1999, 5, 83-94.

[30] Nowotnik, D., P.; Cvitkovic, Adv. Drug Deliv. Rev., 2009, 61 (13), 1214-1219.

[31] National Characterisation Laboratory. 2005, http://ncl.cancer.gov/ncl_business_plan.pdf

[32] Couvreur, P.; Tulkens, P.; Roland, M.; Trouet, A.; Speiser, P., FEBS, Lett., 1977, 84 (2), 323-326.

[33] Ringsdorf, H., J. Polym. Sci. Polym. Symp., 1975, 51, 135-153.

[34] Hurwitz, E.; Levy, R.; Maron, R.; Wilchek, M.; Arnon, R.; Sela, M., Cancer Res., 1975, 35, 1175-1181.

[35] Slepnev, V., I.; Kuzneskova, L., E.; Gubin, A., N.; Batrakova, E., V.; Alakhov, V.; Kabanov, A., V.; Biochem. Int., 1992, 26, 587-595.

[36] Matsumura, Y.; Maeda, H., Cancer Res., 1986, 6, 6387-6392.

or receptor-mediated targeting[37]) and stimulus-triggered drug release ability. The most interesting systems should combine both enhanced site specificity towards diseased organ, cell, intracellular compartment (e.g., nucleus) and local controlled release of the drug. To date this is the main goal of "nanomedicinists".

[37] **Byrne, J., D.; Betancourt, T.; Brannon-Peppas, L., Adv. Drug Deliv. Rev., 2008, 60 (15), 1615-1626.**

1.1.2 HETERO-DIFUNCTIONAL POLYMERS AND THEIR APPLICATIONS

Hetero-difunctional polymers (HDPs) are a class of polymers bearing two different functional groups at theirs chain ends and, if properly synthesized, are able to selectively react with capping agents which provide specific biological properties (Figure 1.1.2 A). Because their chemical versatility, the design of degradable and bioactive HDPs has been received increasing attention for the synthesis of high-performance biomaterials for biotechlogical applications, such as for instance drug conjugates, liposomes, surface modification and protein modification (Figure 1.1.2 A).

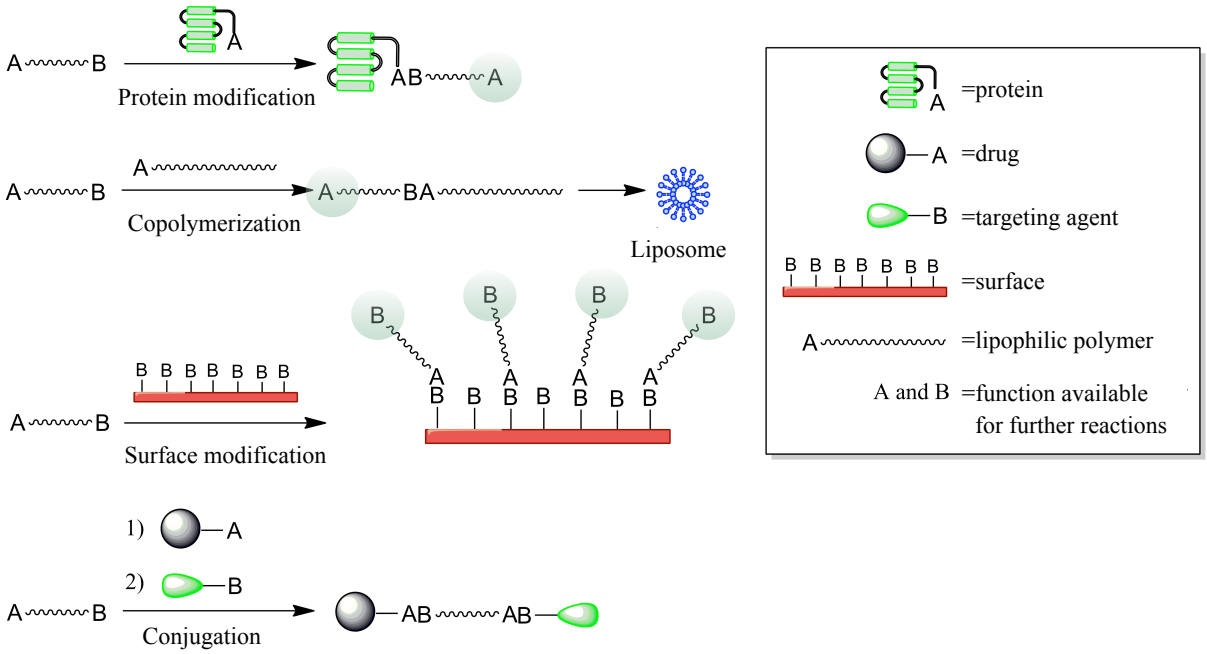

Figure 1.1.2 A. Representation of how HDPs can be used for obtaining protein-conjugate, block-copolymers, surface-modified device, and hetero-diterminated poymers.

For example, hetero-difunctional PEGs have been successful as spacers between two distinct chemical entities and as surface and protein modification agents in drug delivery systems.[38] [39] [40] [41] In such systems the chains of linear PEG are highly flexible and their hydrophilicity improves the solubility of compounds upon conjugation and so ensure good solubility under physiological conditions. In order to manufacture PEG-modified surfaces and proteins, several types of hetero-difunctional PEG are used. Indeed, because PEG chains possessing a functional group at only one end are not suitable for subsequent derivatization/modification, which is frequently crucial for the

[38] Digilio, G.; Barbero, L.; Bracco, C.; Corpillo, D.; Esposito, P., Piquet, G.; Traversa, S.; Aime, S., J. Am. Chem., 2003, 125, 3458-3470.

[39] Lochmann, A.; Nitzsche, H.; von Einem, S.; Schwarz, E.; Mäder, K. J. Control. Release 2010, 147, 92–100.

[40] Vandana, M.; Sahoo, S.K., Biomaterials 2010, 9340–9356.

[41] Gauthier, M., A. and Klok, H., A., Chem. Commun., 2008, 2591-2611.

design of biomaterials or for biomedical applications, and homo-difunctional PEGs can lead to undesired cross-linking molecules, hetero-difunctional PEG is required. Although there are several commercially available hetero-difunctional PEG derivatives, they have a relatively high costs. Moreover, the synthetic pathway used for their synthesis can be considered hazardous, due to the high toxicity and explosiveness of the reagents.[42] [43] In the light of this, PEGylation is so far to be eligible for the synthesis of new generation of biomaterials that should be made considering several aspects: biodegradability, ecocompatibility of reagents, safety of the industrial processes, etc. Mostly, the synthesis of other biodegradable HDPs might be interesting.

Synthetic approaches

In principle, the basic methodology for the synthesis of HDPs obtained by step-polymerization is based upon the condensation or addition reaction of A-A and B-B monomer systems, involving the reaction between the A and B functions until the maximum conversion (Scheme 1.1.2 B).

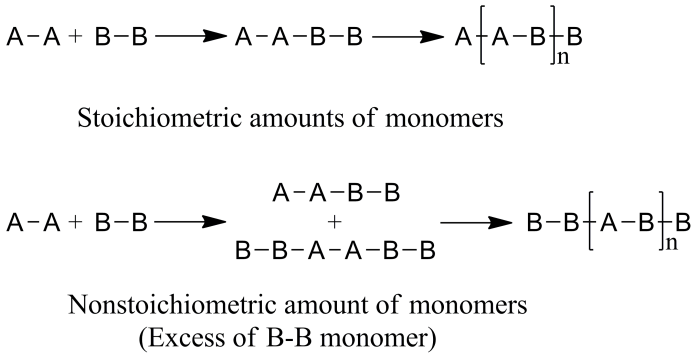

Scheme 1.1.2 B. Products of polycondensation or polyaddition of A-A/B-B systems in stoichiometric and nonstoichiometric conditions.

Unfortunately, this system has serious limitations.[44] The firs drawback, in order of importance, to use the A-A/B-B system is the stringent requirement of exact precision of measurement to ensure equimolar amounts of each monomers. Indeed, high molecular weight polymers can be prepared only if this important aspect is taken in consideration, because the excess of either A-A or B-B monomer leads to the formation of low molecular weight and homo-telechelic macromolecules, due to the termination of growing chains by the excess of functionality. In other words, the polymerization proceeds until one reactant is completely used up and all the chain ends posses the same functional group (the one in excess) (Figure 1.1.2 B). In the face of this marked

[42] **Mahou, K.; Wandrey, C., Polymers, 2012, 4, 561-589.**

[43] **Thompson, M.S.; Vadala, T.P.; Vadala, M.J.; Lin, Y.; Riffle, J.S., Polymer, 2008, 49, 345–373.**

[44] **Odian, G., Principles of Polymerization, Wiley Intersci., New York, 2004.**

shortcomings, others ways have been developed to produce HDPs. In particular, two strategies exist for unequivocally preparing hetero-diterminated polymers, either the ring-opening polymerization of cyclic precursors or the polymerization of hetero-difunctional A-B monomers.

The ring-opening polymerization (ROP) is of commercial interest in a number of systems and is based upon the polymerization of cyclic monomers in the presence of ionic initiators. From the chemical viewpoint ROP is a chain polymerization, consisting of a sequence of initiation, propagation and termination reactions. Indeed, the typical ROP involves the formation and propagation of ionic centers and the molecular weight depends on the conversion degree and the monomer/initiator ratio.[45] One of the potentiality of this approach is that it can be performed living ROPs for the synthesis of block-copolymers and HDPs (Figure 1.1.3 C).

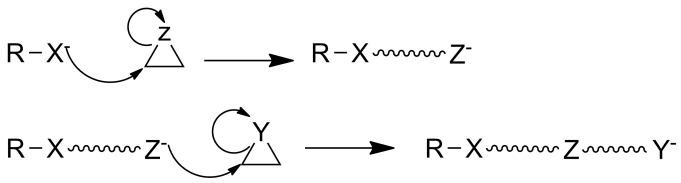

X, Y, Z = heteroatoms
R= other functional group

Figure 1.1.3 C. Mechanism of propagation of a living ring opening polymerization.

Many HDPs have been successfully synthesized using this approach, as for instance PEGs, ε-caprolactam and poly(silyl ester)s. [46] [47] [48] [49] [50] However, cyclic monomers required for this type of polymerization are not so easy to do, most this are toxic and, the last but not the least, they are not available for all polymer types.

As the use of an hetero-difunctional A-B monomer (HDM) let us overcome these problems, since a broad amount of A-B monomers are available for step-polymerization or, alternatively, can be easily synthesized.[51] [52] The self-polymerization of hetero-difunctional A-B monomers avoids the difficulties of controlling the stoichiometric balance of the reacting functions, since they are present

[45] Odian, G., Principles of Polymerization, Wiley Intersci., New York, 2004.

[46] Thompson, M.S.; Vadala, T.P.; Vadala, M.J.; Lin, Y.; Riffle, J.S., Polymer 2008, 49, 345–373.

[47] Raynaud, J.; Absalon, C.; Gnanou, Y.; Taton, D. J. Am. Chem. Soc., 2009, 131, 3201–3209.

[48] Gitto, S., P.; Wooley, K., L., Macromolecules, 1998, 31, 15.

[49] Frisch, K., C. and Reegan, S., L., Ring Opening Polymerization, Marcel Dekker, New York, 1969.

[50] Ivin, K., J. and Saegusa, T., eds., Ring.opening Polymerization, Vols 1, 2, Elsevier, London, 1984.

[51] Mahou, K.; Wandrey, C., Polymers, 2012, 4, 561-589.

[52] Wang, M.; Weinberg, J., M.; Wooley, K.,L., Macromolecules, 2000, 33, 734-742.

within the same molecule. Thus, they can be polymerized to high molecular weight polymers with controlled structures by simply choosing the chain end. HDPs, mono-functional polymers, dendritic polymers and block-copolymers may be synthesized by self-polymerization of the plane HDM, polymerization of the HDM with a monofunctional monomer, polymerization of the HDM in the presence of a multifunctional monomer (number of functions > 3) or step-by-step polymerization of different types of HDMs, respectively (Figure 1.1.2 D).

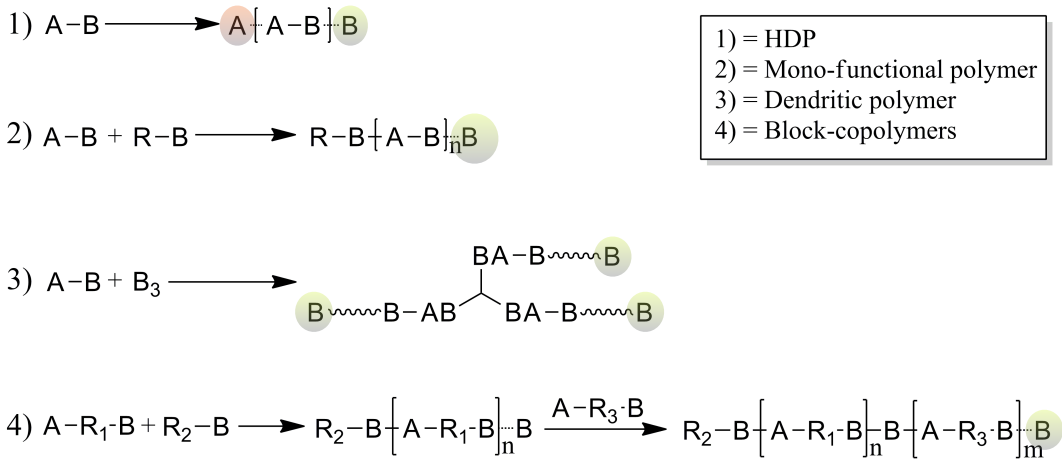

Figure 1.1.2 D. Potentials of HDMs to lead to polymers with outstanding biotechnological applications.

As can be seen in Figure 1.1.2 D, further functionalization of those polymers can be obtained by using the B groups available as chain ends, thus permitting the synthesis of purpose-tailoring biomaterials. Another important aspect, related to the use of HDMs, regards the control of the molecular weight. In the synthesis of polymers one is usually interested in obtaining a product of very specific molecular weight, since the biological and physico-chemical properties of polymers can be highly dependent on molecular weight.[53] [54] [55] Since the degree of polymerization is a function of reaction time, the desired molecular weight can be obtained by quenching the reaction at the appropriate time. Unfortunately, in this manner will be obtained products, which can be liable to subsequent reactions due to the presence of chain ends that can react further with each other. The adding of a chain end monomer, as in the case previously described, avoids this issue because the molecular weight of the product is strictly dependent on the HDM/chain end ratio. The molecular weight distribution in this type of polymerization have been derived statistically for different type

[53] Tanford, C., Physical Chemistry of Macromolecules, Wiley & Sons, INC, New York, London, 1961.

[54] Cavalli, R.; Bisazza, A.; Sess, R.; Primo, L.; Fenili, F.; Manfredi, A.; Ranucci, E.; Ferruti, P., Biomacromolecules, 2010, 11, 2667-2674.

[55] Praker, A., L; Newman, C.; Briggs, S.; Seymour, L.; Sheridan, P., J., Exp. Rev. Mol. Med., 2003, 5, DOI: 10.1017/S1462399403006562.

of monomer systems.[56] [57] Thus, the appropriate use of the HDM/chain end monomer ratio allows to prepare polymers with established molecular weight. Comparison of A-B and A-A/B-B systems have been widely reported for many polymers, including poly(imide)s[58], poly(amide)s[59], poly(silyl esters)s[60], poly(ester)s[61], poly(carbonate)s[62] and poly(quinoline)s.[63] Overall it was found that polymerization via HDMs (A-B) entailed reduced difficulties in reaching the designed polymer architecture, relatively faster propagation rates and higher degree of polymerization.

[56] **Peebles, L.,H.,Jr.; Molecular Weight Distribution in Polymers, Wiley-Intersci., New York, 1971.**

[57] **Shaefgen, J., R.; Flory, J., J. Am. Chem., 1948, 70, 2707.**

[58] **Wang, Z., Y.; Qui, Y.; Bender, T., P.; Gao, G.; P., Macromolecules, 1997, 30, 764.**

[59] **Stevens, M., P., Polymer Chemistry:An Introduction, Oxford University Press, New York, 1990, 424.**

[60] **Wang, M.; Weinberg, J., M. and Wooley, K., L., Macromolecules, 2000, 33, 734, 742.**

[61] **Stevens, M., P., Polymer Chemistry:An Introduction, Oxford University Press, New York, 1990, 392.**

[62] **Bolton, D., H.; Wooley, K., L., J. Polym. Sci. Part A: Polym. Chemistry, 1997, 35, 1133.**

[63] **Harris, R., M.; Stille, J., K., Macromolecules, 1981, 14, 1584.**

1.1.3 DENDRITIC POLYMERS

Dendritic polymers are a class of polymers consisting of high number of treelike branching with well-defined structure, which depends on the functional groups of monomers adopted. [64] [65] [66] [67] This types of polymers have features that differ from the linear one and for this reason growing interest is quite noticeable for research directed towards macromolecules with highly branched structures. The most important difference is that whereas linear polymers have random coil structures and are spatially anisotropic, dendritic polymers have globular shapes with the dimension of the macromolecules about the same in all directions (spatially isotropic). Thereby, the attractive secondary force between the molecules in the linear and dendritic polymers are different. In particular, the attractive secondary forces are greater for linear polymers because the molecules may pack together and attract each other minimizing the free energy of the system (Figure 1.1.3 A).

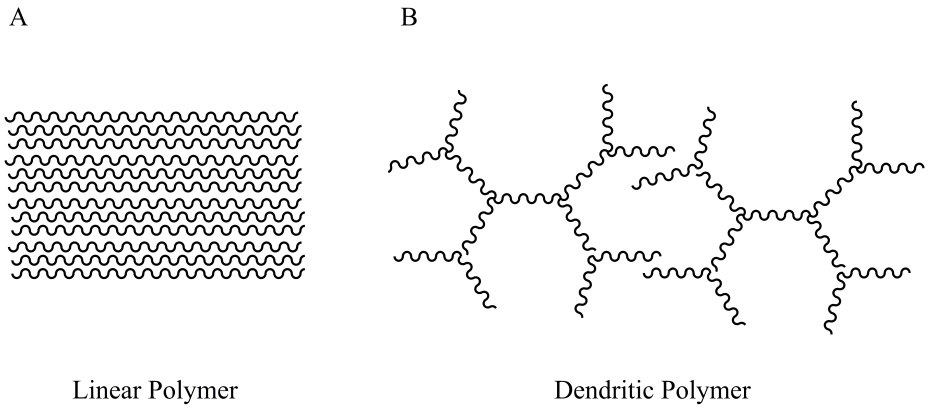

Figure 1.1.3 A. Entanglement of linear polymer chains by comparison with dendritic polymers.

Furthermore, dendritic polymers, having globular shape and limited mobility of their chains, may not undergo chain entanglements as do linear polymers.[68] Thus, unlike the linear polymers, dendritic polymers seldom have sufficient intermolecular interaction to be useful for the preparation of fibers, rubbers and plastics. However, because their low secondary interactions and globular shape, dendritic polymers show higher solubility, lower viscosity and lower hydrodynamic volume if compared with linear polymers, conferring them different biological, physical and chemical properties. In particular, the lower hydrodynamic volume leads the macromolecules to be easily

[64] **Bosman, A., W.; Jannsen, H., M. and Meijer, E. W., Chem. Rev., 1999, 99, 1665**

[65] **Fischer, M.; Vogtel, F., Angew. Chem. Int. Engl. Ed. 1999, 38, 884**

[66] **Frechet, J. and Tomalia, D., eds., Dendrimers and Other Dendritic Polymers, Wiley, New York, 2002**

[67] **Kim, Y., H., J. Polym. Sci. Polym. Chem. Ed., 1998, 36, 1685**

[68] **Odian, G., Principles of Polymerization, Wiley Intersci., New York, 2004**

internalized by the cells [69] [70] and the lower viscosity may facilitate coating, extrusion or other manufacturing processes.[71] Nevertheless, the increasing interest for dendritic polymers is above all related to the presence of a much larger number of chain ends with potential reactive groups, which can be used for further derivatizations of the polymers, such as with targeting agents, monoclonal antibody, drugs and other polymers (Figure 1.1.3 B).

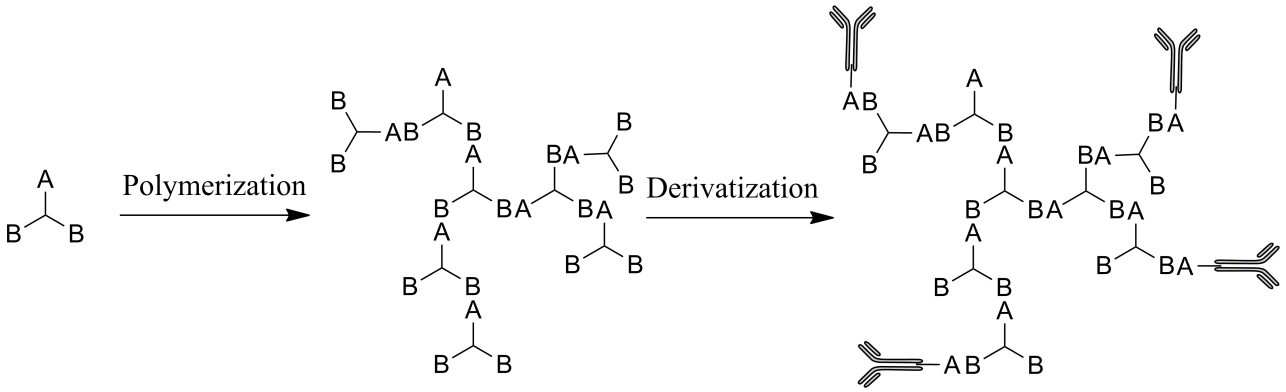

Figure 1.1.3 B. Potential applications of functional dendritic polymers.

Such polymers can be exploited for the development of macromolecular carrier for drug delivery, gene therapy, catalysis and sensors. [72] Two types of dendritic polymers have been developed: hyperbranched polymers and dendrimers (Figure 1.1.3 C). Each of these polymers shows advantages and drawbacks which relate to macromolecular structure and the production economy.

Dendrimers offer the potential for producing polymers whose molecular size and structure are more regular and less polydisperse than hyperbranched polymers, whereas the latter are easier and cheaper to synthesize. Many exciting results related to chemical architecture, synthetic procedure, encapsulating properties, aggregation behavior, self-assembly in solution and surface conjugation with prospective applications in drug delivery, nanocomposite materials have been reported. [73] [74] [75]

However, several factors limit the prospective use of conventional dendrimers for large scale applications, such as: the enormous cost in synthesis and purification steps, due to the exponential reaction time and decreasing yield for each generation of branching, and the steric crowding that

[69] **Ahmed, M.; Narain, R., Biomaterials, 2012, 33, 3990-4001.**

[70] **Battah, S.; Balaratnaml, S.; Casa, A.; O'Neill, S.; Edwards, C.; Batlle, A.; Dobbin, P.; MacRobert, A., J., Cancer Ther., 2007, 6, 876-885.**

[71] **Mishra, M., K.; Kobayashi, S., Eds. Star and Hyperbranched Polymers, New York, Wiley-VCH, 2001.**

[72] **Frechet, J., M., J. and Tomalia, D.,A, eds., Dendrimers and Other Dendritic Polymers, Wiley, New York, 2002.**

[73] **Frechet, J., M., J. and Tomalia, D.,A, eds., Dendrimers and Other Dendritic Polymers, Wiley, New York, 2001.**

[74] **Newkome, G., R.; Moorefield, C., N.; Vogtle, F., eds. Dendrimers and Dendrons: Concept Syntheses Applications. Wiley-VCH, New York, 2001.**

[75] **Paleshanko, S.; Tsukruk, V., V., Prog. Polym. Sci., 2008, 33, 523-580.**

lead to structural defects by distorting the shape of dendrimers. For the purpose of this thesis we will deal with only the hyperbranched polymers, staying away from dendrimers.

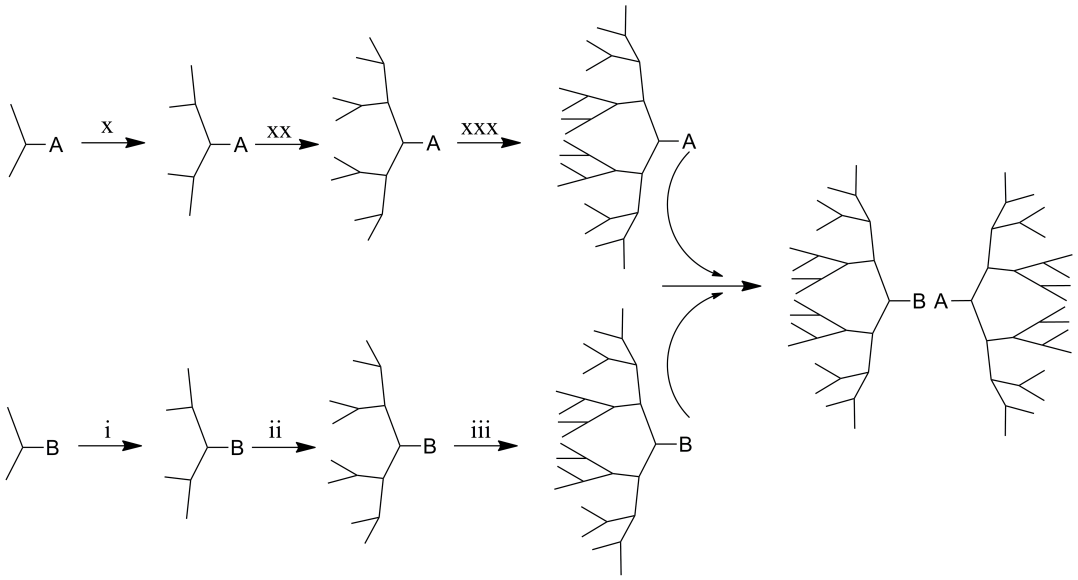

Multi-step synthesis of 3rd generation dendrimers

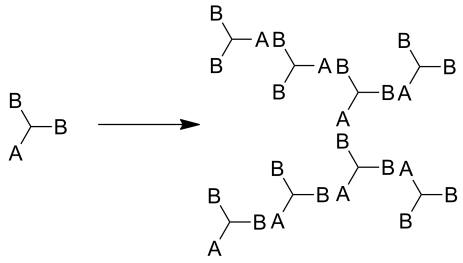

One-pot synthesis of an AB_2 hyperbranched polymers

Figure 1.1.3 C Schematic representation of synthetic approaches for dendrimers (up) and hyperbranched (bottom) polymers

Hyperbranched polymers, also known as random hyperbranched polymers, has branches that occur in a random way and they are usually characterized by the degree of branching (DB), that for high molecular weight polymers is about 0.5 . They compositionally are not so far from conventional dendrimers, but show a lower degree of branching and a less regular architecture (Figure 1.1.3 C). These molecules have attracted the most attention in biomedical field in recent years especially when prospective applications were considered.[76] [77] [78] These polymers are synthesized in one-pot way without lengthy stages of step-wise reaction and purification necessary with traditional dendrimers. Hyperbranched polymers, from the polydisperty point of view, are similar to linear

[76] **Kim, Y., H., J. Polym. Sci. Part A: Polym. Chem. 1998, 36, 1685-1698.**

[77] **Fischer, M.; Vogtle, F., Angew Chem. Int. Ed. 1999, 38, 885-905.**

[78] **Turner, S., R.; Voit, B., I., Polym. News, 1997, 22, 197-202.**

polymers, first of all because they show costitutional isomerism, resulting from the different placement of monomer units. For example, for the polymer derived from an AB_2 multifunctional monomer (Figure 1.1.3 D) it can be noticed many isomers, such as those arising from placement of the lower leftmost AB_2 unit at any the other positions around the perimeter of the molecule.[79]

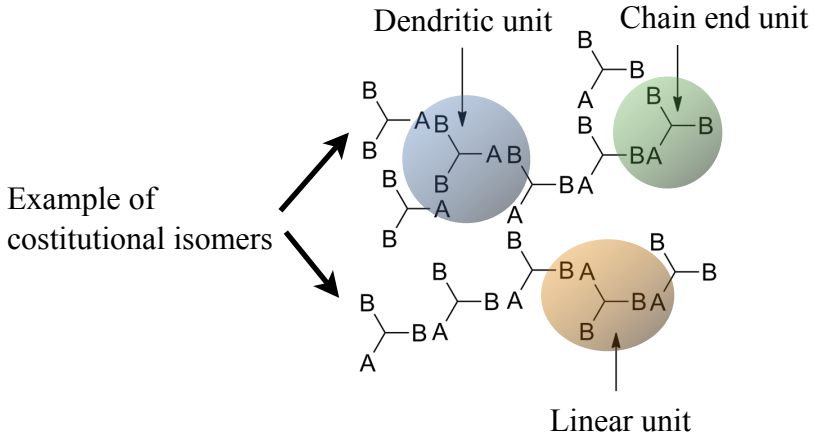

Figure 1.1.3 D. Costitutional isomerism for an AB_2-derived dendritic polymer.

In addition, there are three different types of repeat units: dendritic, linear and terminal units defined as units having two, one and no B groups reacted, respectively. Because this functional heterogeneity, the synthesis of hyperbranched polymers entails inherent and troublesome issues which limit the control of molecular weight and shape.[79] One is the occurrence of intramolecular cyclization, which decreases the functional groups available for polymerization. Another difficulty is the steric crowding, that occurs at the periphery of hyperbranched macromolecules with increasing molecular size, where some reactive functions become inaccessible for the reaction and the reaction take place only along accessible directions.[80] Thus, the steric crowding may not limit the polymer molecular weight, but affects the molecular shape due to the increased linear unit on the macromolecule surface.

Considering these issues related to these two classes of polymers, hyperbranched polymers will probably be used in large-scale applications, where lower cost is a necessity, and dendrimers in particular applications, where higher cost is justified. In spite of that, not too many AB_f monomer are available for the synthesis of new and original hyperbranched polymers, especially in the case of biodegradable and biocompatible polymers such as poly(amidoamine)s, and so further efforts are necessary to afford new synthetic approaches.

[79] Odian, G., Principles of Polymerization, Wiley Intersci., New York, 2004.

[80] de Gennes, P.G. and Hervet, H., J. Phys. Lett., 1983, 44, 351.

Theoretical considerations

Since the lack of B_f monomers, other synthetic pathway for the synthesis of hyperbranched architectures have been developed. When one or more monomers with more than two functional groups are present in the reacting mixture the resulting polymer will be branched instead of linear and with certain monomers crosslinking can also take place. For example, crosslinking of a A-A system will occur when the multifunctional monomer (B_f) carry at least 3 functional groups in the presence of B-B monomer. (Figure 1.1.3 E). Thus, branches of two parallel chains can react together leading to a crosslinked macromolecule because of the presence of the reactive -B-B and -B-A chain ends. When crosslinking statistically prevails the branching reaction, the gel point can be reached and it will be observed the loss of fluidity of the reacting mixture. So, the gelation differs to the crosslinking because it corresponds to the formation of an infinite network whose polymer molecules have been crosslinked to each other.[81] In order to control the crosslinking reaction so that it can be obtained hyperbranched polymers, several theories are available.[82] [83] The Flory[84] [85] and Stockmayer[86] [87] [88] one is statistically derived and represents the best approach to obtain well-defined hyperbranched polymers. Indeed, using this approach, hyperbranched polymers can potentially be synthesized by the $A_2 + B_2 + B_f$ systems, or analogous combinations of monomers, usually used to produce cross-linked polymers (Figure 1.1.3 E). It is possible to synthesize hyperbranched polymers only if cross-linking is minimized by controlling the stoichiometric conditions of the starting mixture (See "Results and Discussion" session).

[81] **Odian, G., Principles of Polymerization, Wiley Intersci., New York, 2004.**

[82] **Carothers, W., H., Trans. Faraday Soc., 1936, 32, 39.**

[83] **Pinner, S., H., J. Polym. Sci., 1956, 21, 153.**

[84] **Flory, P., J., J. Am. Chem. Soc. 1941, 63, 3083, 3091, 3096.**

[85] **Flory, P., J., Principles of Polymer Chemistry, 1953, Cornell Univ. Press, Ithaca, NY.**

[86] **Stockmayer, W., H., J. Chem. Phys., 1943, 11, 45.**

[87] **Stockmayer, W., H., J. Polym. Soc., 1952, 9, 69.**

[88] **Stockmayer, W., H., J. Polym. Soc., 1953, 11, 424.**

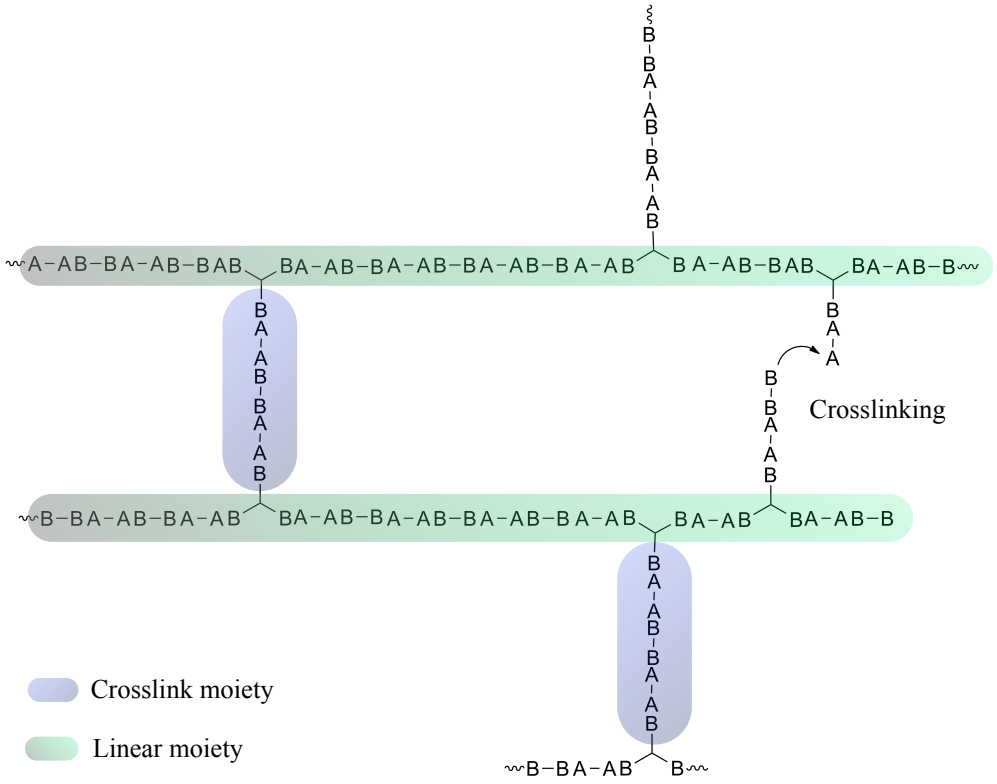

Figure 1.1.3 E. Structure of a cross-linked macromolecules.

1.1.4 POLYMERIC NANOPARTICLES AND THEIR ROLE IN NANOMEDICINE

Recent years have witnessed unprecedented increasing of investigations in the field of nanomedicine and nanotechnology, since nanoparticles brings significant advantages in the diagnosis and treatment of several diseases.[89] Although nanoparticles (NPs) vary in size from 10 to 1000 nm, it is accepted the definition in which NPs are designed as particles with size < 100 nm, because it is recognized that NPs with higher hydrodynamic diameter generally do not show marked improvement of their original physico-chemical properties.[89, 90] In particular, it is known that nanoparticles with the size in the range of 200 nm can accumulate at the solid tumor site by the so called enhanced permeation and retention (EPR) effect, resulting in effective drug targeting (Figure 1.1.4 A). [91]

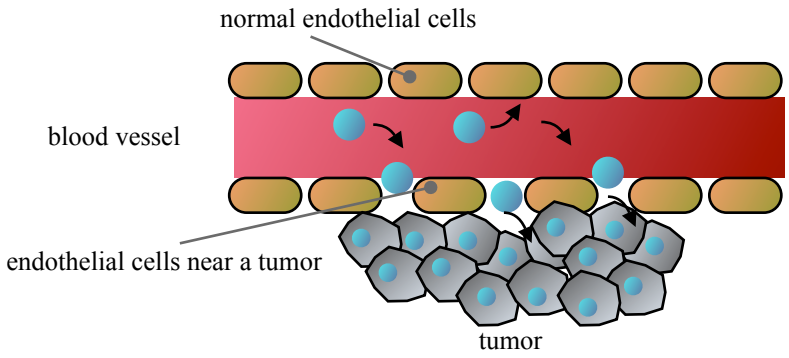

Figure 1.1.4 A. Enhanced permeation and retention effect (EPR) for polymeric nanoparticles: endothelial cells that are close to the tumor are more permeable and the NPs can diffuse across blood vessel towards tumorous cells.

NPs are usually classified on the basis of the materials used for preparing them. Among these, polymeric and inorganic NPs can be distinguished. Those obtained from polymeric material are of great importance because of their chemical and technological versatility. Indeed, biocompatible, biodegradable and functionalized NPs with different phisico-chemical properties may successfully be prepared by using the available polymer architectures. NPs are important tools to accomplish a huge number of medical applications, including drug delivery, gene delivery and diagnosis because of their unique and attractive features, such as: high surface area/mass ratio and their quantum properties.

---

[89] **Duncan, R., Nat. Rev. Drug Disc., 2003, 2, 347-360.**

[90] **The Royal Society and The Royal Accademy of Engineering, 2004, www.nanotech.org.uk/finalReport.htlm.**

[91] **Matsumura, Y.; Maeda, H., Cancer Res., 1986, 46, 6387-6392 .**

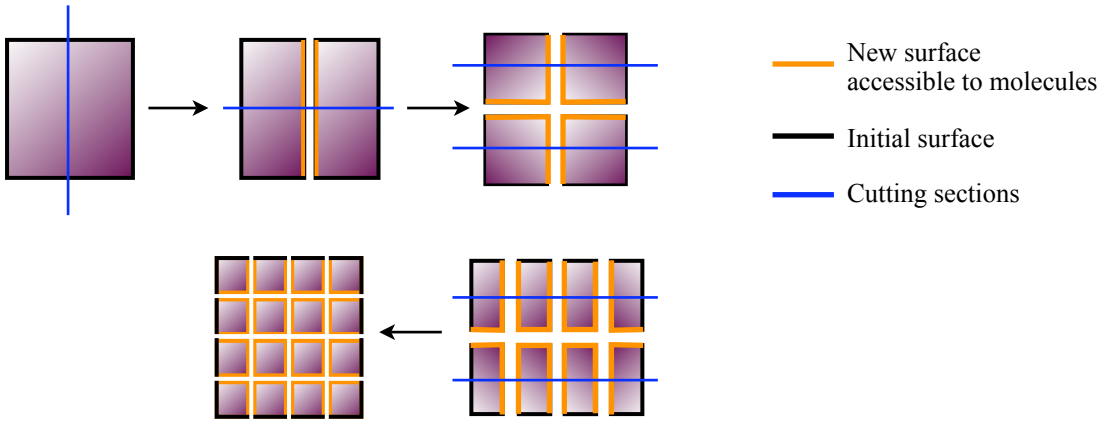

Figure 1.1.4 B. Representation of the process of increasing in accessible surface by consecutive cutting: after each cutting the accessible surface become exponentially greater than the initial surface.

Figure 1.1.4 B shows how the overall surface of a cube can exponentially increases after breaking into small pieces. Increasing surface area, the percentage of molecules on the surface increase, leading to particles of the same material but with different behavior. More precisely, NPs are endowed with peculiar properties, arising from their nanometric size, that make they able to efficiently adsorb and bind bioactive compounds, to diffuse rapidly through the submucosal layer of the gastrointestinal tract and across the endothelial cells into blood vessels, to hardly physically interact with other molecules and cellular membrane.[92] Such particles may efficiently carry drugs, genetic material and proteins in a specific body district and consequently either release their loaded compounds or tagging a specific tissue, organ or tumor. In addition, there are many technological advantages to use NPs. One is that they can be easily formulated as stable liquid by suspending them into an aqueous solution. Indeed, according to the Sokes-Einstain's law, due to their small size, nanoparticles are less prone to gravitationally settling. As particle size decreases to the nanoscale, their settling velocity become less than their Brownian motion, avoiding the gravitational settling. Thus, using NPs homogeneous suspensions with longer shelf life can be obtained. Furthermore, according to Noyes-Whitney equation, the dissolution of poorly water-soluble drugs can be enhanced (until 40%) by preparing nano-sized drugs.[93] NPs can also offer unique magnetic and optical properties with relevance in targeted treatment and diagnostic. For example, ferromagnetic materials lose their magnetization at particle size less than 20 nm, but still respond to a magnetic stimulus. Such particles can be directed to tumors for locally releasing of antitumoral drugs by heating them through pulsed electromagnetic radiation.[94]

[92] De Jong, W., H.; Borm, P., J., A., Int. J. Nanomedicine, 2008, 3, 133-149.

[93] Lipinski, C., A., Curr. Drug Dis., 2001, 17-19.

[94] Gupta, R., B.; Kompella, U., B., eds., Nanoparticles Technology for Drug Delivery, Taylor and Francis, New York, 2006, 159.

Although the use of nanomedicine allows to improve the therapeutic index of many drugs, being the letter the margin between the dose needed for therapeutic effect and the dose inducing adverse effects, the toxicological and environmental evaluation of these systems must be carefully performed. Since the surface of NPs is the crucial determinant of particle response and the unique difference in comparison to bulk material, this should be fully investigated from the toxicological standpoint.[95] [96] [97] Particular emphasis should be dedicated to non degradable or slowly degradable NPs, that, due to the accumulation and and persistence in the site of delivery, might cause chronic inflammatory reaction.[98] However, it cannot be assumed that current assays and analytical procedures are appropriate to detect all potential risks associates with the use of NPs. So additional development of these research field may be needed. Others important aspects that should be better studied are the biopharmaceutics and the pharmacokinetics parameters of NPs after administration, since their body distribution may significantly change in contrast to micro-sized particles.

Polymeric NPs as drug delivery systems

Polymeric nanoparticles are being used as vehicles for drug, gene and protein delivery. The structure, function and biomedical application of these materials have already reviewed.[99] [100] [101] Herein it will report a summary of these example and considerations. Various polymers have been used in drug delivery as they can effectively deliver the drug to a target site and thus increase the therapeutic benefit, while minimizing side effects. PEGylated proteins, antibodies and most recently aptamers have been particularly successful, and the letter are undergoing clinical screening as treatment for cancer, diabetic nephropathy and coronary disease.[102] Among the polymers with potential as drug delivery system, biodegradable polymers allow utilization of higher molecular weight platforms, like NPs, to optimize pharmacokinetics, and they are essential for treatment that require chronic administration of drugs. Overall, drug-loaded polymeric NPs can be obtained by means of two different methods: (i) dispersion of the preformed polymer with drugs and (ii) polymerization of monomers in presence of drugs.

---

[95] **SCHENIHR, EU, Scientific Committee on Emerging and Newly Idendtified Health Risks, 2006, SCENIHR/002/05, http://ec.europa.eu/health/ph_risk/committees/04_scenihr/docs/scenihr_o_003b.pdf.**

[96] **Donaldson, K.; Brown, D.; Clouter, A., 2002, 15, 213-220.**

[97] **Oberdorster,G.; Oberdorster, E.; Oberdorster, J., 2005, Environ. Healt Perpect., 2005, 113, 823-839.**

[98] **De Jong, W., H.; Borm, P., J., A., Int. J. Nanomedicine, 2008, 3, 133-149.**

[99] **Duncan, R., Nat. Rev. Drug Discov., 2003, 2, 347-360.**

[100] **Duncan, R.; Gaspar, R., Mol. Pharmaceutics, 2011, 8, 2101-2141.**

[101] **Parker, A., L.; Newman, C.; Briggs, S.; Seymour, L.; Sheridan, J., 2003, 5, 1-15.**

[102] **Keefe, A., D.; Pai, S.; Ellington, A., Nat. Rev. Drug Discovery, 2010, 9, 537-550.**

Different types of NPs can be obtained depending on the method adopted. The drug can be dissolved, entrapped or encapsulated into a NP, leading to nanoparticles, nanospheres or nanocapsules respectively (Figure 1.1.4 C).

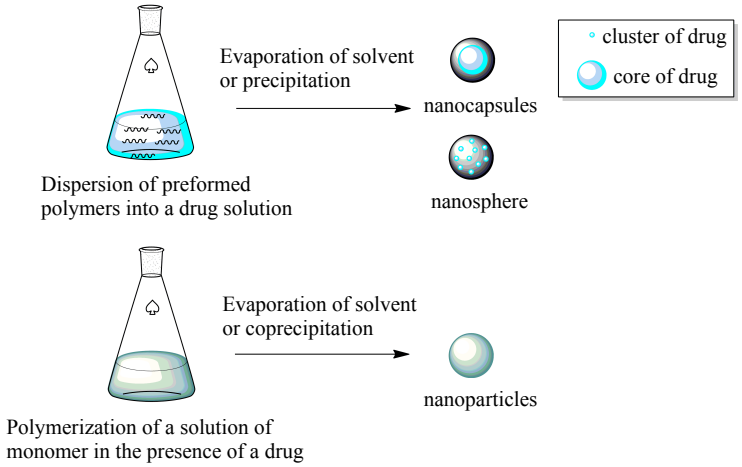

Figure 1.1.4 C. Methods for preparing nano-sized particles: nanocapsules, nanospheres, and nanoparticles.

These usually show various drug release profiles, which can be exploited to make "tailor-made" nanoparticles. Because plasma protein adsorption and phagocytosis of NPs can occur when they are administrated intravenously *in vivo*, thus affording to bioelimination of drugs, the surface of NPs should be carefully studied. Apart from their size, the amount of adsorbed blood circulating proteins (opsonins) are under the influence of surface hydrophobicity, determining the *in vivo* fate of NPs . Indeed, it was observed that PLA NPs, when incubated in human plasma and serum, adsorb high amount of IgG, apolipoprotein-E and C_3 protein (a protein used for recognition of foreign surface) (Figure 1.1.4 D1).[103] [104] Hence, it is necessary to modify NPs surface for designing effective and long circulating NPs.

Several methods of surface modification was developed in order to avoid these issues. In Figure 1.1.4 D are shown some approaches. One is surface coating by adsorbing hydrophilic polymers or surfactants after NPs formation. Although poloxamer[105], poloxamine[106], polysorbate (tween 80)[107] and lauryl ethers (Brij-35) have been widely used for these purpose, PEG-coated NPs have mostly received the attention of researchers because of their well-known toxicity profile.[108] Another road to

[103] Allemann, E.; Patricia, G.; Leroux, J., C.; Luc, B.; Gurnay, R., J. Biomed. Mater. Res., 1997, 37, 229-234.

[104] Blunk, t.; Luck, M.; Calvoer, A.; Hochstrasser, D., F.; Sanchez, J., C.; Muller, B., W.; Muller, R., H., Eur. J. Pharm. Biopharm., 1996, 42, 262-268.

[105] Storm, S.; Belliot, S., O.; Daemen, T.; Lasic, D., D., Adv. Drug Deliv. Rev., 1995, 17, 31-48.

[106] Illum, L.; Davis, S., S.; J. Pharm. Sci., 1983, 72, 1086-1089.

[107] Raessi, S.; Audus, K., J. Pharm. Pharmacol., 1989, 41, 848-852.

[108] Gref, R.; Minamitake, Y.; Peracchia, M., T.; Trubetskoy, V.; Langer, R., Science, 1994, 263, 1600-1603.

lead to this outcome is to prepare NPs by self-assembling of amphiphilic di-block-copolymers in aqueous solution, in which the lipophilic moiety will form the core and the hydrophilic moieties the shell of the NP. Using this technique long circulating poly(lactide-co-glycolide)-PEG (PLGA-PEG) and poly(lactide)-PEG (PLA-PEG) NPs were easily obtained and being particularly popular due to their good biological properties.[109] [110] In particular their half-life was improved by a factor within 180.[111] The protective effect of PEG was explained considering that the presence of hydrophilic and flexible chains onto the NP surface entails a steric effect which prevent NPs from interacting with other macromolecules (e.g. proteins) (Figure 1.1.4 D3).[112] In recent years this technique have provided the forward thrust for developing many long circulating NPs. However, PEGylation is too far to be considered as a versatile strategy and so further studies have to be done for elaborating new and more effective approaches.

A particular type of NPs are interpolyelectolytic complexes (IPEC), obtaining by self-assembling opposite charged polyelectolytes, that are polymers carrying ionizable groups in their polymeric backbone. These NPs have been widely studied for protein and gene delivery as protein-polymer and DNA/siRNA-polymer complexes can be produced by simply mixing the two macromolecules at appropriate ratios, affording to anionic or cationic NPs of nanometric dimensions (<100 nm) and surprisingly homogenous (Figure 1.1.4 E).[113] Usually stable NPs can be obtained since their Z-potential may be modulated by adjusting the starting charge ratio. Several cationic polymers have been evaluated for their ability to get IPEC with DNA, the most significant being poly-L-lysine (pLL) and polyethyleneimine (pEI).[114] [115] However these polymers were quite toxic and cannot be used for clinical applications, thus others efficient polymers have successfully been developed.[116]

Polyampholytes are a class of polymers bearing basic and acidic groups in their polymer chain and have the unique property of changing their overall charge in function of the pH, displaying a self-buffering ability.

---

[109] **Torchilin, V., P., J. Microencapsul., 1998, 15, 1-19.**

[110] **Kim, S., Y.; Shin, I., G.; Lee, Y., M.; J. Control Rel., 1998, 56, 197-208.**

[111] **Bazile, D.; Prud Homme, C.; Bassoullet, M.; Marlard, M.; Spenlehauer, G.; Veillard, M., J. Pharm. Sci., 1995, 84, 493-498.**

[112] **Joen, S., I.; Lee, J., H.; Andrade, J., D.; de Dennes, P., G., J. Colloid. Interf. Sci., 1991, 142, 149-158.**

[113] **Couvreur, P.; Puiseux, F.; Adv., Drug Delyv. Rev., 1993, 5, 141-162.**

[114] **Cherng, J., Y. et al., Pharm. Res., 1999, 16, 1417-1423.**

[115] **Oupicky, D., et al., J. Control Rel., 2000, 65, 149-171.**

[116] **Fisher, D.: Bieder, T.; Li, Y.; Elsasser, H., P.; Kissel, T.; Pharm. Res., 1999, 16, 1273-1279.**

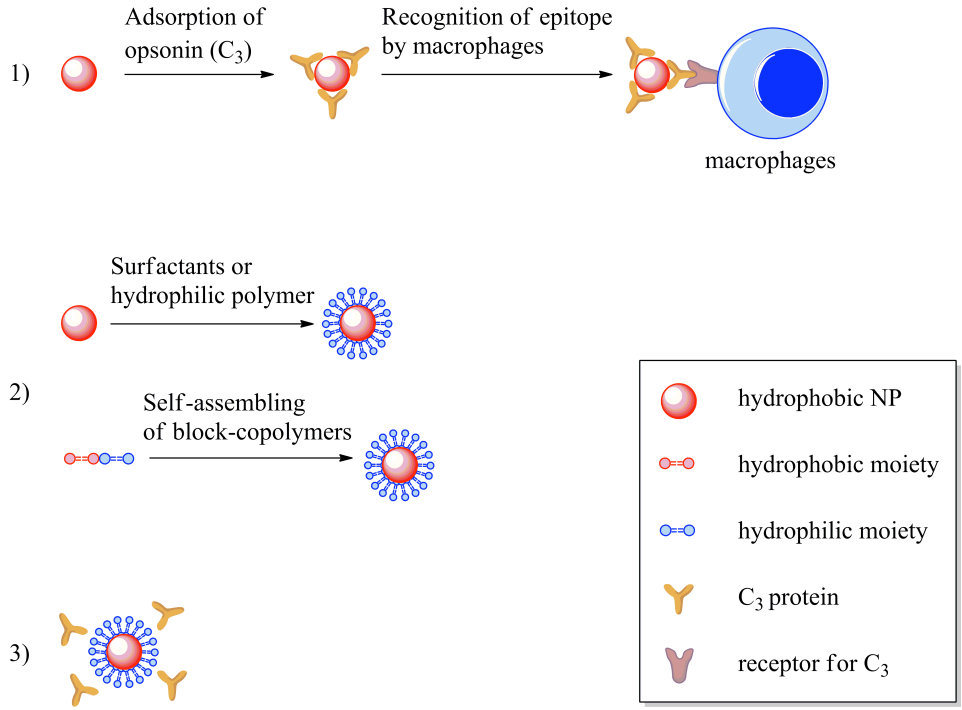

Figure 1.1.4 D Opsonization process of hydrophobic NPs by C_3 protein and their elimination through macrophages (Panel 1); methods to obtain surface modified NPs (Panel 2) and the effect of hydrophilic polymer density on the opsonization process.

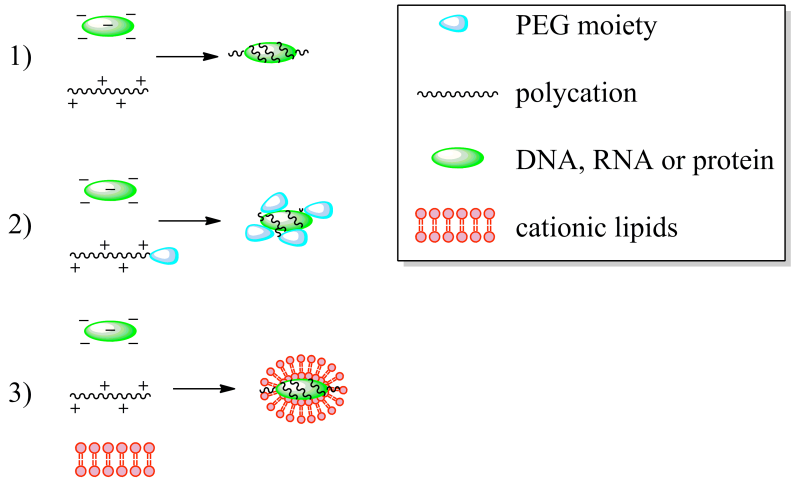

Figure 1.1.4 E This figure represents the formation of IPECs by mixing solutions of genetic material or negative charged protein and polycations (Panel 1); and the formation of PEG/lipid-coating IPEC (Panel 2 and 3 respectively).

For this reason they usually show a minimal toxicity and good transfection efficiency comparing to the purely cationic one.[117] [118] However, IPEC, after intravenous administration, may interact with opposite charged proteins and erythrocytes, causing erythrolysis. PEG-coating IPEC were prepared

[117] **Franchini, J.; Ranucci, E.; Ferruti, P.; Rossi, M.; Cavalli, R., Biomacromolecules, 2006, 7, 1215-1222.**

[118] **Ferruti, P.; Franchini, J.; Bencini, M.; Ranucci, E.; Zara, G., P.; Serpe, L.; Cavalli, R., Biomacromolecules, 2007, 8, 51-58.**

to get round this problem (Figure 1.1.4 E2).[119] PEGylation of IPEC also avoids the inherent inclination of these systems to accumulate into lungs, liver and kidneys, thus being liable to clearance. Despite this, PEGylation reduces the expression efficiency of IPEC by interfering with intracellular trafficking mechanisms, such as for instance the endosomal escaping. Another technique used to avoid the erythrolysis and bioaccumulation is based upon the formation of lipopolyplexes, in which the IPEC has a lipidic and neutral shell obtaining by adding ionic lipids into the IPEC mixture (See Figure 1.1.4 E3). Unfortunately, like liposomes, lipopoliplexes trig opsonization *in vivo* and nedeed further surface modifications. Although a vast number of natural and synthetic polymer-based nanoparticles, IPEC and nanocapsules have been explored, few have progressed into clinical trial. Self-assembling cyclodextrin-polymer conjugate-based nanoparticles pioneered by Davis and colleagues have made this transition as a transferrin targeted siRNA.[120]

NPs as diagnostic devices.

NPs are being actively developed for tumor imaging *in vivo* and biomolecular profiling of cancer biomarkers, because of their superficial characteristics and the EPR effect above mentioned.[121] Many tumor cells express protein biomarkers, namely particular proteins that are overexpressed in status of allostasis (eg, estrogen receptor, progesterone receptor for breast cancers), on which therapeutic regimen is changed. So simultaneous detection and quantification of several proteins on small tumor samples is nedeed in order to monitoring the evolution of specific tumors. Dendrimers, carbon naotubes, niosomes, quantum dots,

gold-conteining NPs, silver-conteining and other polymers are a large and well-established group of organic and inorganic particles that are being used as contrast agent or other diagnostic applications.[122] [123] [124] For example, semiconductor fluorescent nanocrystals, such as quantum dots containing a cadmium selenide core and a zinc sulphide shell surrounded by a coating of amphiphilic polymeric ligands, have been conjugated to antibodies, allowing detection and quantification of these target biomarkers in a tumor section (Figure 1.1.4 F).[125]

---

[119] **Kamimura, M.; Kim, J., O.; Kabanov, A., V.; Bronich, T., K.; Nagasaki, Y., J. Control. Rel., 2012;160(3):486-494.**

[120] **Davis, M., E., Mol. Pharmaceutics, 2009, 6, 659-668.**

[121] **Jain, K., Clin. Chim. acta, 2005, 358, 37-54.**

[122] **Svenson, S.; Tomalia, D., A.; Adv. Drug Deliv. Rev., 2005, 57, 2106-2129.**

[123] **Chan, P.; Yuen, T.; Ruf, F., et al., Nucleic Acids Res., 2005, 33, 161.**

[124] **Fortina, P.; Kricka, L., J.; Surrey, S.; et al., Trends Biotechnol., 2005, 23, 168-173.**

[125] **Gao, X.; Cui, Y.; Levenson, R., M., Nat. Biotechnol., 2004, 22, 969-976.**

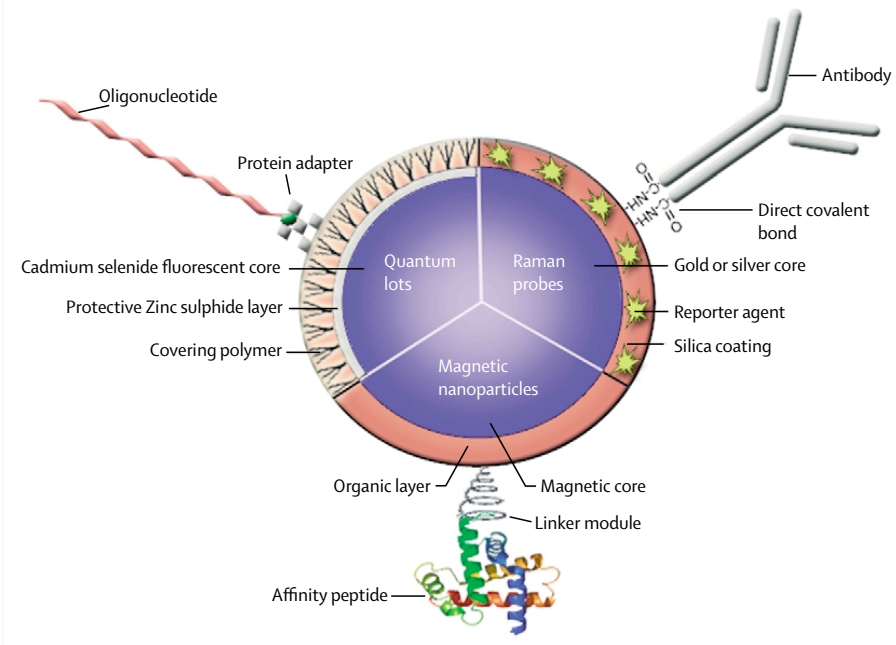

Yezhelyev,M., et al., Lancet Oncology, 2006, 7, 657-667

Figure 1.1.4 F Basic structure of diagnostic NPs (image from reference [126]).

This structure enables quantum dots to emit narrow and symmetrical electromagnetic signals within 450 and 850 nm by changing the size or chemical composition of the nanoparticles, that may be exploited to make different dyed NPs visualizable all together with a light source.[126] Furthermore, measurement of fluorescent intensity permits to quantify the biomarker real-time. Unfortunately, due to the presence of cadmium and other toxic heavy metal cores, quantum dots have limited applications *in vivo*. The use of gold/silver-containing nanoparticles, which are able to generate Raman signals, is another way to obtain reporter NPs for spectroscopic labeling (Figure 1.1.4 F).

Typically a silica shell with the report molecule is present in these systems to allow protein conjugation and Raman scattering. When illuminated with a laser beam, these NPs emit a shifted electromagnetic spectrum, like a fingerprint, which can be used to trace a map of the biomarkers and their amount.[127] Finally, supermagnetic NPs containing a metal core, such as iron, nickel or cobalt, and a polymeric shell, which enable them to be conjugated with proteins, are widely used as contrast enhancement agents to improve the sensitivity of MRI (Figure 1.1.4 F).

Polymer-based NPs as theranostic systems

Theranostic NPs are recent systems developed to carry out a double function, both therapeutical and diagnostical. They show great promise in the emerging field of personalized medicine, because they

[126] **Yezhelyev,M., V.; Gao, X.; Xing, Y.; Al-Hajj, A.; Nie, S.; O'Regan, R., M., Lancet Oncology, 2006, 7, 657-667.**

[127] **Moore, B., D.; Stevenson, L.; Watt, A., et al., Anal. Chem., 2003, 75, 6171-6176.**

permit detection as well as monitoring of an individual patient's cancer at an early stage, and delivering anticancer drugs over an extended period for enhanced therapeutic efficacy (Figure 1.1.4 G).[128] [129]

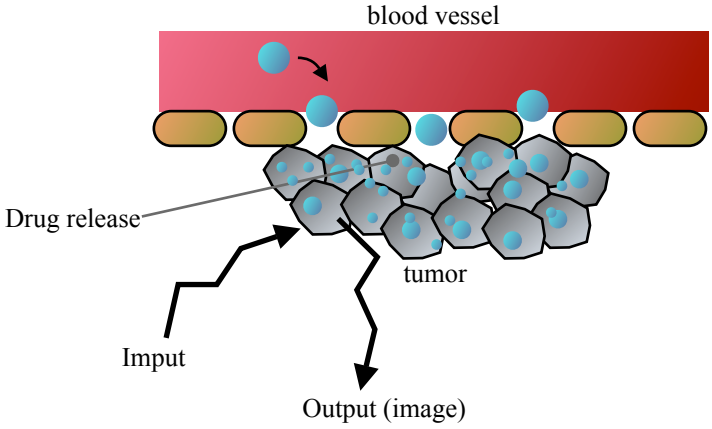

Figure 1.1.4 G. Mechanism of action of a theranostic device.

Furthermore, real-time and non invasive monitoring of the theranostic NPs enables clinicians to rapidly decide whether the regimen is effective in an individual patient or not.[130] Successful application of cancer theranosis require discovery of highly efficient tumor-homing nanoparticles which can diagnose and deliver targeted therapy. Cancer researcher have been investigating various nanoparticles for this purpose, made of lipidic micelles, inorganic particles and polymeric particles.[131] [132] For instance Kim's group have developed very stable chitosan-based NPs that simultaneously execute cancer diagnosis and therapy thanks to their near-infrared fluorescent label and by releasing paclitaxel into tumor site.[133] Fong-Yu Cheng et al. have successfully synthesized quantum dots-loaded FITC-labeled PLGA NPs with different size, demonstrating their potential use for molecular imaging and drug delivery.[134] However, notwithstanding the EPR effect, results have shown a non exhaustive effect.[135]

---

[128] Kim, K.; Kim, J., H.; Park, H.; Kim, Y, Park, K.; Nam, H.; Lee, S.; Park, J., H.; Park, R.; Kim, I.; Choi, K.; Kim, S., Y.; Park, K.; Kwon, I., C., J. control. Rel., 2010, 146, 219-227.

[129] Ozdemir, V.; Williams-Jones, B.; Glatt, S., J.; Tsuang, M., T.; Lohr, J., B.; Reist, C., Nat. Biotechnol., 2006, 24, 942-946.

[130] Weisslender, R., Science, 2006, 312, 1168-1171.

[131] Arap, W.; Pasqualini, R.; Ruoslahti, E., Science, 1998, 377-380.

[132] Peer, D.; Karp, J., M.; Hong, S.; Farokhzad, O., C.; Margalit, R.; Langer, R., Adv. Drug Deliv. Rev., 2002, 54, 631-651

[133] Kim, K.; Kim, J., H.; Park, H.; Kim, Y, Park, K.; Nam, H.; Lee, S.; Park, J., H.; Park, R.; Kim, I.; Choi, K.; Kim, S., Y.; Park, K.; Kwon, I., C., J. control. Rel., 2010, 146, 219-227.

[134] Cheng, F.; Wang, S., P.; Su, C.; Tsai, T.; Wu, P.; Shieh, D.; Chen, J.; Hsieh, P., C., Yeh, C., Biomaterials, 2008, 29, 2104-2112.

[135] Matsumura, Y.; Maeda, H., Cancer Res., 1986, 46, 6387-6392 .

These bad results might be explained in view of the quickly elimination underwent by NPs after administrating into the circulating blood by means of immune system.[136] [137]

It may be concluded that the use of biodegradable polymers for preparing NPs with therapeutic, diagnostic and theranostic purposes is well established, yet currently there is not an high number of commercial available products that utilize this technology. Polymeric nanoparticles have great utility to improve the bioavailability and to vehicle several bioactive agents, like vaccines, anti-tumorals, DNA and siRNA. Many polymeric NPs have been developed to guarantee long circulation of these therapeutic agents, but further approaches should be investigated to better tailor the particles' surface, thus reaching these goals. From the polymer chemistry viewpoint, this can be made by synthesizing new polymers to match the hydrophilic/lipophilic properties of NPs surface towards a specific type of tissue, cell or molecule. Furthermore, it might be expected that friendly processes will be developed.

[136] **Papahadjopulos, D.; Allen, T., M.;Gabizon, A.; Mayhew, E.; Matthay, K.; Huang, S., K.; Lee, K., D.; Woodle, M., C.; Lasic, D., D.; Redemann, C.; et al., Proc. Natl. Acad. Sci. USA, 1991, 88, 11460-11464 .**

[137] **Matsumura, Y.; Hamaguchi, T.; Ura, T.; Muro, K.; Yamada, Y.; Shimada, Y.; Shirao, K.; Okusaka, T.; Ueno, H.; Ikeda, M.; Watanable, N.; Br. J. Cancer, 2004, 91, 1775-1781.**

1.1.5 POLYMER-PRETEIN CONJUGATES

Peptides/protein-synthetic polymer conjugates are hybrid materials, which covalently combine one or more copies of a peptide sequence or protein with one or more synthetic polymer chain (Figure 1.1.5 A).[138][139] From an engineering standpoint, conjugates are interesting because they show biological and chemical features of both the biomacromolecules and the synthetic polymers, allowing the unique opportunity to combine the best of two "parallel worlds" and to overcome the shortcomings inherent to the components alone.

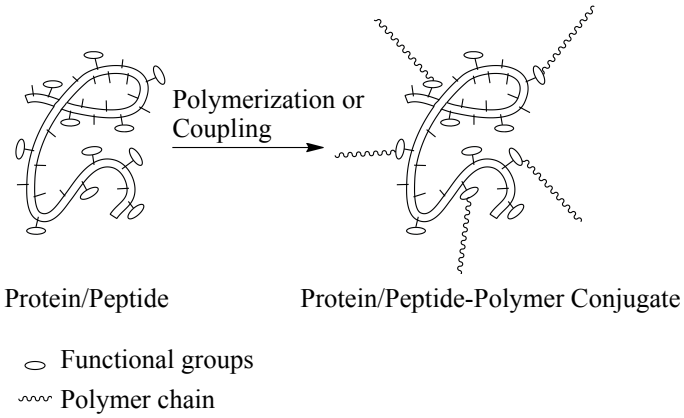

Figure 1.1.5 A. Representation of a Peptide/protein-synthetic polymer conjugates.

In one hand proteins display hierarchical structure formation that provides specific recognition and binding domains useful for obtaining a therapeutical effect. In the other hand synthetic polymers, which show biocompatibility, resistance to enzymatic degradation, increased bioavailability and passive targeting (EPR effect), can be exploited for improving the toxicity, the lack of bioavailability and the immunogeneticity of proteins.[140] Thereby peptides protein-polymer conjugates are of interest to researchers in diverse fields, such as medicine, nanotechnology, medical engineering, polymer chemistry and bioengineering, because combining characteristic properties of peptide or protein and polymers is possible to improve pharmacokinetics with unsubstantial effects on pharmacodynamics.[141] For example covalent attachment of polymers to proteins is known to improve protein efficacy by increasing lifetime *in vivo* and decreasing

[138] **Vandermeulen, G., W., M.; Klok, H., A. Macromol. Biosci. 2004, 4, 383-398.**

[139] **Klok, H., A., J. Polym. Sci. Part A: Polym. Chem. 2005, 43, 1-17.**

[140] **Klok, H., M.; Macromol. 2009, 42, 7990-8000.**

[141] **Grover G., N. and Maynard H.D. Current Opinion in Chem. Biology 2010, 14, 818-827.**

immunogenicity of proteins.[142] [143] [144] In some case, protein-polymer conjugates can exhibit higher biological activity, if compared to the unmodified protein, when attached to surface.[145] In others words this can be translated to fewer doses of drug for patients to reach the same therapeutic effect than the wild-type one. Examples of polymer-protein/peptide conjugation have been throughout summarized.[146] [147] [148] For instance, Davis et al have found that covalent conjugation of linear poly (ethylene glycol) chain (PEGylation) to bovine serum albumin (BSA) and bovine liver catalase was and effective strategy to reduce the immunogenecity of these proteins and increase their bioavailability.[149] [150] PEGylation, to date, is established as a powerful and safe strategy to improve the *in vivo* properties of therapeutics proteins and peptides; because PEGylated biological products exhibit often a reduced affinity for the target receptor that can lead to a lower clearance by target-mediated clearance mechanisms.[151] [152] Maeda et al, in the 1980, discovered that conjugates of neocarcinostatine (NCS) and styrene-maleic anhydride copolymers (SMACS) are able to accumulate in tumor tissue due to a passive targeting mechanism, which was referred to as the enhanced permeability and retention (EPR) effect. [153] Actually, in spite of all these examples, only PEGylation holds an important role in current pharmaceutics applications. In particular, PEG-Interferon® conjugates are good examples of drugs now used in medicine as non immunogenic and highly bioavailable antiviral agents.[154] Although PEGylation is extensively used and safe, there are some recent evidence that show as PEGylated biomolecules might display local and chronic toxicity in kidneys.[155]

---

[142] Glue, P.; Fang, J., W., S.; Rouzier-Panis, R.; Raffanel, C.; Sabo, R.; Gupta S.,K.; Salfi, M.; Jacobs, S.; Hepatitis, C., I., T., G. Clinical Pharmacol. & Therapeutics 2000, 68, 556-567.

[143] Magnusson, J., P.; Bersani, S.; Salmaso, S.; Alexander, C.; Caliceti, P. Bioconj. Chem. 2010, 21, 671-678.

[144] Gao, W.; Liu, W.; Christensen, T.; Zalutsky, M., R.; Chilkoti, A. In Proceedings of the National Academy of Sci. of the U.S.A. 2010, 107, 16432-16437.

[145] Lin P.,C.; Weinrich D.; Waldmann, H.; Macromol. Chemistry and Physics, 2010, 211, 136-144.

[146] Apostolovic, B.; Deacon, S.,P.,E.; Duncan, R.; Klok, H., A. Biomacromol. 2010, 11, 1187-1195.

[147] Osada, K.; Kataoka, K.; Peptide Hybrid Polymers, 2006, 113-153, Advanced in Polym. Sci., vol. 202.

[148] Joralemon, M., J.; McRae, S., Emrick, T. Chemical Communications, 2010,46, 1377-1393.

[149] Abuchowski, A.; van Es, T.; Palczuk, N., C.; Davis, F.,F. J. Biol. Chem., 1977, 252, 3578-3581.

[150] Abuchowski, A.; McCoy, J., R.; Palczuk, N., C.; van Es, T.; Davis, F.,F. J. Biol. Chem., 1977, 252, 3582-3586.

[151] Pasut, G. and Veronese, F., M.; Prog. Polym. Sci., 2007, 32, 933-961.

[152] Webster, R.; Didier, E.; Harris, P.; Siegel, N.; Stadler, J.; Tilbury, L.and Smith, D., Drug Metabolism and Disposition, 2007, 35, 9-16.

[153] Maeda, H.; Takeshita, J.; Kanamaru, R., Int. J. Peptide Protein Res., 1979, 14, 81-87.

[154] Goodman and Gilman's, Brunton, L., L. eds, The Pharmacological Basis of Therapeutis, 2006, p 1263.

[155] Hermansky, S., J.; Neptun, D., A.; Loughran, K., A.; Leung, H., W., Food Chem. Toxicol., 1995, 33 (2), 139-149.

The development of many other improved strategies for the synthesis of new peptide/protein-polymer conjugates is so needed.

Synthetic approach

Preparation of peptides/protein-polymer conjugates, over the past years, paves the way for numerous novel applications of this class of materials. The continuos expansion of the number of synthetic strategy that can be used to prepare these conjugates is due to the development of advanced methodologies for preparing synthetic peptides, creative use of controlled polymerization techniques, chemoselective coupling systems and residue/site specific protein modification reaction, that are reported in Table 1.1.5 A. [156]

Table 1.1.5 A. Main Synthetic strategies for the Preparation of Protein-Polymer Conjugates.

	conjugate synthesis	
peptide/protein synthesis	convergent	divergent
α-amino acid *N*-carboxyanhydride (NCA) ring-opening polymerization	• click coupling of α-alkyne/α-azido polypeptides with alkyne/azide functionalized nonpeptidic polymers	• NCA ring-opening polymerization using primary amine, amido−amine nickelacycle, *N*-trimethylsilylamine, or primary amine hydrochloride macroinitiators • one-pot synthesis using dual initiators for NCA ring-opening polymerization and NMP/ATRP
solid phase peptide synthesis (SPPS)	• N-terminal PEGylation of solid supported peptides • Solution click coupling of azide/alkyne chain end/side chain functionalized synthetic polymers with azide/alkyne functionalized peptides	• SPPS of the peptide segment on a PEG modified solid support • controlled radical polymerization of vinyl monomers using peptide-based initiators or chain transfer agents • (controlled) polymerization of peptide-functionalized monomers
protein biosynthesis	• protein PEGylation • bioorthogonal (Staudinger ligation, click chemistry, and oxidative coupling) conjugation of appropriate functional proteins and synthetic polymers	• ATRP or RAFT polymerization of vinyl monomers using protein-based macroinitiators or chain transfer agents

Table 1.1.5 A shows an overview of the main synthetic approaches that are available for the preparation of protein-polymer conjugates. These are listed according to the method used for the synthesis of the protein moiety as well as with careful consideration to the conjugation strategy used. Briefly, it can be noticed that there are three main techniques used for the synthesis of the protein part involving the (1) N-carboxyanhydride (NCA) ring-opening polymerization, (2) solid phase peptide synthesis (SPPS) and (3) protein biosynthesis. The synthesis of the conjugate can be performed in a convergent, divergent or grafting through fashion. Figure 1.1.5 B reports the three synthetic ways using the controlled radical polymerizations techniques.[157] The *convergent* one involves the coupling of pre-synthesized peptide and polymer building blocks, the *divergent* synthesis can be carried out in two different ways: (1) by polymerization of monomers using a

[156] **Gauthier, M., A.; Klok, H., M., Chem. Commun., 2008, 2591-2611.**

[157] **Grover G., N. and Maynard H.D. Current Opinion in Chem. Biology 2010, 14, 818-82.**

protein as macroinitiator and (2) by synthesizing a peptide on a soluble or solid-supported polymer, whereas the *grafting through* strategy is a mix o the two approaches where all repeat units on the conjugate can bear a pendant peptide or protein moiety .

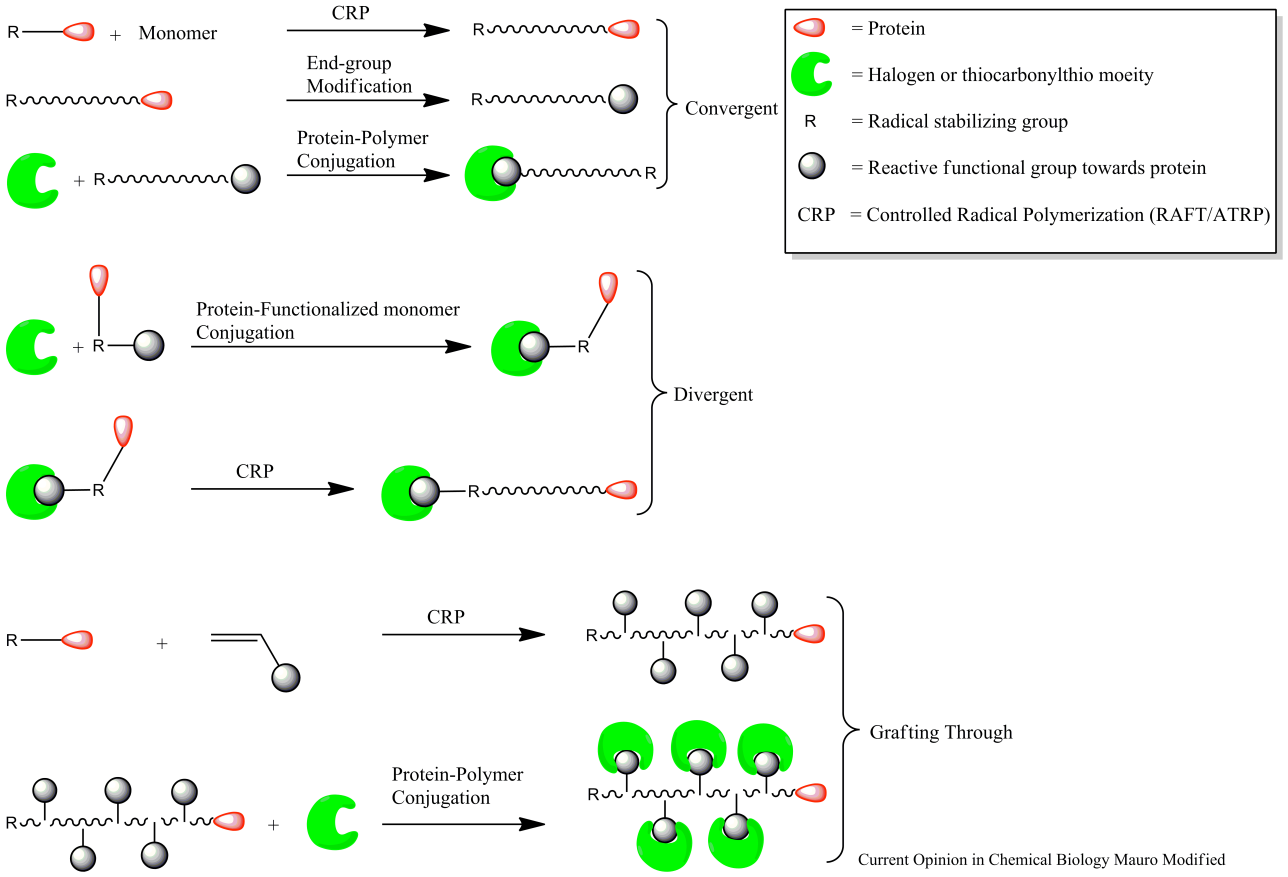

Figure 1.1.5 B. Controlled radical polymerizations for obtaining protein-polymer conjugates.

Each of these synthetic approach has peculiar advantages and drawbacks, which should be taken into consideration in order to obtain the pre-established goal. Nevertheless, in agreement with this scheme, it is rather evident that further functionalizations of the protein-polymer conjugate can not be easily obtained by using the conventional approach. RAFT and ATRP polymerization allow of preparing polymers with a broad range of functional groups that are able to orthogonally react with different chemical and biological species, affording, for example, targeted protein-polymer conjugates. Unfortunately these polymerization ways are very expansive and involve complex and hardly scalable synthetic pathways. This shortcoming can be overcome by using other new and original approaches involving the in-situ polymerization of hetero-difunctional monomers in the presence of soluble protein (Figure 1.1.5 C).

In this way can be prepared functionalized protein-polymer conjugates, with low polydispersity, that might undergo further coupling reactions, namely with targeting agents, or drugs.[158] In the past Paolo Ferruti's group has adopted a synthetic strategy to prepare functionalized BSA employing a large excess of telechelic oligomers carrying Michael acceptor as end-chains (doubly-vinyl terminated oligomers, DVTO). However, despite tedious purification procedures, covalent "bridged" conjugates cannot be excluded.[159]

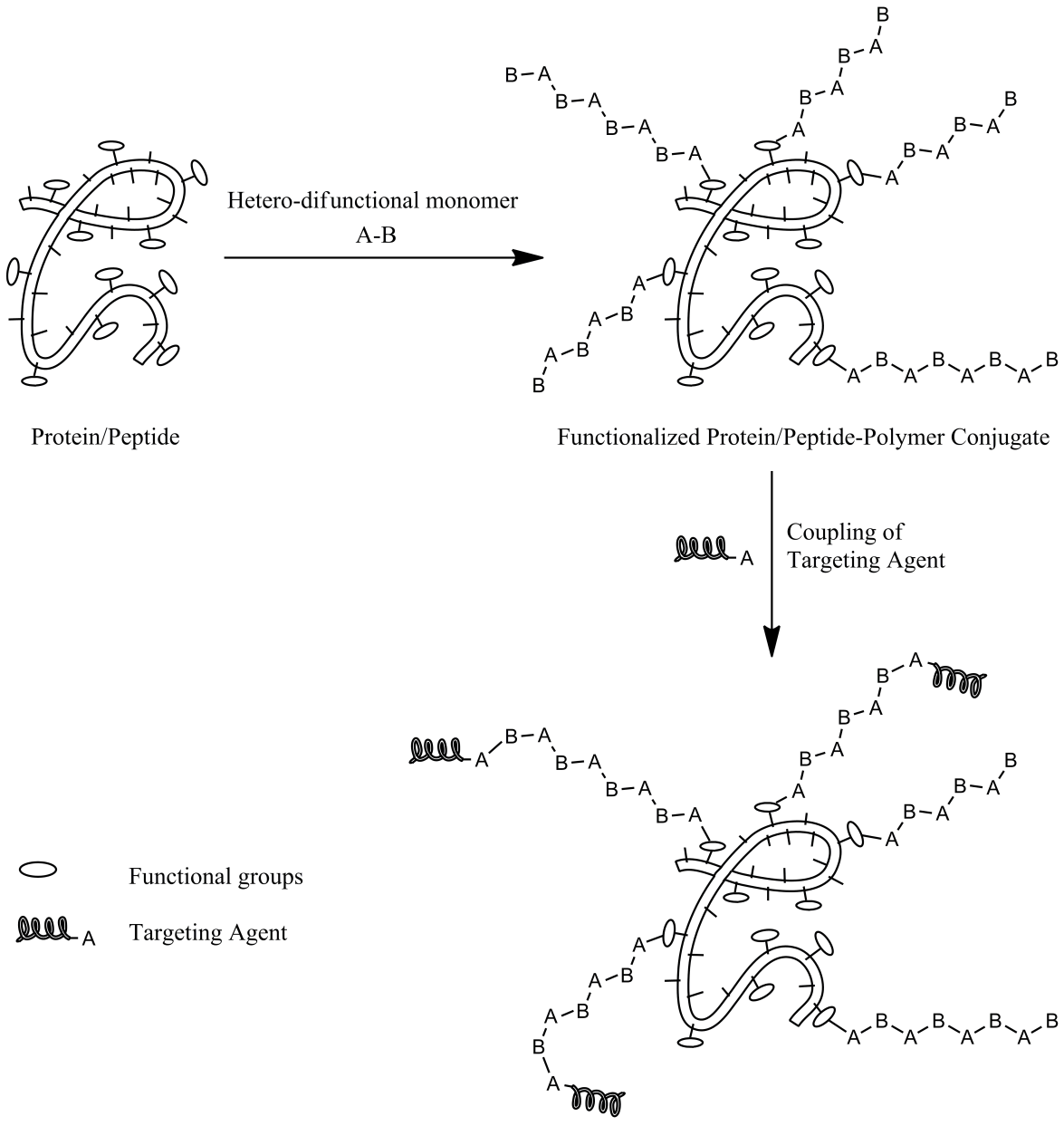

Figure 1.1.5 C. Innovative method for preparing protein-polymer conjugates with targeting agents.

[158] **Ferruti, P.; Mauro, N.; Ranucci, E.; Manfredi, A., J. Polymer Sci. Part A: Polym. Chem., 2012, DOI: 10.1002/pola.26325.**

[159] **Ranucci, E.; Bignotti, F.; Paderno, P. L.; Ferruti, P., Polymer, 1995, 36, 2989-2994.**

1.1.6 HYDROGEL SCAFFOLDS FOR TISSUE ENGINEERING APPLICATIONS

Tissue engineering aims to stimulate or facilitate the re-growth of damaged or diseased tissue by employing a combination of biomaterials, cells and bioactive molecules.[160] To date, thousands of clinical procedures are performed to replace or repair tissues in the human body that have been damaged by disease or trauma. The classical clinical route to replace a damaged tissue is based upon the donor graft tissues technique, consisting in the autografts, allografts, or xenografts of a healthy tissue (Figure 1.1.6 A).

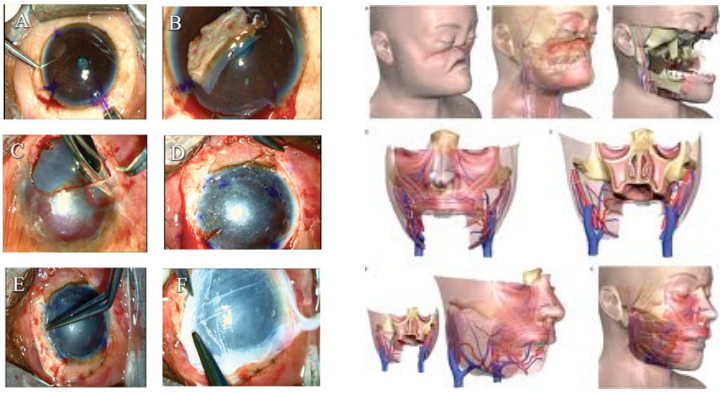

I. Conjunctival autograft

II. Bone allograft

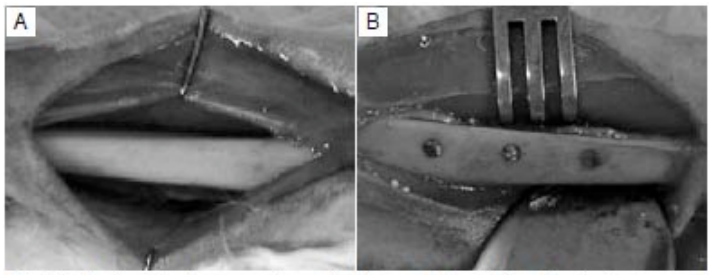

III. Tibial bone xenograft

I.Amar Agarwal, Ocular Surgery News U.S. Edition, 2011
II.Siemionow, M., D. et al, The Lancet, 2009, 374, 203–209
III.Mônica Diuana Calasans-Maia et al, Acta ortop. bras., 2009, 17, 6 São Paulo

Figure 1.1.6 A. Schematic representation of graft techniques useful in tissue engineering. In the panel (I) is reported a step-by-step conjunctival autograft, consisting in harvesting conjunctival limbal from contralateral eye (A, B) and implanting the harvested tissue into the unhealthy eye (C,D,E,F). In the panel (II) can be seen a typical allograft of facial bone after injury, where bones were implanted after their harvesting from a crops**.** In the panel (III) is reported a xenograft of tibial bone in rabbit, in which the tibial gap was filled with hydroxyapatite from bovine bone.

There are many problems associated with this medical practice which point out that the potentialities of this technique are limited, like a shortage of donors or donor sites, transmission of disease, rejection of grafts, donor site pain and morbidity, the volume of donor tissue that can be

[160] **Saltzman W., M.; Olbricht W., L., Nat Rev Drug Discov., 2002, 1, 177–86.**

safely harvested, and the possibility of harmful immune responses.[161] In contrast, tissue engineering, or regenerative medicine, aims to regenerate the damaged tissue by providing a biocompatible scaffold that, stimulating the cellular re-growth and tissue in-growth, allows to restore and maintain tissue functions. Overall, tissue engineering technologies entail the successful interactions between three components: (i) the scaffold that holds the cells together to generate the tissue's physical shape; (ii) the cells that arrange the new tissue; and (iii) the biological signaling molecules, such as growth factors, that direct the cells to express the desired tissue phenotype (Figure 1.1.6 B).[162] [163]

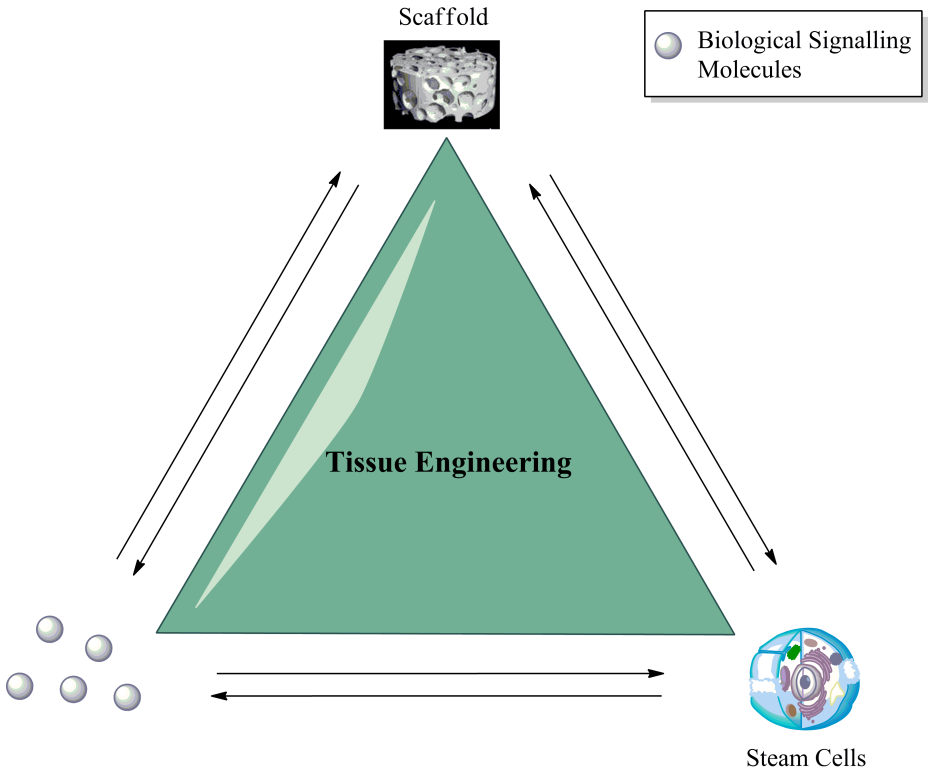

Figure 1.1.6 B. Schematic representation of the interactions that should be take into consideration for reaching the goal in tissue engineering applications: the resorbable scaffold should be able to interact with steam cells present in the unhealthy tissue, supporting them as an extracellular matrix and mimicking physiological release of bioactive signaling molecules, as for instance growth factors.

A scaffold is an artificial structure capable of supporting three-dimensional tissue formation with or without seeded allotropic cells.[163] In particular, biodegradable polymeric scaffolds for tissue engineering have received much attention because they can be gradually replaced with new and functional tissue once it degrades.

[161] Langer R. Biomaterials in drug delivery and tissue engineering: one laboratory's experience. Acc Chem Res., 2000, 33, 94–101.

[162] Lyons, F.; Partap, S.; O'Brien, F., J., Technol Health Care., 2008, 16, 305–17.

[163] Garg, T.; Singh, O.; Arora, S.; Murthy, R., S., R., Critical Rev. Ther. Drug Carrier Syst., 2012, 9, 1-63.

Obviously, the degradation rate of these scaffolds is very important, since it can affect the tissue regeneration: as a too fast degradation rate might not permit a physiologic tissue growth owing to lack of proper structural support, a too slow degradation rate might be a "stopper-like" function towards cellular re-growth. As shown in Figure 1.1.6 C, different types of polymeric scaffolds are available: (i) a typical 3D porous matrix, which is a highly porous and well interconnected open pore structure that allows high cell seeding density and tissue in-growth; (ii) a nanofibrous matrix that is prepared by electrospinning or self-assembly would provide a better resemblance of the physiological environment[164]; (iii) a thermosensitive sol-gel transition hydrogel; and (iv) a porous microspheres. These are already widely utilized as sustained protein-release formulations and have been applied in tissue engineering for the potential use as cell delivery carriers or supportive matrices. Among the polymeric scaffolds, hydrogels play a crucial role, since they are highly biocompatible and similar to the cellular matrix.

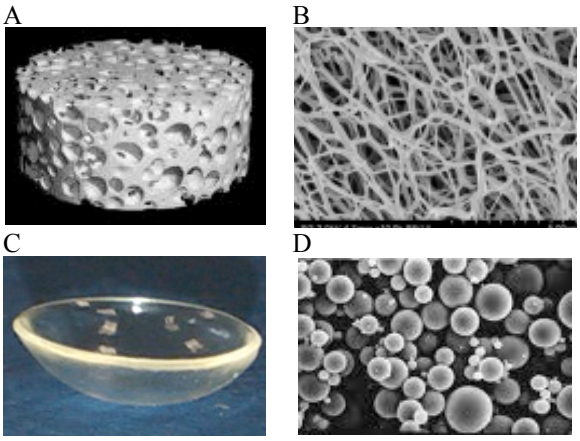

Figure 1.1.6 C Scaffolds for biomedical applications: highly porous polymer (panel A), nanofibrous matrix (B), chemically crosslinked hydrogel (C), porouse microspheres (panel D).

Hydrogel scaffolds

During the last few decades, hydrogels have gained increasing attention as biomaterials for tissue engineering, regenerative medicine and drug delivery applications, because of their water content and biocompatibility.[165] .[166] [167] [168]

[164] Hutmacher, D., W., Biomaterials, 2000, 21, 2529–2543

[165] Hoffman, A.,S.,Adv Drug Deliv Rev. 2002, 43, 3–12.

[166] Van Vlierberghe, S.; Dubruel, P.; Schacht, E., Biomacromolecules, 2011, 12, 1387-1408.

[167] Lee, K., Y.; Mooney, D., J., Chemical Reviews, 2001, 101, 1868-1880.

[168] Hoare, T., R.; Kohane, D., S., Polymer, 2008, 49, 1993-2007.

In Table 1.1.6 A are reported most of the hydrogel commercialized scaffold and their major applications. There are manifold definitions of this material, but the most frequently referred one is given by Peppas, in which the hydrogel is defined as a three dimensional, water-swollen and crosslinked polymeric structure containing (i) covalent bonds, (ii) physical crosslinking due to chain entanglements, (iii) association bonds, or (iiii) crystallites as a result of strong interactions between two or more macromolecular chains.[169] Hydrogels can be classified into different categories depending on various parameters including the macromolecular structure, the overall charge, the nature of the polymer and the mechanical and structural characteristics.

Table 1.1.6 A. Commercial available hydrogel scaffolds and their current applications.

#	Commercial Name of the Scaffold	Current Clinical and Research Applications
1	Apligraft	Artificial skin
2	Revitix	Topical cosmetics
3	VCTO1	Bilayered bioengineered skin
4	inFUSE	Osteoinductive carrier of bone morphogenic protein for spinal fusion
5	Collagraft	Treatment of bone fractures
6	Healos	Bone graft substitute in spina fusion
7	Biomend	Regeneration of periodontal tissue
8	Gelfoam	Hemostati device
9	Gelfilm	Neuro, thoracic and ocular surgery
10	CultiSpher-G	Microcarrier cell culture
11	Nu-Derm, AlgiSite, Curasorb	Injury dressing
12	Hyalgan, Hyalubrix, Artz	Lubrificant or medical support in osteoarthritis
13	Bionect, Jossalind	Surgery and injury healing
14	Orthovisc, Opegan R, Opelead, Healon	Implantation of intraocular lens
15	EmbryoGlue	In vitro fertilization
16	Hyaff	Scaffold for different applications
17	Integra	Dermal regeneration
18	Viscoat	Surgical tool for cataract extraction and intraocular implantation

An exhaustive classification is reported in Table 1.1.6 B. On the basis of the macromolecular structure, homopolymer and copolymer hydrogels can be distinguished. Alternatively, hydrogels can be classified as cationic, anionic, amphoteric and non ionic, depending on the acid-base properties of the starting monomers. Furthermore, hydrogels can also be designated according to their physical status: amorphous, semi-crystalline, hydrogel-bonded, supramolecular, or

[169] **Peppas, N., A.; Bures, P.; Leobandung, W.; Ichikawa, H., Eur. J. Pharm. Biopharm., 2000, 50, 27-46.**

hydrocolloidal. Finally, hydrogel can be made using natural biopolymers, synthetic polymers, or a combination o these (semi-synthetic hydrogels).

Table 1.1.6 B. Classification of hydrogels on the basis of different properties.

Homopolymer	Copolymer		Homopolymer	Copolymer		Copolymer
Natural			Synthetic			Semi-synthetic
		Cationic	Amphoteric	Anionic	Non ionic	
Amorphous	Semicrystalline		Hydrogel-bonded	Supramolecular		Hydrocolloids

Usually they are nanoporous materials and their highly porous structure can easily be tuned by controlling the crosslinking degree of the gel matrix and the affinity of the latter for the aqueous environment in which they are swollen. Their porosity also permits the diffusion of low molecular weight molecules through the matrix, thus ensuring that nutrients and metabolites may be replaced or removed *in vivo* and in vitro at rate dependent on the diffusion coefficient of these molecules. Hydrogels beyond their biocompatible, due to the presence of high water content and the physico-chemical similarity to cellular matrix, are relatively deformable and can conform to the shape of the surface to which they are applied. Despite these advantages, up to now, they show several limitations. In particular, given that they have a very low elastic modulus, that is a measure of the mechanical strength, they can be exploited only for tissue engineering applications encompassing soft tissues, i.e. nerve, liver, spleen, blood vessel, kidney, cartilage, etc. For example, injectable poly (N-isopropylacrylamide) physical hydrogels encapsulating cells have been prepared for cartilage and nerve regeneration.[170] [171] Pluronic/heparin composite hydrogels delivering growth factor also have been studied to induce angiogenesis.[172] Photo crosslinked poly(ethylene glycol) (PEG)–based hydrogels have been utilized for delivery of chondrocytes and osteoblasts. [173] [174] Bone morphogenic protein introduced into the hydrogel material (temperature-sensitive chitosan-polyol salt combination) has been effective in promoting de novo bone and cartilage formation *in vivo*.[175]

[170] **Stile, R., A.; Burghardt, W., R.; Healy, K., E., Macromolecules. 1999;32:7370–9.**

[171] **Park, K., H.; Yun, K., J Biosci Bioeng. 2004;97:374–7.**

[172] **Yoon, J., J.; Chung, H.; Park, T., G., J Biomed Mater Res., 2006, 79, 934–942.**

[173] **Bryant, S., J.; Anseth, K., S., J Biomed Mater Res. 2003;64:70–9 .**

[174] **Burdicka, J., A.; Ansetha K., S., Biomaterials. 2002;23:4315–23.**

[175] **Chenite, A.; Chaput, C.; Wang, D.; Combes, C.; Buschmann, M., D.; Hoemann, C., D.; Leroux, J., C.; Atkinson, B., L., Binette, F.; Selmani, A., Biomaterials, 2000, 21, 2155–2161.**

Poly(lactic acid–glycolic acid) (PLGA) grafted with PEG and PEG grafted with PLGA hydrogels capable of sustained insulin delivery and cartilage repair were synthesized.[176] Pluronic copolymers at a higher concentration have been used to encapsulate chondrocytes and produce engineered cartilage.[177] Amphoteric poly(amidoamine)s hydrogel, carrying RGD-like repeating unit, have been employed as guidance for peripheral nerve regeneration.[178] Although mostly these materials have successfully been used, their inadequate mechanical behavior did not permit their wide use in clinical practice. Looking into convenience and practicability, there are immense interests in developing injectable hydrogel scaffolds, because they are easy to use, versatile, and involve the use of safe adjuvants.[179] Furthermore, new biodegradable and elastic polymers need to be developed to fit for all requirements for surgically implantable scaffolds.

In the light of these, hydrogel scaffolds should be endowed with the following features:

I. Mechanical properties that are sufficient to shield cells from tensile forces without inhibiting biomechanical cues.

II. Desired volume, shape, and mechanical strength.

III. Acceptable biocompatibility.

IV. A highly porous and well-interconnected open pore structure to allow high cell seeding density and tissue in-growth.

V. Bioadsorption at predetermined time period.

VI. Biocompatible chemical compositions and their degradation products, causing minimal immune or inflammatory responses.

VII. Physical structure to support cell adhesion and proliferation, facilitating cell–cell contact and cell migration.

---

[176] **Jeong B, Lee KM, Gutowska A, An YH., Biomacromolecules, 2002, 3, 865–868.**

[177] **Saim AB, Cao Y, Weng Y, Chang C, Vacanti MA, Vacanti CA, Eavey RD., Laryngoscope, 2000, 110, 1694–1697.**

[178] **Magnaghi, V.; Conte, V.; Procacci, P.; Pivato, G.; Cortese, P.; Cavalli, E.; Ranucci, E.; Fenili, F.; Manfredi, A.; Ferruti, P., J. Biomed. Master Res. A, 2011, 98, 19-30.**

[179] **Garg, T.; Singh, O.; Arora, S.; Murthy, R., S., R., Critical Rev. Ther. Drug Carrier Syst., 2012, 9, 1-63.**

There is a troubled challenge in designing and manufacturing hydrogel scaffolds that posses all the above requirements and the abilities to control the release kinetics of bioactive factors over the period of tissue regeneration.[180] Further efforts will definitely be focused on these aspects.

[180] **Papkov M.,S.; ,Agashi K.; Olaye, A.; Shakesheff, K.; Domb, A., J., Adv Drug Deliv Rev. 2007;59:187–206**

1.2 SCAFFOLDS FOR SCHWANN CELLS CULTURING AND PERIPHERAL NERVE REGENERATION

A large proportion of acquired peripheral neuropathies is due to traumatic injuries.[181] Their clinical treatment is usually based on microsurgery techniques, such as end-to-end nerve repair or autologous nerve grafting. However, microsurgery alone seldom leads to a complete functional recovery.[182] [183] Cell-based therapy represents an alternative. To this purpose, Schwann Cells (SC) are the first transplantable cell candidates.[182] [184] SC play an essential role in peripheral nerve regeneration since they are the main cells deputed to form myelin sheets and to secrete growth factors and adhesion molecules supporting the axon elongation and re-myelinization, by this way enhancing the overall rate of functional recovery.[185] [186] However, the use of SC in bioengineered nerve grafts is biased by their poor availability and slow *in vitro* growth rate.[187] Their efficiency may be enhanced *in vitro* by supporting nerve regeneration with conduits made of biocompatible materials favoring in loco SC adhesion and proliferation. The physical guidance of axons is crucial for achieving a satisfactory nerve repair.[188] A conduit for *in vivo* application should form a suitable environment for nerve regeneration by combining cellular stimulating factors with biodegradability. It should be non-toxic, easily fabricated in the convenient size and shape and, in addition, its permeability, swelling and mechanical strength should be tunable, as it is known to play a relevant role for axon elongation *in vivo*. [188]

Several polymeric materials, both of natural and synthetic origin, have been proposed as scaffolds for peripheral nerve regeneration. Among polymers of natural origin, the most promising one is probably collagen, even if modified chitosan, agarose, alginate and fibronectin also received attention. [189] [190] Collagen is the major protein component of the extracellular matrix and is considered by many scientists an ideal scaffold for tissue engineering. It interact favorably with SC

---

[181] Robinson, L. R. Muscle Nerve 2000, 23, 863-873.

[182] Chiono, V.; Tondalnt. Rev. Neurobiol. 2009, 87, 173-198.

[183] Tabesh, H.; Amoabediny, G.; Nik, N. S.; Heydari, M.; Yosefifard, M.; Ranaei Siadat, S. O.; Mottaghy, K. Neurochem. Int. 2009, 54, 73–83.

[184] Chen, Y. S.; Hsieh, C. L.; Tsai, C. C.; Chen, T. H.; Cheng, W. C.; Hu, C. L.; Yao, C. H., Biomaterials, 2000 , 21, 1541-1547.

[185] Mirsky, R.; Woodhoo, A.; Parkinson, D. B.; Arthur J., Peripher. Nerv. Syst. 2008, 13, 122-135.

[186] Mosahebi, A.; Fuller, P.; Wiberg, M.; Terenghi, G., Exp. Neurol. 2002, 173, 213–223.

[187] Terenghi, G.; Wiberg, M.; Kingham, P. J., Int. Rev. Neurobiol. 2009, 87, 393-403.

[188] de Ruiter, G. C. W.;. Malessy, M. J. A; Yaszemski, M. J.; Windebank, A. J.; Spinner, R. J., Neurosurg. Focus 2009, 26, E5 1-9.

[189] Tabesh, H.; Amoabediny, G.; Nik, N. S.; Heydari, M.; Yosefifard, M.; Ranaei Siadat, S. O.; Mottaghy, K. Neurochem. Int. 2009, 54, 73–83.

[190] Friedman, J. A.; Windebank, A. J.; Moore, M. J.; Spinner, R. J.; Currier, B. L.; Yaszemski, M. I.; Bartolomei, J.; Piepmeier, J. M.; Ghu, G.; Fehlings, M. G.; Hodge, C. J.; Wagner, F. C., Neurosurgery 2002, 51, 742–752.

and shows good swelling and degradation. However, its acceptance as medical polymer is biased by the concern about the risk of contamination with prions, or of immunogenic reactions. Compared with polymers of natural origin, synthetic polymers are more reliable as regards reproducibility and lack of immunogenicity.[191] [192] They are not liable to import pathogenic agents and are much more versatile, since their molecular structure can be tailored to tune mechanical properties and degradation rate according to necessities. Among synthetic polymers, by far the most popular ones are polyesters, such as poly(D,L-lactic acid), poly(lactic-co-glycolic acid), poly(β-hydroxybutyrate) and poly(ε-caprolactone).[193] [194] [195] They are easily fabricated, biocampatible and biodegradable to non-toxic products that, however, are strongly acidic and may cause inflammation to the implant surrounding tissues.[196]

Hydrogels can be considered an attractive alternative to rigid hydrophobic scaffolds for the production of conduits for nerve regeneration, since their high water content makes them biomimetic.[197] [198] [199] [200] More recently amphoteric and cross-linked poly(amidoamine)s have been successfully used for *in vivo* nerve repair.[201] Tubes of this biomaterial, implanted in rats, have proved to be biocompatible and capable of inducing peripheral nerve regeneration. However, as a rule, hydrogels need to be improved from the standpoint of mechanical properties.

---

[191] **Willerth, S. M.; SakiyamaAdv. Drug Deliv. Rev. 2007, 59, 325-338.**

[192] **Manzanedo, D. 2005, "Biorubber (PGS): evaluation of a novel biodegradable elastomers", Thesis, Massachusetts Institute of Technology, Department of Material Science and Engineering.**

[193] **Molander, H.; Olsson, Y.; Engkvist, O.; Bowald, S.; Eriksson, I. Muscle Nerve 1982, 5, 54-57.**

[194] **Evans, G. R.; Brandt, K.; Niederbichler, A. D.; Chauvin, P.; Herrman, S.; Bogle, M.; Otta, L.; Wang, B.; Patrick, C. W., J. Biomater. Sci., Polym. Ed. 2000, 11, 869-878.**

[195] **Gregory, R. D.; Brandtb, E. K.; Katzc, S.; Chauvind, P.; Ottod, L.; Bogled, M.; Wangd, B.; Meszlenyie, R. K.; Lue, L.; Mikose, A. G.; Patrick, C. W., Biomaterials 2002, 23, 841–848.**

[196] **Tabesh, H.; Amoabediny, G.; Nik, N. S.; Heydari, M.; Yosefifard, M.; Ranaei Siadat, S. O.; Mottaghy, K. Neurochem. Int. 2009, 54, 73–83.**

[197] **Puppi, D.; Chiellini F.; Piras, A. M.; Chiellini, E., Prog. Polym. Sci. 2010, 35, 403-440.**

[198] **Gunn, J. W.; Turner, S. D.; Mann, B. K.; J. Biomed. Mater. Res. 2005, 72A, 91–97.**

[199] **Rajiv, M.; Munro, C. A.; Dalton, P. D.; Tator, C. H.; Shoichet, M. S. J. Neurosurg. 2003, 99, 555–565.**

[200] **Jabbari, E.; Wang, S.; Lu, L.; Gruetzmacher, J. A.; Ameenuddin, S.; Hefferan, T. E.; Currier, B. L.; Windebank, A. J.; Yaszemsky, M. J., Biomacromolecules 2005, 6, 2503–2511.**

[201] **Magnaghi, V.; Conte, V.; Procacci, P.; Pivato, G.; Cortese, P.; Cavalli, E.; Pajardi, G.; Ranucci, E.; Fenili, F.; Manfredi, A.; Ferruti, P., J. Biomed. Mater. Res. Part A 2011, 98A, 19-30.**

1.3 POLYAMIDOAMINES, A CLASS OF BIOCOMPATIBLE AND BIODEGRADABLE POLYMERS WITH PECULIAR BIOLOGICAL ACTIVITIES

Poly(amidoamine)s (PAAs) are synthetic, biocompatible and biodegradable polyelectrolytes[202] containing *tert*-amine (a) and amide (b) groups regularly arranged along their polymer backbone according to sequences

a-*a*-b or a-*a*-*b*-b

Linear PAAs are obtained by stepwise Michael-type polyaddition of primary or bis-secondary amines to bisacrylamides. The Michael-type addition reaction gives a wide range of polymers from diverse monomers, and corresponding polymers are prepared in environments in which other polymerization mechanism not operate.[203] In biological applications, such as protein derivatization, the mild Michael addition reaction conditions are favorable since high temperatures, oxidizing radicals, and organic solvents are not feasible.[204] It is important to note that temperature and solvent affect this reaction. In particular polyaddition reaction rate is accelerated by increasing temperature, but the resulting polymer have lower molecular weight. This can be explained considering that hydrolysis reaction rate, that competes with the polyaddition, contemporaneously undergo an exponential growth.[205] Concerning solvent effects, more recently, a study showed that mobile hydrogen play a key role in the reaction mechanism of Michael-type addition, and hydrogen mobility strongly influences reaction kinetics.[206] Overall, high molecular weight PAAs can only be prepared in ethylene glycol and water.

The general synthetic procedure for PAAs is reported in Scheme 1.3A. It is clear that to obtain high-molecular weight polymers the functions involved, namely activated double bonds and amine hydrogens, must be stoichiometrically balanced.[207] A perfectly balanced reacting mixture will contain three types of macromolecules, a----a, b----b, and a----b in 1:1:2 ratio. More commonly, unbalanced mixtures will contain the same molecular species, albeit in different ratios, until the minority function is completely consumed.

---

[202] **Ferruti, P.; Manzoni, S.; Richardson, S., C., W.; Duncan, R.; Pattrick, N., G.; Mendichi, R.; Casolaro, M.; Macromolecules, 2000, 33, 7793-7800.**

[203] **Mather, B., D.; Viswanathan, K.; Miller, K., M.; Long, T., E., Progress in Polym. Sci., 2006, 31, 487-531.**

[204] **Elbert. D., L.; Pratt, A., B.; Lutolf, M., P.; Halstenberg, S.; Hubbell, J., A.; J. Control Rel., 2001, 76, 11-25.**

[205] **Ferruti, P.; Ranucci, E.; Bignotti, F.; Sartore, L.; Bianciardi, P.; Marchisio, M., A.; J. Biomater. Sci. Polym. Ed., 1994, 6, 833-844.**

[206] **Mafredi, A.; Suardi, M., A.; Ranucci, E.; Ferruti, P., J. Bioactive Compatible Polymers, 2007, 22(2), 219-231.**

[207] **Ferruti, P.; Mauro, N.; Manfredi, A.; Ranucci, E., J. Polym. Sci. Part: A Polym. Chem., 2012, DOI: 10.1002/pola.26325.**

Only at this point, the product will be entirely constituted of molecules doubly terminated by the excess function. For this reason usually PAAs have a number-average molecular weight in the range of 5,000 - 40,000, with polydispersity index of about 1.9, and needed to be fractionated to enable their use in biomedical field.

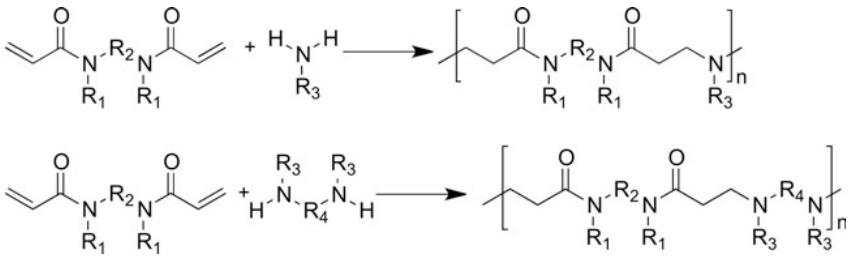

Scheme 1.3 A. General synthesis of linear PAAs by Micheal-type polyaddition.

The polymerization reaction take place in aqueous or alcoholic solutions, at room temperature and without added catalysts. Since under these conditions many functional groups do not interfere in the Michael addition, the structure and the physico-chemical properties of PAAs, including acid-base properties, may be tuned within plentiful limits. Indeed, additional functions may be directly introduced as side substituents, as long as they are not themselves liable to Michael-type reaction. Table 1.3 A shows the functional groups that may be inserted using this approach. For instance, amphoteric PAAs can be synthesized by bringing into starting bisacrylamide an acidic group.[208] A typical amphoteric PAA, named ISA23, obtained by polyaddition of 2,2-bisacrylamidoacetic acid to 2-methylpiperazine, contains as repeating unit a strong acidic carboxyl group (pKa=2.3) an two weakly basic tertiary amine groups (pka= 7.48 and 3.24 respectively). At pH 7.4 the amines are poorly protonated, but carboxyl group is completely deprotonated, and consequently, ISA23 carries excess negative charges. Anyway, PAA are highly functional polymers, thus further post-polymerization functionalizations may be performed in order to make they suitable for specific biomedical applications (Table 1.3A).

Although the ionization profile of polyelectrolytes follows complex laws, acid-base properties of all PAAs are described by the Henderson-Hasselbach equation. In particular they do not depend on the degree of protonation of the whole macromolecule, thus PAAs with specific acid-base behavior may be easily prepared by choosing the acid-base properties of the starting monomers.[209] This means

[208] **Richardson, S.; Ferruti, P.; Duncan, R., J. Drug Targeting, 1999, 6, 391-404.**

[209] **Ranucci, E.; Ferruti, P.; Lattanzio, E.; Manfredi, A.; Rossi, M.; Mussini, P., R.; Chiellini, F.; Bartoli, C., J. Polym. Sci. Part A: Polym. Schem., 2009, 4, 6977.**

that, in principle, it is possible to design a PAA able to pass from a prevailingly anionic to a prevailingly cationic status within narrow pH range.

Table 1.3A. Some functional groups, and their general applications, that can be inserted in PAAs backbone by either pre-polymerization (first column) or post-polymerization reactions (second column).

Functional Group	Further Reactions	Purpose
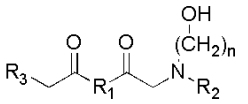	Coupling through EDC/NHSS or EDS/NHS pathway	Conjugation of bioactive agents, seeking mucoadhesion
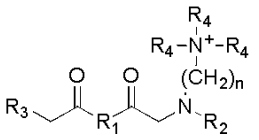	-	Exploring Antibacterial activity
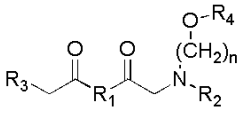	-	Synthesizing PAA-PEG comb copolymers
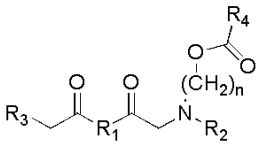	-	Pre-coupling of bioactive agents
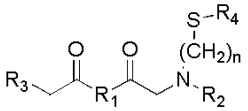	Oxydation to sulfoxide	Seeking mucoadhesion
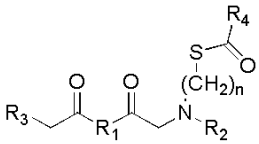	-	Seeking mucoadhesion, pre-coupling of bioactive agents
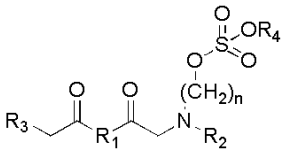	Acid-base	Amphoteric PAAs,
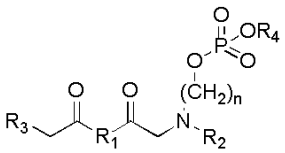	Acid-base	Amphoteric PAAs, targeting towards osteocarcinoma
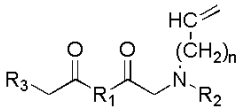	Radical polymerization, Diels-Alder	Highly controlled Cross-linking
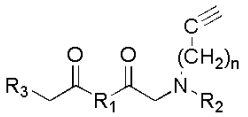	Diels-Alder	Highly controlled Cross-linking
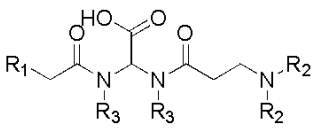	Esterification, Acid-base	Amphoteric PAAs, peptidomimetic structure (e.g. RGD-like)

This phenomenon can be exploited in order to developing smart bioresponsive PAAs able to respond to pH variations in a specific cell or organelle. For instance P. Griffiths et al. have demonstrated that in the case of ISA23, its endosomolytic activity is strictly correlated with its coil expansion on passing from a neutral pH (extracellular) to an acidic pH (endosomal and lysosomal) environments. [210] This conformational change also provides the possibility of designing polymer-drug conjugates that are, following intravenous administration, relatively compacted, thus protecting a drug pay load in the circulation, where the pH is 7.4, but following pinocytic internalization into acidic intracellular compartments unfold, permitting pH-triggered intracellular drug delivery.

The degradability of polymers is also very important to allow a good renal clearance and so to avoid the bioaccumulation of the polymer, which can cause chronic toxicity. The degradation mechanism of several PAAs has been extensively studied in the past decade, in physiological conditions (i.e. 37°C, phosphate buffer pH = 7.4).[211] [212] It can be concisely noticed that PAAs are liable to degradation by means of β-aminolytic and hydrolytic mechanisms. The degradation rate in aqueous media is strongly effected by basic pH and increasing temperature, as well as the nature of both the amine and amide moieties. Furthermore, degradation cannot seem to proceed through enzymatic and retro-Michael way.[213] [214]

Since PAAs are endowed with properly chemical, physico-chemical and biological properties, they represent a class of polymers with recognized potential in nanomedicine and tissue engineering. PAAs, such as ISA23, ISA1 and AGMA1 (See Table 1.3B), can be regarded as potential transfection promoters because they are much less cytotoxic than other commonly used polycations, such as poly-L-lysine (PLL) and poly(ethyleneimine) (PEI).[215] [216] In Table 1.3B are reported the IC_{50} of polycations used at the moment as positive controls by comparison with some PAA. It can be noticed that PAAs are of two order of magnitude less toxic. In addition, amphoteric PAAs are

---

[210] Griffiths, P., C.; Paul, A.; Khayat, Z.; Wan, K.; King, S., M.; Grillo, I.; Schweins, R.; Ferruti, P.; Franchini, J.; Duncanm R., Biomacromolecules, 2004, 5, 1422-1427.

[211] Ranucci, E.; Sartore, L.; Bignotti, F.; Marchisio, M., A.; Bianciardi, P.; Veronese, F., M., Biomaterials, 1994, 15, 1235-1241.

[212] Franchini, J.; Ferruti, P., Chapter 16 in Polymeric Gene Delivery: Principles and Applications, Mansoor, M. Amjii, CRC Press, 2005.

[213] Bignotti, F.; Sozzani, P.; Ranucci, E.; Ferruti, P., Macromolecules, 1994, 27, 7171-7178.

[214] Ranucci, E.; Spagnoli, G.; Ferruti, P.; Sgouras, D.; Duncan, R., J. Biomat. Sci. Polym. Ed., 1991, 2, 303-315.

[215] Lavignac, N.; Lazenby, M.; Foka, P.; Malgesini, B.; Verpilio, I.; Ferruti, P.; Duncan, R., Macromol Biosci., 2004, 4, 922-929.

[216] Richardson, S., C., W.; Ferruti, P., Duncan, R., J. of Drug Targeting, 1999, 6, 391-404.

usually non-cytotoxic (IC_{50} > 5 mg/ml) and have inherent fusogenic properties and stealth-like behavior conferring them good transfecting ability when used as gene delivery systems.[217]

Table 1.3B. Toxicity of some commonly used polycations compared with the IC_{50} of three well-studied PAAs (ISA23, ISA1, and AGMA1).

Name	Structure	IC_{50} (mg/ml)
ISA23	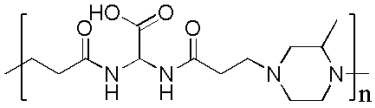	0.5
ISA1	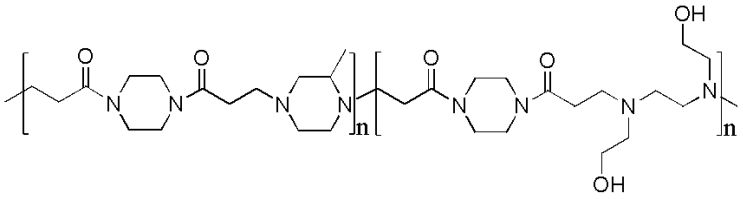	3.0
AGMA1	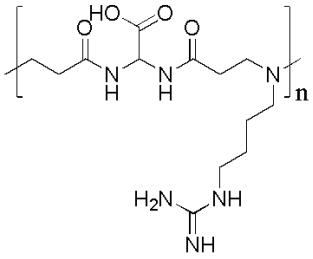	> 5
PLL	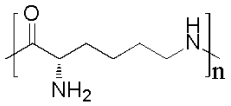	0.012
l-PEI	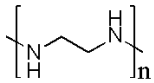	0.010

For a synthetic system to be effective *in vivo*, it should not only be tolerated by the body, but also demonstrate suitable pharmacokinetic profile, i.e. the ability to afford tissue targeting and to be enough bioavailable. PAAs, as ISA23 and ISA1, when studied in this respect exhibit longer circulation time if compared with the other polycations (See Table 1.3 C).

Table 1.3 C. Biodistribution of ^{125}I-labelled ISA23 and ISA1 after intravenous administration in rats.

	Percent Localization			
	ISA23		ISA1	
Body district	After 1 h	After 5 hrs	After 1 h	After 5 hrs
Blood	70	20	1.5	0
Liver	10	8	83	85
Kidney	2	1	7	4
Lungs	2	4	4	3
Urine	13	65	0	15

[217] Ferruti, P.; Franchini, J.; Bencini, M.; Ranucci, E., Biomacromolecules, 2007, 8, 1498-1504.

In particular ISA23 does not seem to be accumulate in liver, lungs or kidney making it suitable for tissue targeting applications *in vivo* either by active or passive targeting (EPR effect)[218] [219]. To reinforce the latter point, biodistribution studies carried out in mice bearing subcutaneous B16F10 melanoma showed that ISA23 and AGMA1 were still accumulating in tumor tissue within 5 hours, enabling their use as tumor targeting carrier in cancer therapy.[220] [221] Biological properties of different PAAs have been widely reported, and encompass the following: antiviral,[222] gene promoter,[221] [223] drug[224] [225] and protein[226] [227] carrier, cell adhesion and proliferation.[228] [229]

[218] **Duncan, R., Pharm. Sci. Technol. Today, 1999, 2, 441.**

[219] **Matsumura, Y.; Maeda, H., Cancer Res., 1986, 46, 6387-6392.**

[220] **Richardson, S., C., W.; Ferruti, P., Duncan, R., J. of Drug Targeting, 1999, 6, 391-404.**

[221] **Ferruti, P.; Franchini, J.; Bencini, M.; Ranucci, E.; Zara, G., P.; Serpe, L.; Primo, L.; Cavalli, R.; Biomacromolecules, 2007, 8 (5), 1498-1504.**

[222] **Ferruti, P.; Cavalli, R.; Ranucci, E.; Lembo, D., WIPO Patent Application WO/2011/145056, 2011.**

[223] **Cavalli, R.; Bisazza, A.; Sessa, R.; Primo, L.; Fenili, F.; Manfredi, A.; Ranucci, E.; Ferruti, P., Biomacromolecules, 2010, 11(10), 2667-2674.**

[224] **Schacht, E.; Ferruti, P.; Duncan, R., PCT, Internat. Pat. Appln., No. PCT/IB94/00259, 1994.**

[225] **Ferruti, P.; Ranucci, E.; Trotta, F.; Gianasi, E.; Evagorou, E.; Wasil, M.; Wilson, G.; Duncan, R., Macromol. Chem., 1999, 200, 1644-1654.**

[226] **Pattrick, N., G.; Richardson, S., C., W.; Casolaro, M.; Ferruti, P.; Duncan, R., J. Contr. Rel., 2001, 77, 225-232.**

[227] **Dempsey, C., E., Biochim. Biophys. Acta, 1990, 1031, 143-161.**

[228] **Jacchetti, E.; Emilitri, E.; Rodighiero, S.; Indrieri, M.; Gianfelice, A.; Lenardi, C.; Podestà, A.; Ranucci, E.; Ferruti, P.; Milani, P., Journal of Nanobiotechnology, 2008, 6, 14.**

[229] **Emilitri, E.; Guizzardi, F.; Lenardi, C.; Suardi, M.; Ranucci, E.; Ferruti, P., Macromol. Symp., 2008, 266, 41-47.**

1.3.1 PAAs AS EFFECTIVE NON-VIRAL GENE DELIVERY SYSTEMS

PAAs have been extensively studied as transfection promoters, as they are able to change their biological behavior depending on the pH of the surrounding medium, thus providing fusogenic properties. [230] Fusogenic polymer are able to form interpolyelectrolytic (IPEC) complexes with genetic material protecting it from the enzymatic degradation, and transfecting it into host cells in order to perform a therapeutic effect. Cationic PAAs, as for instance ISA1, exhibit remarkable efficiency as gene delivery system, even if they are more toxic than the amphoteric one.[231] In this respect, amphoteric PAAs, even those that at physiological pH are prevailingly negative, form stable IPEC with nucleic acids. This might be justified by the fact that cationic and anion charge are located in different spatial position along the polymer chain, thus complexation with other anionic macromolecules may take place. Indeed, an amphoteric PAA, named ISA23, which at pH 7.4 carries excess negative charges, has proved as active as PEI and LipofectIN, and more active than LipofectACE, being non toxic and non-hemolytic. This can be ascribed to the fact that ISA23 can be internalized into cells by pinocytosis and localizes in lysosomes, where the pH in 5.5; here it strongly increases its polycation character, becomes membrane active, and promotes the intracellular trafficking of nucleic acids.[232] [233] [234] Amphoteric PAAs other than ISA23 have also been studied. Those that at pH 7.4 are prevailingly anionic were non-toxic and non-hemolytic. By contrast, AGMA1 apart, those that at the same pH are prevailingly cationic, showed significant toxicity and hemolytic activity.[235] Whereas AGMA1, in spite of being fairly strongly cationic at physiological pH, was neither toxic nor hemolytic in vitro within a vast pH range (4.0 - 7.4).[236] It circulated for a long time in the blood stream when injected in rats. AGMA1 also proved a powerful transfection promoter *in vivo*, with minimal preferential localization in the liver.[237] The transfection ability of this polymer *in vivo* (60% of GFP expressing cells) was definitely comparable to that other commercial available transfection agents, such as the JetPEI, which has 63% of GFP expressing cells.

---

[230] **Griffiths, P., C.; Paul, A.; Khayat, Z.; Wan, K.; King, S., M.; Grillo, I.; Schweins, R.; Ferruti, P.; Franchini, J.; Duncanm R., Biomacromolecules, 2004, 5, 1422-1427.**

[231] **Ferruti, P.; Marchisio, M., A.; Duncan, R., Macromol. Rapid Commun., 2002, 23, 332-355.**

[232] **Hill, I., R.; Garnett, M., C.; Bignotti, F.; Davis, S., S., Biochim. Biophys. Acta, 1999, 1427, 161-174.**

[233] **Hill, I., R.; Garnett, M., C.; Bignotti, F.; Davis, S., S., Anal. Biochem., 2001, 291, 62-68.**

[234] **Richardson, S., C., W.; Pattrick, N., G.; Man, Y., K.; Ferruti, P., Duncan, R., Biomacromolecules, 2001, 2, 1023-1028.**

[235] **Ferruti, P.; Manzoni, S.; Richardson, S., C., W.; Duncan, R.; Pattrick, N., G.; Mendichi, R.; Casolaro, M.; Macromolecules, 2000, 33, 7793-7800.**

[236] **Franchini, J.; Ranucci, E.; Ferruti, P.; Rossi, M.; Cavalli, R., Biomacromolecules, 2006, 7, 1215-1222.**

[237] **Cavalli, R.; Bisazza, A.; Sessa, R.; Primo, L.; Fenili, F.; Manfredi, A.; Ranucci, E.; Ferruti, P., Biomacromolecules, 2010, 11, 2667-2674.**

In conclusion amphoteric PAAs are endowed with unique combination of desirable requirements for a nonviral drug delivery system and warrant further development of this class of polymers as transfection agents *in vivo*. Hyperbranched amphoteric PAAs might be proposed for this research line, because of their complexing ability.

1.3.2 PAA-PROTEIN CONJUGATES

The synthesis of homo-difunctional PAAs carrying acrylic or aminic end chains, liable to subsequent reactions of conjugation, have paved the way for developing PAA-protein conjugates. Using this approach such chimerical macromolecules have been prepared by employing a large excess of doubly vinyl-terminated, low molecular weight PAAs suitable for reacting with the exposed protein functional groups (e.g., thiols, amine groups). Nevertheless, despite tedious purification procedures, this synthetic approach did not ensure a perfect molecular architecture control, i.e., the presence of bridged molecules could not be excluded. In view of this issue a new synthetic pathway for the synthesis of PAA conjugate should be accomplished.

PAA-protein conjugates have been widely investigated in the past for a huge set of different applications in the field of nanomedicine. In particular they were studied as intracellular ribosome-inactivating toxins delivery systems. Ricin is a highly toxic dimeric protein, consisting of an A-chain (RTA), liable for cytotoxicity, and a B-chain (RTB), which acts to promote endocytosis of RTA, linked by a disulphide bridge.[238] [239] Cationic membranes interacting PAAs were chosen to investigate their ability to accomplish intracytoplasmic delivery of RTA chain at tumor cells (B16F10), and proved capable of restoring sito-specific cytotoxic activity of RTA.[240] Comparable results have found for gelonin, that is a toxin unable to diffuse across the cell membrane; hence it may not accomplish its cytotoxicity if not properly released into cells.[240]

ISA23 and ISA1-Mellitin (PAA-MLT) [241] conjugate have been also prepared in order to improve gelonin delivery into tumor cells. Mellitin is a cationic peptide derived from venom of Apis mellifera that display several biological properties, such as anti-tumor and immunostimulating activities. Mellitin has been used as fusogenic agent too, owing to its cationic nature. ISA1-MLT conjugate was able to better delivery gelonin, but, unfortunately, it has shown pH-dependent hemolytic activity at very low concentration, prohibiting its use in biomedical field. Whereas, the counterpart ISA23-MLT did not deliver gelonin.

However, this conjugate was totally non-toxic and non-hemolytic pointing out that it can be exploited as potential anticancer macromolecules.

---

[238] **Endo, Y.; Mitsui, K.; Motizuki, M.; Tsurigi, K., J. Biol. Chem., 1987, 262 (12), 5908-5912.**

[239] **Lord, M.; Roberts, L.; Robertus, J., FASEB J., 1994, 8, 201-208.**

[240] **Pattrick, N., G.; Richardson, S., C., W.; Casolaro, M.; Ferruti, P.; Duncan, R., J. Contr. Rel., 2001, 77, 225-232.**

[241] **Lavignac, N.; Lazenby, Franchini, J.; Ferruti, P.; Duncan, R., Int. J. Pharm., 2005, 300, 101-112.**

PAA-grafted bovine serum albumin (BSA) and human serum albumin (HSA) have been finally synthesized via Michael-type addition reaction involving the accessible amine groups (about 60) and the unique thiol group of the proteins.[242] Two PAAs, one anionic (ISA23) and the other one cationic (ISA1) were chosen to verify the feasibility of the reaction. The synthetic pathway showed proof of high versatility and efficiency, yielding to highly branched proteins with potential in drug delivery.

[242] **Ranucci, E.; Bignotti, F.; Paderno, L.; Ferruti, P., Polymer, 1995, 36 (15), 2989-2994.**

1.3.3 PAA-BASED NANOPARTICLES

One of the goal of pharmaceutic technologist is to solubilise hydrophobic drug that show inherent low solubility in aqueous media, and therefore low bioavailability when administrated *in vivo*. Nanoparticles carrying hydrophobic domains offer the opportunity to circumvent this issue by solubilising these drugs into their hydrophobic domains, thus affording to stable and effective nano-dispersions.

PAA-based nanoparticles have been successfully prepared by using two different strategies: i) the self-assembling of PAA-chelesterol conjugates, and ii) the cosslinking of β-cyclodextrin (β-CD) with di-acrylated PAAs. In the first approach the cholesterol was randomly linked to the polymer as side pendant through redox-sensitive disulphide bonds.[243] Once the polymer was put into aqueous media it self-assembled giving core-shell nanoparticles, in which the shell was characterized by a strong hydration due to the highly hydrophilic nature of PAAs. Such systems were able to load high amount of lipophilic drugs into the hydrophobic core, and yet retained the typical biological behavior of the parent PAA in terms of biocompatibility and biodistribution. In an alternative way PAA-based nanoparticles were obtained by cross-linking β-CD units with telechelic PAA oligomers with acrylic end chains.[244] Not surprisingly, as β-CD are able to complex several hydrophobic small molecules, they proved capable to solubilise paclitaxel up to 5% of their own dry weight, leading to very stable formulations with a shelf-stability of more than 3 years. Finally, biological studies, including *in vivo* hemolytic assay and in vitro MCF-7 cell viability test, have well established that it was biocompatible after intravenous injection. It is important to mention that soluble branched or hyperbranched β-CD/PAA systems did not display comparable results, if ever their performance were enormously lower.

It is noteworthy that both synthetic strategies mostly provided us with the possibility to fulfill effective nanoparticles able to load high amount of hydrophobic drugs. Nevertheless, these roads usually proceed at random and may not permit a good control of the macromolecular architecture, which is a fundamental regulatory request that should carefully considered in modern polymer chemistry.

---

[243] **Ranucci, E.; Suardi, M., A.; Annunziata, R.; Ferruti, P.; Chiellini, F.; Bartoli, C., Biomacromolecules, 2008, 9, 2693-2704.**

[244] **Ferruti, P.; Ranucci, E.; Trotta, F.; Cavalli, R., IT Patent n. MI2007A1173.**

1.3.4 PAAs AS SCAFFOLDS FOR REGENERATIVE MEDICINE

PAAs hydrogel scaffolds can be easily obtained by different manners. Anyway, all procedures are based on the introduction of tetrafunctional monomers into the main polymer chain, thus enabling crosslinking reaction between parallel polymer chains. One of the most efficient means for achieving this, is to polymerize a stoichiometrically balanced mixture of both acrylic (B_2) and amine (A_2) monomers in the presence of primary diamines (A_4) (Scheme 1.3.4 A).[245]

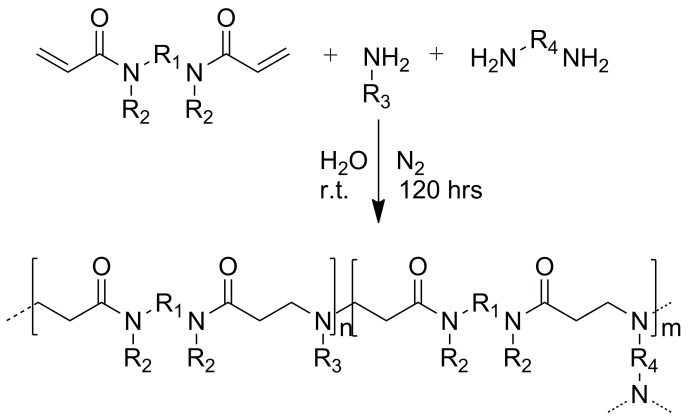

Scheme 1.3.4 A. Synthesis of PAA hydrogels via A_2 B_2 A_4 system.

According with this scheme, having four different mobile hydrogens, the primary amine performs the role of cross-linking agent yielding to hydrogels. Using this technique, depending on the type and the degree of cross-linking, hydrogels absorbing large amounts of water can be obtained without great effort. An alternative widespread way leading to PAAs hydrogels make up of multistep reaction that involves the preparation of linear doubly vinyl-terminated, low molecular weight PAAs, and hence the radical cross-linking of these molecules, after appropriate purification, by means of either UV or radical initiators (Scheme 1.3.4 B).[246] It was found a considerable reduction of degradability due to carbon-carbon bonds, and so the bioelimination of degradation products must be carefully studied before using for biomedical applications. Another possible synthetic method consists of producing linear PAAs carrying primary amino groups as side substituents (NH2-PAAs),[247] which can be used as macromolecular and multifunctional cross-linking agents (Scheme 1.3.4 C).[248]

---

[245] Ferruti, P.; Bianchi, S.; Ranucci, E.; Chiellini, F.; Caruso, V., MAcromol. Biosci., 2005, 5 (7), 613-622.

[246] Magnaghi, V.; Conte, V.; Procacci, P.; Pivato, G.; Cortese, P.; Cavalli, E.; Pajardi, G.; Ranucci, E.; Fenili, F.; Manfredi, A.; Ferruti, P. J. Biomed. Mater. Res. Part A 2011, 98A, 19-30.

[247] Malgesini, B.; Verpilio, I.; Duncan, R.; Ferruti, P., Macromol. Biosci., 2003, 3, 59-66.

[248] Ferruti, P.; Ranucci, E.; Bianchi, S.; Falciola, L.; Mussini, P., R.; Rossi, M., J. Polym. Sci. Part A: Polym. Chem., 2006, 44, 2316-2327.

Owing to its preformed polymer cross-linker, it appears to be particularly convenient for preparing double network hydrogels with different PAA.[249]

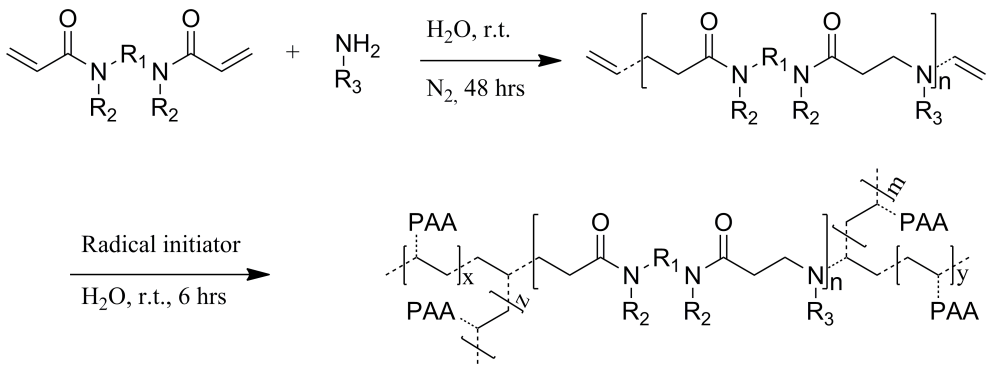

Scheme 1.3.4 B. Synthesis of PAA hydrogels via radical post-polymerization of doubly vinily-terminated PAA.

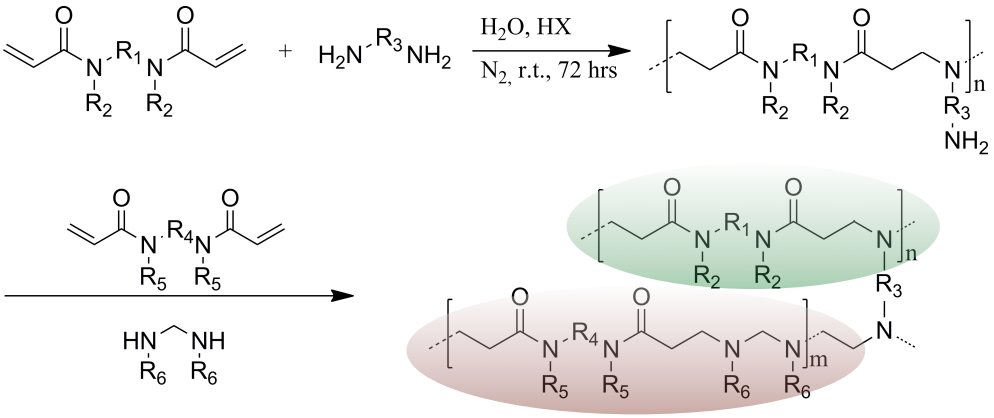

Scheme 1.3.4 C Synthesis of double network PAA hydrogels through insertion of primary amines as pendants: two different PAA networks (one in green and the other in red) occur.

The way in which PAA hydrogels are made affects their physico-chemical performance, such as swelling, degradability, and mechanical strength. Mostly, degradation tests mimicking physiological conditions have shown that PAA degrade at rate dependent on the cross-linking degree, and their degradation product proved completely non-toxic.[250] Furthermore, PAA hydrogels obtained by radical cross-linking degrade more slowly than those synthesized with the other methods, in view of their less amount of water content.

The swelling behavior of PAA hydrogels has been widely described in literature, since it is a key parameter to foresee the biocompatibility of biomaterials.[251]

---

[249] Ferruti, P.; Ranucci, E.; Bianchi, S.; Falciola, L.; Mussini, P., R.; Rossi, M., J. Polym. Sci. Part A: Polym. Chem., 2006, 44, 2316-2327.

[250] Ferruti, P.; Bianchi, S.; Ranucci, E.; Chiellini, F.; Piras, A., M., Biomacromolecules, 2005, 6 (4), 2229-2235.

[251] Magnaghi, V.; Conte, V.; Procacci, P.; Pivato, G.; Cortese, P.; Cavalli, E.; Pajardi, G.; Ranucci, E.; Fenili, F.; Manfredi, A.; Ferruti, P. J. Biomed. Mater. Res. Part A 2011, 98A, 19-30.

Indeed, higher swelling degree usually seems to be connected with higher biocompatibility, because ensure an efficient diffusion of small molecules (e.g., nutrients, metabolites, and degradation products) across the material. PAA hydrogels can be considered super-absorbent material, having the quality to absorb from 120 to 2000 percent of water (v/w). In addition, as role, their swelling degree increases with decreasing their cross-linking degree. Owing to their polyelectrolytic nature, their swelling degree can be influenced by several factors, such as: ionic strength, pH, and specific interaction with biomacromolecules. In particular, the swelling degree of deprotonated or protonated PAA hydrogels is higher than that their acid/base conjugate. As results of their high water content in the swollen state they have inadequate mechanical strength, conferring them a fragile consistency that needed to be improved.[252]

Overall, PAA hydrogels arisen from biocompatible PAAs are biocompatible and were tested as substrate for cell culturing and regenerative medicine.[253] It was found that, as a rule, amphoteric but prevailingly anionic PAA are scarcely adhesive, whereas several cationic or prevailingly cationic PAAs are adhesive towards different cell lines.[254] In particular, hydrogels deriving from an amphoteric but prevailingly cationic PAA, named AGMA1, were particularly considered in this respect. However, AGMA1 hydrogels were not eligible as conduits for peripheral nerve regeneration for the lack of mechanical strength. AGMA1 hydrogels of somewhat improved mechanical properties were obtained by radical post-polymerization of vinyl-terminated AGMA1 oligomers. Tubes of this material, implanted in mice, proved biocompatible and capable of inducing peripheral nerve regeneration.[252]

[252] **Magnaghi, V.; Conte, V.; Procacci, P.; Pivato, G.; Cortese, P.; Cavalli, E.; Pajardi, G.; Ranucci, E.; Fenili, F.; Manfredi, A.; Ferruti, P. J. Biomed. Mater. Res. Part A 2011, 98A, 19-30.**

[253] **Jacchetti, E.; Emilitri, E.; Rodighiero, S.; Indrieri, M.; Gianfelice, A.; Lenardi, C.; Podestà, A.; Ranucci, E.; Ferruti, P.; Milani, P., J. Nanobiotech., 2008, 6, 14.**

[254] **Ferruti, P.; Bianchi, S.; Ranucci, E.; Chiellini, F.; Piras, A., M., Biomacromolecules, 2005, 6 (4), 2229-2235.**

1.4 MALARIA AND ANTIMALARIAL DRUGS

Parasistic infections are of great significance because of the increasing incidence of infections in recent years, especially in the underdeveloped country. Among the parasistic infections, malaria represents the most prevalent and devastating human infection in the world.[255] Indeed, the global burden of the malaria, covered by the portfolio of the World Health Organization's Special Programme of Research and Training in Tropical Diseases, point out that there are 42,280 thousands of infections per year and 1,124 thousands of deaths per year in the world.[256] In 2010, malaria was endemic in 106 countries, 46 of which are in sub-Saharan Africa where the most highly pathogenic of the four malaria parasites (*P. falciparum)* that infect humans and the most effective malaria vector (*Anopheles gambiae*) are widespread.[257]

Malaria in humans can be caused by four species of protozoa of the genus of *Plasmodium: P. falciparum, P. malariae, P. vivax and P. ovale*.[258] The infection of P. *falciparum* is mostly liable for the deaths. Although malaria may be passed though blood transfusion, the principal way to transfer this parasite is the bite of the infected female mosquito of the genus of *Anopheles*. The life cycle of the *Plasmodium* is depicted in Figure 1.4 A.

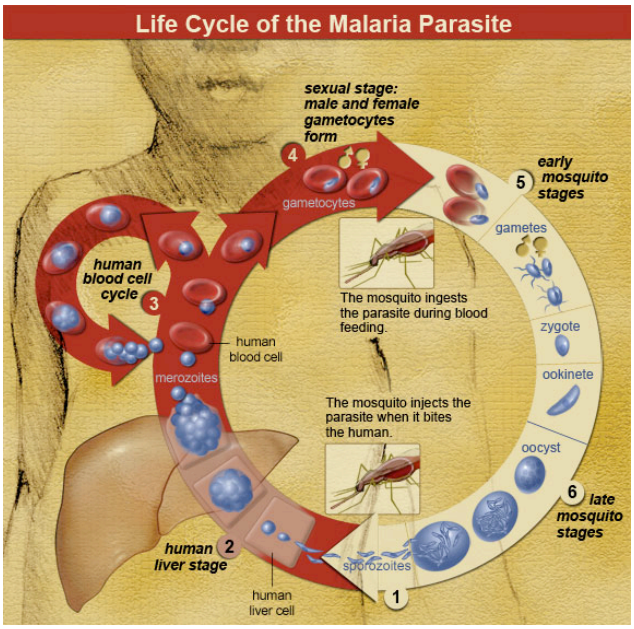

Figure 1.4 A. Illustration of the life cycle of malaria parasite (image from the reference[259]).

[255] Worl Malaria Report, WHO Press, Geneva, 2011.

[256] Stephenson, L., S.; Latham, M., C.; Ottesen, E., A., Parasitology, 2000, 121, S23-S38.

[257] The Africa Malaria Report, WHO Press, Geneva, 2003.

[258] Gardner, M., J.; Hall, N.; Fung, E.; White, O.; Berriman, M.; Hyman, R., W.; Carlton, J., M.; Pain, A.; Nelson, K., E.; Bowman, S.; Paulsen, I., T.; et al., Nature, 2002, 419, 498-511.

[259] NIAID, http://www.niaid.nih.gov/topics/malaria/pages/lifecycle.aspx

In this illustration can be seen that the pathogenic parasite is activated in the liver, affording to merozoites which start and hold the erythrocytic cycle. This enables them to provide erytrolyses and finally the death of the whole organism.

There are many drugs that show an antimalarial activity towards *Plasmodium* at different step of its life-cycle. The pharmacological activity of the most important examples is reported in Table 1.4 A, in which can be noticed that:

- there is not a drug able to perform antisporozoites activity, thus entailing that it may not prevent the infection.
- no drug shows a pharmacological activity upon all hepatic and erythrocytic forms of the parasite.

Table 1.4 A. Activity of the antimalarial drugs: the molecules are classified on the basis of the type of parasite stage that they kill.

	Sporozoite	**Liver Stages**		**Erythrocytic Stages**	
Class I		Schizont	Ipnozoite	Merozoite	Gametocyte
Chloroquine	-	-	-	+	+
Mefloquine	-	-	-	+	-
Quinine, Quinidine	-	-	-	+	+
Pyrimethamine	-	+	-	+	-
Sulphadoxine	-	+	-	+	-
Tetracicline	-	-	-	+	-
Class II					
Atovaquone	-	+	-	+	-
Proguanil	-	+	-	+	-
Class III					
Primaquine	-	+	+	-	+

Hence, a good therapy should be performed by using a combination of two or more antimalarial drugs in order to optimizing the therapeutic effect. Unfortunately, the burgeoning problem of resistance to hitherto effective antimalarial agents in the last decade has added urgency to the necessity to discover new drugs and to make better use of existing ones.[260] However the genome of *Plasmodium falfiparum* has recently been decoded,[258] providing novel drug targets that give researchers new insight into the resistance mechanism of parasite. These advantages have already

[260] **Edwards, G.; Krishna, S., Eur. J. Clin. Microbiol. Infect. Dis., 2004, 23, 233-242.**

afforded to fosfidomycin as novel antimalarial agent thai is now being developed rapidly[261], with more progress sure to follow.[262] Another possibility is to better formulate known drugs to improve their therapeutic index by applying pharmacokinetic and pharmacodynamic principles. Currently, the adopted treatment of malaria is based on administration of artemisinin-derivatives used alone or in combination with other drugs.[263] [264] Artemisinin is a lactone sesquiterpene extracted from *Artemisia Annua*, that is active against all species of *Plasmodium* at all sexual erythrocytic stages. Artemisinin and their derivatives do not bring cross-resistance phenomena, and in a paradox *Plasmodium* that exhibit resistance towards chloroquine can be more sensitive towards artemisinin.[263] Its derivative has a power of about 10-100 times higher than the other drugs and are active towards gametocytes, the sexual stages that are essential for transmission.[265] In spite of its powerful activity, due to its low oral bioavailability, artemisinin is hitherto replaced by its derivatives, including dihydroatemisinin, artesunate, artemether and arteether.[263] However, because of their high lipophilicity, poor water solubility and low stability in gastric medium, these drugs are available only as oily formulations for intramuscular injection, which need sterile dosage and qualified health workforce.[266] As the bioavailability of hydrophobic drugs is hardly improved when incapsulated in a core-shell system, lipid-based and block-copolymer-based micelles have been recently developed for the oral administration of poorly water-soluble antimalarial drugs.[267] [268] Further investigations should be focused upon the targeting of these antimalarial agent into *Plasmodium*-containing erythrocytes, thus avoiding the undesired side effects.

---

[261] Missinou, M., A.; Bormann, S.; Schindler, A.; Issifou, S.; Adegnika, A., A.; Matsiegui, P., B.; Binder, R.; Lell, B.; Wiesner, J.; Baranek, T.; Jomaa, H.; Kremsner, P., G., Lancet, 2002, 360, 1941-1942.

[262] Ridley, R., G., Nature, 2002, 415, 686-693.

[263] Goodman and Gilman's, Brunton, L., L. eds, The Pharmacological Basis of Therapeutis, 2006, p 1020-1024.

[264] Guidelines for the Treatment of Malaria, WHO Press, Geneva, 2010.

[265] White, N., J., Qinghaosu (Artemisininin): the Price of Success, Science, 2008, 320, 330-334.

[266] Drew, M., G.; Metcalfe, M., J.; Dascombe, F., M.; J. Med. Chem., 2006, 49, 6065-6073.

[267] Memvanga, P., B.; Prèat, V., Eur. J. Pharm. Biopharm., 2012, doi/10.1016/j.ejpb.2012.05.004.

[268] Bhadra, D.; Bhadra, S.; Jain, N., K., J. Pharm. Pharmaceut. Sci., 2005, 8(3), 467-482.

CHAPTER 2

AIM OF THE WORK

2.1 HETERO-DIFUNCTIONAL DIMERS AS BUILDING BLOCKS FOR THE SYNTHESIS OF POLYAMIDOAMINES WITH HETERO-DIFUNCTIONAL CHAIN TERMINALS

Though the traditional synthesis of PAAs paved the way for the development of PAAs with interesting biological activities, it has a serious limitations. In order to obtain high-molecular weight products the functions involved in the reaction, that are, activated double bonds and amine hydrogens, must be stoichiometrically balanced. However, reacting mixture will contain at least three kinds of macromolecules, a-.. .. -a, b-.. .. -b, and a-.. .. -b in 1:1:2 ratio. Hence, there is no way, by the traditional method, to straightforwardly obtain PAAs with controlled hetero-difunctional chain terminals, that is, PAAs solely containing molecules of a-.. .. -b type. This precluded to PAAs the access to the remarkable number of biotechnological applications, for instance liposomes preparation, controlled drug conjugation, and protein modification, which have been so far nearly uniquely mastered by hetero-difunctional PEGs that, however, are far to be endowed with the functional versatility of PAAs. Two strategies exits, in principle, for unequivocally synthesizing hetero-diterminated PAAs, either the ring-opening polymerization of cyclic precursors or the self-polymerization of hetero-difunctional a-a-b-b or a-a-b dimers (HDDs). The first strategy was ruled out because it was thought difficult to design a cyclic PAA precursor amenable to thermal or catalytic ring-opening polymerization, especially in the case of purpose-tailored PAAs carrying reactive side-substituents, as for instance carboxyl groups, liable to interfere in these processes. Therefore, the preparation of HDDs, in particular those of the a-a-b-b type, expected to polymerize according to Scheme 2.1 A, was preferred. We focalized our investigation to these HDDs because the procedure adopted in this investigation was not easily applicable to the preparation of the a-a-b ones.

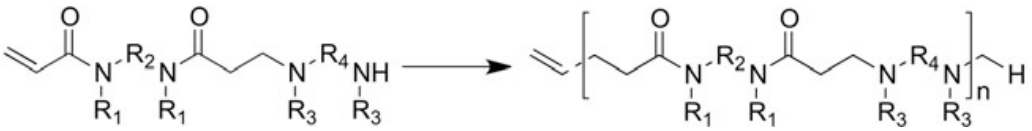

Scheme 2.1 A. Self-polymerization of the a-a-b-b type HDDs.

The synthetic scope of HDDs is manifold. They can be polymerized to high-molecular weight PAAs without bothering with stoichiometric balance. PAAs of controlled average molecular weight and mono-functionalized with an acrylamide or a sec-amine group at one end chain can be prepared by adding, respectively, a controlled amount of mono-functional acrylamides or se-amines, wheras the

addition of multifunctional acrylamides or amines will lead to star-like PAAs. Block PAA-PAA or PAA-PEG copolymers with controlled structure will be easily obtained. “Velvety-like” grafting of PAA chains to properly functionalized surface can be achieved. PAA chains of controlled average length can be grafted to proteins with non risk of undesirable side reactions such as protein-protein coupling or crosslinking. “Tadpole-like” conjugate with hydrophobic moieties forming in aqueous media “liposomes” or core-shell polimeric nanomicelles can be prepared as functional drug carriers. Based on this premise, the aim of this work is to report on the preparation of some model HDDs corresponding to PAAs extensively studied for biomedical applications and to provide selected factual examples of their synthetic potential.

2.2 HYPERBRANCHED POLYAMIDOAMINES FOR THE SYNTHESIS OF HIGH-PERFORMANCE BIOMATERIALS

PAA-based nano-sized systems have been widely studied for using in biological and biomedical field. For instance, PAAs have been found to be able to complex and transport gene, siRNA, and proteins into different cytotypes, enabling specific delivery of many biocative macromolecules at subcellular level.[1] [2] Furthermore, PAAs containing hydrophobic moiety as side pendant have proved capable to form nanoparticles with hydrophobic core able to solublise and consequently release several hydrophobic drugs.[3] Up to now, only linear PAAs have been considered for these purposes, although highly branched macromolecules have proved to be more effective due to the smaller size, more compact shape, and high concentration of terminal groups in their surface.[4] In addition, they generally exhibit much lower solution viscosity compared with linear polymers of the same molar mass, a characteristic that may help facilitate all technological and manufacturing and medical processes, including the administration. To our knowledge, no clear reports on branched or hyper-branched PAAs have been published so far, while plenty of information are available on the structurally related (but not identical) PAMAM polymers, prepared by self-polycondensation of 2-aminoethylacrylamide hydrochloride that, being an "AB_2" type monomer, automatically gives rise to hyperbranched structures. [5] On the other hand, hydrogels consisting of cross-linked PAAs are well known and have been studied either as scaffolds for tissue engineering or as heavy metal ions absorbing resins.[6] [7] The easiest way for preparing crosslinked PAAs is to partially or totally substitute in their polymerization recipes amines bearing three or more reactive hydrogen atoms for the primary monoamines or the secondary bis-amines normally employed as monomers. Theoretical considerations led us to suppose that by properly adjusting the reaction conditions and particularly the monomers' stoichiometric ratio, branched soluble PAAs could be obtained in the same way. A set of experiments was performed to substantiate this assumption. The aim of this work is to report on the results obtained.

---

[1] Richardson, S., C., W.; Pattrick, N., G.; Stella Man, Y., K.; Ferruti, P.; Duncan, R., Biomacromolecules, 2001, 2 (3), 1023-1028.

[2] Ferruti, P.; Franchini, J.; Bencini, M.; Ranucci, E., Biomacromolecules, 2007, 8, 1498-1504.

[3] Ranucci, E.; Ferruti, P.; Suardi, M. ,A.; Manfredi, A., Macromol. Rapid Commun., 2007, 28, 1243-1250.

[4] Peleshanko, S.; Tsukruk, V., V., Prog. Polym. Sci., 2008, 33, 523-580.

[5] Tomalia, D., A.; Naylor, A. M.; Goddard, W., A., Angew Chem., 1990, 29, 119-157.

[6] Ferruti, P.; Bianchi, S.; Ranucci, E., Biomacromolecules, 2005, 6, 2229-2235.

[7] Ferruti, P.; Ranucci, E.; Bianchi, S.; Falciola, L.; Mussini, P., R.; Rossi, M., J. Polym. Sci.: Part A: Polym. Chem., 44, 2316-2327.

2.3 POLYAMIDOAMINE-BASED MULTILAYER NANOPARTICLES AS POTENTIAL GENE AND PROTEIN DELIVERY SYSTEMS

Synthetic polymers are receiving increasing attention as drug and gene delivery vehicles as rational design makes it possible to modify the polymer properties, and thereby to optimize the structure-activity relationships to induce a desired pharmokinetic profile. A common mechanism to engineer structures is to use electrostatics, and one can envisage a situation where multilayer vehicles are prepared from synthetic, positively and negatively charged polymers that also incorporate electrostatically negatively charged biological macromolecules such as DNA or RNA.[8] Delivery of the cargo is effected when such nanoparticles disassemble inside the cell as a result of pH changes, and the DNA is then able to be transported to the nucleus.[9] Due to the versatility of layer-by-layer techniques, a range of structurally diverse nanoparticles with wide potential application in the field of gene and protein delivery is accessible from a small number of components. Further tailoring of the outermost layer allows for specific intracellular up-take and, potentially, more control from the delivery profile point of view, since interaction with a specific cytotype or an appropriate biodistribution profile can be achieved by modifying the surface of nanoparticles with peptides, antibodies and lipids;[10] Zhang et al have made lipid-based polyplexes to alter, through hydrophobic tails, the delivery properties of the system,[11] a surface modification that reduces the interaction of the nanoparticles with various serum proteins that would otherwise cause aggregation or degradation of the particles, thereby improving delivery; Kim et al have modified polyethylenimine (PEI) to produce non-toxic interpolyelectolyte complexes for use as a carrier for siRNA.[12] PEGylation of the surfaces of nanoparticles can confer stealth-like behavior of the nanoparticles due to decreasing interaction with plasma proteins and reticulo-endothelial system (RES). Whilst such approaches have had some success, these polymers are not totally biodegradable or exhibit cytotoxicity in-vivo that has hindered practical application.[13] By contrast, PAAs are degradable and biocompatible synthetic polyelectrolytes. Therefore, the encapsulation of drugs, proteins or genetic material in multilayer PAA-based nanoparticles can efficiently provide a method for assembling gene/protein delivery systems with appropriate biodistribution characteristics and biocompatibility. Recently, we showed that the

[8] **Shmueli RB, Anderson DG, Green JJ, Expert Opin. Drug Deliv., 2010, 7(4), 535-550.**

[9] **Reibetanz U, Claus C, Typlt E et al., Macromol. Biosci., 2006, 6(2), 153–60.**

[10] **Brannon-Peppas L, Blanchette JO, Adv. Drug Deliv. Rev., 2004, 56 (11), 1649-59.**

[11] **Zhang S, Zhao B, Jiang H, et al., J. Control Release, 2007, 123(1), 1-10.**

[12] **NaJung K, Dahai J, Jacobi AM, et al., Int. J. Pharm., 2012, 427(1), 123-133.**

[13] **Hu-Lin J, Seong-Ho H, You-Kyoung K, et al., Int. J. Pharm., 2011, 420(2), 256-265.**

degree of ionization of each ionic group is only weakly dependent on the ionization state of the entire PAA molecule and thus, the charge distribution of the polymer can be engineered through an appropriate choice of monomer,[14] enabling a more facile and modular approach to nanoparticle design. Taking that insight as a reference for current study, the aim of this work was to investigate the feasibility of PAA-based multilayer nanoparticles prepared using layer-by-layer approaches as gene or protein delivery systems, focusing on four possible combinations of biocompatible PAAs. Experimentally, the focus has been the charge, size and localized dynamics of each particular layer within the nanoparticle assembly, against a background of an acceptable cytotoxicity profile.

[14] **Ranucci E, Ferruti P, Lattanzio E, et al., J. Polym. Sci. Pt. A-Polym. Chem. 47(24), 6977-6991, (2009).**

2.4 ISA23-BSA CONJUGATE AS ANTIMALARIAL DELIVERY SYSTEMS

Malaria is one of the main medical concerns worldwide because of the numbers of people affected, the severity of the disease, and the complexity of the life cycle of its causative agent, the protozoan Plasmodium. The arsenal of strategies deployed to hinder this infection has included chemotherapy by using combination of drugs and vaccination approaches, none of them being capable yet of claiming victory.[15] The emergence of drug resistance severely limits the arsenal of available drugs against protozoal pathogens.[16] The development of resistance is favored in any situation in which parasites are exposed to a low level of antimalarial drug, for instance where a full course of treatment is not completed, or where long-acting drugs are administered, which are eliminated slowly from the body. With the advent of nanomedicine, renewed hopes have appeared of finally obtaining the magic bullet against malaria. Novel delivery formulations are likely to optimize the therapeutic efficacy of antimalarials. In particular, targeted nanovectors, such as liposomes, solid-lipid nanoparticles, nano-/microemulsions and polymer-based nanocarriers have been receiving special attention in order to minimize the side effects of drug therapy and achieve the intake of doses sufficiently low to be innocuous for the patient but locally high enough to be lethal for the malaria parasite.[17] [18] The aim of this work was to design a prototype nanovector for the targeted delivery of antimalarial drugs exclusively to P. falciparum-infected red blood cells (pRBC), and capable of reaching the preclinical pipeline in the short term. Preliminary targeting analysis by fluorescence-assisted cell sorting (FACS) indicated that fluorescein-labeled ISA23 has an almost complete target specificity towards pRBC. Furthermore, in vitro experiments demonstrated that ionic complexes of ISA23 with primaquine significantly increased its activity. In the light of this, highly water-soluble ISA23/albumin graft-copolymers, sharing the stealth-like properties of ISA23 and the drug binding ability of the albumin core, have been developed. Overall, the binding ability and the antimalarial activity were explored in order to assemble a Troyan horse “nanocapsule” targeting pRBC with complete specificity of delivering its antimalarial cargo inside these cells, and of eliminating detectable parasitemia both in P. falciparum cultures and in malaria-infected mice.

---

[15] P.L. Alonso, Malaria, Int. Microbiol. 2006, 9, 83-93.

[16] N.S. Santos-Magalhães, V.C. Mosqueira, Adv. Drug Deliv. Rev. 2010, 62, 560-75.

[17] P. Murambiwaa, B. Masola, T. Govender, S. Mukaratirwa, C.T. Musabayane, "Anti-malarial drug formulations and novel delivery systems: A review", Acta Tropica, 2011, 118, 71-79; (b) Humanitarian Practice Network (HPN): http://www.odihpn.org/humanitarian-exchange-magazine/issue-31/malaria-in-emergencies-treatment-diagnosis-and-vulnerable-groups.

[18] M. Enserink, Science 2010, 328, 844-846.

2.5 POLYAMIDOAMINE HYDROGELS AS SCAFFOLDS FOR IN VITRO CULTURING OF PERIPHERAL NERVOUS SYSTEM CELLS

Hydrogels can be considered an attractive alternative to rigid hydrophobic materials for the production of conduits for nerve regeneration, since they are biomimetic because of their high water content.

PAAs are synthetic water soluble polymers, and most of them are endowed with physico-chemical and biological properties making them appealing as biomaterials. Cross-linked PAAs can be obtained by using as cross-linking agents multifunctional amines, affording to hydrogel which absorb large amounts of water. In addition, PAA hydrogels arisen from biocompatible linear PAAs are usually biocompatible and biodegradable to non-toxic products. Although several PAA hydrogels were tested as substrate for cell culturing and conduits for peripheral nerve regeneration, actually, neither of them display suitable characteristics for achieving nerve regeneration in vivo owing to their scarce mechanical strength.[19] In view of clinical applications, this work deal with the evaluation of two families of PAA hydrogels, prepared by polyaddition of piperazine and 1,2-diaminoethane as cross-linking agent with N,N'-methylenebisacrylamide or 1,4-bisacryloylpiperazine, as scaffolds for Schwann cells (SC) and dorsal root ganglia (DRG) neuron culturing.

The aim was to obtain new hydrogel materials combinig mechanical properties with ability to promote SC and DRG cell adhesion and/or proliferation, to be used as tubular conduits for *in vivo* peripheral nerve regeneration. The rationale was to capitalize on the structure-forming ability of these PAAs as linear polymers, which might be maintained, to some extent, in the cross-linked form.

[19] Magnaghi, V.; Conte, V.; Procacci, P.; Pivato, G.; Cortese, P.; Cavalli, E.; Pajardi, G.; Ranucci, E.; Fenili, F.; Manfredi, A.; Ferruti, P., J. Biomed. Mater. Res. Part A 2011, 98A, 19-30.

CHAPTER 3

MATERIALS AND METHODS

3.1 MATERIALS

2,2-Bis(acrylamido)acetic acid (BAC) and 1,4-bis(acryloyl)piperazine (BP) were synthesized as previously described.[1] [2] Lithium hydroxide monohydrate (98%), piperazine hexahydrate (P) (99%), 1,4,8,11-tetrazacyclotetradecane (Cyclam) (98%), di-(tert-butyl)dicarbonate (97%), thiocholesterol (TC), bovine serum albumin (BSA) (96%), 4-acryloylmorpholine (97%), morpholine (99.5%), guanidine hydrochloride (98%), glacial acetic acid, hydrochloric acid (37%), sodium hydroxide (98.5%), sodium chloride (99%), dichloromethane (reagent grade), trifluoroacetic acid, DOWEX MAC-3 ion exchange resin, deuterium oxide (99.9 atom % D), N,N'.methylenebisacrylamide (MBA) (99%), PBS, chlorotrimethylsilane (98%), ethanol (95%), 4-amino-TEMPO (TEMPO) (98%), N,N'-bis(2-hydroxyethyl)ethylenediamine (HEEDA) (98%), potassium hydroxide (99%) sodium dodecyl sulphate (SDS) (98%) and 1-amino-4-guanidinobutane sulphate salt (Agmatine) (97%), tris(hydroxymethyl)aminomethane (tris) (99%), chloroquine bisphosphate (98%), primaquine bisphosphate (98%), fluorescein 5-isothiocyanate (FITC) were purchased from Sigma-Aldrich and used as received. 1,2-diaminoethane (ethylenediamine) (99%) and 1,4-diaminobuthane was purcheased from Fluka and purified just before use by distillation. Piperazine anhydrous (99%), 2-(R, S)-methylpiperazine (MP) (95%), and *trans*-2,5-dimethylpiperazine (98%) were purcheased from Sigma-Aldrich and purified before use by sublimation.

ISA1, ISA23, AGMA1, BACEDDA were synthesized as previously described,[3] [4] their salient features are reported in Table 3.2.3 B.

---

[1] Ferruti, P.; Ranucci, E.; Trotta, F.; Gianasi, E.; Evagorou, G.; Wasil, M.; Wilson, G.; Duncan, R., Macromol. Chem. Phys., 1999, 200, 1644-1654.

[2] Ferruti, P., Macromol. Synth., 1985, 9, 25-29.

[3] Ranucci, E.; Ferruti, P.; Lattanzio, E.; Manfredi, A.; Rossi, M.; Mussini, P.; Chiellini, F.; Bartoli, C., J. Polym. Sci.: Part A: Polym. Chem., 2009, 47, 6977-6991.

[4] Richardson, S.; Ferruti, P.; Duncan, R., J. Drug Targeting, 1999, 6 (6), 391-404.

3.2 METHODS

Nuclear Magnetic Resonance (NMR) Spectra. ^{1}H NMR, ^{13}C NMR, distortionless enhanced by polarization transfer (DEPT), ^{1}H- ^{1}H correlation (COSY), heteronuclear multiple bond correlation (HMBC), and heteronuclear correlation (HETCOR) spectra were run at room temperature on a Bruker Advance 400 spectrometer operating at 400.132 and 100.623 MKz, respectively.

Electron Paramagnetic Resonance (EPR) Spectra. EPR spectra were recorded using a cw-Bruker EMX spectrometer (BrukerBiospin, UK) fitted with a high-sensitivity cavity (ER 4119HS) operating at X-band frequencies (9.5 GHz) at room temperature,with 100 kHz field modulation and 10mW microwave power.

Size Exclusion Chromatography (SEC). SEC traces were obtained using a Knauer Pump 1000 equipped with a Knauer Autosampler 3800, TKSgel G4000 PW and G3000 PW TosoHaas columns connected in series, using a light scattering (LS)/viscosimeter Viscotek 270 Dual Detector, coupled to a refractive index detector (Waters model 2410). The mobile phase was a 0.1 M Tris buffer (pH 8.0 ± 0.05) with 0.2 M sodium chloride. The sample concentration was 2% (w/v) and the flow rate 1 mL/min Triple detector SEC allowed determining, besides the molecular weight, the long chain branching (LCB) frequency of star-like PAAs by means of the dedicated Viskotech software, which compared their Mark-Houwink plots with those of samples of their linear counterparts of approximately the same molecular weight and used common Zimm-Stockmayer equation and methods.[5]

Dynamic Light Scattering (DLS). DLS analysis was performed to evaluate the hydrodynamic diameter of polymeric micelles and self-assembled nanoparticles using a Malvern NanoZS instrument (Malvern Instruments, Worcesterchire, UK) with a laser fitted at 532 nm and fixed 173° scattering angle.

[5] **Zimm, B.; Stockmayer, W., H., J. Chem. Phys., 1949, 17, 1301-1314.**

3.2.1 HETERO-DIFUNCTIONAL DIMERS AS BUILDING BLOCKS FOR THE SYNTHESYS OF POLYAMIDOAMINES WITH HETERO-DIFUNCTIONAL CHAIN TERMINALS

Synthesis of 4-N-Boc-2-(R, S)-methylpiperazine (MP-Boc). Typically, 2-(R,S)-methylpiperazine (MP) (21.1 g, 0.200 mol) was dissolved in tap water (1.2 L) and glacial acetic acid (12.0 g, 0.197 mol) was added. The mixture was gently stirred for 15 minutes then cooled to 0 °C. After this time, a solution of di-(tert-butyl)dicarbonate (34.9 g, 0.160 mol) in methanol (150 mL) was added dropwise in 30 minutes to the reactive mixture. During this time the reaction was vigorously stirred and the temperature gradually warmed up to room temperature. The reaction was maintained under this condition for further 20 minutes, then the precipitated formed filtered and the pH was adjusted to 5.5 with 1M HCl. The aqueous phase was extracted with CH_2Cl_2 (2x100 mL) to separate the disubstituted derivative then the pH was adjusted to 9.5 with 1M NaOH. The desired product was recovered by repeated extraction with CH_2Cl_2 (5x200 mL), the organic layers collected and dried over anhydrous sodium sulphate. The solvent was evaporated to afford the crude solid. Yield: 90 %.

^{1}H NMR ($CDCl_3$, δ, ppm): 0.99 (d, $HNCH_2CHC\mathbf{H_3}$), 1.41 (s, $(C\mathbf{H_3})_3C$), 1.57 (br, $N\mathbf{H}CH_2CH$), 2.34 (br, axial $NHC\mathbf{H}_2CH$), 2.64 (m, $NHCH_2C\mathbf{H}$), 2.72 (m, axial $NHCH_2C\mathbf{H}_2NBoc$), 2.90 (m, equatorial $NHC\mathbf{H}_2CH$), 2.95 (br, equatorial $NHC\mathbf{H_2}C\mathbf{H}_2N$). ^{13}C NMR ($D_2O$, δ, ppm): 19.16 ($\mathbf{C}H_3CH$), 28.15 ($(\mathbf{C}H_3)_3CO$), 45.71 ($HN\mathbf{C}H_2\mathbf{C}H_2N$, $CH_3CH\mathbf{C}H_2N$), 51.65 ($CH_3\mathbf{C}H$), 79.51 ($(CH_3)_3\mathbf{C}O$), 154.70 ($N\mathbf{C}O$). Anal. Calcd for: $C_{10}H_{20}N_2O_2$: C, 59.97; H, 10.07; N, 13.99. Found: C, 59.12; H, 10.13; N, 13.75.

Synthesis of N-Boc-Piperazine (P-Boc). P-Boc was synthesized following the same procedure above described for MP-Boc using piperazine hexahydrate (25.0 g, 0.129 mol), glacial acetic acid (7.6 g, 0.127 mol), di-(*tert*-butyl)dicarbonate (23.2 g, 0.103 mol) and tap water (1.2 L). Yield: 87%.

^{1}H NMR ($CDCl_3$, δ, ppm): 1.47 (s, $(C\mathbf{H_3})_3C$), 1.82 (br, $N\mathbf{H}CH_2CH_2NBoc$), 2.81 (m, $HNC\mathbf{H_2}CH_2NBoc$), 3.40 (m, $NHCH_2C\mathbf{H_2}NBoc$). ^{13}C NMR (D_2O, δ, ppm): 28.97 ($(\mathbf{C}H_3)_3CO$), 45.21 ($HN\mathbf{C}H_2\mathbf{C}H_2N$), 79.52 ($(CH_3)_3\mathbf{C}O$), 154.84 ($N\mathbf{C}O$). Anal. Calcd for: $C_9H_{18}N_2O_2$: C, 58.04; H, 9.74; N, 15.04. Found: C, 56.12; H, 10.78; N, 14.46.

Synthesis of BAC-P. To a vigorously stirred solution of *N*-Boc-piperazine (1.3200 g, 7.042 mmol) in bidistilled water (15 mL) cooled at 0 °C, a solution of 2,2-bis(acrylamido)acetic acid (BAC) (2.8000 g, 14.084 mmol) and $LiOH{\cdot}H_2O$ (0.5963 g, 14.084 mmol) in bidistilled water (30 mL) was added dropwise. The reaction was maintained at 0 °C and left under stirring for 2 days. After this

period, the crude reaction mixture was purified by ionic exchange chromatography on Dowex Mac-3 (8x60 cm) using bidistilled water (500 mL), and then an acid concentration elution gradient passing from 10^{-4} M to 0.1 M hydrochloric acid (1000 mL total). The product obtained was freeze-dried then dissolved in trifluoroacetic acid to obtain a 1 M solution maintained for 3 hours under gentle stirring in nitrogen atmosphere. The product was precipitated by addition of diethyl ether (10 mL), washed with fresh solvent (3 x 10 mL) and dried under vacuum affording a white and deliquescent solid. Yield: 55%.

The full NMR characterization (D_2O) is reported in Table 3.2.1 A. Anal. Calcd for: $C_{12}H_{20}N_4O_4$: C, 50.69; H, 7.09; N, 19.71. Found: C, 49.46; H, 7.31; N, 18.83.

Synthesis of BAC-MP. The reaction and purification of BAC-MP were carried out as previously described for BAC-P using BAC (2.8000 g, 14.084 mmol), $LiOH \cdot H_2O$ (0.5963 g, 14.084 mmol) and 4-*N*-Boc-2-methylpiperazine (1.4100 g, 7.042 mmol) as reagents. Yield: 60%.

The full NMR characterization (D_2O) is reported in Table 3.2.1 A. Anal. Calcd for: $C_{13}H_{22}N_4O_4$: C, 52.34; H, 7.43; N, 18.78. Found: C, 50.47; H, 7.62; N, 17.89.

Synthesis of MBA-P. To a solution of MBA (4.7438 g, 30.77 mmol) in bidistilled water (220 mL) a solution of *N*-Boc-piperazine (1.9297 g, 10.46 mmol) in bidistilled water (50 mL) was added dropwise under stirring at 0 °C. The reaction was maintained at 0 °C for 48 hours and monitored by TLC using 2-propanol/water/0.15 M acetate buffer pH 5.5 = 2:2:6 ($^v/_v$) as eluant. During this time a precipitate was formed that was filtered off and the solution acidified at pH 3.0 using 1 M hydrochloric acid. Unreacted MBA was successfully eliminated by repeated extraction with diethyl ether (5x100 mL) and ethyl acetate (2x150 mL). The aqueous solution was treated with 5 % hydrochloric acid (4.6 mL) and stirred for 24 hours. The mixture was then freeze dried and the product obtained as a white solid. Yield: 70%.

The full NMR characterization (D_2O) is reported in Table 3.2.1 A. Anal. Calcd for: $C_{11}H_{20}N_4O_2$: C, 54.98; H, 8.39; N, 23.32. Found: C, 49.98; H, 8.83; N, 21.14.

Table 3.2.1 A. Full NMR characterization (D_2O, δ) of all HDDs.

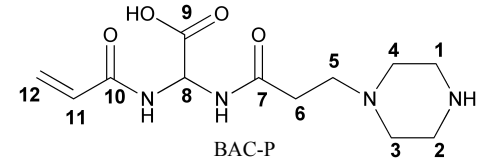

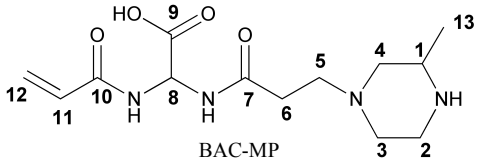

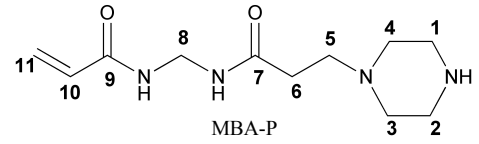

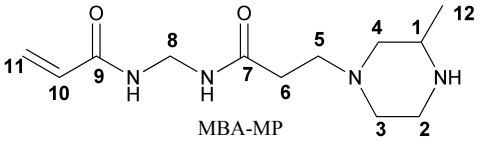

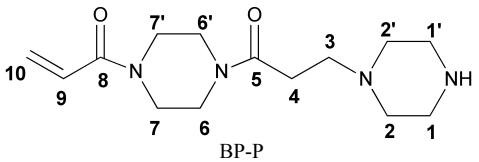

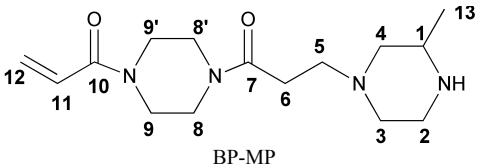

		1	2	3	4	5	6	7	8	9	10	11	12	13
BAC-P	^{1}H	3.49	3.49	3.49	3.49	3.49	2.74		5.73			5.68	6.13	
	^{13}C	48.56	48.56	52.62	52.62	41.39	28.81	170.79	56.61	168.15	170.79	128.75	129.10	
BAC-MP	^{1}H	3.24	3.40[a] 3.78[b]	3.40	3.63	3.63	2.81		5.78			6.21	5.75	1.43
	^{13}C	57.38	46.43	49.00	48.14	40.30	29.23	170.75	57.41	168.40	170.75	129.74	129.53	13.97
MBA-P	^{1}H	3.58	3.58	3.58	3.58	3.47	2.73		4.58		5.71	6.14		
	^{13}C	45.7	45.7	49.89	49.89	42.09	29.22	171.68	53.60	171.68	128.42	129.75		
MBA-MP	^{1}H	3.19	3.38[a] 3.71[b]	3.38	3.60	3.38	2.72		4.60		5.74	6.19	1.40	
	^{13}C	58.12	46.23	48.94	48.15	40.29	29.17	171.79	53.58	171.79	128.45	129.56	13.85	
BP-P	^{1}H	3.61	3.61	3.61	3.01	-	3.61	3.61	-	5.79	6.14[c] 6.67[d]			
	^{13}C	48.95	53.11	44.53	27.42	169.73	40.70	41.33	169.73	127.35	129.02			
BP-MP	^{1}H	3.87	3.44[a] 3.77[b]	3.42	3.77	3.56	2.98		3.58	3.65		5.75	6.08[c] 6.64[d]	1.47
	^{13}C	56.76	45.26	47.83	45.06	44.85	27.59	169.64	40.04	41.37	169.64	127.23	128.97	13.49

[a] equatorial, [b] axial, [c] cis, [d] trans

Synthesis of MBA-MP, BP-P, BP-MP. The same procedure above described for MBA-P was followed.

MBA-MP

The full NMR characterization (D_2O) is reported in Table 3.2.1 A. Anal. Anal. Calcd for $C_{12}H_{22}N_4O_2$: C, 56.67; H, 8.72; N, 22.03. Found C, 51.92; H, 9.11; N, 19.74.

BP-P

The full NMR characterization (D_2O) is reported in Table 3.2.1 A. Anal. Anal. Calcd for $C_{14}H_{24}N_4O_2$: C, 59.98; H, 8.63; N, 19.98. Found: C, 59.43; H, 8.73; N, 19.59.

BP-MP

The full NMR characterization (D_2O) is reported in Table 3.2.1 A. Anal. Anal. Calcd for $C_{15}H_{26}N_4O_2$: C, 61.20; H, 8.90; N, 19.03. Found: C, 61.25; H, 9.02; N, 18.98.

Synthesis of BAC-MP Homopolymer (ISA23). To a solution of BAC-MP (0.4 g, 1.3408 mmol) in bidistilled water (450 μL) 1 M NaOH was added dropwise until pH 9 and the reaction kept under stirring at room temperature for 5 days in nitrogen atmosphere After this period the mixture was acidified to pH 4.4-5.5 with 37% HCl, filtered through a paper filter then ultrafiltered through a membrane with nominal cut-off of 3000. The product was obtained after freeze-drying as a yellowish solid. Yield: 79%.

*M*n = 38000, *M*w = 50000, *M*w/ *M*n = 1.32, *R*h = 7.4 nm, [η] = 0.567 dL/g, *a* = 0.773, log*K* = -3.855. ^{1}H NMR (D_2O, δ, ppm): 1.26 (d, C**H$_3$**CH), 2.64 (m, C**H$_2$**CONH), 2.85 (m, C**H**CH_3), 3.07 (br, NC**H$_2$** MP ring), 3.28 (br, equatorial NC**H$_2$**CH_2 MP ring), 3.28 (br, axial NC**H$_2$**CH_2N MP ring, NC**H$_2$**CH_2), 5.51, 5.45 (ds, C**H**COOH and C**H**COO^-).

Synthesis of BP-P Homopolymer. The reaction was carried out as above reported, starting from BP-P (0.7200 g, 5.569 mmol) dissolved in bidistilled water (1.4 mL). After 5 days under gentle stirring the mixture was acidified with concentrated HCl, filtered through a paper filter then ultrafiltered through a membrane with nominal cut-off of 3000. The pure product was recovered after freeze-drying. Yield: 72.5 %.

*M*n = 30900, *M*w = 38000, *M*w/ *M*n = 1.13, *R*h = 3.808 nm, [η] = 0.294 dL/g, *a* = 1.01, log*K* = -4.703. ^{1}H NMR (D_2O, δ, ppm): 2.58 (br, C**H$_2$**CONH), 3.06 (s, NC**H$_2$** piperazine ring), 3.12 (m, NC**H$_2$**CH_2), 3.31 (br, C**H$_2$**NCO piperazine ring), 3.38 (br, C**H$_2$**NCO piperazine ring).

Synthesis of BAC-MP-Acryloylmofpholine Conjugate. Acryloylmorpholine (4.4 mg, 0.035 mmol) was dissolved in 0.1 M sodium hydroxide (150 μL) and BAC-MP (100.0 mg, 0.335 mmol) was added under vigorous stirring until a clear solution was obtained. Then 1 M NaOH was dropped into the reaction mixture until pH 8.5 was reached, and the reaction was kept 3 days at room temperature under nitrogen atmosphere. After this time the mixture was acidified at pH 5 by the addition of 1 M HCl. The final product was obtained after freeze drying. Yield: 97%.

*M*n = 3200, *M*w = 4100, *M*w/ *M*n = 1.28, *R*h = 6.8 nm, [η] = 0.234 dL/g, *a* = 0.781, log*K* = -3.74. ^{1}H NMR (D_2O) is reported in Table 3.2.1 B.

Table 3.2.1 B. ^{1}H NMR chemical shifts (δ) of BAC-MP-AM conjugate, star-like BAC-MP-Cyclam (BAC-MP-Cy), star-like BP-MP-Cyclam (BP-MP-Cy) in D_2O.

BAC-MP-AM

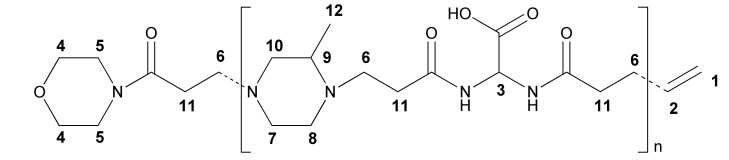

BAC-MP-Cy

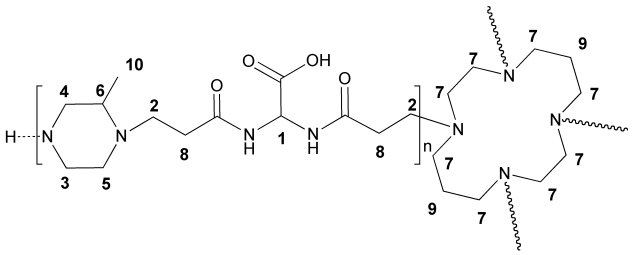

BP-MP-Cy

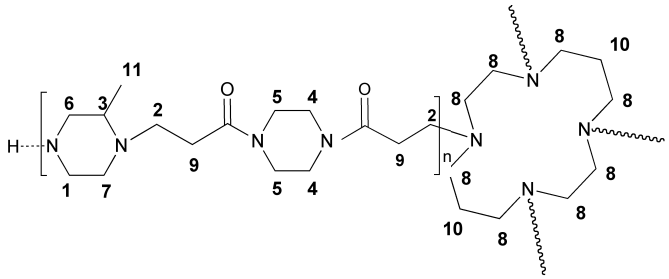

#		1	2	3	4	5	6/7	8	9	10	11
BP-MP-Cy	^{1}H	3.87 [a]; 3.48 [b]	3.79	3.68	3.63	3.57	3.48	3.05	2.99	1.85	1.48; 1.38
#		1	2	3	4/5/6	7	8	9	10		
BAC-MP-Cy	^{1}H	5.65	3.78	3.78[a]; 3.44[b]	3.44	3.16	2.82	1.96	1.45; 1.38		
#		1	2	3	4	5/6	7/8/9/10	11	12		
BAC-MP-AM	^{1}H	6.22	5.77	5.62; 5.56	4.05	3.62	3.20	2.75	1.39		

[a] equatorial, [b] axial

Synthesis of Star-like BAC-MP. To a solution of cyclam (2.0 mg, 0.001 mmol) in 0.5 M NaOH (150 μL), BAC-MP (100.0 mg, 0.335 mmol) was added and the reaction left 5 days at pH 8 under gentle stirring. After this time the mixture was freeze-dried and the dry product recovered. Yield: 98%.

*M*n = 10800, *M*w = 11660, *M*w/ *M*n = 1.08, [η] = 0.125 dL/g, *a* = 0.607, log*K* = -3.706, branching frequency = 2.17. . ^{1}H NMR (D_2O) is reported in Table 3.2.1 B.

Synthesis of Star-like BP-MP. The same procedure above described was followed using cyclam (20.4 mg, 0.102 mmol), 0.5 M sodium hydroxide (550 μL) and BP-MP (300.0 mg, 1.020 mmol). The reaction was filtered through a paper filter and the crude product freeze-dried. Yield: 97%.

*M*n = 3300, *M*w = 3900, *M*w/ *M*n = 1.21, [η] = 0.128 dL/g, *a* = 0.521, log*K* = -3.823, branching frequency = 2.08. . ^{1}H NMR (D_2O) is reported in Table 3.2.1 B.

Synthesis of BAC-P-grafted-BSA. Guanidine hydrochloride (0.5056 g, 5.190 mmol) was dissolved in bidistilled water (5 mL), BSA (1.5065 g, 0.023 mmol) was added and the mixture was vigorously stirred for 10 minutes until a clear solution was obtained. BAC-P (0.3190 g, 1.122 mmol) was then added to the mixture and the pH was adjusted at 8.0 by the addition of solid Na_2CO_3. The reaction was kept under nitrogen atmosphere and gentle stirring for 5 days. The mixture was purified by dialysis against water (membrane cut-off 50000) and the pure product collected after freeze-drying. Yield: 72%.

*M*n = 1,01,000, *M*w/ *M*n = 1.07, *R*h = 6.1 nm, [η] = 0.203 dL/g, *a* = 0.203, log*K* = -2.74.

Synthesis of BAC-MP-grafted-BSA. The reaction was carried out following the same procedure described for BAC-P-grafted-BSA using guanidine hydrochloride (0.5056 mg, 5.190 mmol), BSA (1.5065 g, 0.023 mmol), BAC-MP (0.3347 g, 1.122 mmol). The pure product was obtain after the usual ultrafiltration procedure and freeze drying. Yield: 84%.

*M*n = 84,900, *M*w/ *M*n = 1.17, *R*h = 4.11 nm, [η] = 0.053 dL/g, *a* = 0.265, log*K* = -2.58.

Synthesis of BP-P-grafted-BSA. The same procedure as in the previous case was followed using guanidine hydrochloride (0.5056 mg, 5.190 mmol), BSA (1.5065 g, 0.023 mmol), BP-P (0.3146 mg, 1.122 mmol). The usual work-up afforded the pure product. Yield: 79%.

*M*n = 88,100, *M*w/ *M*n = 1.14, *R*h = 5.90 nm, [η] = 0.083 dL/g, *a* = 0.163, log*K* = -2.04.

Synthesis of Hetero-difunctional BAC-MP-TC. To a solution of BAC-MP (103.3 mg, 0.251 mmol) in bidistilled water (1 mL), thiocholesterol (TC) (10.1 mg, 0.025 mmol) dissolved in diethyl ether (0.1 mL) was added and the formation of a macroemulsion was observed. The pH was adjusted to 7.0 by the addition of 3 M NaOH and the mixture vigorously stirred for 2 days. Then, 1 M NaOH was added until pH 9 and the reaction maintained in this condition under stirring for further 5 days. After this time, the mixture was acidified to pH 5 by the addition of 1 M HCl and purified by dialysis against water (membrane cut-off 3500) for 2 hours. The crude product collected after freeze drying was suspended in diethyl ether (2 mL) to remove unreacted thiocholesterol, and dried in vacuum. Yield: 38%.

Anal. Calcd for $(C_{13}H_{22}N_4O_4)_{10}$-$(C_{27}H_{46}S)$: C, 55.69; H, 7.92, N, 16.55. Found: C, 51.98; H, 8.46, N, 18.15.

Synthesis of Hetero-difunctional MBA-P-TC. The reaction was carried out following the same procedure as in the previous case using MBA-P (60.3 mg, 0.251 mmol) and TC (10.1 mg, 0.025 mmol). Yield: 29%.

Anal. Calcd for $(C_{11}H_{20}N_4O_2)_{10}$-$(C_{27}H_{46}S)$: C, 58.64; H, 8.84; N, 19.97. Found: C, 58.00; H, 8.76; N, 20.56.

Synthesis of Hetero-difunctional BP-P-TC. The reaction was carried out following the same procedure as in the case of ISA23-TC using: BP-P (70.4 mg, 0.251 mmol) and TC (10.1 mg, 0.025 mmol). Yield: 44%.

Anal. Calcd for $(C_{14}H_{24}N_4O_2)_{10}$-$(C_{27}H_{46}S)$: C, 62.56; H,8.99; N, 17.48. Found: C, 61.42 ; H, 8.83; N, 18.60.

Synthesis of Hetero-difunctional BP-MP-TC. The reaction was carried out following the same procedure as in the case of ISA23-TC using: BP-MP (73.9 mg, 0.251 mmol) and TC (10.1 mg, 0.025 mmol). Yield: 36%.

Anal. Calcd for $(C_{15}H_{26}N_4O_2)_{10}$-$(C_{27}H_{46}S)$: C, 63.53; H, 9.21; N,16.74. Found: C, 62.75; H, 9.11; N, 17.50.

Dynamic Light Scattering (DLS). DLS analysis was performed to evaluate the hydrodynamic diameter of polymeric micelles using a Malvern NanoZS instrument (Malvern Instruments, Worcesterchire, UK) with a laser fitted at 532 nm and fixed 173° scattering angle. DLS measurements were carried out on two sets of experiments. In the first, samples were prepared in phosphate buffer solution (PBS) saline in the concentration range of 0.1-1 mg/ml and measurements were performed at fixed temperature (25 °C). In the second one, the sample was prepared in PBS saline with concentration of 1 mg/ml, and the measures were performed varying the temperature: 20, 25, 30, 35, 40, 45, 50, 55, and 60 °C. Before each analysis, the samples were filtered though a syringe filter (5 μm pore size; Watmann, UK) to remove the dust. All data were evaluated as numeral distribution of the hydrodynamic diameter.

Transmission Electron Microscopy (TEM). TEM analysis of self-assembled polymeric BAC-MP-TC micelles was captured using the negative staining technique. A solution of BAC-MP-TC (1 mg/ml) in ultrapure water at pH 7.4 was prepared; then a 5 μl aliquot was deposited onto a Formvar-coated Cu grid (400 Mesh). After adsorption, the grid was stained with 1% uranyl acetate solution (5 μl), wiped away by means of a paper filter and died at room temperature. Observation was made

by using a LEO 912 AB energy-filtering transmission electron microscopy (EFTEM; Carl Zeizz, Obercochen, Germany) operating at 80 kV. Digital images were collected by Proscan 1K slow-scan charge-coupled device camera (Proscan Scheuting, Germany).

3.2.2 HYPERBRANCHED POLYAMIDOAMINES FOR THE SYNTHESIS OF HIGH-PERFORMANCE BIOMATERIAL

Polymerization: General procedure.

BAC series (reaction 1.1 from Table 3.2.2 A as model of synthesis). BAC (555.8 mg , 2.6250 mmol, purity 93.6%) was dissolved in 1.00 mL deoxygenated doubly distilled water under nitrogen atmosphere in the presence of lithium hydroxide (63.5 mg, 2.6250 mmol). The amines (EDA,22.8 mg, 0.3750 mmol ; and P, 254.2 mg, 3.0000 mmol) were then added at once all together and the mixture gently stirred until homogeneous and maintained at 20°C under nitrogen for 7 days with intermittent stirring. After this time, the reaction mixture was acidified to pH ≅ 4 (1M HCl). The product, if soluble, was purified by dissolving in water and ultrafiltering through a membrane with nominal cut-off 1000. It was finally recovered by freeze-drying and the yield determined. Characterizations were performed on the final product. In the case of gel formation, the gel time was estimated and the polymerization was then allowed to proceed as described. The final product, after acidification, was thoroughly extracted with water, dried, and the yield determined. The soluble extracts, if any, were not further characterized. The exact amounts of all reagents for each preparation are reported in Table 3.2.2 A and Table 3.2.2 B.

Table 3.2.2 A. Amount of reagent for the system based on 2,2'-bisacrylamidoacetic acid and ethylenediamine.[a)]

N°	BAC (Mol x 10^{-3})	EDA (Mol x 10^{-3})	P (Molx 10^{-3})	M (Mol x 10^{-3})
1.1	2.6250	0.3750	3.0000	-
1.2	2.4975	0.3750	3.0000	-
1.3	3.1875	0.3750	3.0000	-
1.4	1.6665	0.2500	2.0000	-
1.5	4.9342	0.3750	3.0000	-
1.6	5.1370	0.3750	3.0000	-
1.7	5.6222	0.3750	3.0000	-
1.8	3.9280	0.4550	3.0000	2.0000
1.9	3.5000	1.3333	3.0000	-
1.10	3.3333	1.3333	3.0000	-
1.11	4.2500	1.3333	3.0000	-
1.12	5.0000	0.8889	2.0000	-
1.13	4.8000	1.3333	3.0000	2.0000

[a)] BAC= 2,2'-bisacrylamidoacetic acid, EDA=ethylenediamine, P=piperazine, M=morpholine.

Table 3.2.2 B. Amount of reagent for the system based on 2,2'-bisacrylamidoacetic acid and cyclam as multifunctional monomer.[a)]

N°	BAC (Mol x 10^{-3})	Cy (Mol x 10^{-3})	P (Mol x 10^{-3})	M (Mol x 10^{-3})
3.1	2.6250	0.3750	3.0000	-
3.2	2.4975	0.3750	3.0000	-
3.3	3.1875	0.3750	3.0000	-
3.4	1.5630	0.1250	1.0000	-
3.5	3.3000	0.1250	1.0000	-
3.6	3.3000	0.1250	1.0000	-
3.7	3.9280	0.4550	3.0000	2.0000

[a)] BAC= 2,2'-bisacrylamidoacetic acid, Cy=cyclam, P=piperazine, M=morpholine.

BP series (reaction 2.1 from Table 3.2.2 C as model of synthesis). BP (509.8 mg, 2.6250 mmol) was dissolved in 0.9 mL deoxygenated doubly distilled water under nitrogen atmosphere. The amines (EDA,22.8 mg, 0.3750 mmol ; and P, 254.2 mg, 3.0000 mmol) were then added at once all together, and the mixture gently stirred until homogeneous and maintained at 20°C under nitrogen for 4 days with intermittent stirring. After this time, the reaction mixture was acidified to pH ≅ 4 (1M HCl), diluted and ultrafiltered through a membrane with nominal cut-off 1000. The product was finally recovered by freeze-drying and characterized. In the case of gel formation the same procedure as in the previous case was followed. The exact amounts of all reagents for each preparation are reported in Table 3.2.2 C.

Table 3.2.2 C. Amount of reagent for the system based on bisacryloylpiperazine and ethylenediamine as multifunctional monomer.[a)]

N°	BP (Mol x 10^{-3})	EDA (Mol x 10^{-3})	P (Mol x 10^{-3})	M (Mol x 10^{-3})
2.1	2.6250	0.3750	3.0000	-
2.2	2.4975	0.3750	3.0000	-
2.3	3.1875	0.3750	3.0000	-
2.4	1.6665	0.2500	2.0000	-
2.5	4.9342	0.3750	3.0000	-
2.6	5.1370	0.3750	3.0000	-
2.7	5.6222	0.3750	3.0000	2.0000
2.8	3.9280	0.4550	3.0000	2.0000
2.9	3.5000	1.3333	3.0000	-
2.10	3.3333	1.3333	3.0000	-
2.11	4.2500	1.3333	3.0000	-
2.12	5.0000	0.8889	2.0000	-
2.13	4.8000	1.3333	3.0000	2.0000

[a)] BP=bisacryloylpiperazine, EDA=ethylenediamine, P=piperazine, M=morpholine.

3.2.3 POLYAMIDOAMINE-BASED MULTILAYER NANOPARTICLES AS POTENTIAL GENE AND PROTEIN DELIVERY SYSTEM

Synthesis of Spin-labelled PAA (ISA1-TEMPO of Table 3.2.3 A). 1,4-bis(acryloyl)piperazine (4.000 g, 20.5952 mmol) was dissolved in water (6.6 mL) by gently stirring. TEMPO (0.3634 g, 2.0595 mmol), MP (0.9771 g, 9.2678 mmol) and HEEDA (1.4161 g, 9.2678 mmol) were then added together and the mixture maintained 3 days at room temperature under nitrogen with occasional stirring. After this time, it was diluted with distilled water (50 mL), acidified to pH 4-4.5 with dilute hydrochloric acid and then ultrafiltered through a membrane with nominal molecular weight cut-off 10000. The retained fraction was freeze-dried and the product obtained as a white powder. Yield: 65%. The other spin-labelled polymers were obtained using stoichiometric ratio indicated in Table 3.2.3 A. The molecular weight of the polymers are reported in Table 3.2.3 B, including the polymers without labelling.

Table 3.2.3 A. Reagent used in the synthesis of spin-labelled PAAs.

Reagent	ISA1-TEMPO	ISA23-TEMPO	AGMA1-TEMPO
Water / mL	6.60	6.60	6.60
BAC / mmol	-	20.08	20.08
BISPIP / mmol	20.60	-	-
2-MP / mmol	9.27	18.07	-
HEEDA / mmol	9.27	-	-
TEMPO / mmol	2.06	2.00	2.00
LiOH / mmol	-	20.08	38.16
Agmatine / mmol	-	-	18.08

Table 3.2.3 B. Molecular weight of the PAAs used for self-assembly experiments.

Sample	M_n	M_w	PD
ISA1	21400	26000	1.21
ISA1-TEMPO	12000	16000	1.30
ISA23	25000	28600	1.15
ISA23-TEMPO	13700	19300	1.40
AGMA1	18400	24100	1.31
AGMA1-TEMPO	21800	25900	1.18
BACEDDA	22500	26300	1.17

Core Preparation. Polymeric nanoparticles, with all possible binary combinations of cationic and predominantly anionic PAAs, were prepared from polymer solutions at pH 7.4 (Table 3.2.3 C).

Table 3.2.3 C. Pairs of polymers used for obtainig nano-sized cores with or without spin-labelled probe.

Name	Cationic polymer	Anionic Polymer
NP1	ISA1	ISA23
NP2	ISA1	BACEDDA
NP3	AGMA1	ISA23
NP4	AGMA1	BACEDDA

Briefly, stock solutions of polymers (1 mg/mL) were prepared by dissolving the polymer in water, and then adjusting the pH to 7.4 using potassium hydroxide 2M. In order to prepare the polymeric core, the required amount of cationic polymer solution was transferredto a vial, and the anionic polymer solution added under vigorous stirring. Each pair of polymers was prepared using the cationic/anionic charge ratio (c/a) within a range 1:1 to 10:1. The charge/repeating unit of the polymers at pH 7.4 are reported in Table 3.2.3 D.

Table 3.2.3 D. Equivalent charge per mol of the PAAs at pH 7.4.

Sample	Cationic (charge/mol)	Anionic (charge/mol)
ISA1	1.020	-
AGMA1	0.529	-
ISA23	-	0.333
BACEDDA	-	1.979

Multilayer Nanoparticle Preparation. Typically, multilayer nanoparticles were prepared following the same simple procedure, namely adding oppositely charged polymers, layer-by-layer, by sequential addition of the appropriate polymer solution. All nanoparticles were prepared starting witha core obtained using the procedure describedabove with c/a ratio of 1:5. After core formation, cationic or anionic polymer was added step-by-step, waiting 5 minutes for each layer formation, to obtain nanoparticles with 6 layers.

Measurement of Core and Multilayer Stability Using DLS and Z-potential analysis. Dynamic light scattering measurements were carried out at 20° C, on a Malvern Zetasizerwith wavelength 488 nm. A scattering angle of 90° was chosen. Before analysis, the nanoparticlesolutions, at a fixed concentration of 1 mg/mL, were filtered througha 5-micron pore size syringe filter (Whatman, UK). The

intensity autocorrelation function analysed by the method of cumulantswas used to obtain the average diffusion coefficient and polydispersity of the nanoparticles, and thus, the hydrodynamic diameter via the Stoke-Einstein equation. ζ-potential analyses were carried out using the same instrument. To determine the ζ-potential samples were diluted with 0.1 mMKCl and placed in an electrophoretic cell, where an electric field was applied for 2 minutes. Each sample was analysed in triplicate, and the average mobility reported here.

Preparation of Multilayer Nanoparticles for EPR Studies. TEMPO spin-labelled nanoparticles with 4 layers were obtained in an analogous manner, except that the spin-labelled polymer was incorporated into the nanoparticles in only one layer at a time, to obtain three different labelled nanoparticles, specifically, where the label resides in the core and in the first and third layer, Table 3.2.3 E.

Table 3.2.3 E. Spin-labelled multilayer (4 layer) nanoparticles obtained at pH 7.4 labelled in the core (NP1{n=1}), (NP2 {n=1}), (NP3{n=1}), in the first (NP1{n=2}), (NP2 {n=2}), (NP3{n=2}) and in the third (NP1{n=4}), (NP2 {n=4}), (NP3{n=4}).

Sample	ISA1	AGMA1	ISA23	BACEDDA
NP1{n=1}	+	-	(+)	-
NP1{n=2}	+	-	(+)	-
NP1{n=4}	+	-	(+)	-
NP2{n=1}	(+)	-	-	+
NP2{n=2}	(+)	-	-	+
NP2{n=4}	(+)	-	-	+
NP3{n=1}	-	(+)	+	-
NP3{n=2]	-	(+)	+	-
NP3{n=4}	-	(+)	+	-
NP4{n=1}	-	(+)	-	+
NP4{n=2}	-	(+)	-	+
NP4{n=4}	-	(+)	-	+

The spin-labelled probe is reported in parentheses.

Preparation of Multilayer Nanoparticles for Toxicological Studies. The nanoparticles reported in Table 3.2.3 C were also prepared without spin-labelled polymers as previously described for assessment in the toxicology studies.

Preparation of Lypopolyplexes for EPR Studies. 200 mg of SDS was dissolved in water to make 100 mL of solution (2 mg/mL). This stock solution was used to make solutions with decreasing concentration of SDS by serial dilution. 1 mL of these SDS solutions was added to 1 mL of spin-labelled nanoparticles, as previously prepared and labelled in the third layer (n=4), in order to pre-

pare lipopolyplexes with SDS concentrations of 0.05 and 1 mg/mL. The mixture was subjected to vigorous stirring for 15 minutes.

Investigation of PAA Mobility in Multilayer Nanoparticles. For each nanoparticle, the EPR analysis was carried out in triplicate and the spectra analysed in terms of the rotational correlation time (τ_r) of the TEMPO label, and the polarity that the probe senses. The EPR spectra of the TEMPO-labelled PAA nanoparticles were compared with pure spin-labelled polymers in water at pH 7.4, and the same polymer species in SDS solutions.

Analysis of the spectra, in terms of τ_r,were carried out using the well-known equation,[6]

$$\tau_r = 6.5 \times 10^{-10} \Delta H_o \left(\sqrt{\frac{H_o}{H_{-1}}} - 1 \right) \qquad \text{(eq. 1)}$$

where ΔH_0 is the linewidth of the central peak and H_0 and H_{-1} are the intensities of the central and high field peak respectively. These values were evaluated by the instrument software (WinEPR, Bruker) in order to calculate the rotational correlation time (τ_r) and the hyperfine coupling constant (polarity) sensed by the probe. This type of analysis can be used for weakly and mildly immobilized spin-labels, as they are in our case ($10^{-10}<\tau_r<10^{-9}$). Small changes in peak intensity arising due to slight changes in instrument gain were removed by normalising each spectrum to the maximum peak intensity in each spectrum. The τ_r sensed by a spin-labelled ISA1-TEMPO, AGMA1-TEMPO or ISA23-TEMPO can also be quantified by analysing its EPR spectrum. Changes on that environment induced by molecular interactions are accordingly easily detected.

Evaluation of In-vitro Toxicity. An assessment of toxicity was performed in vitro as previously described.[7] Briefly, the nanoparticles described herein, were reconstituted in DMEM cell culture media to a final concentration of 5mg/mL. Sterile flat bottomed 96-well plates were seeded with Vero and B16 cells, respectively, at a cell density of $1x10^4$ cells per well and incubated for 16 h at 37°C in an atmosphere of 5% (v/v) CO_2. Cells were exposed to the nanoparticles using a final concentration range of 0.5-5 mg/mL. After incubation for 68 hours (37°C; 5% (v/v) CO_2), cell viability was assessed using the 3-(4,5-dimethylthiazol-2-yl)- 2,5-diphenyltetrazolium bromide (MTT) assay. MTT solution was added (5µL of a sterile 5mg/mL MTT in PBS) and incubated for a further 4 hours (total incubation of 72h), during which time the yellow tetrazolium dye was converted to an

[6] Griffiths P., C.; Paul, A., Heenan, R., K.; et al., J. Phys. Chem. B, 2004, 108 (12), 3810-3816.

[7] Richardson, S., C., W.; Ferruti, P.; et al., J. Drug Target., 1999, 6 (6), 391-404.

insoluble blue formazan salt. The cell culture media was removed and formazan salt crystals were dissolved in DMSO (100µL/well). Plates were evaluated spectrophotometrically by measuring absorbance at 550nm and the results compared to a negative control (dextran (D1662, Sigma, Dorset UK); concentration range 0.5-5mg/mL) and positive control (poly(ethyleneimine) (PEI) (181978 Sigma, Dorset, UK); concentration range 0.5-5mg/mL) respectively. Results were recorded as percentage viability measured against an untreated population of cells and expressed as a mean (±S.E.M.). IC_{50} values were calculated using the Prism software package by Graphpad Software Inc., (La Jolla, CA, USA).

3.2.4 ISA23-BSA CONJUGATE AS ANTIMALARIAL DELIVERY SYSTEMS

Synthesis of 4-N-Boc-2-(R, S)-methylpiperazine (MP-Boc). Typically, 2-(R,S)-methylpiperazine (MP) (21.1 g, 0.200 mol) was dissolved in tap water (1.2 L) and glacial acetic acid (12.0 g, 0.197 mol) was added. The mixture was gently stirred for 15 minutes then cooled to 0 °C. After this time, a solution of di-(tert-butyl)dicarbonate (34.9 g, 0.160 mol) in methanol (150 mL) was added drop-wise in 30 minutes to the reactive mixture. During this time the reaction was vigorously stirred and the temperature gradually warmed up to room temperature. The reaction was maintained under this condition for further 20 minutes, then the precipitated formed filtered and the pH was adjusted to 5.5 with 1M HCl. The aqueous phase was extracted with CH_2Cl_2 (2x100 mL) to separate the disub-stituted derivative then the pH was adjusted to 9.5 with 1M NaOH. The desired product was recov-ered by repeated extraction with CH_2Cl_2 (5x200 mL), the organic layers collected and dried over anhydrous sodium sulphate. The solvent was evaporated to afford the crude solid. Yield: 90 %.

^{1}H NMR ($CDCl_3$, δ, ppm): 0.99 (d, $HNCH_2CHC\mathbf{H_3}$), 1.41 (s, $(C\mathbf{H_3})_3C$), 1.57 (br, $N\mathbf{H}CH_2CH$), 2.34 (br, axial $NHC\mathbf{H}_2CH$), 2.64 (m, $NHCH_2C\mathbf{H}$), 2.72 (m, axial $NHCH_2C\mathbf{H}_2NBoc$), 2.90 (m, equatorial $NHC\mathbf{H}_2CH$), 2.95 (br, equatorial $NHC\mathbf{H_2}C\mathbf{H}_2N$). ^{13}C NMR ($D_2O$, δ, ppm): 19.16 ($\mathbf{C}H_3CH$), 28.15 ($(\mathbf{C}H_3)_3CO$), 45.71 ($HN\mathbf{C}H_2\mathbf{C}H_2N$, $CH_3CH\mathbf{C}H_2N$), 51.65 ($CH_3\mathbf{C}H$), 79.51 ($(CH_3)_3\mathbf{C}O$), 154.70 ($N\mathbf{C}O$). Anal. Calcd for: $C_{10}H_{20}N_2O_2$: C, 59.97; H, 10.07; N, 13.99. Found: C, 59.12; H, 10.13; N, 13.75.

Synthesis of BAC-MP. To a vigorously stirred solution of 2,2-bis(acrylamido)acetic acid (BAC) (2.8000 g, 14.084 mmol) and $LiOH{\cdot}H_2O$ (0.5963 g, 14.084 mmol) in bidistilled water (30 mL) cooled at 0 °C, a solution of *N*-Boc-piperazine (1.4100 g, 7.042 mmol) in bidistilled water (15 mL) was added dropwise. The reaction was maintained at 0 °C and left under stirring for 2 days. After this period, the crude reaction mixture was purified by ionic exchange chromatography on Dowex Mac-3 (8x60 cm) using bidistilled water (500 mL), and then an acid concentration elution gradient passing from 10^{-4} M to 0.1 M hydrochloric acid (1000 mL total). The product obtained was freeze-dried then dissolved in trifluoroacetic acid to obtain a 1 M solution maintained for 3 hours under gentle stirring in nitrogen atmosphere. The product was precipitated by addition of diethyl ether (10 mL), washed with fresh solvent (3 x 10 mL) and dried under vacuum affording a white and deli-quescent solid. Yield: 60%.

The full NMR characterization (D_2O) was already reported in Table 2.2.1 A. Anal. Calcd for: $C_{13}H_{22}N_4O_4$: C, 52.34; H, 7.43; N, 18.78. Found: C, 50.47; H, 7.62; N, 17.89.

Synthesis of BAC-MP-grafted-BSA (ISA23-BSA conjugate). Guanidine hydrochloride (0.5056 g, 5.190 mmol) was dissolved in bidistilled water (5 mL), BSA (1.5065 g, 0.023 mmol) was added and the mixture was vigorously stirred for 10 minutes until a clear solution was obtained. BAC-MP (0.3347 g, 1.122 mmol) was then added to the mixture and the pH was adjusted at 8.0 by the addition of solid Na_2CO_3. The reaction was kept under nitrogen atmosphere and gentle stirring for 5 days. The mixture was purified by dialysis against water (membrane cut-off 50000) and the pure product collected after freeze-drying. Yield: 84%.

Mn = 1,01,000, Mw/ Mn = 1.07, Rh = 6.1 nm, [η] = 0.203 dL/g, a = 0.203, log$K$ = -2.74.

Synthesis of FITC-labelled BAC-MP-grafted-BSA (ISA23-BSA-FITC). ISA23-BSA conjugate previously synthesized (100 mg) was solubilized in bidistilled water (2 ml), and the pH was adjusted to 8.0 by using 2 M sodium carbonate. To this mixture FITC (1 mg) were added under stirring and the reaction was maintained under nitrogen atmosphere for 48 h and occasionally stirred. After this time, it was diluted with bidistilled water (4 ml), acidied with hydrochloric acid to pH 6.5 and then ultrafiltered though a membrane with nominal cut-off 50,000. The fraction retained was finally freeze-dried and the product collected as a yellow powder. Yield 98 %.

Equilibrium dialysis test. Equilibrium dialysis was performed using Teflon dialysis chamber with standard membrane (millipore). Experiments were carried out in triplicate using 1 ml of the PBS containing chroloquine (CQ) or primaquine (PQ) against 1 ml of PBS containing ISA23-BSA conjugate (30 mg/ml). Equilibrium time was determined spectrophotometrically for the two drugs using 200 ng/ml of CQ and 100 ng/ml of PQ and was found to be 4 h. Thereby, dialysis was carried out for 5 h in all experiments and at 25 °C. The binding of CQ and PQ was determinated within the range of 25-600 ng/ml. CQ and PQ were quantified by HPLC analysis.[8] Protein binding was calculated using the formula $(C_c\text{-}C_t)/C_c$ x 100, where C_c is drug concentration in the compartment containing the conjugate and C_t the concentration in PBS after dialysis.

Preparation of the ISA23-BSA/Chloroquine formulation (ISA23-BSA/CQ). The ISA23-BSA conjugate previously synthesized (300 mg) was dissolved in PBS (300 ml), and then chloroquine diphosphate (60 mg) was added into the mixture with vigorous stirring. The mixture was filtered through a syringe filter with pore size of 0.2 μm, freeze-dried and recovered as a yellowish solid.

[8] **Alvàn, G.; Ekman, L.; Lindstrom, B., J. Chromatogr., 1982, 229, 242-247.**

Preparation of the ISA23-BSA/Primaquine (ISA23-BSA/PQ) Formulation. This formulation was prepared using the same procedure previously reported for the formulation of ISA23-BSA/CQ.

Cryo-Transmission Electron Microscopy (Cryo-TEM). The cryo-TEM of ISA23-BSA conjugate was prepared by punge-freezing. Briefly, a lacey carbon filmed grid was placed in a pair of weezers at the end of a road in a controlled-atmosphere box. One drop of the particle-containing solution (1 mg/ml) was applied on the grid and most of the liquid was removed by a paper filter to leave a thin layer covering the holes. The rod was then shot vertically to plunge the grid into a liquid ethane bath cooled down to -180 °C. The grid was then transferred to a cryo-holder (Oxford CT-3500) cooled with liquid nitrogen below 180 °C. Microscopy was performed using a Philips CM120 BioTWIN transmission electron microscope operated at 120 kV, which was equipped with an objective lens to enhance contrast.

Hemolysis Assays. RBCs were diluted in PBS to yield a solution with 3% hematocrit. 200 µl of RBCs from this suspension and 2 µl of each ISA23-BSA solution were added to a 96-well plate. After incubating for 3h, 6h, and 24h at 37 °C, samples were collected in eppendorf tubes, spun at 16,000 g per min, and the supernatant absorbance was measured spectrophotometrically at 541 nm. Each assay was performed in triplicate, including positive (1% Triton X-100 from Sigma Aldrich) and negative (PBS) controls.

Cytotoxicity Assays. Cytotoxicity assays were performed using 3T3 and HUVEC cells . 5,000 cells/well were plated in 96-well plates and after 24h at 37 °C in 5% CO_2 the medium was substituted by 100 µl of ISA23-BSA solution obtained using culture medium without FBS, and incubation was resumed for 48h. 10 µl of 4-[3-(4-iodophenyl)2-(4-nitrophenyl)- 2H-5-tetrazolio]-1,3-benzene disulfonate labeling reagent (WST-1 Sigma Aldrich) was added to each well, and the plate was incubated in the same condition for 3 h. After thoroughly mixing for 1 min on a shaker, the absorbance of the sample was measured at 400 nm using a Benchmark Plus microplete reader. WST-1 in the absence of cells was used as blank and were prepared in triplicate for each experiments.

Immunofluorescence Assays. ISA23-BSA-FITC solutions at concentration of 0.2 and 0.5 mg/ml were obtained in PBS and filtered through a syringe filter with pore size of 0.2 µm. Then polymer solutions were incubated with 3D7 *P. falciparum* infected Red Blood Cells (pRBCs) for 90 min at 37 °C with gentle stirring. Parasite nuclei were stained with 4'-6-diamino2-

phenylindole (DAPI by Sigma Aldrich) and the RBC membrane was labelled with wheat germ agglutinin (WGA)-tetramethylrhodamine conjugate (Sigma Aldrich). Samples were imaged with a Leica TCS SP5 laser scanning confocal microscope.

Flow Cytometry (FACS). P. falciparum cells (pRBCs) cultures at a parasitemia of 5% (*5,000 cells per test tube)* were incubated in a test tube with 100 µl of ISA23-BSA-FITC (0.5 mg/ml) for 90 min at 37 °C with gentle stirring. Parasite nuclei were stained with Hoetch reagent (Sigma Aldrich), and then samples were analyzed using a Gallios multi-color flow cytometry instrument.

Plasmodium Falciparum Growth Inhibition Assay. Parasitemia of *P. falciparum* 3D7 cultures was adjusted to 1.5% with more than 90% of parasites at ring stage after sorbitol synchronization. 100 µl of this culture was plated in 96-well plates and incubated for 48 h at 37 °C, under a gas mixture of 92% N_2, 5% CO_2, and 3% O_2, in the presence of ISA23-BSA/PQ or ISA23-BSA/CQ solutions at different concentration. Parasitemia was determined after incubation by microscopic counting of blood smears, or by fluorescence-assisted cell sorting (FACS). The ratio of infected versus non-infected RBCs was also determied by microscopic analysis. The average of Plasmodium growth inhibition with free drug or drug formulation was expressed as percentage of reduction respective to the parasitemia of controls.

In vivo Toxicity of ISA23-BSA conjugate. ISA23-BSA conjugate was diluted in PBS in order to obtain a solution at concentration of 0.5 mg/ml. This solution was injected in tail's mice to yield a dose within 10-200 mg/Kg. Each dose was tested on three mouse with different weight. The acute toxicity was evaluated as percentage of death caused after polymer administration.

In vivo Antimalarial Activity of ISA23-BSA/PQ. The *in vivo* antimalarial activity of ISA23-BSA/PQ formulation was evaluated by comparison with plane primaquine using the 4-days suppressive test. Biefly, $2x10^5$ RBCs from the rodent malaria parasite *Plasmodium yoelii yoelii* 17XL (PyL) MRA-267 were inoculated in mice by intraperitoneal injection (i.p.). Two therapeutic regimen were chosen to establish the dose-dependence. In the first group, three mouse were treated with a dose equivalent to 12.5 mg/Kg of primaquine, whereas in the second one a dose of 6.25 mg/Kg was applied. The chemotherapy treatment started 2 h later (day 0) by an i.p. injection of formulation solution in PBS followed by identical dose of primaquine for the following 3 days. The negative and positive control groups received saline and the same dose of plane primaquine bisphosfate in PBS

respectively. Parasitemia was monitored daily by microscopic examination of Wright's-stained thin-blood smears.

3.2.5 POLYAMIDOAMINE HYDROGELS AS SCAFFOLDS FOR IN VITRO CULTURING OF PERIPHERAL NERVOUS SYSTEM CELLS

Linear PAAs from N-N'-methylenebisacrylamide and Piperazine (MBA-P). N,N'-methylenebisacrylamide (2.600 g, 16.696 mmol) was dissolved in ethylene glycol (5.6 mL) by gently heating at 80°C. Piperazine hexahydrate (3.276 g, 16.696 mmol) was then added and the mixture maintained 3 days at room temperature under nitrogen with occasional stirring. After this time, it was diluted with distilled water (30 mL), acidified to pH 4-4.5 with dilute hydrochloric acid and then ultrafiltered though a membrane with nominal molecular weight cut-off 10000. The retained fraction was freeze-dried and the product obtained as a white powder. Yield: 90%.

^{1}H NMR (D_2O): δ (ppm) 2.64 (t, NHCOC**H$_2$**), 3.24 (br, $NHCOCH_2C$**H$_2$**), 3.26 (br, NC**H$_2$C H$_2$**N), 4.51 (s, NHC**H$_2$**NH). ^{13}C NMR (D_2O): δ (ppm) 30.21 ($NHCO$**C**H_2), 44.36 (NH**C**H_2NH), 49.70 (N**C**H_2**C**H_2N), 52.41 ($NHCOCH_2$**C**H_2), 172.14 (NH**C**OCH_2).

Molecular weight: M_n=1,09,500, M_w=171000, PD=1.56.

Linear PAAs from N,N'-methylenebisacrylamide and 2-methylpiperazine (MBA-MP) or trans-2,5-dimethylpiperazine (MBA-DMP). N,N'-methylenebisacrylamide (2.600 g, 16.696 mmol) was dissolved in water (5.6 mL) by gently heating at 80°C. 2-Methylpiperazine (1.724 g, 16.696 mmol) or (*trans*-2,5-dimethylpiperazine (1.945 g, 16.696 mmol) was then added and the mixtures processed as in the previous case. Yields: 65% (*MBA-MP*) and 70% (*MBA-DMP*).

^{1}H NMR (D_2O) (*MBA-MP*): δ (ppm) 1.32 (d, C**H$_3$**CH), 2.63 (br, NHCOC**H$_2$**), 2.88 (br, NC**H$_2$**), 3.08 (br, br, NC**H$_2$**), 3.38 (br, NC**H**), 3.59 (br, $NHCOCH_2$C**H$_2$**), 4.51 (s, NHC**H$_2$**NH). ^{13}C NMR (D_2O) (*MBA-MP*): δ (ppm) 13.79 (**C**H_3CH), 29.68 ($NHCO$**C**H_2), 44.39 (NH**C**H_2NH), 48.33 ($NHCOCH_2$**C**H_2), 52.54 (N**C**H_2**C**H_2N), 54.83 (NCH**C**H_2N), 56.22 (CH_3**C**H), 172.14 (NH**C**OCH_2).

^{1}H NMR (D_2O) (*MBA-DMP*): δ (ppm) 1.32 (d, C**H$_3$**CH), 2.69 (br, NHCOC**H$_2$**), 2.94 (br, NC**H$_2$**), 3.15 (br, NC**H$_2$**), 3.38 (br, NC**H**), 3.55 (br, $NHCOCH_2$C**H$_2$**), 4.51 (s, NHC**H$_2$**NH). ^{13}C NMR (D_2O) (*MBA-DMP)*: δ (ppm) 13.98 (**C**H_3CH), 29.59 ($NHCO$**C**H_2), 44.39 (NH**C**H_2NH), 48.35 ($NHCOCH_2$**C**H_2), 53.55 (N**C**H_2CHN), 56.07 (CH_3**C**H), 172.15 (NH**C**OCH_2).

Molecular weights: *MBA-MP*: M_n=38,500, M_w=48,900 PD = 1.27; *MBA-DMP*: M_n=37,200, M_w=52,400, PD=1.41.

Linear PAA from 1,4-Bis(acryloyl)piperazine and piperazine (BP-P). 1,4-Bis(acryloyl)piperazine (2.500 g, 12.871 mmol) was dissolved in water (4.2 mL) at room temperature and piperazine hexahydrate (2.525 g, 12.871 mmol) was added under stirring. After about 5 minutes, the formed oligomers crystallized out. The system became homogeneous on heating at 60-70 °C and at this temperature the reaction proceeded to some extent, as apparent from the viscosity increasing. Eventually, however, the polymer precipitated again. It was retrieved by lyophilization of the whole reaction mixture.

Linear PAA from 1,4-Bis(acryloyl)piperazine and 2-methylpiperazine (BP-MP) or trans-2,5-dimethylpiperazine (BP-DMP). 1,4-Bis(acryloyl)piperazine (2.500 g, 12.871 mmol) was dissolved in water (4.2 mL) by stirring and then 2-methylpiperazine (1.359 g, 12.871 mmol) or trans-2,5-dimethylpiperazine (1.500 g, 12.871 mmol) was added. The reaction was maintained at r.t. under nitrogen atmosphere for 3 days with gentile stirring. After this time the reaction was treated as in the case of MBA-P. Yield: 65%

^{1}H NMR (D_2O) (*BP-MP*): δ (ppm) 1.30 (d, C**H$_3$**CH), 2.82 (br, NHCOC**H$_2$**), 2.88 (br, NC**H$_2$**), 3.07 (br, NC**H$_2$**), 3.25 (br, NC**H**), 3.51 (br, $NHCOCH_2C$**H$_2$**) 3.56, 3.63 (m, NC**H$_2$**C**H$_2$**N). ^{13}C NMR (D_2O) (*BP-MP*): δ (ppm) 14.48 (**C**H_3CH), 27.90 (NHCO**C**H_2), 41.61 (N**C**H_2**C**H_2N), 44.67 ($NHCOCH_2$**C**H_2), 45.29 (N**C**H_2**C**H_2N), 50.75 (NCH**C**H_2N), 56.09 (CH_3**C**H), 170.94 , 170.88 (NH**C**OCH_2).

^{1}H NMR (D_2O) (BP-DMP): δ (ppm) 1.29 (d, C**H$_3$**CH), 2.84 (m, NHCOC**H$_2$**, NC**H$_2$ ax.**), 3.09 (br, NC**H**), 3.24 (br, NC**H$_2$ eq.**), 3.49 (br, $NHCOCH_2C$**H$_2$**), 3.56, 3.62 (m, NC**H$_2$**C**H$_2$**N). ^{13}C NMR (D_2O): δ (ppm) 14.41, 15,22 (**C**H_3CH), 27.82 (NHCO**C**H_2), 41.61 (N**C**H_2**C**H_2N), 44.64 ($NHCOCH_2$**C**H_2), 48.41 (N**C**H_2CHN), 55.11, 56.01 (CH_3**C**H), 170.94, 170.88 (NH**C**OCH_2).

Molecular weight: BP-*MP*: M_n=22,200, M_w=29,100 PD = 1.31; *BP-DMP*: M_n=17,100, M_w= 23,000, PD =1.35.

Mold Preparation. As a rule, the hydrogels were prepared in the form of sheets using molds consisting of two silanized glass plates of size 10 x 10 x 0.2 cm, with a 1 mm-thick silicone spacer. The glass plates were rendered non-adhesive by soaking 5 hrs in aqua regia at room temperature, then washing several times with water, drying and exposing to chlorotrimethylsilane vapors for 3 days in a closed chamber. The plates were then soaked in toluene (20 mL), ethanol (2 × 20 mL) and water (3 × 20 mL). Finally, they were gently wiped with soft paper and used immediately. Hydrogels in the form of solid cylinders were obtained using thin glass tubes as molds. They were treated in the

same way as plates, but often the final product could be recovered only by carefully breaking the mold. Hydrogels in the form of hollow tubes were obtained with molds consisting of polystyrene cylinders with coaxial wires of graphite. No previous treatment was required in this case, since both materials are intrinsically non-adhesive towards PAA hydrogels.

MBA-P Hydrogels: a Model of Synthesis (MBA-P10 of Table 3.2.5 A). N,N'-methylenebisacrylamide (2.600 g, 16.696 mmol) was dissolved in water (5.6 mL) at 80 °C and stirred until a homogeneous solution was obtained. Piperazine hexahydrate (2.948 g, 15.026 mmol) and 1,2-diaminoethane (0.0507 g, 0.835 mmol) were then added under the same conditions. The solution was then injected into the mold, and placed in an oven at constant temperature (25 °C). Gelation occurred after about 30 h, but the reaction time was extended to 5 days. After this time, the glass plates were separated and the product recovered as a transparent, flexible hydrogel, which was purified from soluble impurities by first extracting with ethanol (200 mL) for 16 h and then with water (200 mL) for 3 h. This extraction cycle was repeated three times.

BP-P Hydrogels: a Model of Synthesis (BP-P25 of Table 3.2.5 A). Bisacryloylpiperazine (3.2440 g, 16.696 mmol) was dissolved in water (5.6 mL) at room temperature and stirred until a homogeneous solution was obtained. Piperazine hexahydrate (2.4567 g, 12.522 mmol) and 1,2-diaminoethane (0.1261 g, 2.087 mmol) were then added with vigorous stirring for 3 minutes. The solution was then injected into the mold, and placed in an oven at constant temperature (25 °C). Gelation occurred after about 12 h, but the reaction time was extended to 3 days. After this time, the glass plates were separated and the product recovered as a transparent, flexible hydrogel, with naked-eye visible opaque microdomain, which was purified from soluble impurities by first extracting with ethanol (200 mL) for 16 h and then with water (200 mL) for 3 h. This extraction cycle was repeated three times.

Other Hydrogels. The preparaion recipes of all other hydrogels considered in this work are reported in Table 3.2.5 A.

Table 3.2.5 A. Reagents used in the synthesis of PAA hydrogels.

Hydrogel	Water [mL]	MBA [mmol]	BP [mmol]	P [mmol]	EDA [mmol]
MBA-P10	5.60	16.70		15.00	0.80
MBA-P15	5.60	16.70		14.20	1.30
MBA-P30	5.60	16.70		11.70	2.50
BP-P25	5.60	-	16.70	12.53	2.09
BP-P30	5.60	-	16.70	11.69	2.51
BP-P40	5.60	-	16.70	10.02	3.34

Solid-state Infrared Spectroscopy (FT-IR ATR). FT-IR ATR spectra were obtained using a Spectrum 100 FT-IR scpectrometer connected with universal ATR sampling accessory produced by PerkinElmer.

Differential Scanning Calorimetry (DSC) Analysis. DSC analyses were performed using METTLER TOLEDO DSC 823 instrument. DSC measures were performed on BP-P polymer and BPP-base hydrogels in an atmosphere of nitrogen (flow 20 mL · min−1), using about 15 mg of sample contained in open aluminum crucible. The heating rate applied was: 25 - 110 °C, 20 °C · min−1; 110 °C, 4 min; 110 - 320 °C, 10 °C · min−1.

Swelling Kinetics in Differet Media. Swelling experiments were performed in water, ethanol and phosphate buffer solution (PBS) pH 7.4 on hydrogel discs 1 mm in thickness and with a base diameter of 18 mm. All samples were dried to constant weight at 25 °C and 0.1 Tor before undergoing swelling experiments. Each disc was put into a test tube containing 40 mL of the swelling medium and maintained at 25 °C. At regular intervals the disc was retrieved, gently wiped with soft filter paper, weighed and reintroduced into the test tube. Maximum swelling was observed after about 1 h. The extent of swelling, SW%, was determined using the following equation: where Wo is the weight of the dry disc and Wt is the weight of the swollen disc at any time. In all tests the percent mean variation coefficient, CV%, was lower than 5%. The reported values were the average of 6 experiments.

Swelling in aqueuos media at different pH. These experiments were performed as described previously, using a starting aqueous solutions with pH in the range 1-11. After the incubation of the hy-

drogels with the aqueous medium, the external solution was equilibrated at the fixed pH by adding 2 M sodium hydroxide or 2 M hydrochloric acid dropwise. The CV% was lower than 5%.

Degradation Kinetics. Degradation was monitored by following the weight loss of the hydrogel samples maintained at 37 °C in PBS pH 7.4 for prolonged time. The percent residual weight, W_r%, was calculated according to the equation:

$$W_r\% = \frac{(W_{td})}{W_o} x100 \qquad \text{eq. 3.2.5 A}$$

where W_o is the weight of the dry disc at initial time, and W_{td} is the weight of the dried disc at time t. All experiments were performed in triplicate. In all tests the mean CV% was ≤5%. The degradation was also indirectly monitored by measuring under the same conditions the trend of SW% on time.

Accelerated Degradation Test. These experiments were carried out as indicated in the previous case. The degradation was evaluated at 60 °C until a complete degradation was observed.

Rheological Test. Rheological measurements were performed using an ARES strain controlled rheometer (Rheometric Scientific). All tests were carried out at 25 °C using a parallel plate geometry (d = 25 mm). The linear viscoelastic zone was measured by applying a shear strain ramp from 0.05 to 10% at frequency of 6.28 rad/s (1 Hz). The frequency sweep tests were performed at strain of 0.1% over a frequency range from 0.1 to 10 rad/s. A different compressive force of 0.2, 0.5 and 1.0 N were applied to hydrogels during the measurements. To prevent dehydratation during rheological measurements, a thin layer of silicon oil was placed on the peripheral surface of the hydrogel held between the plates. Each measurement was performed at least twice on different disc specimens of the same hydrogels sample.

Schwann Cells (SC) Culture. SC were isolated from Sprague–Dawley 3-day-old rats (Charles River, Calco, Italy) accordingly to institutional guidelines and in compliance with the policy on the use of animals approved by the European Communities Council Directive (86/609/EEC). Sciatic nerves explanted were digested with 1% collagenase and 0.25% trypsin (Sigma, Milan, Italy) then filtered through a 30 μm nylon membrane and centrifuged 10 min at 280 x g. Pellets were solubilized in Dulbecco's modified Eagle's medium (DMEM) (Serotec, Oxford, UK) supplemented with 10% fetal calf serum (FCS; Invitrogen, Monza, Italy) and plated onto 35 mm Petri dishes coated with poly-L-Lysine (PLL; Sigma). 24 h after plating, the medium was supplemented with 10 μM arabinoside C (Sigma) then after 48 h the cultures were treated with a stream of cold DMEM-FCS 10%. The re-

maining cells were plated in DMEM-FCS 10 vol.% supplemented with 10 μM forskolin (Sigma) and bovine pituitary extract 200 μg · mL−1 (Invitrogen). Cells became confluent in 10 days. Immunopanning for final purification was carried out incubating the cells for 30 min with mouse anti rat Thy1.1 antibody (Serotec) followed by 500 μL of baby rabbit complement (Cedarlane, Ontario, Canada). The cell suspension (3 x 105) was seeded on 6 cm Petri dishes and grown in presence of 2 μM forskolin and bovine pituitary extract 200 μg · mL−1. At the third passage in vitro SC cultures were trypsinized and cell suspension used for hydrogel experimentation. Tissue culture polystyrene (TCPS) PLL-coated dishes were used as a positive control and empty disks were used as negative control for comparisons. The SC purity (more than 98%) was assessed by immunocytochemistry with a specific antibody against the SC markers protein S100 and glycoprotein P0,[9] [10] analyzed by fluorescence microscopy by Axiovert 2000 microscope (Zeiss, Gottingen, Germany) and the images processed using Adobe Photoshop 5.0.2.

Dorsal Root Ganglia (DRG) Neuron Culture. DRG were harvested from adult rat of Sprague–Dawley (Charles River) accordingly to institutional guidelines (86/609/EEC). DRG were dissociated in 0.125% collagenase type IV (Worthington, Lakewood, NJ, USA) in F12 medium (Invitrogen) for 1 h x 2 and then incubated in 0.25% trypsin (Worthington) in F12 medium for 30 min. Trypsin was inactivated by the addition of 10 vol.% foetal bovine serum (Invitrogen) in F12 medium. The DRG were then washed three times in F12 medium to remove all traces of serum and were mechanically dissociated by gentle trituration, filtered and centrifuged (200 g x 5 min). Cells were resuspended in F12 medium and centrifuged (600 g x 10 min) with 15% bovine serum albumin (BSA; Sigma). The cells debris supernatant was removed leaving the bolus of dissociated neurons. The neurons were re-suspended in modified Bottenstein and Sato's medium (BS medium) containing 0.1 mg · mL−1 transferrin, 20 nM progesterone, 100 μM putrescine, 30 nM sodium selenite, 1 mg · mL−1 BSA, 0.01 mM cytosine arabinoside, 10 pM insulin (all Sigma). Finally the neurons were plated on hydrogels. Neurons seeded onto TCPS dishes pre-coated with 2 μg · mL−1 laminin-1 (Sigma) were used as positive control. After 2 h, 150 ng · mL−1 NGF (Sigma) was added to allow neurons to develop neurites for 7 days.

Application of SC and DRG neuron to hydrogel scaffolds. Under sterile conditions hydrogel round scaffolds (diameter 12 mm) were transferred into 12-well plate (smooth side faces upwards). The

---

[9] **Magnaghi, V.; Conte, V.; Procacci, P.; Pivato, G.; Cortese, P.; Cavalli, E.; Pajardi, G.; Ranucci, E.; Fenili, F.; Manfredi, A.; Ferruti, P., J. Biomed. Mater. Res. Part A, 2011, 98A, 19.**

[10] **Magnaghi, V.; Balabbio, M.; Cavarretta, I., T., C.; Froestl, W.; Lambert, J., J.; Zucchi, I.; Melcagni, R., C., Eur. J. Neurosci, 2004, 19, 2641.**

SC or DRG neuron suspension was then seeded onto the hydrogels at proper concentrations: 5 x 104 cells/well in DMEM-FCS 10 vol.% plus 2 μM forskolin for SC and 2 x 104 cells/well in BS medium for DRG neurons. The cells were grown in a tissue incubator at 37 °C in a humidified atmosphere with 5% CO2 for a period of 1, 3, 5, 7, 10 days of cell culture, and analyzed at each time point by contrast phase light microscopy using a Zeiss inverted microscope Axioskop 2000 or processed for MTS assay of cell proliferation.

Cell proliferation. The cell proliferation on the scaffolds were determined using the colorimetric MTS assay (CellTiter 96 AQueous One solution; Promega, Madison, WI, USA). The reduction of yellow tetrazolium salt in MTS (3-(4,5-dimethylthiazol-2-yl)-5-(3-carboxymethoxy -phenyl)-2-(4-sulfophenyl)-2H-tetrazolium) to form purple formazan crystals by the dehydrogenase enzymes secreted by mitochondria of metabolically active cells forms the basis principle of this assay. The formazan dye shows absorbance at 490 nm and the amount of formazan crystals formed is directly proportional to the number of cells. To process for MTS assay, the samples were rinsed with PBS to remove unattached cells and incubated with 20 vol.% MTS reagent for a period of 3 h at 37 °C. Absorbance of the obtained dye was measured at 490 nm using a spectrophotometric plate reader (ELx800 Absorbance Microplate Reader; BioTek USA)

DRG neuron immunocytochemistry. DRG neuron were fixed in 4% paraformaldehyde r.t. for 30 min, then rinsed 1h with PB-0.25% BSA and incubated overnight (4 °C) with primary antibodies for β-tubulin (1:500, mouse monoclonal; Abcam, Milan, Italy). The cells were then incubated for 2 h FITC-coniugated mouse anti-β-tubulin (1:200; GE Healthcare Europe GmbH, Milan, Italy). The slides were mounted with VectashieldTM mounting medium for fluorescence containing DAPI (4′, 6-diamidino-2-phenylindole) for nuclear staining (Vector Laboratories, Peterborough, UK) and examined under a fluorescence Zeiss inverted microscope Axioskop 2000.

Statistical Analysis. All the biological data presented in this work were plotted and best-fit growth curve constructed (GraphPad Prism, GraphPad Software, San Diego, CA, USA).

CHAPTER 4

RESULTS AND DISCUSSION

4.1 HETERO-DIFUNCTIONAL DIMERS AS BUILDING BLOCKS FOR THE SYNTHESIS OF POLYAMIDOAMINES WITH HETERO-DIFUNCTIONAL CHAIN TERMINALS

The aim of this work was to prepare hetero-diterminated PAAs as well as some novel PAA derivatives not previously obtained by simple methods. Hetero-difunctional dimers (HDDs) were the simplest building blocks capable of exactly reproducing the same sequence of amide-and *tert*-amine groups along the polymer chain of PAAs, while unequivocally ensuring hetero-difunctional chain terminals. As mentioned in Introduction, linear PAAs can be prepared by the stepwise polyaddition of bisacrylamides and either *prim*-monoamines or *sec*-bisamines, which yields PAAs with different chain structures. The investigation reported in this work concerned only HDDs leading to PAAs with "a—a—b—b" sequence of amide- and amine groups along the polymer chain, that is, HDDs obtained by the mono-addition of bis-*sec*-amines to bisacrylamides (Scheme 4.1 A).

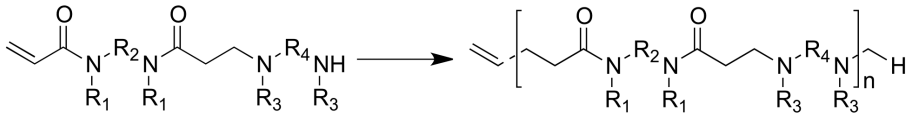

Scheme 4.1 A. Self-polyaddition of "a—a—b—b" type HDDs.

Six HDDs were prepared starting from 2,2-bisacrylamidoacetic acid (BAC), 1,4-bisacryloylpiperazine (BP) and N,N'-methylenebisacrylamide (MBA) as bisacrylamides and piperazine (P) and 2-methylpiperazine (MP) as amines. BAC was selected because, in combination with MP, it gives ISA23, the highly biocompatible "stealth-like" amphoteric PAA mentioned in Introduction. BP and MBA were chosen because with P and MP they give PAAs extensively studied as components of bioactive hydrogels (data not shown). Moreover, P and MP are endowed with high reactivity towards Michael polyaddition, coupled with limited basicity leading, as a rule, to good biocompatibility of the resultant PAAs.[1 2 3 4 5]

[1] Ferruti, P.; Marchisio, M.; Duncan, R., Macromol. Rapid Commun., 2002, 23, 332-335.

[2] Richardson, S.; Ferruti, P.; Duncan, R., J. Drug Targeting, 1999, 6, 391-404.

[3] Ranucci, E.; Spagnoli, C.; Ferruti, P.; Souras, D.; Duncan, R., J. Biomater. Sci. Polym. Ed., 1991, 2, 303-315.

[4] Richardson, S., C., W.; Pattrick, N., G.; Lavignac, N.; Ferruti, P.; Duncan, R., J. Controlled Release, 2010, 142, 78-88.

[5] Ferruti, P.; Ranucci, E.; Trotta, F.; Gianasi, E.; Evagorou, G., E.; Wasil, M.; Wilson, G.; Duncan, R., Macromol. Chem. Phys., 1999, 200, 1644-1654.

The six HDDs obtained by combining the above building blocks were named BAC-P, BAC-MP, BP-P, BP-MP, MBA-P and MBA-MP after their parent compounds. Their structures are reported in Figure 4.1A.

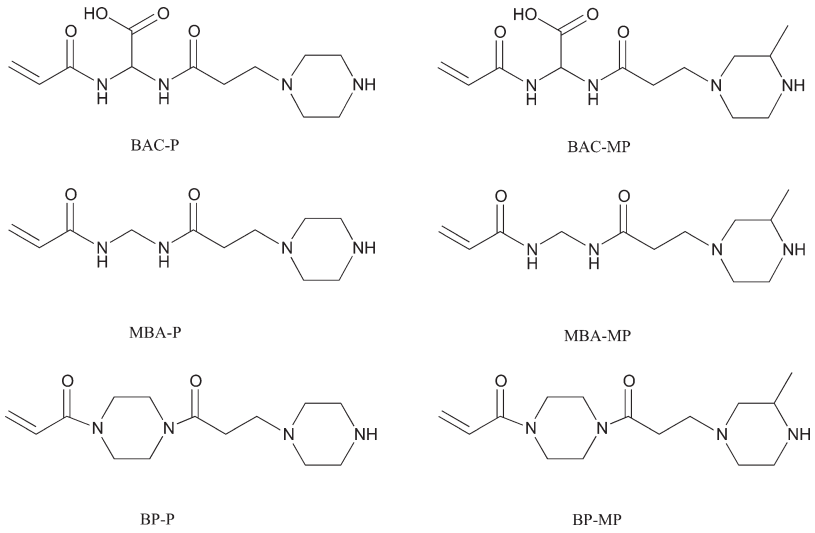

Figure 4.1 A. Structures of the HDDs synthesyzed.

The general synthetic procedure adopted for preparing HDDs is depicted in Scheme 4.1 B. It involved the synthesis of mono-Boc-protected P and MP [Step (a)] followed by reaction with moderate excess bisacrylamide, isolation and purification of the mono-addition product, and cleavage of the protecting group [Step (b)]. Both steps deserve comments.

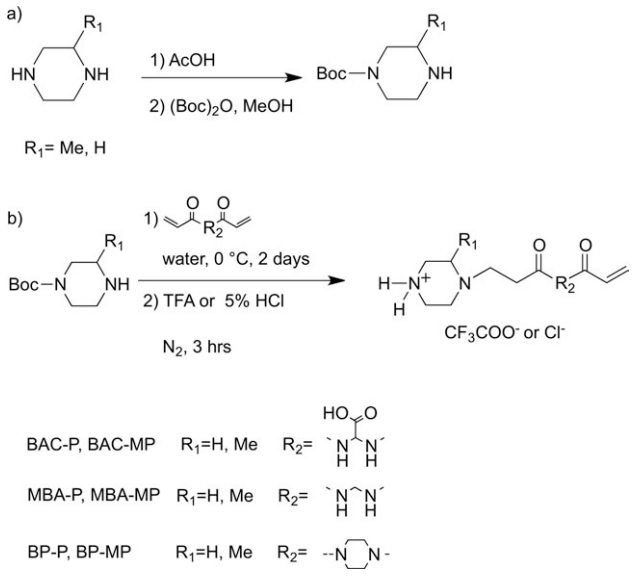

Scheme 4.1 B. General synthetic pathway for the preparation of HDDs. Step (a): synthesis of mono-Boc-protected P and MP. Step (b): Michael-type reaction with bisacrylamide, and cleavage of the protecting group.

In step (a), Boc-P and Boc-MP were prepared from quasi-stoichiometric amounts of di-(*tert*-butyl)dicarbonate and mono-protonated P and MP, in turn obtained by in situ adding acetic acid to the amine in 1:1 molar ratio. Only a slight excess of amine mono-acetate was required to maximize the yield of the mono-substituted products, since the two pK_a values of both amines differ by approximately four orders of magnitude, and under the conditions adopted the amount of doubly-protonated molecules and, correspondingly, of uncharged molecules amenable to react twice was minimal. In step (b), the addition reactions of Boc-P and Boc-MP to BAC, BP and MBA were carried out for two days in water at 0 °C, using 2- to 3-fold excess bisacrylamide. Under these conditions, the double addition to the same bisacrylamide molecule was minimized. It may be noticed that the excess bisacrylamide required to achieve this result was significantly lower than expected from purely statistical calculations. It would appear that at 0 °C the amine addition to one of the two double bonds biased the reactivity of the other notwithstanding the fairly long distance between them. However, at room temperature and with the same stoichiometric ratios significant amounts of the double-addition products were formed. The product work-up depended on the bisacrylamide employed. In the case of BAC, the reaction mixtures contained excess BAC, protected BAC-P (or BAC-MP) and small amounts of di-addition products, that is, di-protected trimers of the "b—b—a—a—b—b" type. All these products were highly polar and hardly extractable from water with organic solvents. Therefore, they were isolated by ion-exchange chromatography employing a weakly acid (carboxylated) resin and following a two-step elution protocol. The first step was carried out with bidistilled water as eluant, the second step with an acid concentration elution gradient passing from 10^{-4} M to 0.1 M hydrochloric acid (Figure 4.1 B). Unreacted BAC was eluted in the first step. In the second step, the mono-addition products were eluted first, followed by the di-substituted products, which were discarded. The combined fractions containing the mono-addition products were then lyophilized and pure BAC-P and BAC-MP finally obtained by de-protection with trifluoroacetic acid.

The addition reactions of MBA or BP with Boc-P or Boc-MP gave protected MBA-P, MBA-MP, BP-P and BP-MP, respectively. The reaction mixtures, containing dimers and residual bisacrylamide, were acidified to pH 3 and the bisacrylamides fractionally extracted with organic solvents. Under these conditions, the protected dimers, being ionized, remained in the aqueous phase and were retrieved by freeze-drying. Since the products were insoluble in TFA, the de-protection step was carried out with 5% hydrochloric acid.

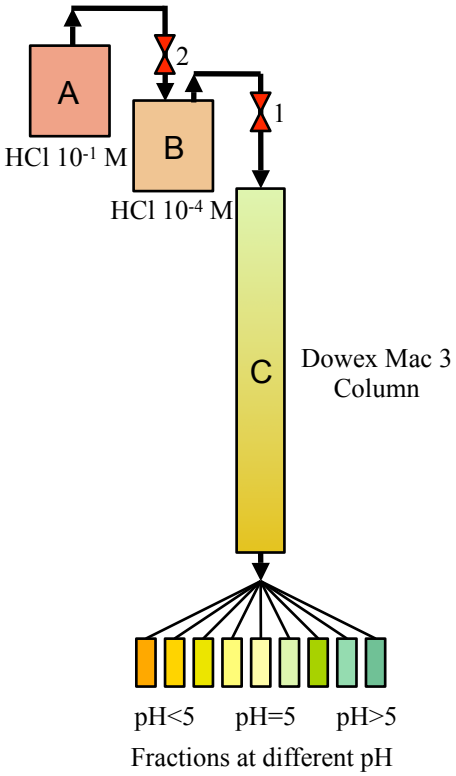

Figure 4.1 B. Equipment adopted to obtain the hydrochloric acid gradient used in the second elution step of BAC-P and BAC-MP purification. Column C was connected through Valve 1 to Flask B containing 10^{-4} M hydrochloric acid, in turn connected through Valve 2 to Flask A containing 10^{-1} M hydrochloric acid. Each drop flowing out the column drew a drop from Flask B, immediately replaced by a drop from Flask A, thus obtaining the desired acid concentration gradient.

All protected HDDs were characterized by ^{1}H NMR. All de-protected HDDs were fully characterized by elemental analysis, ^{1}H NMR, ^{13}C NMR (Figures S4.1 A-F), distortionless enhanced by polarization transfer (DEPT), ^{1}H-^{1}H correlation (COSY), heteronuclear multiple bond correlation (HMBC) and heteronuclear correlation (HETCOR) (Table 4.1 A). The results of these characterizations were in agreement with the proposed structures. C/N ratios by elemental analysis are reported in Table 4.1 B. Since all HDDs were isolated as trifluoroacetates or hydrochlorides and vacuum dried or lyophilized, some loss of acid was inevitable and, therefore, the absolute values of elemental analyses were not fully reliable. However, the C/N ratios were not liable to be significantly affected by the isolation procedures and provided a reliable confirmation that the product structures were as expected. All HDDs, as either hydrochlorides or trifluoroacetates, could be stored for a long time at 0÷5 °C, if protected from moisture, and did not polymerize at room temperature. In aqueous solution, polymerization was triggered by rising pH above 7.5 with bases inert towards Michael addition, such as inorganic hydroxides or tertiary amines. The molecular weights of the resultant

polymers were usually high and obviously related to the reaction time, whereas all practical difficulties to achieve a precise balance among the reactant functions were got round.

Table 4.1 A. Full NMR characterization (D_2O, δ) of all HDDs.

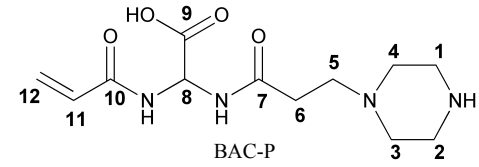

BAC-P

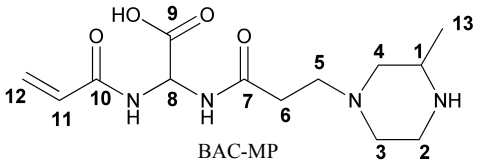

BAC-MP

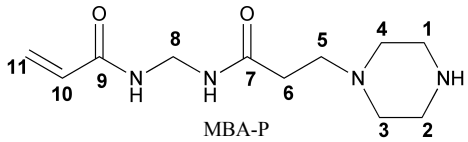

MBA-P

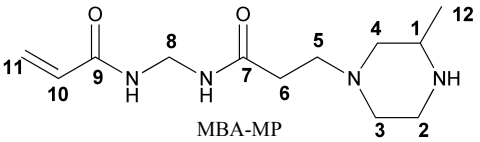

MBA-MP

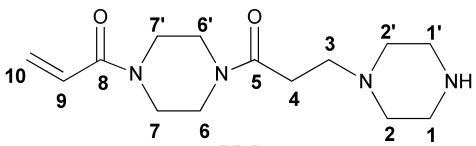

BP-P

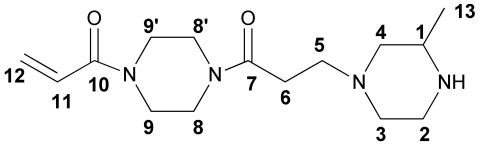

BP-MP

		1	2	3	4	5	6	7	8	9	10	11	12	13
BAC-P	^{1}H	3.49	3.49	3.49	3.49	3.49	2.74		5.73			5.68	6.13	
	^{13}C	48.56	48.56	52.62	52.62	41.39	28.81	170.79	56.61	168.15	170.79	128.75	129.10	
BAC-MP	^{1}H	3.24	3.40[a] 3.78[b]	3.40	3.63	3.63	2.81		5.78			6.21	5.75	1.43
	^{13}C	57.38	46.43	49.00	48.14	40.30	29.23	170.75	57.41	168.40	170.75	129.74	129.53	13.97
MBA-P	^{1}H	3.58	3.58	3.58	3.58	3.47	2.73		4.58		5.71	6.14		
	^{13}C	45.7	45.7	49.89	49.89	42.09	29.22	171.68	53.60	171.68	128.42	129.75		
MBA-MP	^{1}H	3.19	3.38[a] 3.71[b]	3.38	3.60	3.38	2.72		4.60		5.74	6.19	1.40	
	^{13}C	58.12	46.23	48.94	48.15	40.29	29.17	171.79	53.58	171.79	128.45	129.56	13.85	
BP-P	^{1}H	3.61	3.61	3.61	3.01	-	3.61	3.61	-	5.79	6.14[c] 6.67[d]			
	^{13}C	48.95	53.11	44.53	27.42	169.73	40.70	41.33	169.73	127.35	129.02			
BP-MP	^{1}H	3.87	3.44[a] 3.77[b]	3.42	3.77	3.56	2.98		3.58	3.65		5.75	6.08[c] 6.64[d]	1.47
	^{13}C	56.76	45.26	47.83	45.06	44.85	27.59	169.64	40.04	41.37	169.64	127.23	128.97	13.49

[a] equatorial, [b] axial, [c] cis, [d] trans

Table 4.1 B. C/N Ratio of all HDDs synthesized.

	C/*N* Ratio	
HDD	Calculated	Found
BAC-P	2.57	2.63
BAC-MP	2.79	2.82
MBA-P	2.35	2.36
MBA-MP	2.57	2.63
BP-P	3.00	3.04
BP-MP	3.22	3.23

The synthetic potential of HDDs was assessed by performing model reactions, namely self-polyaddition, preparation of monofunctional PAA oligomers with controlled molecular weight, of star-like PAA architectures, of protein-PAA conjugates and of tadpole-like PAA-cholesterol amphiphiles. The aim was to test the general aptitude of HDDs to be employed for these reactions and was limited to a few examples involving only some of the prepared dimers at a time. It may be noticed that most of the reaction products were hardly obtainable by the traditional PAA preparation method.

The self-polyadditions of BAC-MP and BP-P were carried out as model syntheses of PAAs via the corresponding HDDs. The reaction progress was monitored by ^{1}H NMR until signals at 5.78, 6.13 and 6.67 ppm, relative to the acrylic hydrogens, fell below the detection threshold of the instrument. The products had, respectively, *M*n 38000 and 30900, with *M*w/*M*n 1.32 and 1.13. These molecular weight values were significantly higher than those of the corresponding PAAs obtained by the traditional methods after the same reaction times, with lower polydispersities.

The polymerization of HDD mixtures with either monofunctional acrylamides or amines with approximately the same reactivity as the corresponding function present in HDDs, leads at 100% conversion to an average polymerization degree equal to:

$$\overline{X}_n = \frac{N_{\mathrm{HDD},0}}{N_{\mathrm{monofunctional},0}} \qquad \text{eq. 4.1 A}$$

Where $N_{HDD,0}$ is the initial number of HDD molecules and $N_{monofunctional,0}$ is the initial number of mono-functional compound. Obviously, *M*n is given by the product of X_n times the molecular weight of the HDD employed, added by the molecular weight of the mono-functional compound. The resultant polymer will be terminated at one terminus with the unreactive group and at the opposite terminus with the excess reactive function.

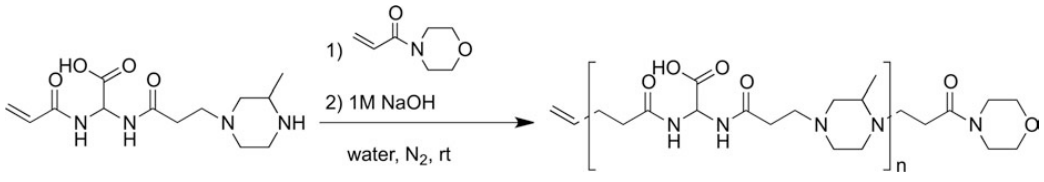

Scheme 4.1 C. Synthesis of the mono-functionalized ISA23 oligomer by polymerization of BAC-MP in the presence of 4-acryloylmorpholine.

The preparation of an ISA23 oligomer mono-functionalized at one terminus with an activated double bond by polymerization of BAC-MP in the presence of 4-acryloylmorpholine is reported in

Scheme 4.1 C. The reaction was carried out adopting a 10/1 BAC-MP/4-acryloylmorpholine molar ratio. The reaction progress was monitored by ^{1}H NMR by comparing the signals at 6.22 and 5.62 ppm, relative to the end-chain acrylic group and the CH-COO^{-} hydrogen of BAC, respectively (Figure 4.1 C).

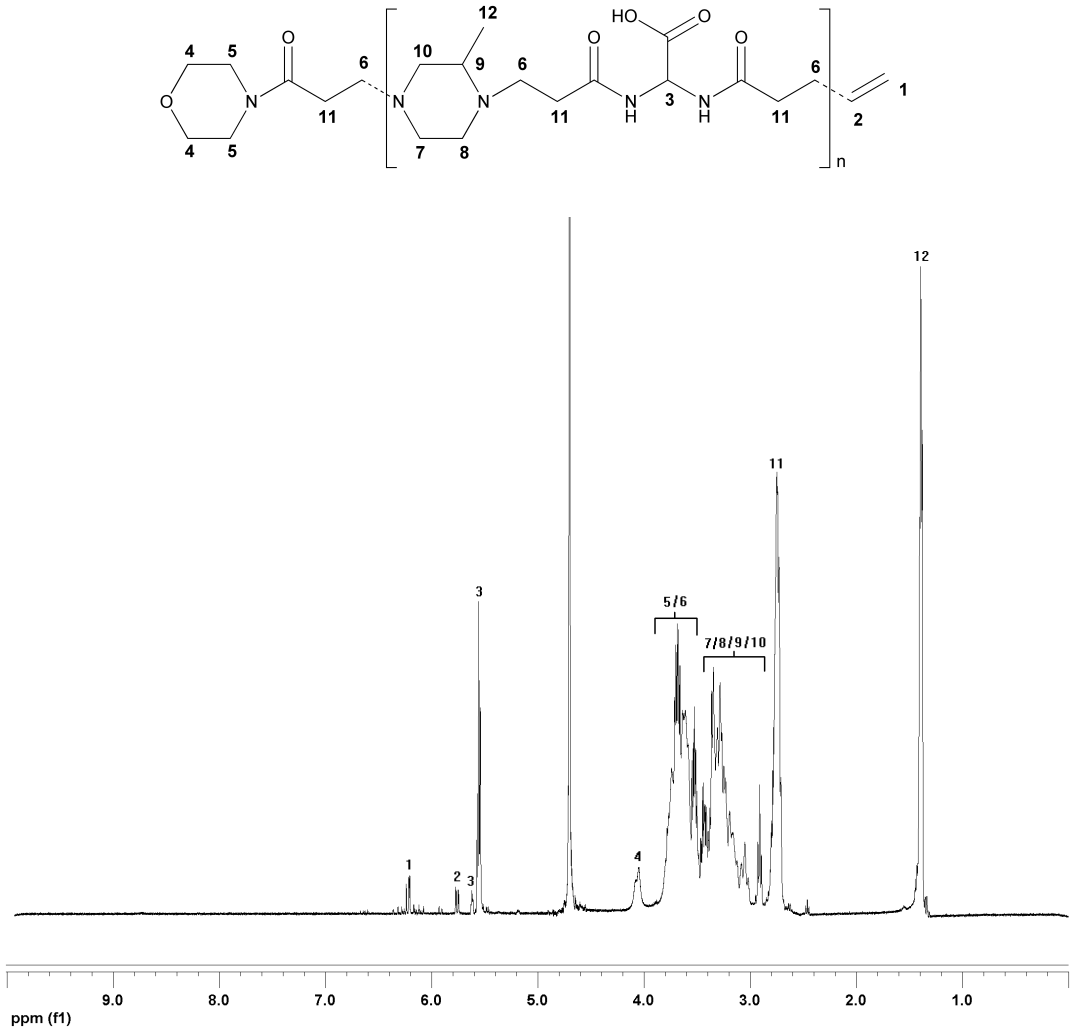

		1	2	3	4	5/6	7/8/9/10	11	12
BAC-MP-AM	^{1}H	6.22	5.77	5.62; 5.56	4.05	3.62	3.20	2.75	1.39

Figure 4.1 C. ^{1}H NMR of BAC-MP-4-acryloylmorpholine conjugate (BAC-MP-AM).

The reaction was stopped when in the NMR spectrum the ratio of the reference peaks' integrals remained constant with time and was consistent with the presence of a double bond every 10 BAC-MP units, that is, the reaction yield had approached 100%.

The *M*n of the product was 3200, with *M*w/ *M*n 1.28. This molecular weight value was very close to the expected value of 3150, as calculated from Eq. 4.1 A.

Four-arm star-like PAAs (BP-MP-C and BAC-MP-C) were synthesized from BP-MP and BAC-MP and 1,4,8,11-tetraazacyclotetradecane (cyclam) (Scheme 4.1 D). The polymerization reactions were performed, as usual, in aqueous solution at pH 9 and monitored by ^{1}H NMR (Figures S4.1 G and H). The products were isolated when the signals attributed to the double bond hydrogens fell below the instrument's detection threshold.

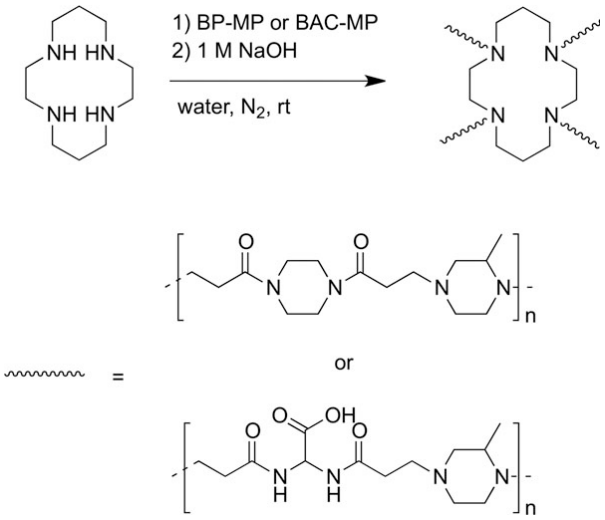

Scheme 4.1 C. Synthesis of four-arm star-like PAAs from BP-MP and BAC-MP and cyclam.

In the case of BP-MP-C, the adopted HDD/cyclam molar ratio was 10. The *M*n of the product was 3300, with *M*w/ *M*n 1.21. These values were in close agreement with the values of 3400 and 1.29 calculated from the classic literature's formulas[6] [7] extrapolated for $p = 1$ (Eq.s 4.1 B and C):

$$\bar{X}_n = \frac{(frp + 1 - rp)}{(1 - rp)} \qquad \text{Eq. 4.1 B}$$

$$\frac{\bar{X}_w}{\bar{X}_n} = 1 + \frac{frp}{(frp + 1 - rp)^2} \qquad \text{Eq. 4.1 C}$$

Where f is the number of reactive functions of the multifunctional monomer (four for cyclam), r = $N_a/(N_b + \mathrm{f}\, N_{b'})$, $N_a = N_b$ is the molar amount of HDD and $N_{b'}$ is the molar amount of the multi-functional monomer. In the case of BAC-MP-C the adopted HDD/cyclam molar ratio was 34.2. The product had *M*n 10800 with *M*w/ *M*n 1.08, to be compared with the calculated values of 10700 and 1.26. It may be observed that *M*n was in excellent agreement with the expected value, whereas the *M*w/ *M*n ratio was remarkably lower. In fact, the product obtained was quasi-monodisperse. Inter-

[6] Khalili, F.; Henni, A.; East, A., L., L., J. Chem. Eng. Data, 2009, 54, 2914-2917.

[7] Peebles, L., H. Eds., In Molecular Weight Sistribution in Polymers, Wiley Interscience, New York, 1971.

estingly, this effect was not observed with BP-MP, suggesting that the zwitterionic nature of BAC-MP was largely responsible for it. Possibly, BAC-MP reversibly interacted with cyclam, resulting in a local catalytic activity of the latter favoring the growth of the chains attached to it over that of "free" molecular species. Thus, the behavior of the BAC-MP/ cyclam system as regards the molecular weight distribution of the resultant polymer approached that of a cyclic monomer growing on a multifunctional center. The long chain branching (LCB) frequency of BP-MP-C and BAC-MP-C was determined by SEC connected in series with RI, light scattering and viscometric detectors (see Experimental) and found in both cases of approximately 2 side chains per macromolecule. This LCB frequency value was consistent with the expected four-arm architecture originating from a cyclam core.

BAC-P, BAC-MP, BP-P and BSA were chosen as model HDDs and protein for the preparation of PAA-protein graft copolymers. This was simply achieved by triggering the HDD polymerization in aqueous medium in the presence of BSA that participated in the polymerization through its exposed NH_2 and SH groups. To give an example, the synthesis of BAC-MP-g-BSA is reported in Scheme 4.1 E. The occurrence of PAA grafting onto BSA was evaluated by SEC connected in series with RI, light scattering and viscometric detectors.

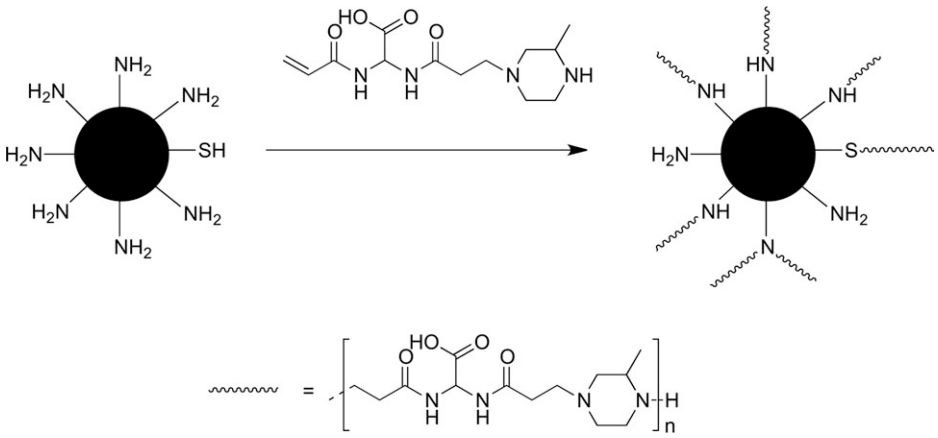

Scheme 4.1 E. Synthesis of BAC-MP-g-BSA by polymerization of BAC-MP in the presence of BSA.

The data, reported in Table 4.1 C, provided clear evidence of the increasing of the molecular weight of copolymers with respect to native BSA, always accompanied by low polydisperisities and higher values of the Mark-Houwink constants, hence higher hydrodynamic radii. A further confirmation was provided by the far higher solubility in aqueous media of the copolymers compared with virgin BSA.

Table 4.1 C. Molecular weight and viscosimetric data of PAA-g-BSA samples compared with BSA.

Sample	M_n[a]	M_w/M_n[b]	$[\eta]$[c] (dL/g)	a[d]	log K[e]	R_h[f] (nm)
BSA	67,000	1.04	0.054	0.034	−1.45	3.92
BAC-MP-*g*-BSA	1,01,000	1.07	0.067	0.203	−2.74	6.1
BAC-P-*g*-BSA	84,900	1.17	0.053	0.265	−2.58	4.11
BP-P-*g*-BSA	88,100	1.14	0.083	0.163	−2.04	5.90

[a] Number average molecular weight; [b] Polydispersity index; [c] Intrinsic viscosity; [d,e] Mark-Houwink constants; [f] Hydrodynamic radius.

The BP-P-g-BSA copolymer was further characterized by comparing the tracing of its potentiometric titrations with those of virgin BSA/linear BP-P mixtures of known composition (Figure 4.1 D), as previously reported.[13] The titration curves of the copolymer and of the BSA/BP-P mixtures exhibited two evident inflections at pH values close to the inflections of the BP-P titration curve, whereas the BSA curve was characterized by a semi-continuous decrease of pH upon acid addition without clearly detectable inflections.

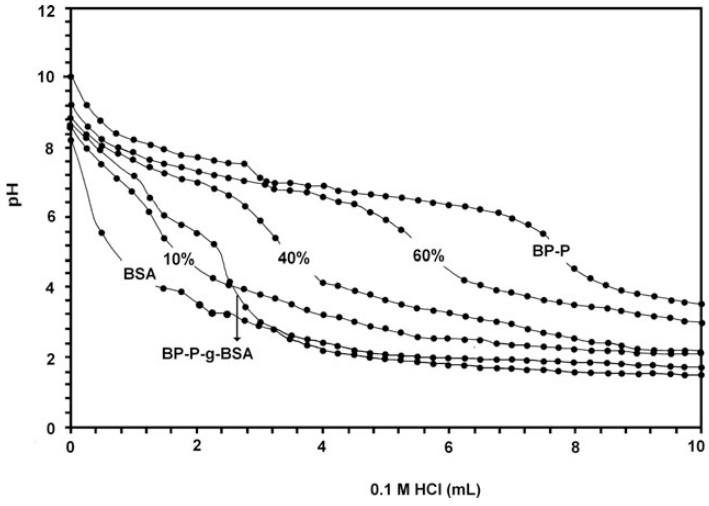

Figure 4.1 D. Potentiometric titration curves of BP-P-g-BSA copolymer and of BSA/linear BP-P mixtures of known composition.

Considering that the amine character of the albumin -NH_2 groups involved in the grafting reaction is preserved, we may reasonably suppose that PAA/BSA mixtures are good models for PAA-grafted albumin, as far as titration is concerned. Therefore, from the family of titration curves reported in Figure 4.1 D, the PAA content in the grafted product can be determined as approximately 20% by weight. This value was consistent with the molecular weight difference of the BP-P-g-BSA copolymer with respect that of BSA (calculated 18000, experimentally found 21100). Assuming that

no BP-P was present, since the copolymer had been extensively ultrafiltered through a membrane with molecular weight cut-off 50000, this correspondence confirmed that grafting reaction occurred as expected. No titration experiments were carried out with BAC-MP-g-BSA and BAC-P-g-BSA since the acid-base properties of BAC-MP and BAC-P are close to those of BSA.

"Tadpole-like" PAA-cholesterol amphiphiles were obtained by carrying out the polymerization of HDDs in the presence of thiocholesterol (TC), which participates in the Michael polyaddition through its SH group (Scheme 4.1 F).

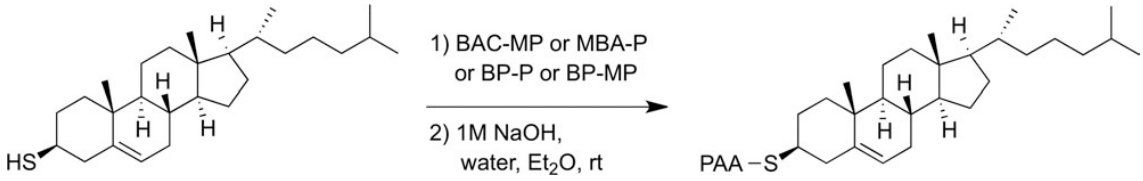

Scheme 4.1 F. Synthesis of "tadpole-like" PAA-Cholesterol amphiphiles by polymerization of HDDs in the presence of thiocholesterol (TC).

These reaction systems closely resembled the preparation of mono-functional PAAs by copolymerization of HDDs with monofunctional amines or acrylamides, since the SH group reacts with activated double bonds in the same way as the amine groups.[8] Being thiocholesterol insoluble in water, the preparations of HDD-TC conjugates were carried out in a diethylether/water slurry. Thiocholesterol resided in the former solvent and the HDDs in the latter. The two solutions were vigorously stirred under nitrogen at room temperature in a closed vessel until the signals due to the acrylic hydrogens of bisacrylamides were no longer detectable in the ^{1}H NMR spectra of the aqueous phases. The feasibility of this process was ascertained with BAC-MP, MBA-P, BP-P and BP-MP. A 10:1 HDD/TC molar ratio was employed for obtaining polymers with 10 repeating units of HDD per TC molecule.

This value was chosen because literature data[9] [10] suggest it as leading to a suitable hydrophilic/lipophilic balance for micelle formation in aqueous media. In the case of BAC-MP-TC and MBA-P-TC, their amphiphilic nature led to phase segregation both in aqueous media and organic solvents. Consequently, their ^{1}H NMR spectra showed neither traces of the PAA backbone in deuterated water, nor of the cholesterol moiety in deuterated chloroform, as expected. BP-P turned to be hardly soluble in both solvents, probably due to the tendency of the BP-P chain to crystallize (data

[8] **Flory, P., J., J. Am. Chem. Soc., 1948, 70, 2709-2718.**

[9] **Ranucci, E.; Ferruti, P., Macromolecules, 1991, 24, 3747-3752.**

[10] **Perrin, P.; Monfreux, N.; Lafruma, M., Colloid Polym. Sci., 1999, 277, 89-94.**

not shown). Only in the case of BP-MP-TC both components were soluble in deuterated chloroform. This allowed obtaining clear homogeneous solutions and running ^{1}H NMR spectra in this solvent. These spectra did not significantly differ from those of a previously synthesized BP-MP PAA carrying pendant TC moieties,[11] and showed the presence of the diagnostic peaks of both components. The calculated and experimentally determined C/N ratios for all the PAA-TC polymers synthesized are reported in Table 4.1 D.

Table 4.1 D. C/N Ratio of "Tadpole-like" PAA-Cholesterol Amphiphiles

Sample	*C/N*[a]	*C/N*[b]	HDD/TC[c]
BAC-MP-TC	3.21	2.98	4.52
MBA-P-TC	2.94	2.82	7.97
BP-P-TC	3.58	3.30	5.17
BP-MP-TC	3.80	3.59	6.61

[a] Calculated; [b] Found; [c] Molar ratio between the HDD repeat unit and the TC moiety as calculated from C/N found values, to be compared with a 10:1 HDD/TC molar ratio in the reaction feeding.

It may be observed that the experimental values were invariably lower than the theoretical ones, pointing to cholesterol content somewhat lower than expected, doubtless due to the heterogeneous reaction conditions adopted. All PAA-TC samples formed nanoparticles in aqueous media, as confirmed by dynamic light scattering (DLS) and TEM analyses. As example, the DLS curves of BAC-MP-TC and the TEM analysis are reported in Figure 4.1 E. It may be noticed that the correlogram is consistent with a neat homogeneous monomodal size distribution. Furthermore, TEM analysis showed a quasi-spherical shape of these nanoparticles. The other PAA-TC samples gave similar results.

The average PAA-TC nanoparticle sizes in PBS solution pH 7.4 as a function of concentration and temperature are reported in Figures 4.1 F and 4.1 G, respectively. It may be observed that particle formation at 25 °C in PBS started at concentrations in the range 0.15-0.60 mg/mL, their size increased sharply, reached a maximum at about twice these values, then remained approximately constant and finally decreased for concentrations higher than 1 mg/mL. Consequently, the critical micelle concentration (CMC) deduced from the graphs varied from 0.16 to 0.7 mg/mL, following the trend BP-P<BP-MP≤ MBA-P<<BAC-MP. This trend is consistent with the relative hydrophilicities of the PAA portions. The apparent exception provided by BP-P-TC can be explained by the previ-

[11] **Astafieva, I.; Zhong, X., F.; Eisemberg, A., Macromolecules, 1993, 26, 7339-7352.**

ously mentioned structure-forming tendency of its PAA portion. Nanoparticle average sizes at 1 mg/mL concentration varied in the range 13–28 nm and, not surprisingly, followed the same trend as the CMC, the most hydrophilic ones giving larger nanoparticles.

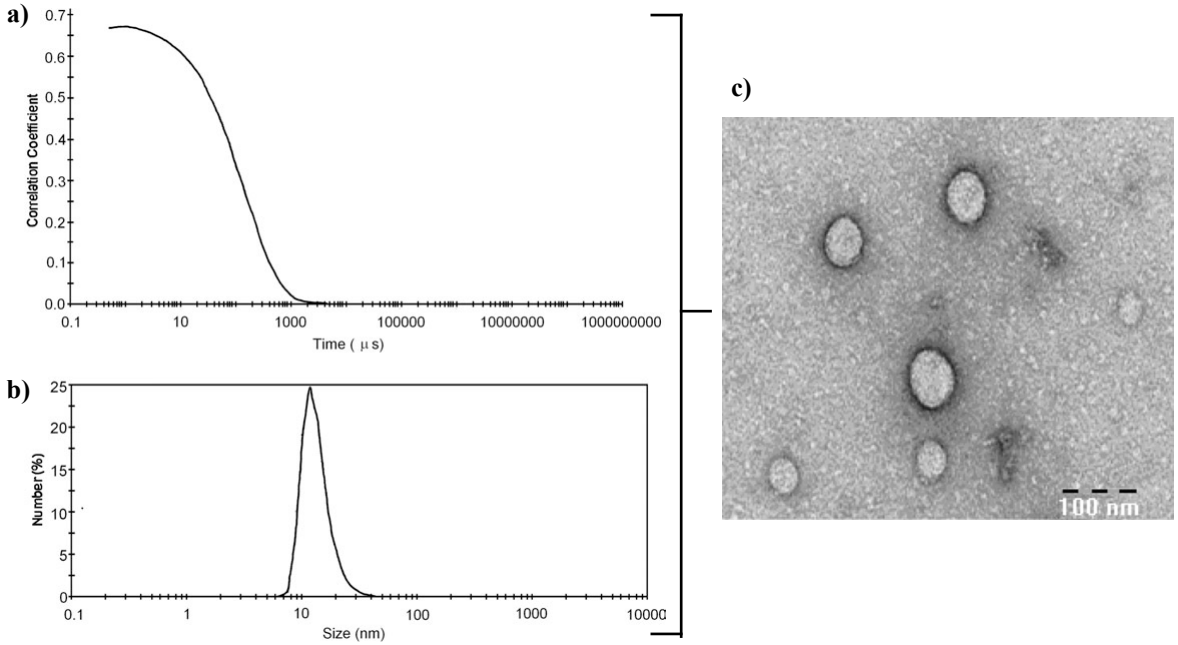

Figure 4.1 E. DLS an TEM analyses of BAC-MP-TC nanoparticles in PBS (1 mg/ml) at 25 °C. Panel (a): correlogram; panel (b): number size-distribution. Panel (c): TEM micrograph obtained by negative staining microscopy using uranyl acetate.

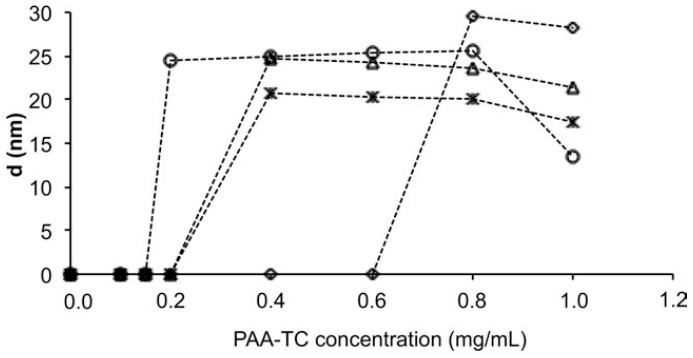

Figure 4.1 F. Hydrodynamic diameter of PAA-Cholesterol micelles in PBS at 25 °C as function of polymer concentration: BAC-MP-TC (--◊--); MBA-P-TC (--△--); BP-P-TC (--○--); BP-MP-TC (--✳--).

The temperature dependence of nanoparticle average size in the range 25-60 °C are reported in Figure 4.1 G. All curves, leaving apart BAC-MP, show qualitatively the same trend.

The average size initially decreased until about 30 °C, remained approximately constant in the range 30-45 °C and then increased until the maximum tested temperature of 60 °C. In the case of

BAC-MP the trend was initially the same and the average size decreased until about 30 °C, but immediately after started to increase until 60 °C.

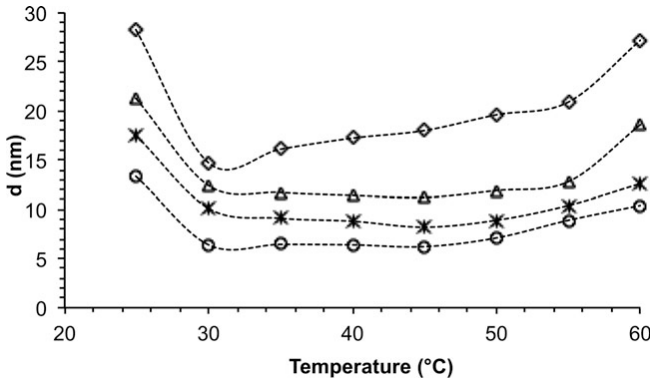

Figure 4.1 G. Hydrodynamic diameter of PAA-Cholesterol micelles in PBS at concentration of 1 mg/ml as function of temperature: BAC-MP-TC (--◊--); MBA-P-TC (--△--); BP-P-TC (--○--); BP-MP-TC (--✳--).

Supplementary Figures.

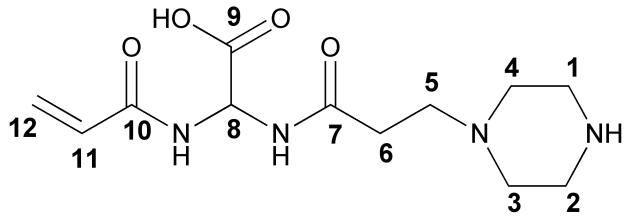

a)

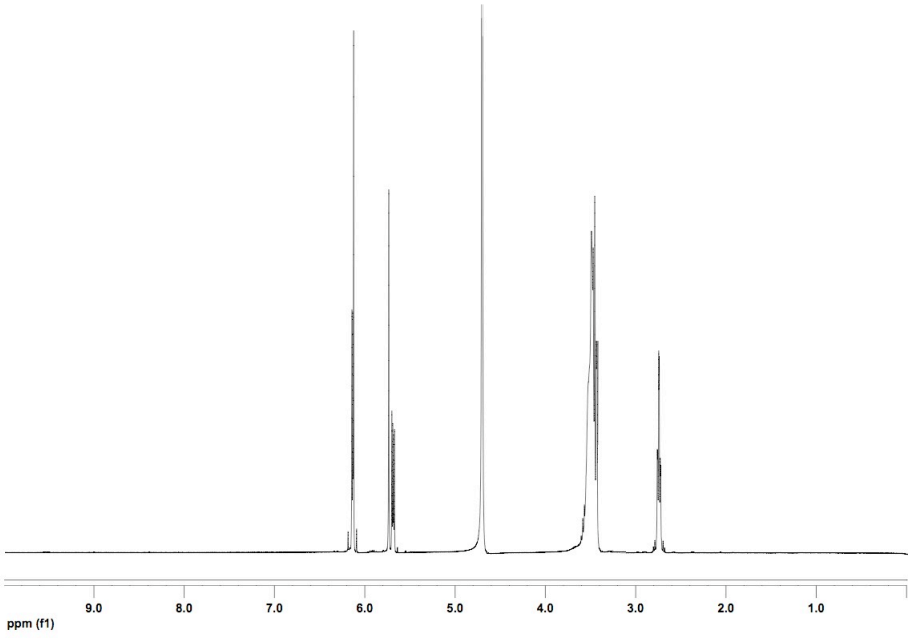

b)

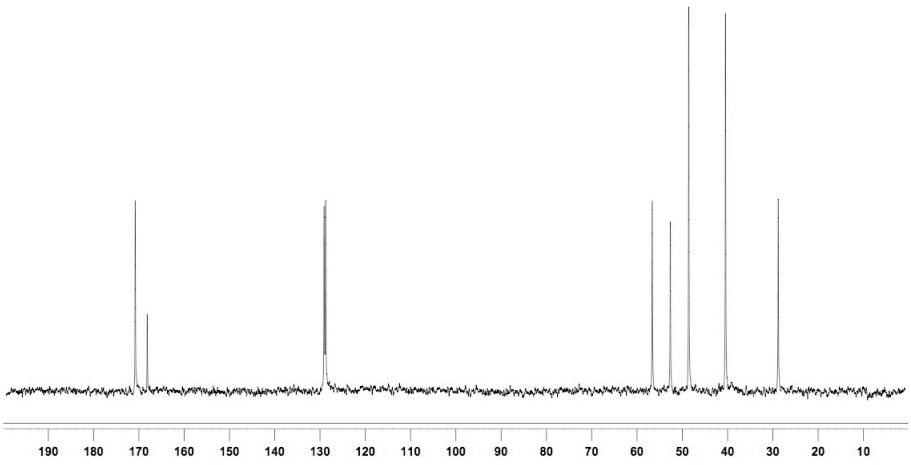

Figure S4.1 A. ^{1}H (Panel a) and ^{13}C (Panel b) NMR spectra (D_2O, ppm) of BAC-P dimer.

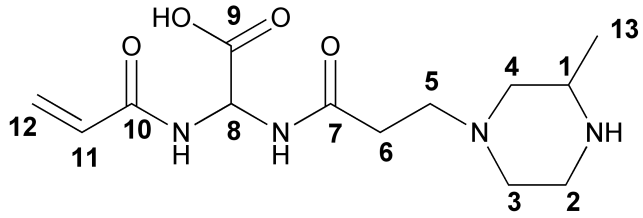

a)

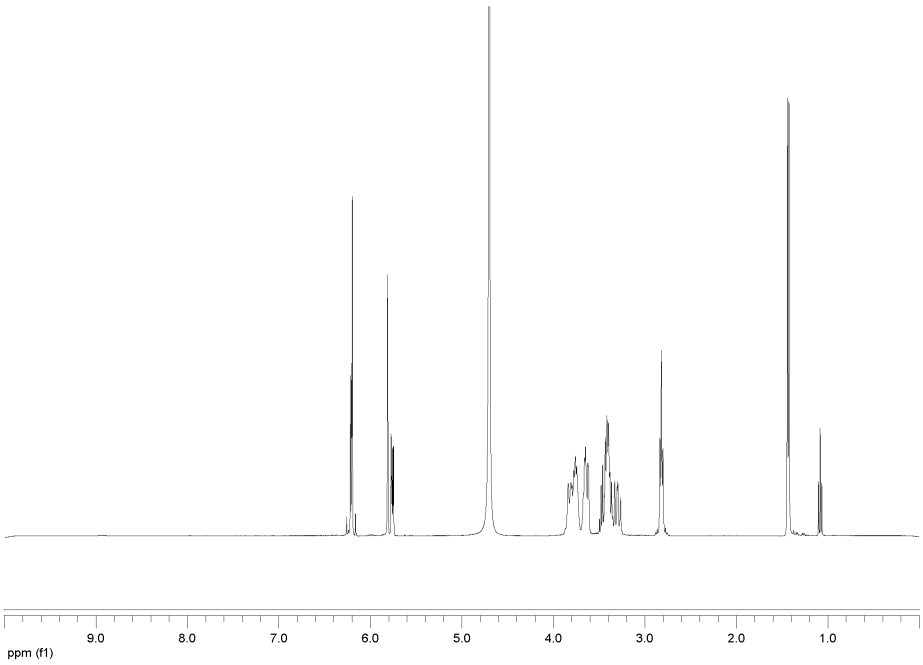

b)

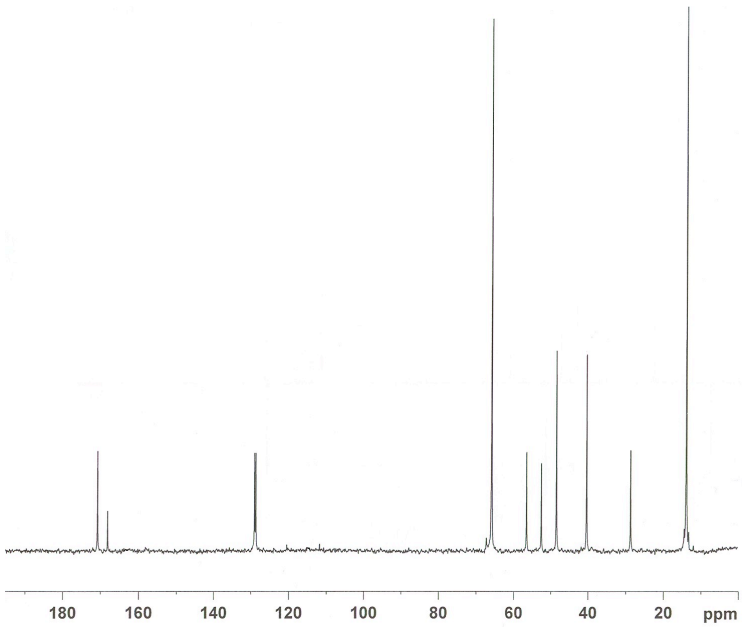

Figure S4.1 B. ^{1}H (Panel a) and ^{13}C (Panel b) NMR spectra (D_2O, ppm) of BAC-MP dimer.

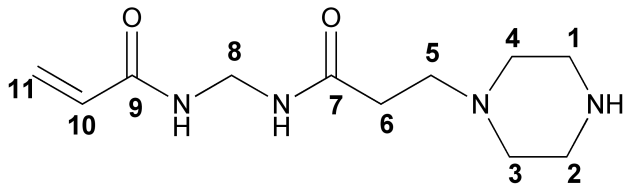

a)

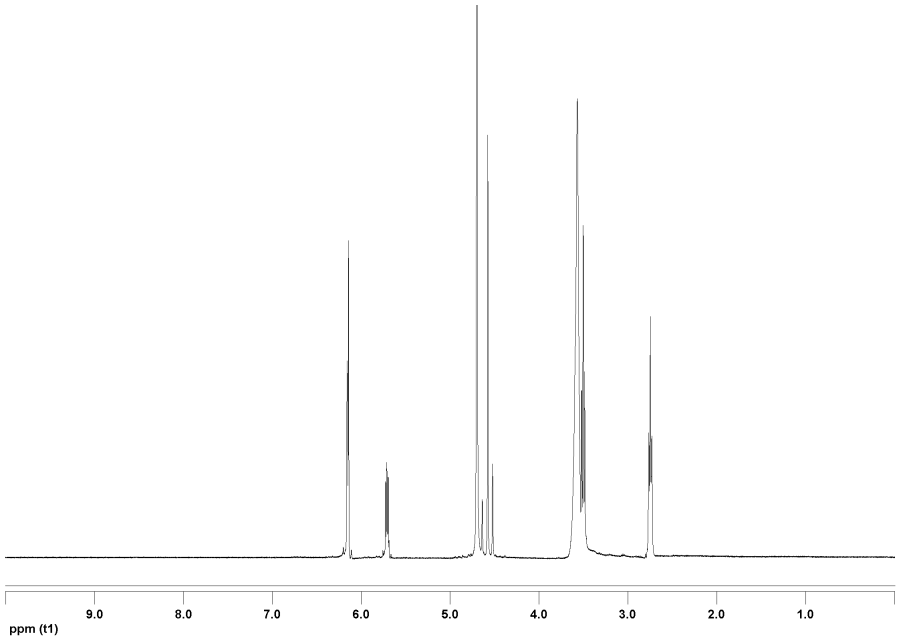

b)

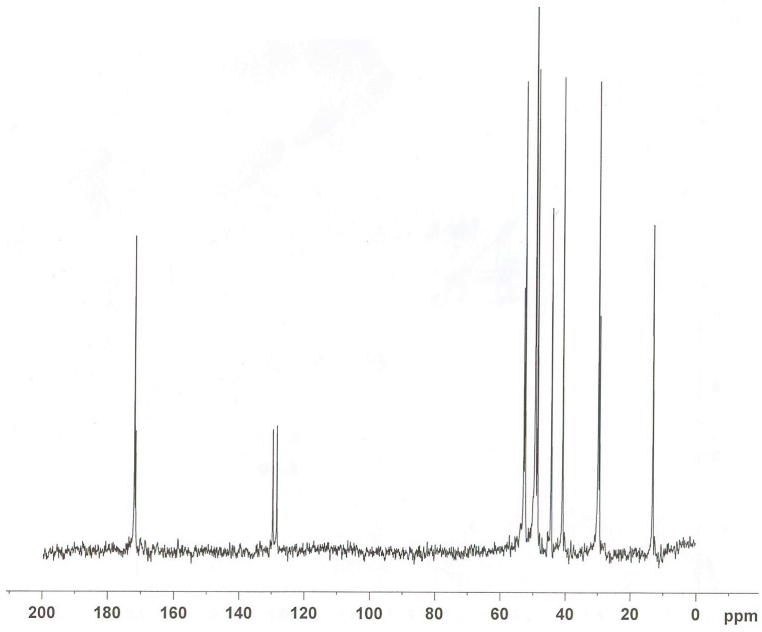

Figure S4.1 C. ^{1}H (Panel a) and ^{13}C (Panel b) NMR spectra (D_2O, ppm) of MBA-P dimer.

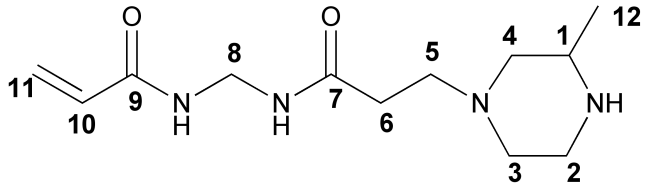

a)

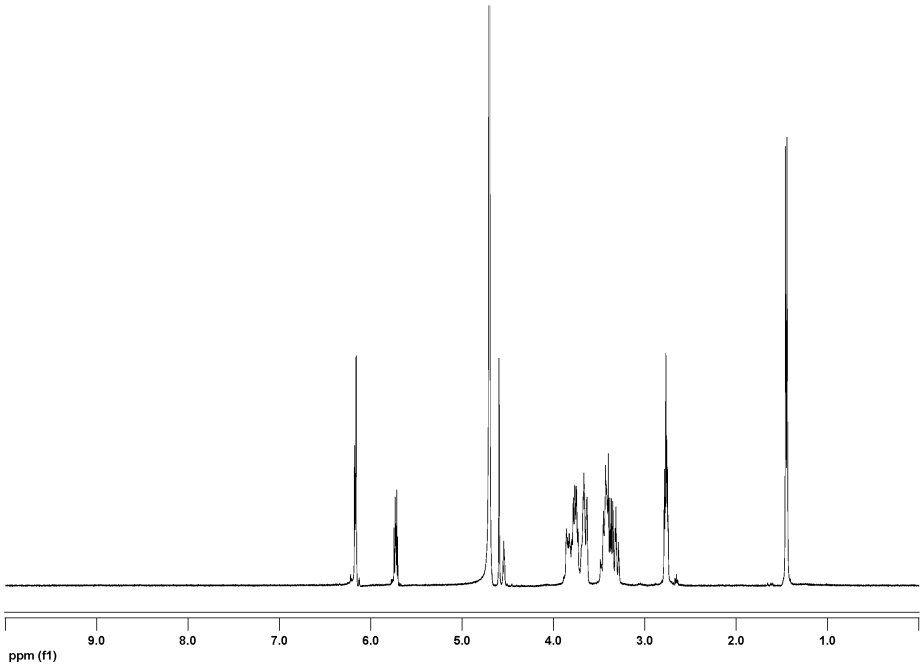

b)

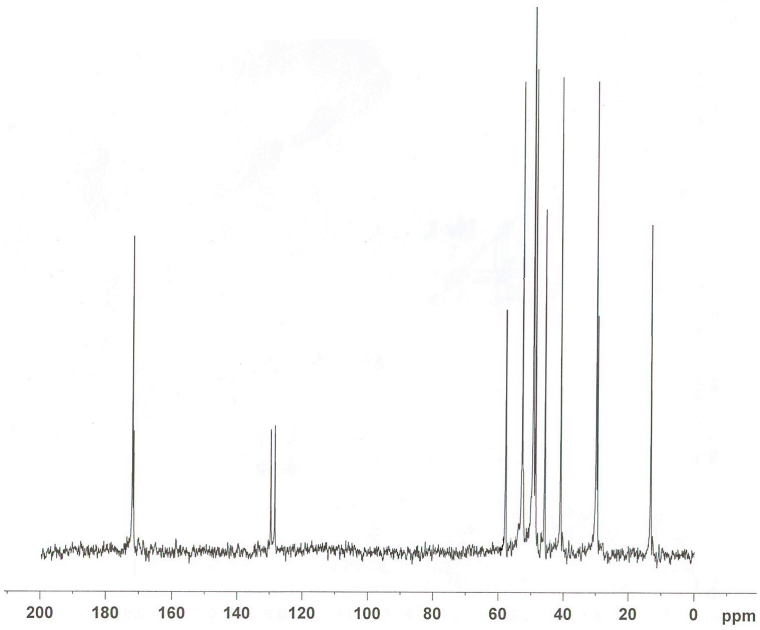

Figure S4.1 D. ^{1}H (Panel a) and ^{13}C (Panel b) NMR spectra (D_2O, ppm) of MBA-MP dimer.

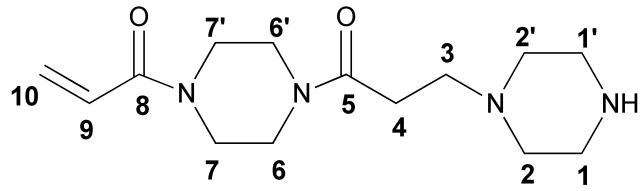

a)

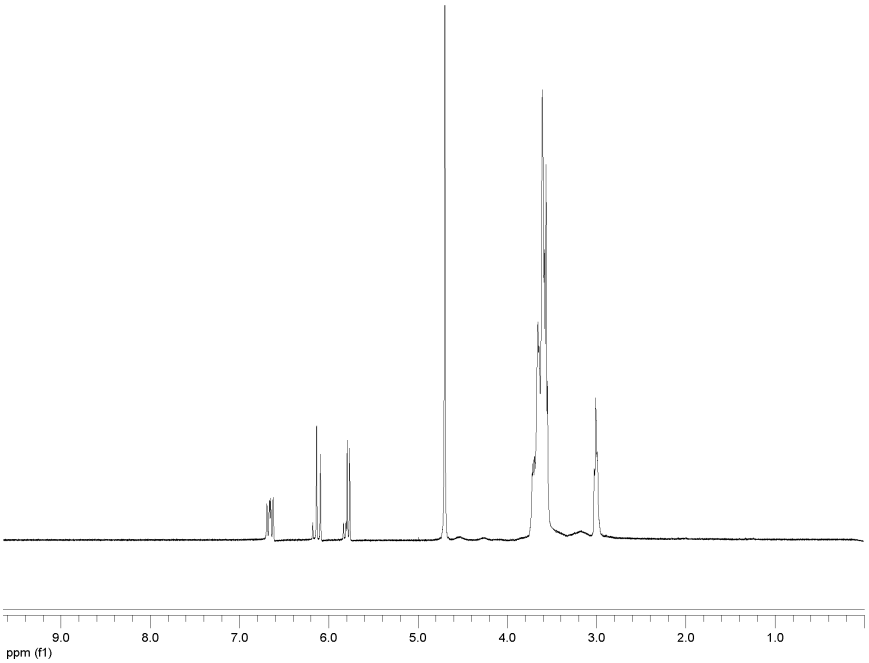

b)

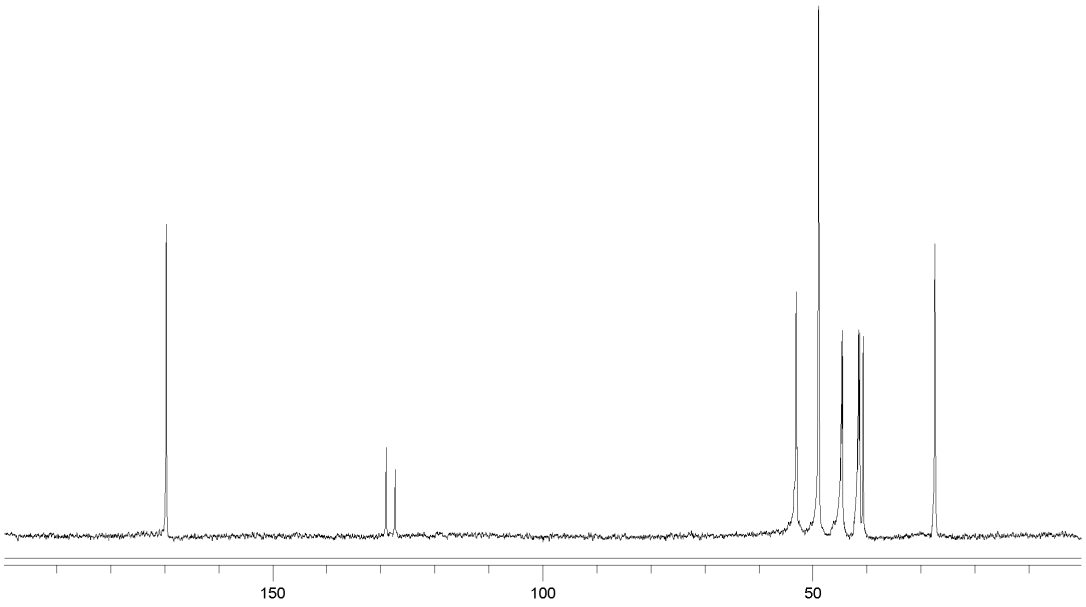

Figure S4.1 E. ^{1}H (Panel a) and ^{13}C (Panel b) NMR spectra (D_2O, ppm) of BP-P dimer.

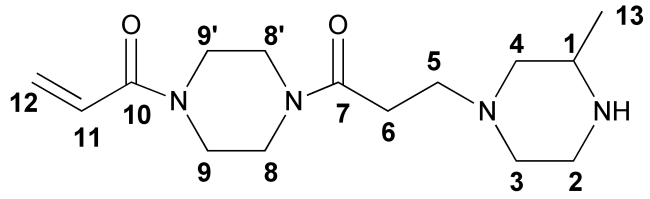

a)

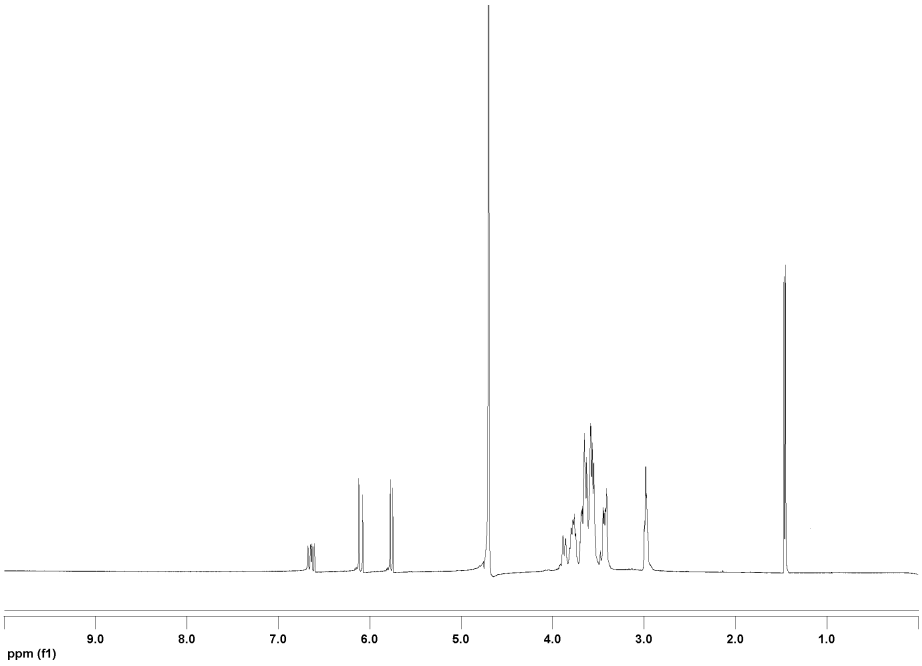

b)

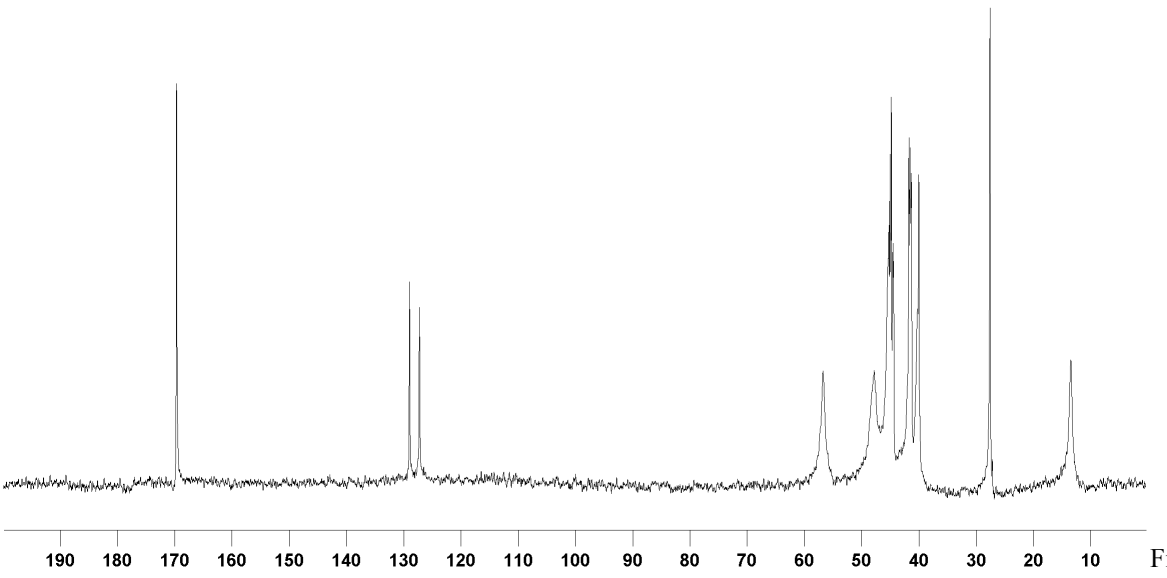

Figure S4.1 F. ^{1}H (Panel a) and ^{13}C (Panel b) NMR spectra (D_2O, ppm) of BP-MP dimer.

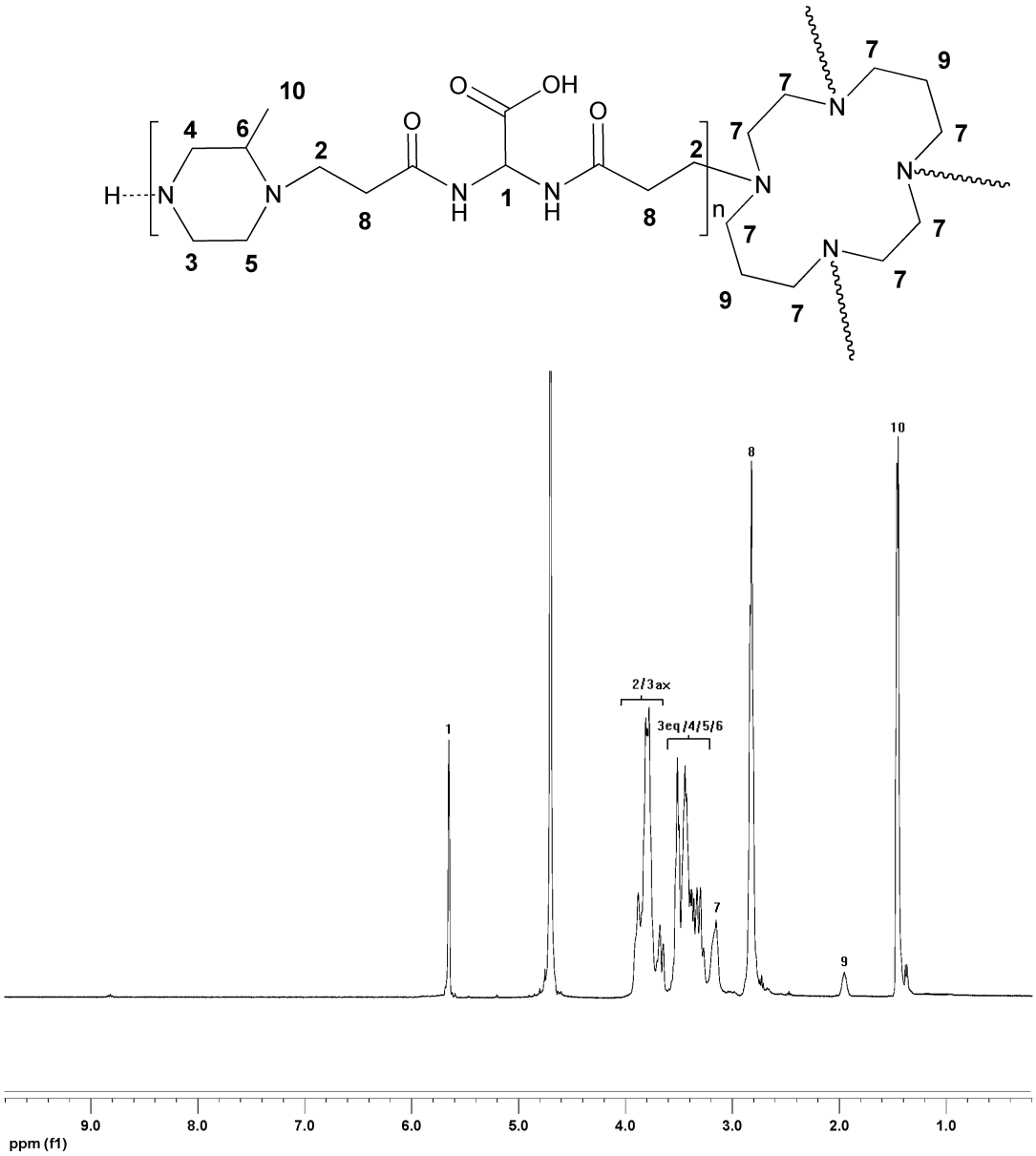

#		1	2	3	4/5/6	7	8	9	10
BAC-MP-Cy	^{1}H	5.65	3.78	3.78; 3.44	3.44	3.16	2.82	1.96	1.45; 1.38

Figure S4.1 G. ^{1}H NMR spectrum (D_2O, ppm) of BAC-MP-Cyclam star-like polymer.

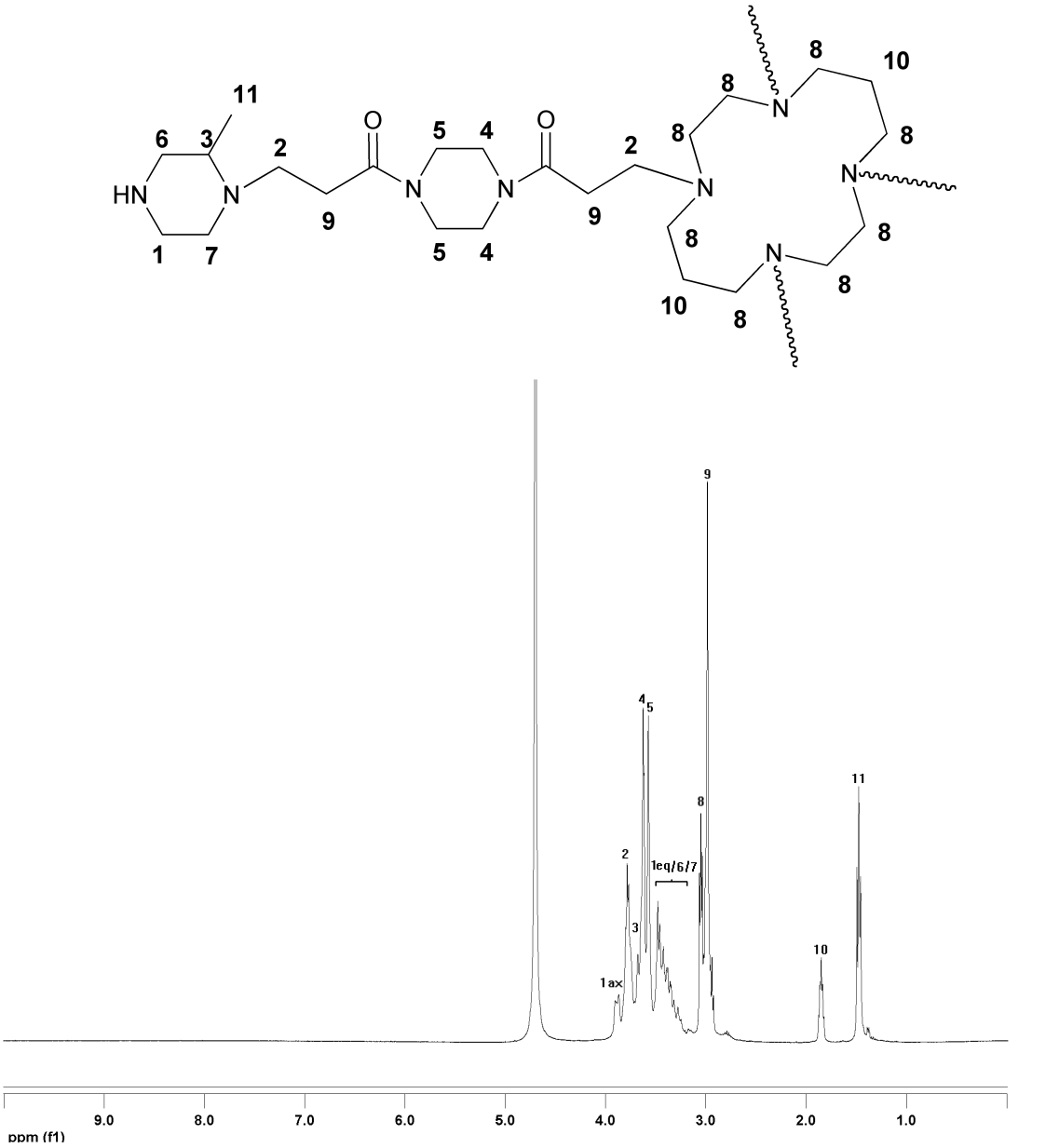

#		1	2	3	4	5	6/7	8	9	10	11
BP-MP-Cy	^{1}H	3.87; 3.48	3.79	3.68	3.63	3.57	3.48	3.05	2.99	1.85	1.48; 1.38

Figure S4.1 H. ^{1}H NMR spectrum (D_2O, ppm) of BP-MP-Cyclam star-like polymer.

4.2 HYPERBRANCHED POLYAMIDOAMINES FOR THE SYNTHESIS OF HIGH-PERFORMANCE BIOMATERIAL

Theoretical considerations. It is commonplace that in polycondensations involving monomers carrying separately two types of complementary functions *"a"* (for instance, reactive hydrogens) and *"b"* (for instance, activated double bonds) of which the minority function is by convention *"a"*, the ruling parameters are the initial stoichiometric ratio *"r"* and the conversion degree *"p"*, defined as in Eq.s 4.2. A and 4.2. B, respectively:

$$r = Na_0/Nb_0 \qquad \text{(Eq. 4.2. A)}$$

Where Na_0 and Nb_0 are the number of *a* and *b* functions initially present

$$p = (Na_0 - Na)/Na_0 \qquad \text{(Eq. 4.2. B)}$$

Where *Na* is the number of *a* functions present at the observation time.

It is apparent that by definition, both *r* and *p* are ≤1. Polycondensations involving monomers bearing more than two functional groups (multi- or polyfunctional polycondensations) lead to insoluble cross-linked products at *p* values higher than a particular value called "critical advancement degree", *"p_c"*. For $p > p_c$ the system looses its mobility, and for this reason p_c is also called "gel point".

When only one polyfunctional monomer is present, the critical advancement degree p_c is predicted by the Flory-Stockmayer formula (Eq. 4.2 C)

$$p_c = \frac{1}{\left[r\left[1 + \rho(f - 2)\right]\right]^{1/2}} \qquad \text{(Eq. 4.2 C)}$$

Where ρ is the fraction of functions belonging to the monomer with functionality >2 with respect to the total amount of the functions of the same type initially present in the system, *f* is the number of functions of the poly functional monomer and *r* is defined as above. It is worth noticing that in Eq. 4.2 C the p_c value depends solely on stoichiometric parameters. In Eq. (4.2 C), p_c and *r* are related. In particular, it exists a "critical stoichiometric ratio", which we sign r_c, under which the system is unable to gel and yields branched, but still soluble polymers. Since *p* (and therefore also p_c) cannot by definition be > 1, the theoretical r_c value is obtained from Eq. (4.2 A) by putting $p_c = 1$ and solving for *r*.

Then we have:

$$r_c = \frac{1}{1 + \rho(f - 2)} \qquad \text{(Eq. 4.2 D)}$$

If ρ= 1, that is, the multifunctional monomer is the only one with this type of function, Eq. (4.2 D) reduces to:

$$r_c = \frac{1}{f - 1} \qquad \text{(Eq. 4.2 E)}$$

Eq. (4.2 C) is not valid in the presence of mono functional compounds. These systems obey to Eq. (4.2 F):

$$p_c = \frac{1}{\left[r(f_{W.A} - 1)(f_{W,B} - 1)\right]^{1/2}} \qquad \text{(Eq. 4.2 F)}$$

Where $f_{W,A}$ and $f_{W,B}$ are the weight average of the monomers functionalities, including the mono functional ones (Eq. 4.2 G):

$$f_{W,A} = \frac{\sum f_{A,j}^2 N_{A,j}}{\sum f_{A,j} N_{A,j}} \quad ; \quad f_{W,B} = \frac{\sum f_{B,j}^2 N_{B,j}}{\sum f_{B,j} N_{B,j}} \qquad \text{(Eq. 4.2 G)}$$

Where *"$f_{A,j}$"* and *"$f_{B,j}$"* represent the functionality of each monomer of type "A" and "B", respectively, and where N_{Aj} and N_{Bj} are the corresponding moles number in the system.

Also in this case it is possible to define a critical ratio, rm_c, below which the system cannot settle into a gel. This will be determined by putting in Eq. 4.2 G $p_c = 1$ and resolving for r. The resultant equation is:

$$rm_c = \frac{1}{(f_{W.A} - 1)(f_{W,B} - 1)} \qquad \text{(Eq. 4.2 H)}$$

In these systems there are two main ways for preparing branched, but completely soluble stepwise polymers, namely employing recipes with $\boldsymbol{r} > \boldsymbol{r_c}$, but stopping the reaction at $\boldsymbol{p} < \boldsymbol{p_c}$, or employing recipes with $\boldsymbol{r} < \boldsymbol{r_c}$ and pushing the reaction to $\boldsymbol{p} \approx 1$. The former method has received attention,[12] [13] but is of rather difficult application, in that the necessary conditions for rendering it reproducible is

[12] **Stockmayer, W., H., J. Chem. Phys., 1943, 11, 45; J. Polym. Soc., 1952, 9, 69.**

[13] **Flory, P., J.; J. Am. Chem. Soc., 1939, 61, 3334; 1941, 63, 3083-3096.**

the perfect knowledge of the polymerization kinetics coupled with the thorough control of all reaction parameters. These conditions, once adjusted for a given system, are hardly extensible to other systems. By contrast, the latter method involves only the reagents' stoichiometric control in the polymerization recipe, which is far easier, and in principle can be extended to all similar systems. Therefore, this method was the only considered in this investigation.

Systems adopted. According to Flory, the equations reported in the previous paragraph are expected to hold if all the functions of the same type present in the system have equal reactivity. We supposed that for the Michael-type additions leading to PAAs this condition was approached by employing from one side symmetrical bisacrylamides, owing the relatively long distance between the activated double bonds, and from the other side symmetrical bis-*sec*-amines and symmetrical macrocyclic polyamines. In particular, we chose a model system (System A) consisting of 2,2-bis-acrylamidoacetic acid as bisacrylamides, piperazine as difunctional amine, 1,4,8,12-tetraazacyclotetradecane as tetra functional amine and, when opportune, morpholine as monofunctional amine. In both cases we performed six polymerization reactions: two with $\boldsymbol{r} > \boldsymbol{r_c}$ and excess amine hydrogens, one with $\boldsymbol{r} > \boldsymbol{r_c}$ and excess double bonds, one with $\boldsymbol{r} < \boldsymbol{r_c}$ and excess mobile hydrogens, one with $\boldsymbol{r} < \boldsymbol{r_c}$ with excess activated double bonds, and one starting from $\boldsymbol{r} > \boldsymbol{r_c}$, but driven to $\boldsymbol{rm} < \boldsymbol{rm_c}$ by the addition of morpholine. The reaction conditions were the same in all cases and according to previous experience should allow reaching $\boldsymbol{p}$ values close to 1.

For comparison purposes, we also studied a parallel a system (System B) in which 1,4,8,12-tetraazacyclotetradecane was replaced by 1, 2-diamonoethane (ethylenediamine), all other reagents being equal. The two systems are not equivalent in that the four mobile hydrogen atoms of ethylenediamine are not expected to be equally reactive towards Michael addition. In fact, the reaction constants of the two hydrogen atoms of primary amines with model acrylamides are known to differ by at least one order of magnitude.[14] Nevertheless, ethylenediamine had been often employed in the past as cross-linking agent for preparing PAA hydrogels.[15] [16]

Compliance with the theory. The results obtained for the system A employed BAC as bisacrylamide are reported in Table 4.2.A.

---

[14] Mather, B., D; Viswanathan, K.; Miller, K., M.; Long, T., E., Progress Polym. Sci., 2006, 31, 487-531.

[15] Ferruti, P., Salamone J., C. Eds, CRC Press Inc.: Boca Ranton, FL, 1996; Vol. 5, pp 3334-3359.

[16] Ferruti, P.; Marchisio, M., A.; Duncan, R., Macromol. Rapid. Commun., 2002, 23, 332-355.

Table 4.2 A. Results obtained for the system A. [a], [e]

N°	BAC	CY	P	M	Excess	r_c [c]	r	$r - r_c$	Mn	Mw
	Mol 10^{-3}	Mol 10^{-3}	Mol 10^{-3}	Mol 10^{-3}					10^{-3}	10^{-3}
3.1	2.6250	0.3750	3.0000	-	H	0.714	0.7	-0.014	4.7	6.1
3.2	2.4975	0.3750	3.0000	-	H	0.714	0.667	-0.047	3.9	5.7
3.3	3.1875	0.3750	3.0000	-	H	0.714	0.85	+0.136	-[b]	-[b]
3.4	1.5630	0.1250	1.0000	-	=	0.714	0.800	+0.086	-[b]	-[b]
3.5	1.0004	0.1250	1.0000	-	H	0.714	0.800	+0.086	-[b]	-[b]
3.6	1.7863	0.1250	1.0000	-	=	0.714	0.709	-0.005	3.7	9.1
3.7	3.9280	0.4550	3.0000	2.0000	H	0.857[d]	0.800	-0.057	3.4	4.6

[a]BAC=2,2'-bisacrylamidoacetic acid, CY=cyclam, P=piperazine, M=morpholine; [b]Formation of microgels was observed after about 7 hrs; [c]Theoretical r_c [d] rm_c value [e] All experiments were performed in triple

The polyaddition experiments with excess double bonds and $r > r_c$ (3.4 of Table 4.2 A) ultimately gave a gel. Apparently, the polyaddition experiment with excess mobile hydrogens and $r > r_c$ (3.3 and 3.5 of Table 4.2 A) did not gel, as expected, but DLS analysis revealed that it contained microgels, a behavior already observed for widely different systems where the principle of equal reactivity was not strictly obeyed. This result suggests that three of the four hydrogens of 1,4,8,12-tetraazacyclotetradecane are significantly more reactive than the fourth one. All polyaddition systems with $r < r_c$ (3.1, 3.2 and 3.6 of Table 4.2 A) did not gel irrespective of the nature of the excess function, including 3.7 of Table 4.2 A, in which the addition of morpholine brought to non-gelling conditions a system that otherwise would have gelled. DLS analysis excluded in all of these systems the presence of micro-or nanogels.

The results obtained with System B are reported in Table 4.2 B. In this case, two different bisacrylamides, namely BAC and BP, were used. Conflicting results were obtained among the polyaddition experiments performed with excess amine hydrogens (1.1-1.4, 1.8-1.11, 1.13, 2.1-2.4, 2.8-2.11, 2.13 of Table 4.2 B) and those with excess double bonds (1.5-1.7, 1.12, 2.5-2.7, 2.12 of Table 4.2 B). In the former case, when $r > r_c$ the substitution of ethylenediamine for 1,4,8,12-tetraazacyclotetradecane, with the exception of the reactions 1.3, 1.11, 2.3 and 2.11, led to reaction mixtures that neither gelled, nor contained microgels.

Table 4.2.2. Results obtained for the system B.[a], [e]

N°	BAC	EDA	P	M	Excess	r_c[c]	r	$r - r_c$	Mn	Mw
	Mol 10^{-3}	Mol 10^{-3}	Mol 10^{-3}	Mol 10^{-3}					10^{-3}	10^{-3}
1.1	2.6250	0.3750	3.0000	-	H	0.714	0.700	-0.014	4.3	6.8
1.2	2.4975	0.3750	3.0000	-	H	0.714	0.667	-0.047	3.9	5.7
1.3	3.1875	0.3750	3.0000	-	H	0.714	0.850	+0.136	-[b]	-[b]
1.4	1.6665	0.2500	2.0000	-	H	0.714	0.667	-0.047	2.8	4.3
1.5	4.9342	0.3750	3.0000	-	=	0.714	0.760	+0.046	-[b]	-[b]
1.6	5.1370	0.3750	3.0000	-	=	0.714	0.730	+0.016	-[b]	-[b]
1.7	5.6222	0.3750	3.0000	-	=	0.714	0.667	-0.047	2.2	3.5
1.8	3.9280	0.4550	3.0000	2.0000	H	0.857[d]	0.800	-0.057	3.4	4.6
1.9	3.5000	1.3333	3.0000	-	H	0.515	0.618	+0.103	3.4	5.3
1.10	3.3333	1.3333	3.0000	-	H	0.515	0.588	+0.073	2.9	4.7
1.11	4.2500	1.3333	3.0000	-	H	0.515	0.750	+0.235	-[b]	-[b]
1.12	5.0000	0.8889	2.0000	-	=	0.515	0.756	+0.241	-[b]	-[b]
1.13	4.8000	1.3333	3.0000	2.0000	H	0.606[d]	0.720	+0.114	3.1	4.2
N°	BP	EDA	P	M	Excess	r_c[c]	r	$r - r_c$	Mn	Mw
	Mol 10^{-3}	Mol 10^{-3}	Mol 10^{-3}	Mol 10^{-3}					10^{-3}	10^{-3}
2.1	2.625	0.3750	3.0000	-	H	0.714	0.700	-0.014	5.1	7.9
2.2	2.4975	0.3750	3.0000	-	H	0.714	0.667	-0.047	4.2	6.5
2.3	3.1875	0.3750	3.0000	-	H	0.714	0.850	+0.136	-[b]	-[b]
2.4	1.6665	0.2500	2.0000	-	H	0.714	0.667	-0.047	3.3	4.9
2.5	4.9342	0.3750	3.0000	-	=	0.714	0.760	+0.046	-[b]	-[b]
2.6	5.1370	0.3750	3.0000	-	=	0.714	0.730	+0.016	-[b]	-[b]
2.7	5.6222	0.3750	3.0000	-	=	0.714	0.667	-0.047	2.5	3.9
2.8	3.928	0.4550	3.0000	2.0000	H	0.857[d]	0.800	-0.057	3.1	4.2
2.9	3.5000	1.3333	3.0000	-	H	0.515	0.618	+0.103	3.4	5.3
2.10	3.3333	1.3333	3.0000	-	H	0.515	0.588	+0.073	2.9	4.7
2.11	4.2500	1.3333	3.0000	-	H	0.515	0.750	+0.235	-[b]	-[b]
2.12	5.0000	0.8889	2.0000	-	=	0.515	0.756	+0.241	-[b]	-[b]
2.13	4.8000	1.3333	3.0000	2.0000	H	0.606[d]	0.720	0.114	2.9	3.8

[a]BAC=2,2'-bisacrylamidoacetic acid, EDA=ethylenediamine, P=piperazine, M=morpholine; [b]Formation of microgels was observed after about 7 hrs; [c]Theoretical r_c [d] rm_c value [e] All experiments were performed in triple

By contrast, the results of the polyadditions performed with excess double bonds gelled, in full agreement with the theory. Perhaps, in the latter case considerable excess of double bonds provides a suitable environment to make possible the reaction of all four amine hydrogens without significant difference in reactivity. The ***r*** and r_c values reported in 4.2 A and 4.2 B were calculated by putting forward as a hypothesis that both 1,4,8,12-tetraazacyclotetradecane and ethylenediamine carry four reactive hydrogens, that is, they react as tetrafunctional monomers. In Tables 4.2 C and 4.2 D, the same results of Tables 4.2 A and 4.2 B are correlated with ***r*** and r_c values calculated by hypothesizing that the same amines react as trifunctional monomers.

Table 4.2 C. Results obtained for system A considering cyclam as trifuntional monomers. [(a), (e)]

N°	BAC Mol 10^{-3}	CY Mol 10^{-3}	P Mol 10^{-3}	M Mol 10^{-3}	Excess	r_c	r	$r - r_c$	Mn 10^{-3}	Mw 10^{-3}
3.1	2.6250	0.3750	3.0000	-	H	0.864	0.737	-0.127	4.7	6.1
3.2	2.4975	0.3750	3.0000	-	H	0.864	0.701	-0.163	3.9	5.7
3.3	3.1875	0.3750	3.0000	-	H	0.864	0.895	0.031	-	-
3.4	1.5630	0.1250	1.0000	-	=	0.864	0.760	-0.104	-	-
3.5	1.0004	0.1250	1.0000	-	H	0.864	0.842	-0.022	-	-
3.6	1.7863	0.1250	1.0000	-	=	0.864	0.665	-0.199	3.7	9.1
3.7	3.9280	0.4550	3.0000	2.0000	H	1.000	0.839	-0.161	3.4	4.6

[(a)]BAC=2,2'-bisacrylamidoacetic acid, CY=cyclam, P=piperazine, M=morpholine; [(b)]Formation of microgels was observed after about 7 hrs; [(c)]Theoretical r_c [(d)] rm_c value [(e)] All experiments were performed in triple

It is immediately apparent that as regards gelling 1,4,8,12-tetraazacyclotetradecane does not fit into this hypothesis and reasonably follows the theory only as tetrafuctional monomer. Ethylenediamine reacts as tetrafunctional monomer only with excess double bonds, while with excess hydrogens it follows the theory only as trifunctional monomer, with the additional qualification that even as such it has a tendency to form microgels instead of gelling completely (1.8 of Table 4.2 D). Apparently, two out of the four hydrogens, of ethylenediamine (one per nitrogen) are significantly more reactive than the third one, which in turn is more reactive than the fourth one. In other words, the experimental data suggest that ethylenediamine contains three kinds of amine hydrogens of unequal reactivity. The first two belong to primary amines and can be reasonably expected to be highly reactive.

Table 4.2 D. Results obtained for system B considering EDA as trifuntional monomers. [a], [e]

N°	BAC	EDA	P	M	Excess	r_c[c]	r	$r - r_c$	Mn	Mw
	Mol 10^{-3}	Mol 10^{-3}	Mol 10^{-3}	Mol 10^{-3}					10^{-3}	10^{-3}
1.1	2.6250	0.3750	3.0000	-	H	0.864	0.737	-0.127	4.3	6.8
1.2	2.4975	0.3750	3.0000	-	H	0.864	0.701	-0.163	3.9	5.7
1.3	3.1875	0.3750	3.0000	-	H	0.864	0.895	+0.031	-[b]	-[b]
1.4	1.6665	0.2500	2.0000	-	H	0.864	0.701	-0.163	2.8	4.3
1.5	4.9342	0.3750	3.0000	-	=	0.864	0.736	-0.128	-[b]	-[b]
1.6	5.1370	0.3750	3.0000	-	=	0.864	0.693	-0.161	-[b]	-[b]
1.7	5.6222	0.3750	3.0000	-	=	0.864	0.634	-0.230	2.2	3.5
1.8	3.9280	0.4550	3.0000	2.0000	H	1.000[d]	0.839	-0.161	3.4	4.6
1.9	3.5000	1.3333	3.0000	-	H	0.714	0.7000	-0.014	3.4	5.3
1.10	3.3333	1.3333	3.0000	-	H	0.714	0.6666	-0.047	2.9	4.7
1.11	4.2500	1.3333	3.0000	-	H	0.714	0.8500	+0.136	-[b]	-[b]
1.12	5.0000	0.8889	2.0000	-	=	0.714	0.6666	-0.048	-[b]	-[b]
1.13	4.8000	1.3333	3.0000	2.0000	H	0.857[d]	0.8000	-0.057	3.1	4.2
N°	BP	EDA	P	M	Excess	r_c[c]	r	$r - r_c$	Mn	Mw
	Mol 10^{-3}	Mol 10^{-3}	Mol 10^{-3}	Mol 10^{-3}					10^{-3}	10^{-3}
2.1	2.625	0.3750	3.0000	-	H	0.864	0.737	-0.127	5.1	7.9
2.2	2.4975	0.3750	3.0000	-	H	0.864	0.701	-0.163	4.2	6.5
2.3	3.1875	0.3750	3.0000	-	H	0.864	0.895	+0.031	-[b]	-[b]
2.4	1.6665	0.2500	2.0000	-	H	0.864	0.702	-0.163	3.3	4.9
2.5	4.9342	0.3750	3.0000	-	=	0.864	0.736	-0.128	-[b]	-[b]
2.6	5.1370	0.3750	3.0000	-	=	0.864	0.693	-0.161	-[b]	-[b]
2.7	5.6222	0.3750	3.0000	-	=	0.864	0.634	-0.230	2.5	3.9
2.8	3.928	0.4550	3.0000	2.0000	H	1.000[d]	0.839	-0.161	3.0	3.9
2.9	3.5000	1.3333	3.0000	-	H	0.714	0.7000	-0.014	3.4	5.3
2.10	3.3333	1.3333	3.0000	-	H	0.714	0.6666	-0.047	2.9	4.7
2.11	4.2500	1.3333	3.0000	-	H	0.714	0.8500	+0.136	-[b]	-[b]
2.12	5.0000	0.8889	2.0000	-	=	0.714	0.6666	-0.048	-[b]	-[b]
2.13	4.8000	1.3333	3.0000	2.0000	H	0.857[d]	0.8000	-0.057	2.9	3.8

[a]BAC=2,2'-bisacrylamidoacetic acid, EDA=ethylenediamine, P=piperazine, M=morpholine; [b]Formation of microgels was observed after about 7 hrs; [c]Theoretical r_c [d] rm_c value [e] All experiments were performed in triple

The remaining two belong to already reacted amine groups and according to previous findings are expected to be significantly less reactive. Moreover, when one of them has reacted, the remaining one probably reacts even more sluggishly owing to the steric hindrance provided by the double substitution to the neighboring nitrogen, which in this sense is probably more effective if inserted in a branched molecular context. Then, reaction systems containing excess amine hydrogens cannot behave in the same way as those containing excess double bonds. In the former case, the more reactive hydrogens react first leaving little or no double bonds available for the last one that under these conditions does not act as structure-forming, but rather as structure-breaking group. This explains why ethylenediamine follows the theory as a trifunctional monomer as regards gelling. On the opposite, with excess double bonds all hydrogens are ultimately forced to react and contribute to structure formation irrespective of their relative reactivities. Consequently, ethylenediamine fully displays its potential as tetrafunctional monomer and complies with the theory as such.

Properties of the polymers. According to theory,[17] the branched PAAs obtained under non-gelling conditions should have a modest average polymerization degree ($X_n \approx 4$), coupled with high polydispersity ($X_w \approx 10$). We did not endeavor to study in detail the compliance with theory of our systems up to the point of molecular weight distribution. Instead, we aimed at establishing a synthetic protocol for preparing branched PAAs with reasonably high molecular weight and narrow- to moderate molecular weight distribution. To this purpose, we had to resort to fractionation techniques. The crude products were ultrafiltered through a membrane with theoretical cut-off 1000 and the retained fraction recovered by lyophilization. The molecular weights of the resultant products were then determined by SEC-LALS. The results are reported in Tables 4.2 A and 4.2 B. The reaction yield for all reactions was whitin 45-55 %. It may be observed that, in agreement with the theory, the final products were obtained in relatively low yields and with molecular weights in the order of a few thousands, that is, significantly lower that those usually achieved by linear PAAs. In front of this, each polymer molecule had multiple chain ends carrying only one type of reactive function, either amine or activated double bond according to the excess function present in the polymerization recipe. This opens the way to further functionalization useful for the synthesis of tailor-made polymers.

[17] **Odian, G., Principles of polymerization, Wiley Intersci., New York, 2004, p 106.**

4.3 POLYAMIDOAMINE-BASED MULTILAYER NANOPARTICLES AS POTENTIAL GENE AND PROTEIN DELIVERY SYSTEM

The investigation reported in this section concerned PAAs affording to multilayer nanoparticles via their layer-by-layer self-assembling in aqueous solutions at pH 7.4. Four PAAs, named ISA1, AGMA1, ISA23 and BACEDDA,[18] [19] were synthesized, with or without spin label (TEMPO), as previously described in order to obtain four couple of oppositely charged polyelectrolytes, namely ISA1/ISA23, ISA1/BACEDDA, AGMA1/ISA23 and AGMA1/BACEDDA, able to form nanoparticles when mixed at proper charge ratio. Their salient characteristics are shown in Table 4.3 A.

Table 4.3 A. Equivalent charge per mol of the PAAs at pH 7.4.

Sample	Cationic (charge/mol)	Anionic (charge/mol)
ISA1	1.020	-
AGMA1	0.529	-
ISA23	-	0.333
BACEDDA	-	1.979

Briefly, ISA1 and BACEDDA are purely cationic and purely anionic, respectively; whereas ISA23 and AGMA1 are amphoteric polyelectrolytes able to change their average charge as function of the pH. In particular, at pH 7.4 ISA23 is prevailingly anionic and AGMA1 is prevailingly cationic. Among PAAs, these were chosen because of their widely assessed high biocompatibility.

Core formation at different charge ratios (pH 7.4). Attempts were performed to prepare different nanoparticles from the four PAAs at different cationic/anionic mole ratio, for screening the best conditions in which stable and small cores could be made. At pH 7.4, ISA1 bears a full positive charge per monomer unit, whereas ISA23 is negatively charged, but less so, -0.33/monomer unit (Table 4.3 A). When used to prepare the core for subsequent particles, these two polymers form structures that are circa 1.0 (± 0.2) μm in diameter, with a surface charge of -20.0 (± 7.0) mV, with no obvious correlation of these properties on cationic to anionic monomer mole ratio ([cat]/[an]), Figure 4.3 A. For the ISA1/BACEDDA pair, where the latter polymer is anionic but bears twice as much charge/monomer as the cationic component ISA1 (-1/monomer), the complexes formed from these two polymers are much smaller than the ISA1/ISA23 pair, namely 0.5 (±0.1) μm in diameter,

[18] Richardson, S.; Ferruti, P.; Duncan, R., J. Drug Targeting, 1999, 6, 391-404.

[19] Ranucci, E.; Ferruti, P.; Lattanzio, E.; Manfredi, A.; Rossi, M. Mussini, P.; et al., J. Polym. Sci.: Part A:Polym. Chem., 2009, 47, 6977-6991.

with a surface charge that increases from -40.0 (± 5.0) to +10 (± 5.0) mV with increasing cationic/ anionic mole ratio, Figure 4.3 B.

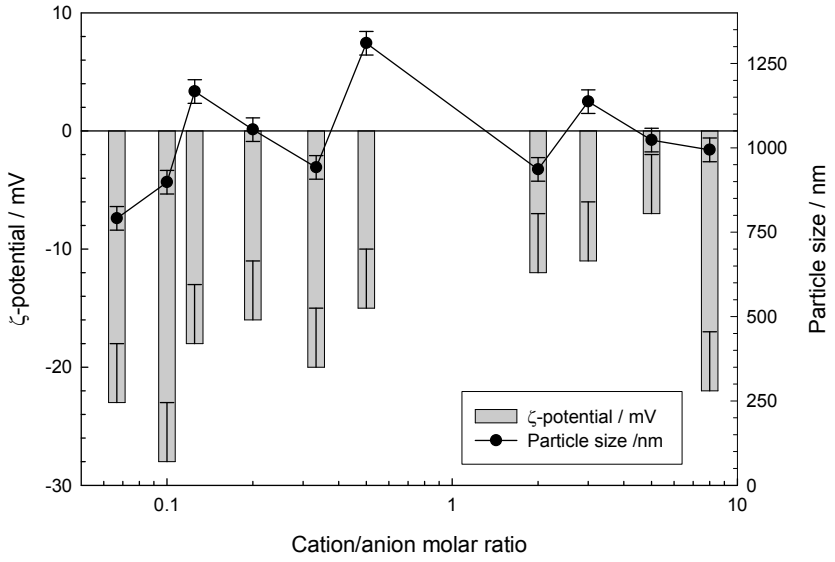

Figure 4.3 A. ζ-potential and particle size for nanoparticles formed from NP1 (ISA1/ISA23) as a function of mole ratio.

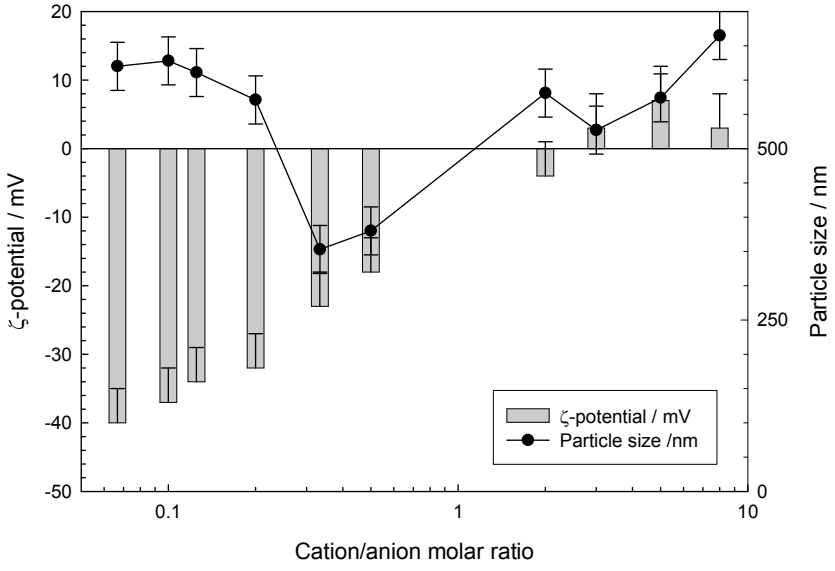

Figure 4.3 B. ζ-potential and particle size for nanoparticles formed from NP2 (ISA1/BACEDDA) as a function of mole ratio.

The particle size goes through a minimum around [cat]/[an] = 0.4. Similarly, the AGMA1/ISA23 pair show a pronounced dependence of size and surface charge on composition, with the size increasing from 200 to 600 (± 50.0) nm and the charge -15 to +3 (± 5.0) mV, reflecting the relative charges on the AGMA1 (+0.5/monomer) and ISA23 (-0.33/monomer) units, Figure 4.3 C. For this system, the minimum in particle size is shifted towards lower [cat]/[an] = 0.2. Finally, for the AGMA1/BACEDDA complexes, there is a pronounced switch from anionic surface charge to cati-

onic surface charge with increasing cationic/anionic ratio, passing through the point of zero charge (PZC) at a mole ratio of 2, roughly consistent with the relative charges on the AGMA1 (+0.5/monomer) and BACEDDA (-2/monomer) monomer units. Here, the size of the complex mirrors the charge, increasing with mole ratio, Figure 4.3 D. Again a minimum is seen in the particle size vs composition dependence, but at a [cat]/[an] = 0.5.

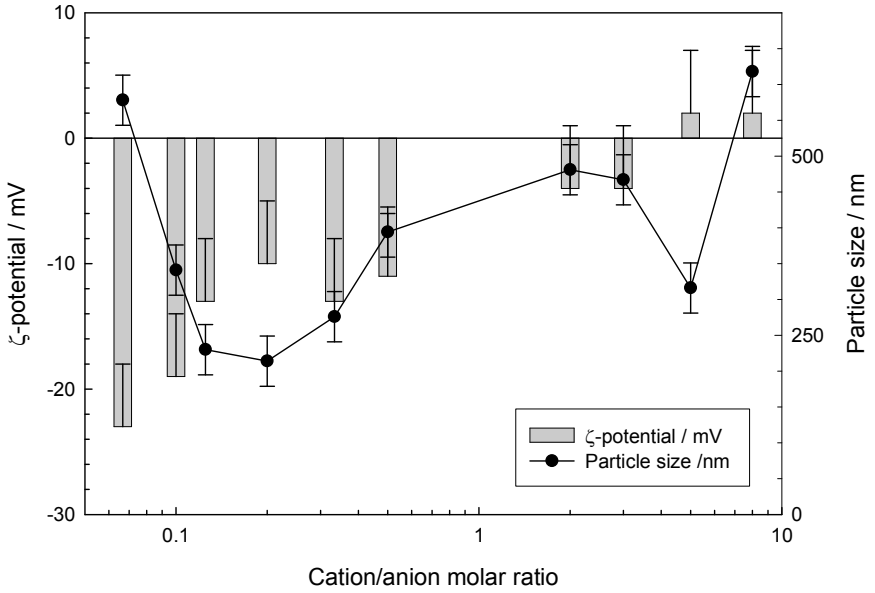

Figure 4.3 C. ζ-potential and particle size for nanoparticles formed from NP3 (AGMA1/ISA23) as a function of mole ratio.

At high values of [cat]/[an], viz5-8, the charge on the particles follows the order ISA1/ISA23 < AGMA1/ISA23 < ISA1/BACEDDA < AGMA1/BACEDDA whereas at low values of [cat]/[an], the order is somewhat different AGMA1/BACEDDA < ISA1/BACEDDA < ISA1/ISA23 < AGMA1/ISA23; both of these trends are consistent with the charge on the respective monomers at pH 7.4 [ISA1 (+1), AGMA1 (+0.5), ISA23 (-0.33), BACEDDA (-2)].

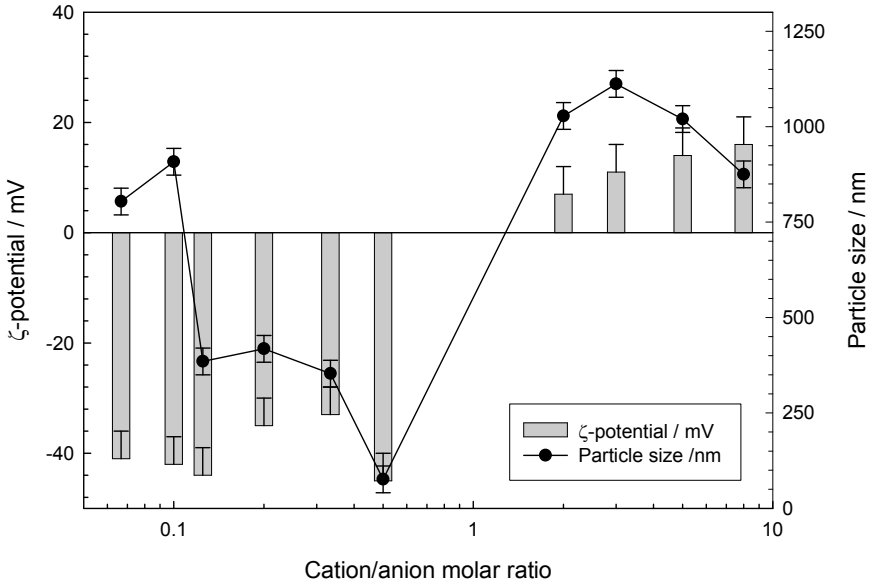

Figure 4.3 D. ζ-potential and particle size for nanoparticles formed from NP4 (AGMA1/BACEDDA) as a function of mole ratio.

Formation of multilayer nanoparticles (pH 7.4). Given this detailed knowledge of the charge and size of these polymer-polymer complexes, a fixed ratio of two oppositely charged polymers was selected in the various combinations, to form the core of the particles on which to build the layer-by-layer assemblies. Such self-assembling structures were formed successfully from all combinations of these polymers, with three nanoparticle assemblies (ISA1/BACEDDA – NP2; ISA23/ AGMA1 – NP3; AGMA1/BACEDDA – NP4) showing charge inversion through the various layers, and some electrostatic induced collapse of the particle size, Figures 4.3 E-H.

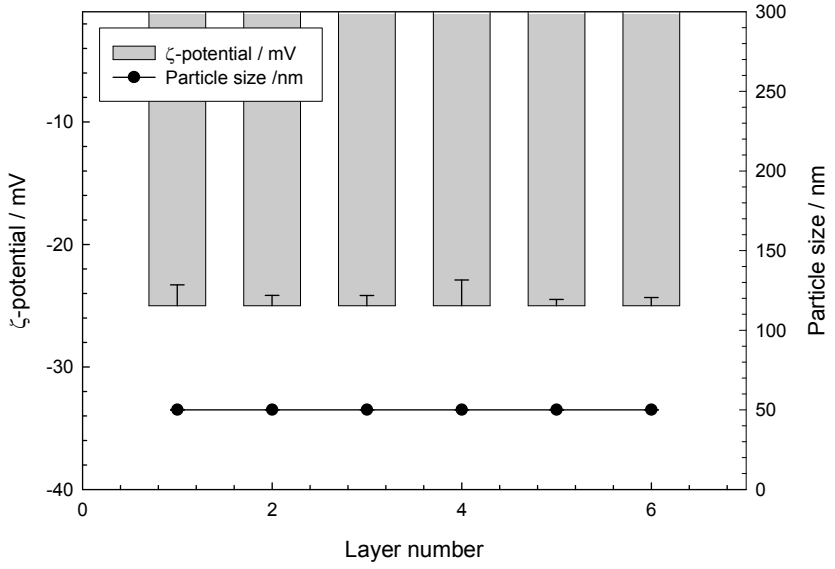

Figure 4.3 E. ζ-potential and particle size for nanoparticles formed from NP1 (ISA1/ISA23).

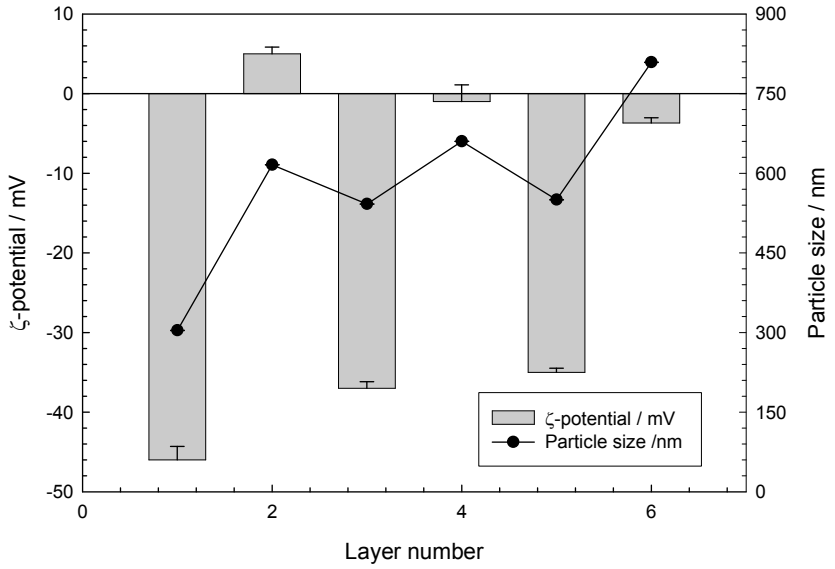

Figure 4.3 F. ζ-potential and particle size for nanoparticles formed from NP2 (ISA1/BACEDDA).

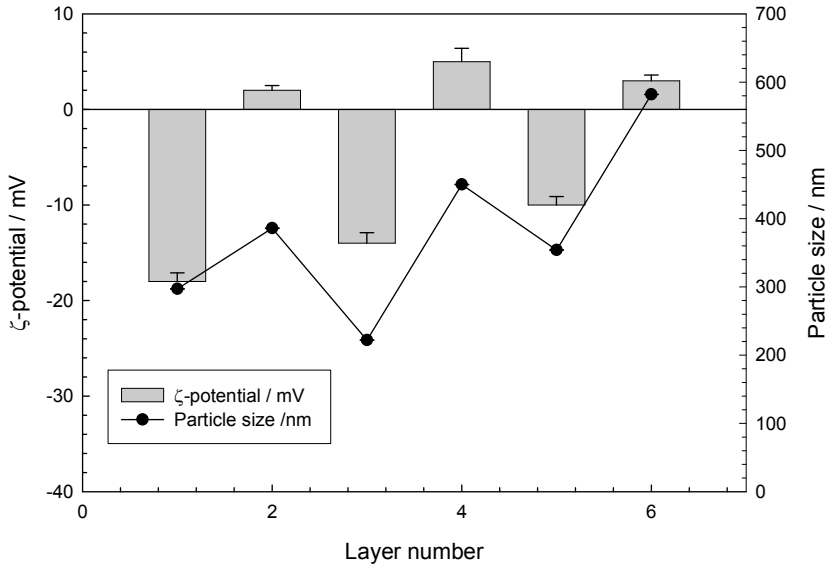

Figure 4.3 G. ζ-potential and particle size for nanoparticles formed from NP3 (AGMA1/ISA23).

The ISA1/ISA23 (NP1) combination showed no such charge inversion, and we conclude that stable nanoparticles were not formed. Charge inversion arises due to the presence of excess of either the cationic or anion charge within the alternating layers. For NP2, NP3 and NP4, the absolute zeta-potential and the change in that potential as the layer number increases are greater when the difference in charge/monomer is largest c.f. Figure 4.3 F, NP2 formed from the combination of the +1 charge on ISA1 and the -2 on BACEDDA and Figure 4.3 G, NP3 formed from the +0.5 charge on AGMA1 and -0.33 on ISA23. The seemingly erratic increase in particle size is a manifestation of an expansion of the structure as the layers are built up, with a smaller superimposed collapse ascribed

to an electrostatically driven association of the oppositely charged monomers, with the greatest effect imposed by the much greater charge density of the anionic component.

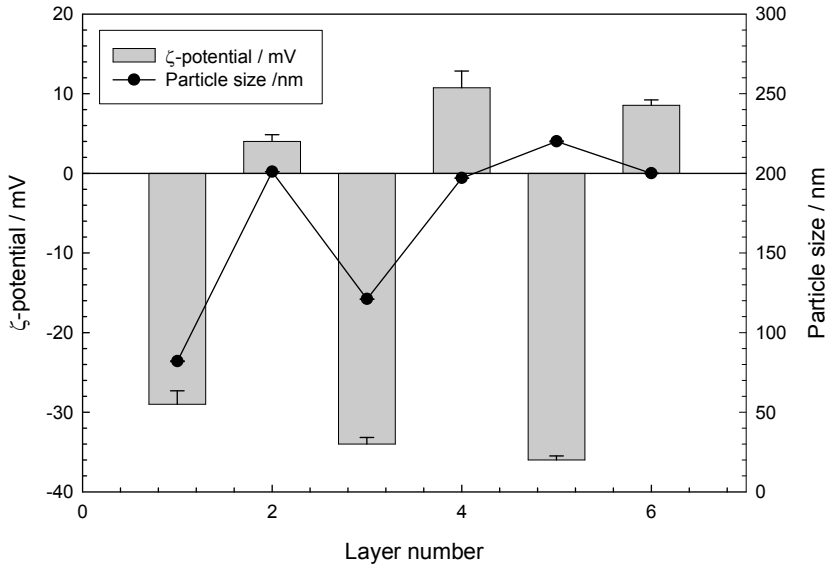

Figure 4.3 H. ζ-potential and particle size for nanoparticles formed from NP4 (AGMA11/BACEDDA).

One approach to quantify the structure and dynamics within the various layers forming the multi-layer particles is to use an EPR label grafted to one of the polymers located within a specific layer. Here, TEMPO-labelled versions of ISA23, ISA1 and AGMA1 have been incorporated into the particles, as per Scheme 4.3 A. The spin-labelled nanoparticles obtained by using these method are reported in Table 4.3 B.

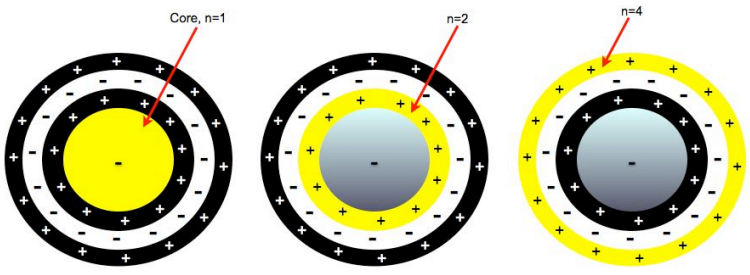

Scheme 4.3 A. Nomenclature pertaining to the location of the spin-label within the multi-layer nanoparticles. The anionic core particle is defined as n=1, such that the first i this example, cationic polymer layer corresponds to n=2, the second to n=4, whereas the anionic polymers is n=3.

Table 4.3 B. Spin-labelled multilayer (4 layer) nanoparticles obtained at pH 7.4 labelled in the core (NP1{n=1}), (NP2 {n=1}), (NP3{n=1}), in the first (NP1{n=2}), (NP2 {n=2}), (NP3{n=2}) and in the third (NP1{n=4}), (NP2 {n=4}), (NP3{n=4}).

Sample	ISA1	AGMA1	ISA23	BACEDDA
NP1{n=1}	+	-	(+)	-
NP1{n=2}	+	-	(+)	-
NP1{n=4}	+	-	(+)	-
NP2{n=1}	(+)	-	-	+
NP2{n=2}	(+)	-	-	+
NP2{n=4}	(+)	-	-	+
NP3{n=1}	-	(+)	+	-
NP3{n=2]	-	(+)	+	-
NP3{n=4}	-	(+)	+	-
NP4{n=1}	-	(+)	-	+
NP4{n=2}	-	(+)	-	+
NP4{n=4}	-	(+)	-	+

The spin-labelled probe is reported in parentheses.

Two independent quantities are measurable in an EPR spin-label experiment, the hyperfine coupling constant (polarity) sensed by the spin-label (defined largely by the degree of hydration) and the rotational correlation time, the former extracted from the position of the resonance lines, the latter from the lineshapes, Figures 4.3 I-M. Also presented for comparison, is the equivalent parameter for the TEMPO-labelled polymer in free solution, i.e. in the absence of any second complexing polymer.

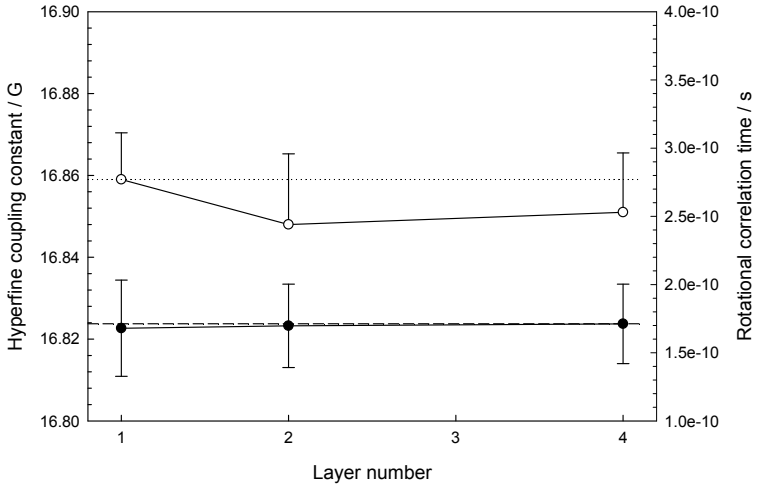

Figure 4.3 I. Hyperfine coupling constant (open symbols) and rotational correlation time (filled symbols) as a function of label position for nanoparticles formed from NP1 (ISA1/ISA23). The dotted line corresponds to the hyperfine coupling constant for the labelled polymer in solution, whereas the dashed line is its rotational correlation time.

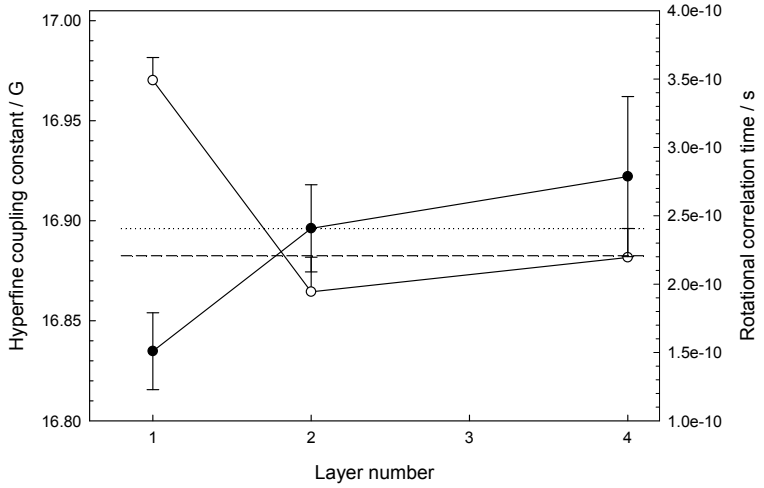

Figure 4.3 K. Hyperfine coupling constant (open symbols) and rotational correlation time (filled symbols) as a function of label position for nanoparticles formed from NP2 (ISA1/BACEDDA). The dotted line corresponds to the hyperfine coupling constant for the labelled polymer in solution, whereas the dashed line is its rotational correlation time.

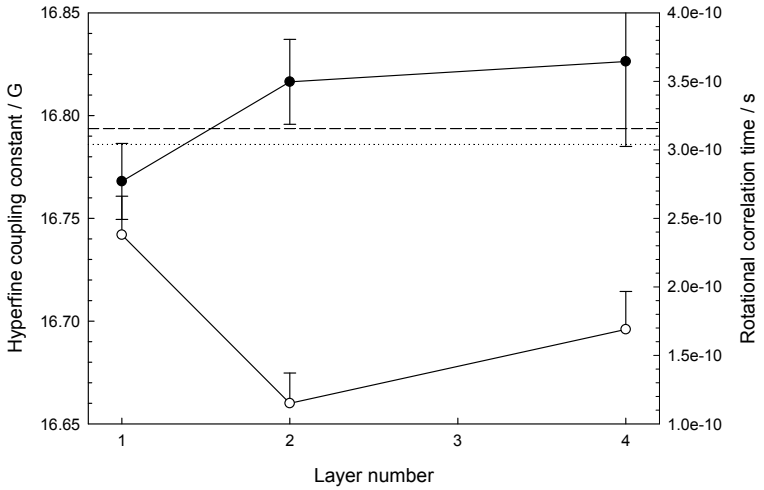

Figure 4.3 L. Hyperfine coupling constant (open symbols) and rotational correlation time (filled symbols) as a function of label position for nanoparticles formed from NP3 (AGMA1/ISA23). The dotted line corresponds to the hyperfine coupling constant for the labelled polymer in solution, whereas the dashed line is its rotational correlation time.

For NP2, NP3 and NP4, the rotational correlation time for the TEMPO label in layer i (τri) increases with increasing layer number in all three cases. Interestingly, $\tau rcore$ is smaller than the equivalent value for the corresponding polymer in solution, $\tau rsoln$, implying that the probe experiences a more mobile environment within the core compared to the solution environment. As the layers are built up, τri increases ($\tau rcore < \tau r1 < \tau r3$) and appears to reach a value that is comparable to (NP4) or slightly greater than $\tau rsoln$ (NP2,3). Since a long correlation time corresponds to slow motion, the increasing correlation time corresponds to a decrease in mobility. For these three nanoparticles, this implies that the core environment is rather mobile, and that the polymer chains added to the periphery of the particle are somewhat less mobile than the core suggesting a densification of

the outer layers. Changes in the polarity sensed by the probe in the various locations as the particles are built up are small. For NP1, NP2 and NP3, the polarity decreases from the core to the first layer but subsequently increase in the third layer.

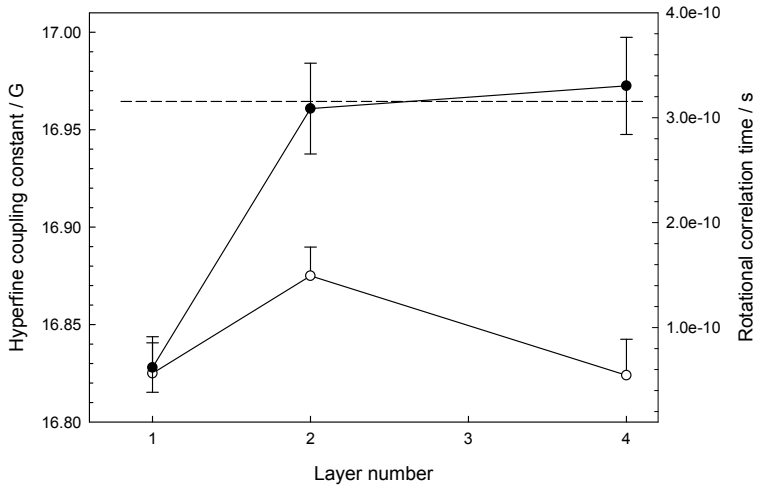

Figure 4.3 M. Hyperfine coupling constant (open symbols) and rotational correlation time (filled symbols) as a function of label position for nanoparticles formed from NP4 (AGAM1/BACEDDA). The dotted line corresponds to the hyperfine coupling constant for the labelled polymer in solution, whereas the dashed line is its rotational correlation time.

For NP4, a maximum (rather than a minimum) is shown in polarity within layer n=2. These two combined EPR insights, coupled with the particle size/zeta-potential analysis, imply that NP2, NP3 and NP4 possess rather loose, flexible internal structures that are somewhat similar to the polymer in solution, with some collapse of the polymer structure around the surface of the particle. They are rather different to solid-core nanoparticles. This flexible character has interesting implications for their ability to solubilise and release any encapsulated material. For NP1, the structures formed from ISA1/ISA23 show a behavior that is analogous to the labelled ISA23, and we conclude that these structures are rather ill-defined and consequently, were not further considered.

Cytotoxicyty assay of Multilayer Nanoparticles. All multilayer nanoparticles described herein were evaluated from the toxicity point of view on B16 and VERO cells. The MTT assay was performed to quantify the cell viability after incubation for 68 hours at 37 °C at concentration whitin 0.5-5 mg/ml. The cytotoxicyties (IC_{50}) of all four samples (the three nanoparticles NP2, NP3 and NP4, as well as the structures present in the NP1 mixture) were found to be largely independent of the nanoparticle structure and type, Figure 4.3 N, much higher than PEI controls, and comparable to the cytotoxicity of the component polymers themselves[20].

[20] **Richardson, S.; Ferruti, P.; Duncan, R., J. Drug Targeting, 1999, 6, 391-404.**

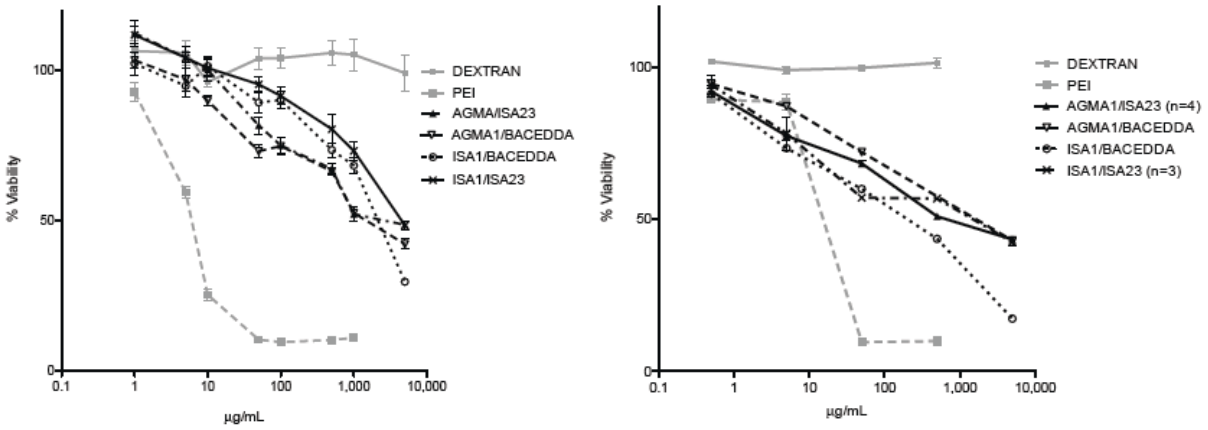

	IC_{50} (mg/mL)				
	AGMA/ISA23	AGMA1/BACEDDA	ISA1/BACEDDA	ISA1/ISA23	PEI
Vero	3.32 (±0.28)	3.82 (±0.13)	0.32 (±0.007)	2.63 (±0.15)	0.027 (±0.0009)
B16	4.32 (±0.38)	3.09 (±0.23)	2.83 (±0.16)	4.63 (±0.31)	0.006 (±0.0002)

Figure 4.3 N. IC_{50} for the nanoparticles studied here in epithelial (Vero) and murine (B16) cells.

Nanoparticle disassembly. In order to understand how the nanoparticle will disassemble in solution, the interaction of the labelled polymers in solution and in various layers within the nanoparticles has been examined in the presence of common surfactants. The interaction of the simple TEMPO-labelled polymers with the anionic surfactant sodium dodecylsulphate, SDS, or the cationic surfactant cetyltrimethylammonium bromide, CTAB, was first examined, Figures 4.3 O and 4.3 P. Clearly, the rotational correlation time is unchanged on addition of SDS for ISA23, which can be understood as found previously, by a lack of an interaction due to the anionic nature of both polymer and surfactant. The other two polymers, ISA1 and AGMA1, show a decrease in correlation time with increasing [SDS], at least above [SDS] = 0.5 mM, indicating the onset of surfactant binding. Below that value, the rotational correlation time for the TEMPO probe is unchanged for AGMA1, implying that the critical amount of SDS for an interaction (CMC(1)) is 0.5 mM, and that CMC(1) increases slightly for ISA1 consistent with its greater cationic character. A similar response may be induced in the ISA23 case by addition of the cationic surfactant, CTAB, highlighting the electrostatic nature of the interaction.

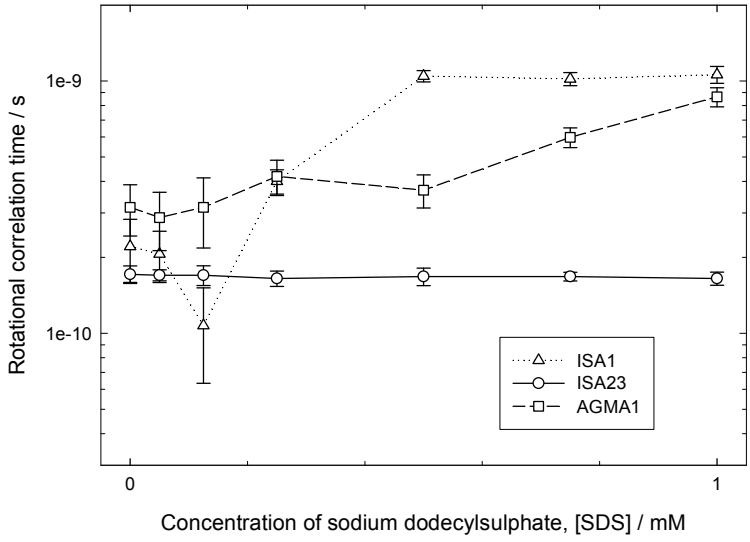

Figure 4.3 O. Rotational correlation time for parent polymers in the presence of sodium dodecylsulphate (SDS).

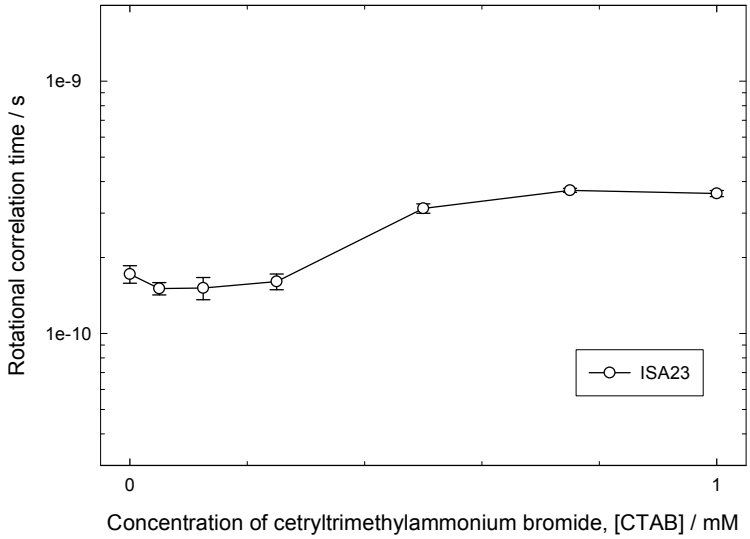

Figure 4.3 P. Rotational correlation time for ISA23 in the presence of cetyltrimethylammonium bromide (CTAB).

For the nanoparticles, figures 4.3 Q-S, there is a general increase in the rotational correlation time with increasing [SDS], indicating that the spin-label is reported a more rigid environment. The polarity behavior is rather more complex, but in essence, the polarity rises to a maximum – more hydrated - before subsequently starting to decrease at high [SDS]. Over this surfactant concentration range, it is probable that there is not full dissolution of the nanoparticle, but the anionic surfactant is complexing with the cationic polymer, making the polymer conformation around the spin-label rather rigid but hydrated given the ionic interaction.

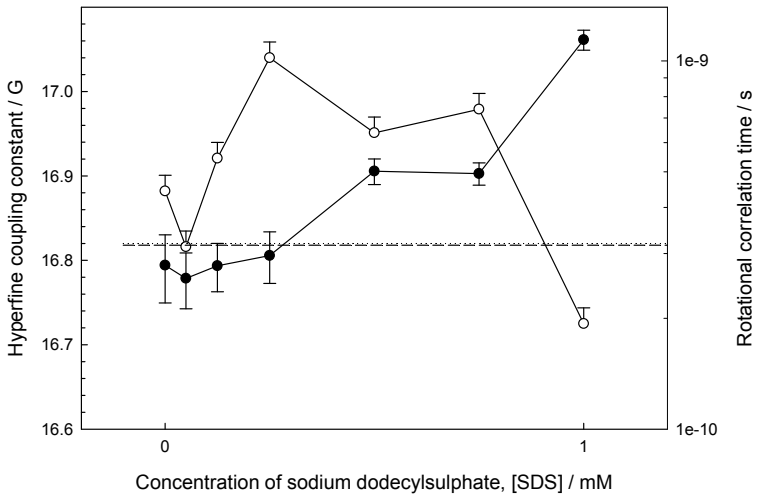

Figure 4.3 Q. Hyperfine coupling constant (open symbols) and rotational correlation time (filled symbols) for nanoparticles formed from NP2 (ISA1/BACEDDA) in the presence of sodium dodecylsulphete (SDS).

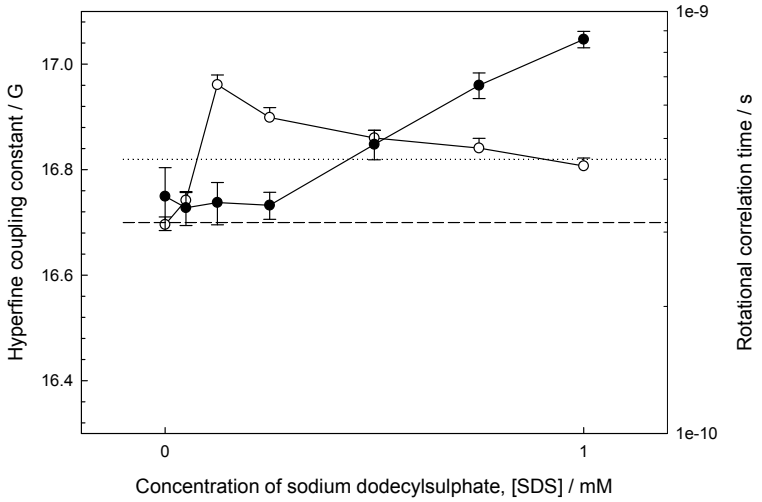

Figure 4.3 R. Hyperfine coupling constant (open symbols) and rotational correlation time (filled symbols) for nanoparticles formed from NP3 (AGMA1/ISA23) in the presence of sodium dodecylsulphete (SDS).

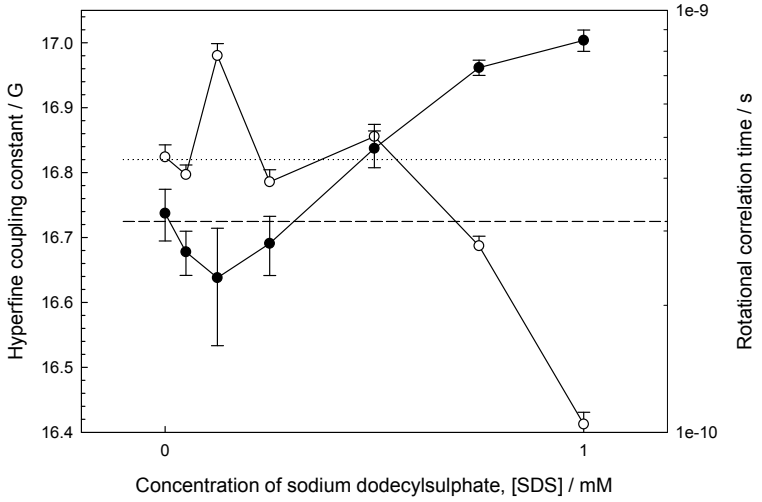

Figure 4.3 S. Hyperfine coupling constant (open symbols) and rotational correlation time (filled symbols) for nanoparticles formed from NP4 (AGMA1/BACEDDA) in the presence of sodium dodecylsulphete (SDS).

4.4 ISA23-BSA CONJUGATE AS ANTIMALARIAL DELIVERY SYSTEM

BAC-MP, previously mentioned in the section 4.1, was chosen as hetero-difunctional dimer for synthesizing PAA-protein graft copolymers because the resultant polymer shell (ISA23) was found to be highly biocompatible and stealth-like.[21] BSA was chosen because of its binding ability against drugs and its high molecular weight that ensures a suitable clearance of the payloaded drug. In spite of the fact that it usually binds acidic drugs, we expected acidic moyety of ISA23 shell to provide binding ability towards basic drugs, such as primaquine and chloroquine. This was simply achieved by triggering the BAC-MP polymerization in aqueous medium in the presence of BSA that participated in the polymerization through its exposed NH_2 and SH groups (Scheme 4.4 A). The occurrence of BAC-MP grafting onto BSA was evaluated by SEC connected in series with RI, light scattering and viscometric detectors.

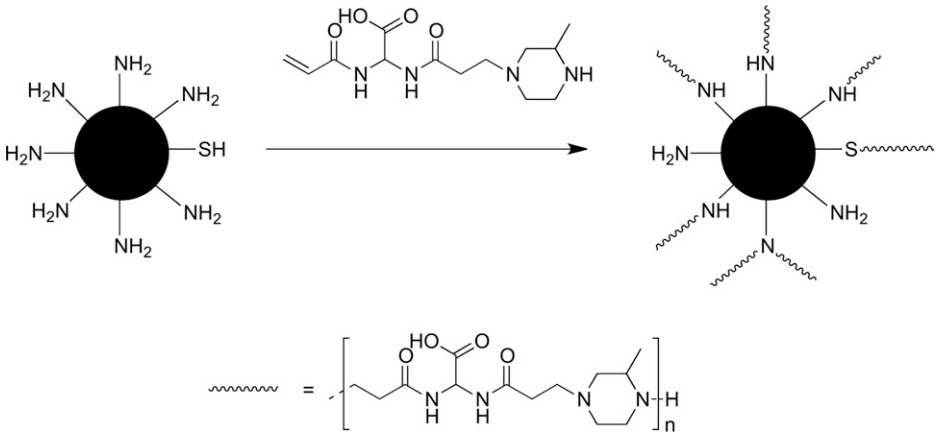

Scheme 4.4 A. Synthesis of ISA23-BSA conjugate by polymerization of BAC-MP in the presence of BSA. The BAC-MP dimer was obtained as previously described in chapter 4.1.

The data, reported in Table 4.4 A, provided clear evidence of the increasing of the molecular weight of the copolymer with respect to native BSA, always accompanied by low polydisperisities and higher values of the Mark-Houwink constants, hence higher hydrodynamic radii.

Table 4.4 A. Molecular weight and viscosimetric data of BAC-MP-g-BSA sample compared with BSA.

Sample	M_n[a]	M_w/M_n[b]	$[\eta]$[c] (dL/g)	a[d]	log K[e]	R_h[f] (nm)
BSA	67,000	1.04	0.054	0.034	−1.45	3.92
BAC-MP-*g*-BSA	1,01,000	1.07	0.067	0.203	−2.74	6.1

[a] Number average molecular weight; [b] Polydispersity index; [c] Intrinsic viscosity; [d,e] Mark-Houwink constants; [f] Hydrodynamic radius.

[21] **Richardson, S.; Ferruti, P.; Duncan, R., J. Drug Targeting, 1999, 6, 391-404.**

A further confirmation was provided by the far higher solubility in aqueous media of the copolymers compared with virgin BSA. The copolymer size was also investigated by cryo-TEM analysis, that showed a quasi-spherical shape of the polymeric nanovector (Figure 4.4 A). This point out that this system might efficiently circulate throughout the body for reaching specific cell districts, without leading to thrombosis-like events caused by shear stress after intravenous administration.[22] [23] Furthermore, it is generally recognized that nanoparticles with dimensions in the range 200-300 nm may be internalized into cells in vitro, but are unsuitable for *in vivo* use, whereas 150 nm represents the highest threshold size value for nonspecific cell uptake *in vivo*.

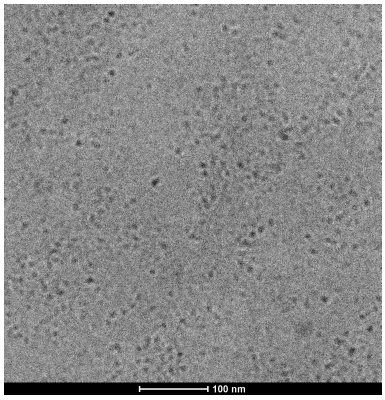

Figure 4.4 A. cryo-TEM analysis of ISA23-BSA conjugate

The binding ability of the copolymer was evaluated by equilibrium dialysis test in which primaquine (PQ) or chloroquine (CQ) solutions were dialyzed against a solution of BSA at fixed concentration. The copolymer binding data are shown in Figure 4.4 B, where the absence of an outstanding relationship between drug concentration and copolymer binding can be seen. Nevertheless, the percent of binding seems to decrease by increasing the pre-dialysis concentration of the drug, almost certainly due to the saturation of copolymer binding sites. The binding data showed also significant differences between CQ and PQ (59.1±1.3% *vs* 78.3±1.5%), giving us an insight into the higher affinity of the copolymer for PQ rather than CQ. The higer binding of PQ may be explained by the hypothesis that it can interact more easly with the copolymer for the simple reason that it is sterically favorite by the presence of a primary amine instead of a *tert*-amine. Furthermore, primary amine may form hydrogen bond, strengthening the binding to the copolymer.

[22] **Lesieur, S.; Gazeau, F.; Luciani, N.; Ménager, C.; Wilhelm, C., J. Materials Chem., 2011, 21, 14387-14393.**

[23] **Maalej, N.; Folts, J., D., American Heart Association, 1996, 93, 1201-1205.**

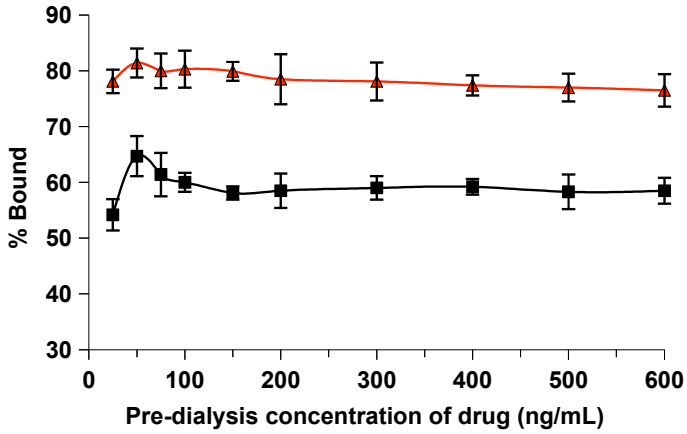

Figure 4.4 B. Plotting of ISA23-BSA binding ability towards CQ (black) and PQ (red) obtained by equilibrium dialysis test.

The copolymer considered in this study was also characterized in terms of cytotoxicity on HUVEC cells. Figure 4.4 C (Panel A) shows the cytotoxicity profile of this sample. It can be noticed that ISA23-BSA conjugate was found to be definitely non-toxic, even if compared with Dextran (95% availability). Owing to after intravenous injection of polyelectrolytes hemolysis can occur, the hemolytic activity of the copolymer was studied. Results are reported in Figure 4.4 C (Panel B).

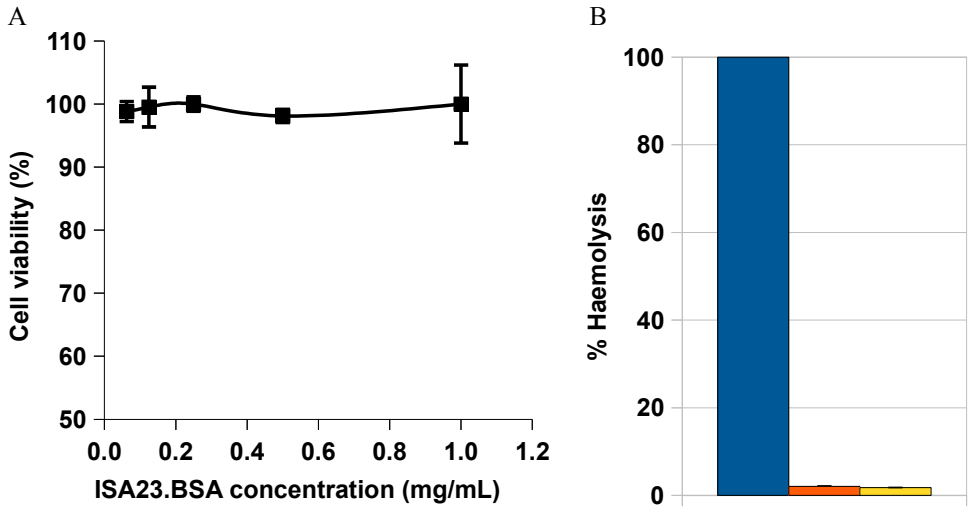

Figure 4.4 C. Cytotoxicity and hemolytic profile of ISA23-BSA conjugate. Cytotoxicity on HUVEC cells (Panel A). Hemolysis activity of ISA23-BSA (1 mg/mL) (yellow) on RBCs by comparison with TritonX-100 (blue) and dextran (orange) as positive and negative control respectively (standard deviation was smaller than 4%).

As expected, no significant hemolytic activity was observed for the copolymer at concentration of 1 mg/mL after 24 hrs incubation in RBC with 3% hematocrit at 37 °C. Hence it combines strong binding ability towards PQ and CQ with negligible cytotoxicity and hemolytic activity up to a concentration of 1 mg/mL. This positive combination of properties makes the copolymer rather excep-

tional as antimalarial nanovector and lead us to consider its as valuable candidate as PQ and CQ carrier not only *in vitro*, but also *in vivo*.

To assess passive targeting of the copolymer towards *Plasmodium*-infected red blood cells (pRBC) we performed *in vitro* immunofluorescence experiments, where *Plasmodium* parasites were colocalized together with the polymer and RBC (Figure 4.4 D). In fact, pRBC usually shows a significant increasing of membrane permeability, arising from the physiological allostasis, that is liable for bioaccumulation of such systems.

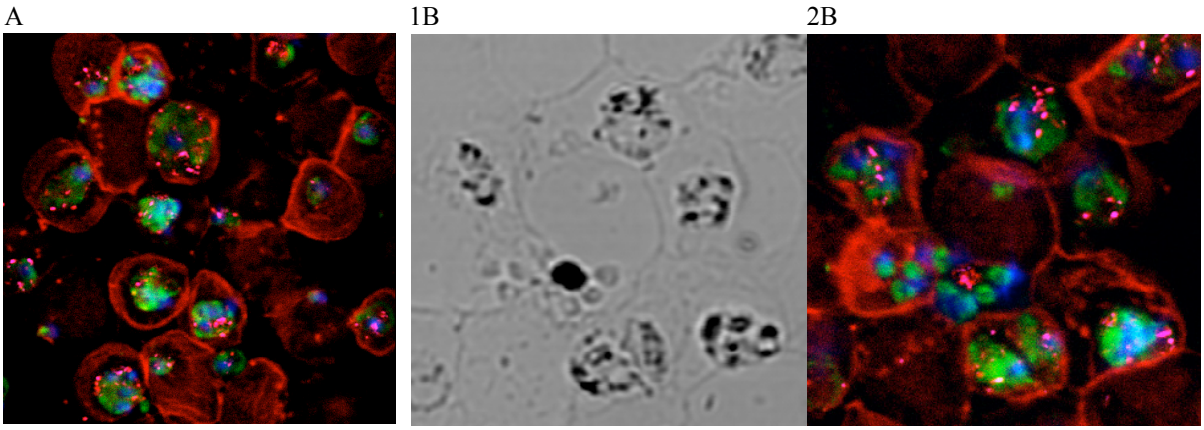

Figure 4.4 D. Confocal fluorescence microscopy analysis of the interaction of ISA23-BSA-FITC conjugate with infected pRBCs: single confocal section (Panel A, Panel 2B). RBC plasma membrane (red), ISA23-BSA-FITC conjugate (green), nuclei (blue) and hemozoin (pink). Light microscopy image of the selected field (Panel 1B).

Immunofluorescence results indicated that FITC-labelled ISA23-BSA conjugate interacts preferentially with pRBC and seems to colocalize with the parasite. In addition, flow cytometry experiments confirmed immunofluorescence results without reservations. This results clearly highlighted a remarkable passive targeting of the copolymer into pRBC, that can be exploited to selectively increase the local concentration of CQ and PQ into pRBC providing a better efficacy of drugs. Furthermore, the higher amount of drugs inside pRBC rather than RBC and plasma avoids side effects and resistance mechanisms that usually jeopardize the therapeutic efficacy of the treatment.

On account of the above considerations, we prepared two isotonic formulations of ISA23-BSA/drug complex, one for each drug (PQ and CQ), in PBS at pH 7.4. This was accomplished by simply mixing the copolymer solution with a PBS solution of PQ or CQ dropwise, obtaining a formulation with 5.5% (w/w) PQ or CQ. The copolymer was found to have PQ and CQ binding ability due to the hinerent properties of native BSA to bind both drugs [24] and as consequence of the presence of the ISA23 shell, in which carboxylic groups may electrostatically interact with the amino group of

[24] Ofori-Adjei, D.; Ericsson, O.; Lindstrom, B., Sjoqvist, F., Br. J. clin. Pharmac., 1986, 22, 356-358.

both drugs. However, it might be expected that a bit of free drug (22% and 41% respectively) must be in solution as consequence of the impending thermodynamic equilibrium between three species (see also Figure 4.4 B):

$$\text{ISA23-BSA} \cdot \text{PQ} \underset{}{\overset{K_d}{\rightleftharpoons}} \text{ISA23-BSA} + \text{PQ}$$

The amount of free drug is hardly influenced by the drug/ISA23 ratio, as it depends primarily from the maximum loading threshold of the polymer (11.2±0.9% and 7.9±1.1% w/w). Thus exceeding this threshold the drug obviously became free.

To establish if the formulations were able to enhance the efficacy of the two drugs, we measured the reduction of parasitemia *in vitro* on pRBC after incubation for 48 h and with respect to the same concentration of the plane drugs. The *in vitro* antimalarial activity of ISA23-BSA/PQ and ISA23/ CQ formulations are reported in Figure 4.4 E as function of the logarithm of drug concentration (Panel A and B respectively).

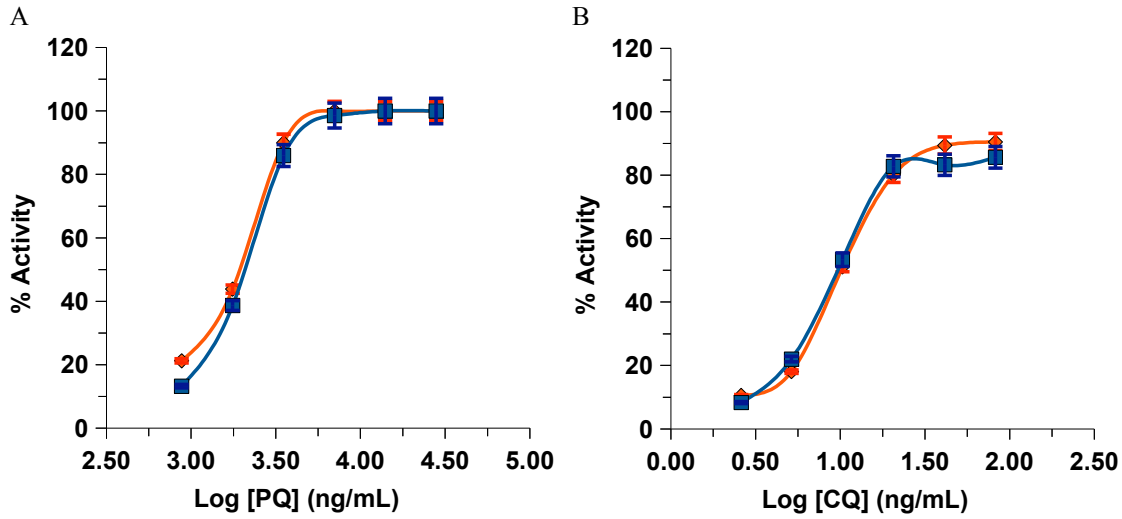

Figure 4.4 E. *In vitro* antimalarial activity of PQ and CQ formulations expressed as percentage of parasite reduction respective to the parasitemia of controls (%Activity). Panel A: PQ (blue line) and ISA23-BSA/PQ formulation (red line) formulation. Panel B: CQ (blue line) and ISA23-BSA/CQ formulation (red line).

Results obtained show significant differences between the effect of the copolymer on PQ and CQ antimalarial activity. As ISA23-BSA/CQ formulation followed the same trend than that observed for the plane CQ (Figure 4.4 E, Panel B), in the case of ISA23-BSA/PQ sample the antimalarial activity was slightly higher with respect to the plane PQ, especially at low drug concentration (Figure 4.4 E, Panel A). The small increase in antimalarial activity of PQ observed when encapsulated in ISA23-BSA conjugate can be explained considering that it can not be easily released in a mono-

compartimental system, in which the *in vitro* experiments are usually performed. In fact, in a mono-compartimental system, where the sink condition was not held, the release of drug at equilibrium may not quickly occurred due to the very slow clearance of the free drug from the medium.

Along this line, ISA23-BSA/PQ formulation was hence selected to perform further studies *in vivo* on mice. The *in vivo* toxicity of the copolymer was first investigated in mice with 100 mg/Kg dose and 200 mg/Kg dose. Results shown that it is endowed with negligible toxicity after intraperitoneal injection at high dose too, enabling it to be used for *in vivo* medical applications (Figure 4.4 F).

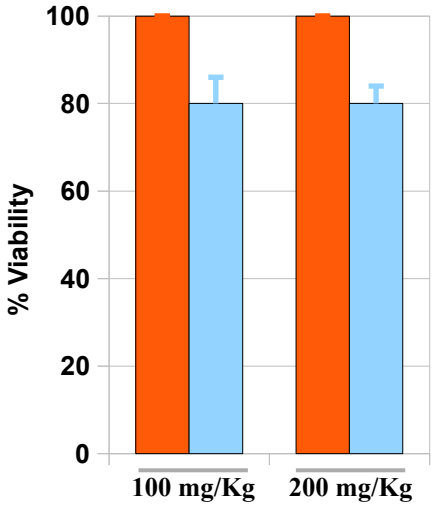

Figure 4.4 F. Acute Toxicity *in vivo* of ISA23-BSA/PQ formulation (blue) after *i.p.* injection in mice compared with PBS injection as control (orange).

The *in vivo* antimalarial activity of ISA23-BSA/PQ formulation was evaluated by using a 4-days suppressive test, in which parasite-infected mice were treated with an intraperitoneal injection (*i.p.*) of the formulation after 2 h from the *Pasmodium yoelii yoelii* 17XL (Pyl) inoculation, followed by identical administration for 3 days. Usually ineffective doses, that means non suitable chemotherapy treatment, lead to mice death within four days; in contrast, the administration of a proper therapy provides healthy mice avoiding death. For comparative purposes, all results were reported together the activity perceived after *i.p.* of the same amount of plane PQ (Figure 4.4 G). Results obtained on day 4 indicate that in the lower SA23-BSA/PQ dose (6.25 mg/Kg PQ equivalent dose) there is an increased antimalarial activity of ISA23-BSA/PQ formulation if compared with plane PQ. Much as no significant difference is observed in mice treated with higher dose of drug (6.25 mg/Kg).

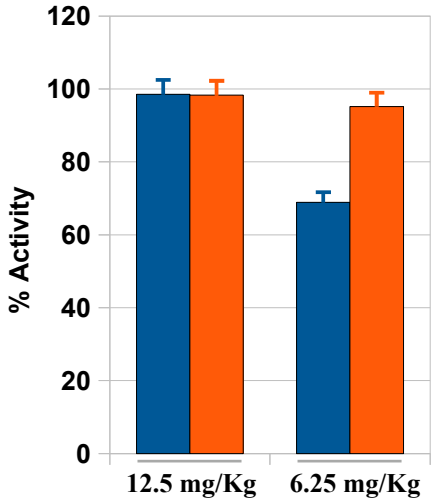

Figure 4.4 G. 4-day suppressive test on mice. *In vivo* antimalarial activity of plane PQ (blue) and ISA23-BSA/PQ formulation (orange) after 4 days. The values of the *in vivo* antimalarial activity (% activity) are expressed as percentage of parasite reduction respective to the parasitemia of controls.

Furthermore, in spite of the results observed *in vitro*, mice treated with ISA23-BSA/PQ formulation (6.25 mg/Kg daily dose of PQ) were found to be healthy after 4 days and after 7 days they without doubt achieved clearance of the parasitemia. However, only 2 out of 3 mice treated with the higher dose of ISA23-BSA/PQ (12.5 mg/Kg daily dose of PQ) were cured. Surprisingly, the other one died after 2 days, maybe owing to a paroxysmal toxic effect. The apparent higher toxicity observed for high dose treatment might be explained by the greater oncotic pressure due to the presence of high amount of copolymer, that in some case provides water retention that might afford to cardiac infarct. In contrast, all mice treated with the identical amount of the plane PQ died whitin 4 days, indicating that the ISA23-BSA/PQ formulation was much more effective after *i.p.* administration *in vivo*. Pharmacokinetics studies should be needed to better investigate why this complex improve the PQ efficacy *in vivo*. Still this imply that the ISA23-BSA conjugate releases the PQ payload only into pRBC, where the parasite is placed, holding high amount of drug only in the site of action and thus avoiding resistance mechanisms. We have no data, at the present, to ascertain which specific mechanism allow the PQ payload from the formulation *in vivo*. Nevertheless, broadly speaking, it is reasonable to think that the clearance of the drug from plasma compartment (Sink conditions) provides suitable environment to release PQ payload from the complex at non-equilibrium circumstance. This also make clear to us sharp differences in antimalarial activity observed by *in vivo* and *in vitro* experiments.

4.5 POLYAMIDOAMINE HYDROGELS AS SCAFFOLDS FOR IN VITRO CULTURING OF PERIPHERAL NERVOUS SYSTEM CELLS

Planning structures. MBA hydrogels were prepared by polyaddition of piperazine with *N*,*N*'-methylenebisacrylamide, using 1,2-diaminoethane as cross-linking agent (Scheme 4.5 A).

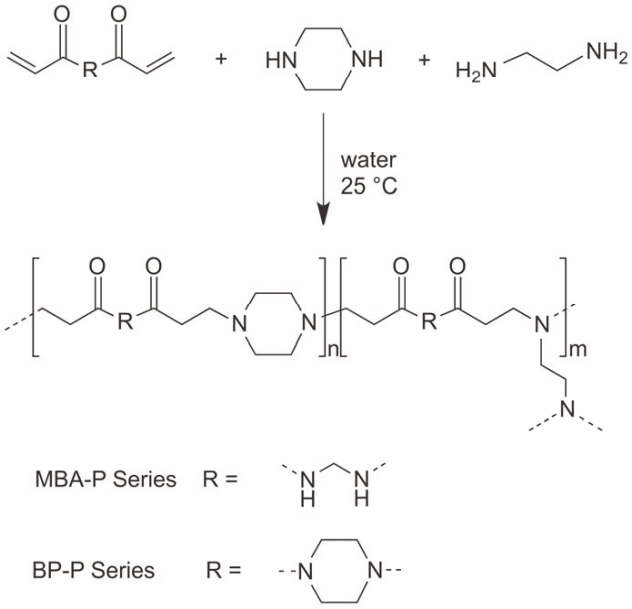

Scheme 4.5 A. General synthesis of MBA-P and BP-P hydrogels.

These monomers were chosen considering that the main aim of this study was to obtain hydrogels combining mechanical strength in the swollen state with biocompatibility. The mechanical strength might be expected to increase in the presence of amide hydrogen bonds and cyclic structures along the polymer chain. *N*,*N*'-methylenebisacrylamide provided the former and piperazine the latter. On the other side, the biocompatibility of PAAs is usually higher the lower their cationic charge at pH 7.4. A library of acid-base properties of PAAs indicates that the piperazine-deriving ones are the weakest of all, with pKa_1 and pKa_2 in the order of 7.4 and 3.8, respectively, independently of the structure of the bisacrylamide moiety.[25] Therefore, it can be predicted that at physiological pH only one–half of the piperazine moieties bears a positive charge, resulting in a modest density of positive charges along the polymer chain, on the average one every 500 Da. Moreover, the physico-chemical properties of the linear PAA deriving from the polyaddition of piperazine, 2-methylpiperazine or *trans*,2,5-dimethylpiperazine with *N*,*N*'-methylenebisacrylamide pointed out that only PAA deriving from piperazine is able to form highly ordered structures that can be exploited to prepare hydro-

[25] **E. Ranucci, P. Ferruti, E. Lattanzio, A. Manfredi, M. Rossi, P. R. Mussini, F. Chiellini, C. Bartoli, J. Polym. Sci., Part A: Polym. Chem. 2009, 47, 6977.**

gels with suitable mechanical strenght. In particular, the higher molecular weight and the lower solubility in water of the piperazine-based polymer, namely MBA-P, led us to this conclusion.

BP hydrogels were prepared by polyaddition of piperazine with *N*,*N*'-bisacryloylpiperazine, using 1,2-diaminoethane as cross-linking agent (Scheme 4.5 A). These monomers were chosen based on the knowledge on the physico-chemical and biological properties of the linear PAA deriving from the polyaddition of piperazine, 2-methylpiperazine or *trans*,2,5-dimethylpiperazine with *N*,*N*'-bisacryloylpiperazine. Among these PAAs, that obtained with piperazine proved in preliminary experiments to be highly crystalline in the solid state and to have a strong tendency to crystallize from its aqueous solutions at pH ≥ 7 and at temperatures ≤ 40 °C. The latter property prompted the hypothesis, later on confirmed by experiments, that it could partially crystallize even when inserted into a cross-linked structure and that crystalline domains could be maintained in the swollen hydrogel, thus increasing the hydrogel's strength.

Preparation and properties of linear PAAs. The linear counterparts of the hydrogels, namely MBA-P, MBA-MP, MBA-DMP and BP-P, BP-MP and BP-DMP were prepared first in order to obtain exact information on the physico-chemical polymer properties, such as for instance solubility and thermal behavior, thus facilitating the interpretation of the hydrogel performance. The preparation conditions for MBA-MP, MBA-DMP, BP-MP and BP-DMP were 2 M concentration of both monomers in water at 25 °C and no added catalysts. In the case of MBA-P, the preferred reaction medium was ethylene glycol because in water, at the same concentration, some of the product precipitated in gel form. Gel precipitation could be avoided by performing the reaction at higher dilution, but this practice reduces the molecular weight of the resultant PAAs. In the case of BP-P, carrying out the polymerization reactions in aqueous solution and at room temperature, as usual for PAAs, after the first reaction steps a sharp phase separation due to crystallization occurred. The system became homogeneous on heating at 60-70 °C and at this temperature the reaction proceeded to some extent, as apparent from the viscosity increasing. Eventually, however, the polymer precipitated again. Much interesting, BP-P was insoluble at r.t. in all common solvents, but soluble in boiling water. DSC analysis revealed a melting peak centered at approximately 278 °C (see below). On the opposite, the others PAAs was soluble in aqueous media and high molecular weight samples were obtained (Table 4.5 A). They were apparently amorphous in the dry state, as revealed by DSC analysis. Furthermore their molecular weight follow the trend P>MP>DMP, probably because the methyl group in α position to the amine bias the rate of the polyaddition reaction.

Table 4.5 A. Number average and weight average molecular weight (M_n and M_w respectively), polydispersity index (M_w/M_n) and water solubility of linear PAAs.

Sample	M_n	M_w	M_w/M_n	Solubility [a] (mg/mL)	Solubility [b] (mg/mL)
MBA-P	109500	171000	1.56	490	> 1000
MBA-MP	38500	48900	1.27	> 1000	n.d[c]
MBA-DMP	37200	52400	1.41	> 1000	n.d[c]
BP-P	n.d[c]	n.d[c]	n.d[c]	<1	645
BP-MP	22200	29100	1.31	>1000	n.d[c]
BP-DMP	17100	23000	1.35	> 1000	n.d[c]

[a] Solubility at r.t.; [b] solubility at boiling point; [c] not determined

Hydrogel synthesis. Cross-linked MBA-P and BP-P hydrogels were obtained by partially substituting 1,2-diaminoethane for piperazine in the polymerization recipes (Scheme 4.5 A). This cross-linking method did not introduce non-biodegradable segments in the hydrogels structure. All polymerizations were performed in aqueous solution with precise stoichiometric equivalence between double bonds and amine hydrogens. Two hydrogel series were prepared, one for each bisacrylamide and, within each series, three different cross-linking degrees (calculated as the percentage of amine hydrogens pertaining to 1,2-diaminoethane over the total amount of N-H functions) were chosen, in particular 10, 15 and 30% for MBA-P hydrogels and 25, 30 and 40 % for BP-P ones. The choice of the cross-linking degree of the latter hydrogels was based upon preliminary experiments that allowed identifying 25% as the minimum threshold value needed to ensure gelation. All reaction mixtures set within 30 hrs. However, in order to maximize the reaction yield, the products were isolated after five days. In the case of MBA-P, transparent homogeneous hydrogels were invariably obtained, with no evidence of phase separation. In the case of BP-P, partial precipitation occurred since the initial stages, due to the formation of crystalline domains inside the polymer network during hydrogel formation. Nonetheless, all resultant hydrogels were elastic and pliable. As a rule, hydrogel samples were prepared as 10 x 10 x 0.1 cm sheets, measured on the swollen phase, although hydrogels in the form of solid cylinders and hollow tubes of various dimensions were also prepared for demonstration purposes. All hydrogels were tough and pliable irrespective of shape and dimension (Figure 4.5 A).

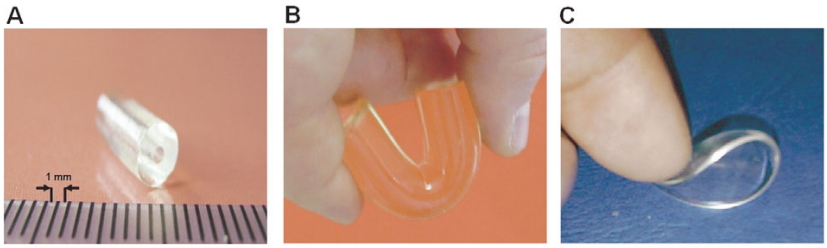

Figure 4.5 A. Example of PAA hydrogels obtained with different shape: MBA-P30 tubing (A), cylinder of MBA-P10 (B) and sheet of BP-P30 (C).

Hydrogel swelling behavior. The swelling behavior of MBA-P and BP-P hydrogels in water, PBS pH 7.4 and ethanol is reported in Figure 4.5 B.

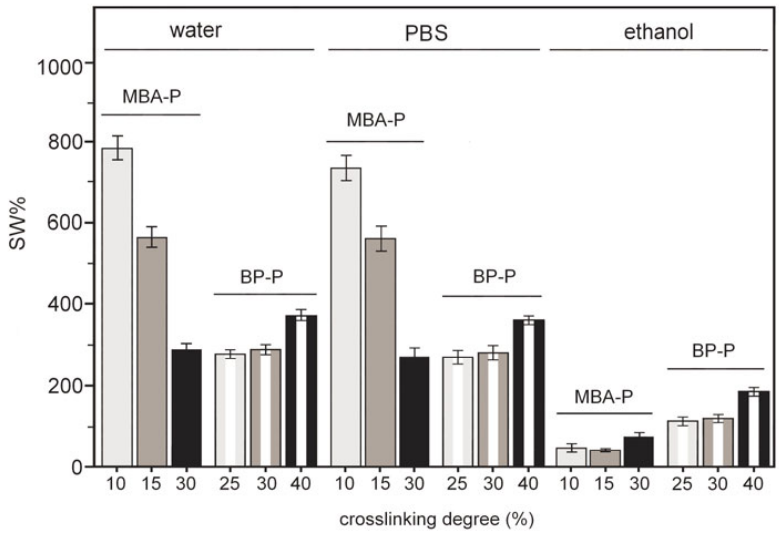

Figure 4.5 B. Swelling behavior of MBA hydrogels in water, PBS and ethanol: MBA-P and BP-P.

It may be observed that in the MBA-P series the equilibrium swelling decreased by increasing the cross-linking degree, as expected. No significant differences were observed between swelling in PBS and water. The swelling behavior of the BP-P hydrogels exhibited the opposite trend. This apparent inconsistency was explained by the loss of crystallinity following the formation of the polymer network. Unexpectedly, this factor was not balanced by the reduction in the mesh size normally causing shrinking. The hydrogel swelling turned to be pH sensitive, albeit to a minor extent for BP-P, as shown in the diagrams reported in Figure 4.5 C. It is apparent that swelling increased from pH 5 downward, reaching a maximum between pH 3 and 1. There is little doubt that this behavior corresponded to the protonation of the amine groups of the repeating units, one of which is only weakly basic. Not surprisingly, the pH sensitivity was higher for the less cross-linked samples. The less pronounced pH sensitivity of BP-P hydrogels was no doubt due to the presence of crystalline domains.

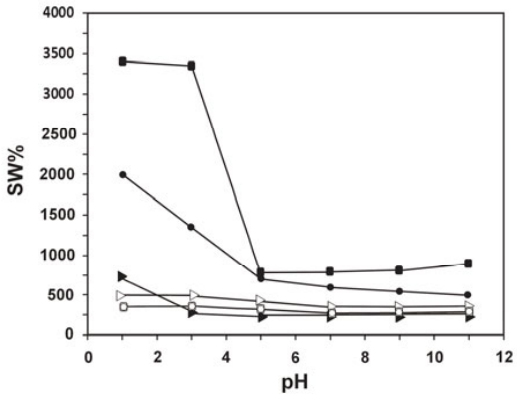

Figure 4.5 C. Swelling percent of the MBA-P and BP-P hydrogels at different pH. For MBA-P series: 10% cross-linker (■), 15% cross-linker (●) and 30% cross-linker (▶). For BP-P series: 25% cross-linker (□), 30% cross-linker (○) and 40% cross-linker (▷).

Degradation kinetics. The hydrogel degradation rate was studied at 37 °C in PBS buffer pH 7.4. The variations of the percent residual weight and swelling on time of the hydrogels are reported in Figure 4.5 D.

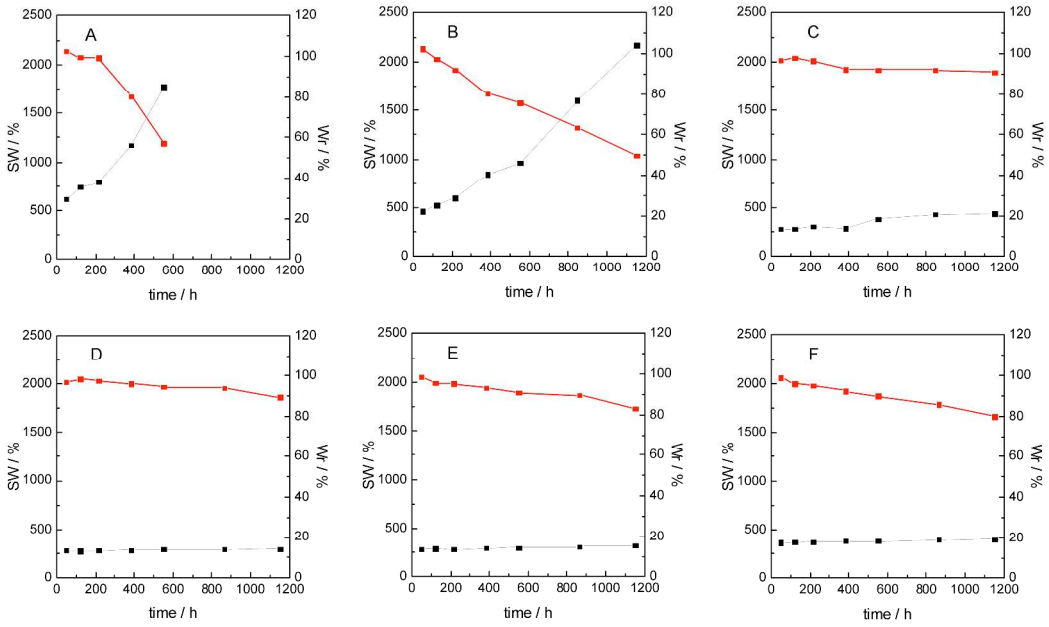

Figure 4.5 D. Degradation profiles in PBS and 37 °C of MBA-P10 (A), MBA-P15 (B) MBA-P30 (C), BP-P25 (D), BP-P-30, and BP-P40. *SW%* (black symbol) and *Wr%* (red symbol).

Under the above conditions MBA-P10 dissolved completely within 35 days, but the dissolution times of MBA-P15 and MBA-P30 were higher than 48 days. The intersection of the swelling and the residual weight curves provided a comparative estimate of the degradation rate. In fact, the for-

mer increased and the latter decreased as effect of the progressive bond cleavage, resulting in two curves whose slopes were of opposite sign and of absolute values higher the faster the sample degraded. Both curves obviously vanished after a certain degradation degree, when the samples dissolved. For comparison purposes, the intersection point and dissolution time of all hydrogels are reported in Table 4.5 B.

Table 4.5 B. Intersection time of the SW% and Wr% degradation curve of PAA hydrogels.

Hydrogel	**Degradation time [h]**	**Intersection time [h]**
MBA-P10	780	465
MBA-P15	>1580	790
MBA-P30	>1580	>1580
BP-P25	>1580	>1580
BP-P30	>1580	>1580
BP-P40	>1580	>1580

Unlike the MBA hydrogels, the percent residual weight of the BP-P hydrogels decreased by increasing the cross-linking degree. In particular, after 45 days BP-P25 degraded up to 10 wt.%, whereas BP-P30 and BP-P40 degraded up to 17 and 20 wt.%, respectively. This behavior followed the swelling degree trend, the more swollen samples degrading faster.

Table 4.5 C. Degradation time of PAA hydrogels at 60 °C in PBS.

Hydrogel	**Time [h]**
MBA-P10	96
MBA-P15	168
MBA-P30	816
BP-P25	580
BP-P30	520
BP-P40	510

Rapid degradation tests were also carried out at 60 °C in PBS, in order to demonstrate within reasonable times the complete hydrogel dissolution. The results, reported in Table 4.5 C, confirmed the complete degradability of all hydrogels with a trend consistent with that of the degradation experiments at 37 °C.

Thermal characterization. The degree of crystallinity of BP-P hydrogels was evaluated by DSC analysis of dry samples by comparison with linear BP-P, taken as reference. DSC profiles of both linear BP-P and BP-P hydrogels are shown in Figure 4.5 E.

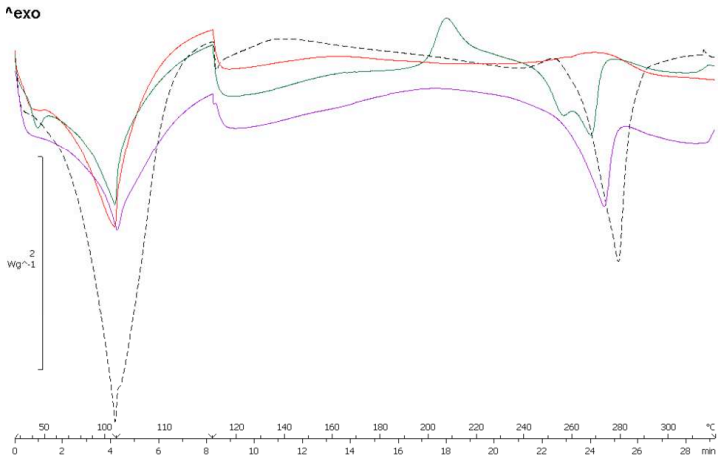

Figure 4.5 E. DSC profiles of BP-P hydrogels by comparison with the linear BP-P: BP-P25 (light purple line), BP-P30 (green line), BP-P40 (red line) and linear BP-P (black dotted line).

All traces revealed endotherms in the range 60-110 °C due to evaporation of residual water. No melting peaks were observed in the trace of the totally amorphous BP-P40, whereas both BP-P25 and BP-P30 exhibited broad endotherms due to the melting of crystalline domains. In particular, BP-P25 exhibited one single endotherm with minimum at 272 °C.

Table 4.5 D. Crystallinity degree of BP-P hydrogels obtained by DSC.

Sample	**Peak 1** [°C]	**Enthalpy 1** [J . g^{-1}]	**Peak 2** [°C]	**Enthalpy 2** [J . g^{-1}]	**Peak 3** [°C]	**Enthalpy 3** [J . g^{-1}]	**%C**[a)]
BP-P	278.1	-166.2	-	-	-	-	100.0
BP-P25	272.0	-63.4	-	-	-	-	38.2
BP-P30	207.3	36.4	255.6	-36.7	266.6	-40.7	24.5
BP-P40	-	-	-	-	-	-	0.0

[a)] The crystallinity degree (%C) of the BP-P hydrogels was calculated comparing the enthalpy of the linear polymer (BP-P) with the hydrogels

By contrast, BP-P30 displayed a crystallization exotherm centered at 207 °C, and two partly overlapping melting peaks in the range 240 – 275 °C with minima placed at 256 and 267 °C, respectively, the first ascribed to the melting of the crystalline component generated during the heating process and the second of the native crystalline domains. The relative crystallinity degree was calculated by comparing the enthalpy of the BP-P hydrogels with linear BP-P using the following for-

mula: $(H^h/H^l)\cdot 100$. Where H^l is the enthalpy of the linear BP-P and H^h is the enthalpy of the BP-P based hydrogel. Results are shown in Table 4.5 D. As expected, the crystallinity decreased by increasing the hydrogel cross-linking degree, due to higher amount of amorphous-like phase generated by the replacement of piperazine with 1,2-diaminoethane.

Confocal microscopy analysis. The confocal microscopy analysis of BP-P hydrogels was performed to characterize the morphology of the crystalline domains embedded in the swollen phase of BP-P25 and BP-P30 hydrogels. As shown in Figure 4.5 F, spherulites were observed in BP-P25 and in BP-P30 with average diameters of about 15 and 7 μm, respectively; whereas no presence of crystallites was observed in BP-P40, in agreement with DSC data.

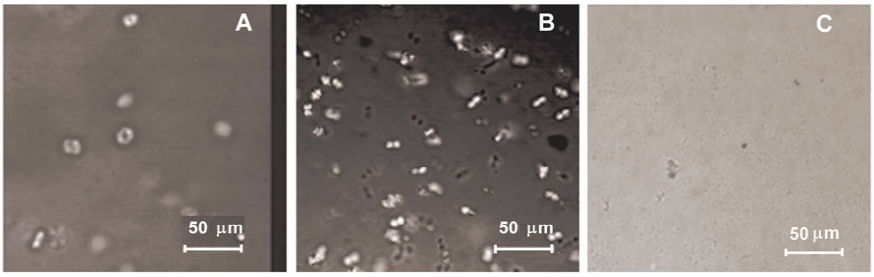

Figure 4.5 F. Confocal microscopy coupled with diffraction-limited laser beam of BP-P hydrogels: BP-P25 (Panel A), BP-P30 (Panel B) and BP-P40 (Panel C).

Rheological characterization. The rheological characteristics of hydrogels are key parameters to understand their structure and consequently their application fields. To define the linear viscoelastic zone, the samples were subjected to a strain sweep analysis in which they were deformed at different shear strains at 1.0 Hz frequency, while compressive forces of 0.2, 0.5 and 1.0 N were applied to the samples. A typical strain sweep analysis is shown in Figure 4.5 G for sample MBA-P10. The shear storage modulus *G'* stayed relatively constant below 1% shear strain. Above 1% shear strain, *G'* decreased as the shear strain increased, thus indicating a transition from linear to non-linear behavior.[26] At very high strain (>3%), the collapse of the hydrogel network was observed due to macroscopic damage of the sample.

[26] D. Ma, X. Xie, M. L. Zhang, J. Polym Sci. Part B: Polym. Phys. 2009, 47, 740.

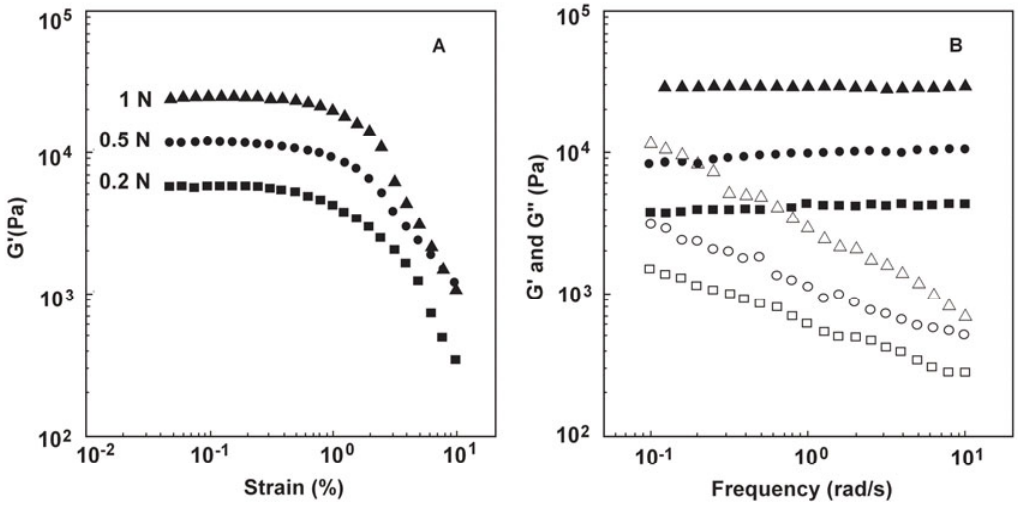

Figure 4.5 G. Strain sweep tests at different compressive force for MBA-P10 (Panel A): 0.2 N (■), 0.5 N (●) and 1 N (▲). B. Frequency sweep tests at different compressive force for MBA-P15 (*G'* solid symbol and *G"* empty symbol): 0.2 N (□), 0.5 N (○) and 1 N (△).

Consequently, a deformation of 0.1% was chosen in the subsequent tests to ensure that each measurement was made in the linear viscoelastic region. Each sample was then subjected to a frequency sweep over the range of frequencies from 0.1 to 10 rad $\cdot$ s^{-1}. The viscoelastic behavior of all the samples was qualitatively similar. As illustrated for sample MBA-P15 in Figure 4.5 G, a strongly solid like behavior was observed (*G'*>> *G"*) and *G'* was always independent of the applied frequency, thus indicating the formation of well-developed cross-linked and mechanically robust network.[27] The frequency sweeps were repeated by applying different compressive forces and the storage modulus *G'* was found to increase as the compressive force increased. This effect was probably due to a parallel decrease of the equilibrium water content.[28] The storage modulus *G'* at 10 rad $\cdot$ s^{-1}, recorded during the frequency sweep tests at different compressive forces, are collected in Table 4.5 E. The trend of the storage modulus *G'*, at the fixed compressive force of 1.0 N, as a function of the cross-linker amount for the two hydrogel series are depicted in Figure 4.5 H. In all cases, *G'* increased with the cross-linker amount.[29] [30] In addition, there was a straightforward relation between the elastic modulus and the swelling degree. The elastic modulus within MBA-P series decreased regularly as the swelling degree increased following the decrease of the cross-linking density (Figure 4.5 H).

[27] **A. S. Sarvestani, X. He, E. Jabbari, Biopolymers 2006, 85, 370.**

[28] **E. Karpuskin, M. Dušková-Smrčková, T. Remmler, M. Lapčiková, K. Dušek, Polym. Int. 2012, 61, 328.**

[29] **K. S. Anseth, C. N. Bowman, L. Brannon-Peppas, Biomaterials 1996, 17, 1647.**

[30] **J. L. Trompette, E. Fabrégue, G. Cassanas, J. Polym Sci., Part B: Polym. Phys. 1997, 35, 2535.**

Table 4.5 E. Storage modulus *G'* of PAA hydrogels at 10 rad·s^{-1} obtained at different compressive force.

Hydrogel	0.2 N	0.5 N	1 N
MBA-P10	3.9	7.5	9.5
MBA-P15	4.2	10.3	28.9
MBA-P30	9.7	16.7	37.6
BP-P25	11.1	27.3	41.4
BP-P30	24.6	34.3	55.6
BP-P40	61.2	71.2	81.9

The reverse behavior shown within the BP-P series, in which both the elastic modulus and the swelling degree increased by increasing the cross-linking degree, was probably related to the semicrystalline nature of these hydrogels. As the amount of the cross-linking agent increased, the amount of crystalline regions decreased, thus giving the network a great freedom to swell.

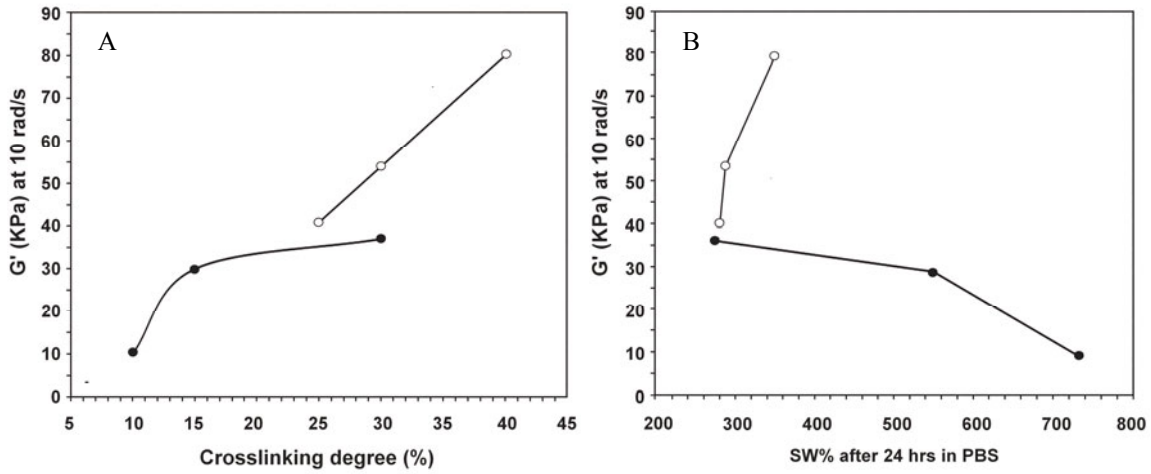

Figure 4.5 H. Trend of storage modulus *G'* of PAA hydrogels at 10 rad·s^{-1} and compressive force of 1 N. Panel A: *G'* as function of % of cross-linker; MBA-P (●) and BP-P (○). Panel B: *G'* as function of swelling degree in PBS; MBA-P (●) and BP-P (○).

Biological experiments: SC culturing. To compare validity and reliability of the experiments, SC culture seeded on PLL-coated dishes were first used to verify and characterize that SC populations were a pure culture. Primary Schwann cultures showed a typical morphology with spindle-shaped bodies and bipolar processes. Moreover, SC were characterized by immunofluorescence with spe-

cific antibodies against the SC markers protein S100 (Figure 4.5 I, Panel A) and glycoprotein P0,[31] revealing a cell purity higher than 98 %. Additionally, SC were grown under standard culture condition (i.e. DMEM-10% FCS, forskolin 2 μM onto TCPS PLL-coated dishes), monitored at 1, 3, 5, 7 and 10 div and used as control for proliferation and cytocompatibility assays. As shown in Figure 4.5 I (panels B, C and D) the SC were already at confluence at 3 div (Figure 4.5 I, panel B), whereas cell proliferation did not substantially changed at later times in vitro, 5 and 10 div respectively (Figure 4.5 I Panels C and D).

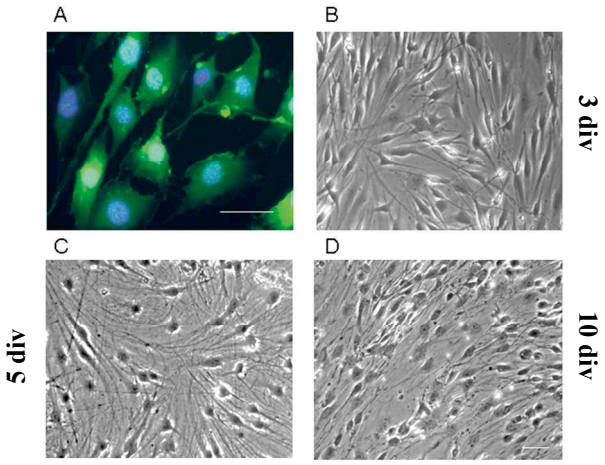

Figure 4.5 I. Immunofluorescence of SC seeded on TCPS PLL-coated dishes by an antiS100 antibody revealing a cells purity more than 98% (Panel A). SC growth was then monitored at 3, 5 and 10 day in vitro (div). SC were at confluence at 3 div (Panel B), whereas cell proliferation did not substantially change at later times, 5 and 10 div respectively (panels C and D). Scale bar 20 μm.

SC cytocompatibility and proliferation on hydrogels. The hydrogels were evaluated as scaffold for SC cultures to assess in parallel the cytocompatibility, the cell proliferation and the degradation rate of the material at 3, 5 and 10 div. SC at 3 div culture assumed a typical spindle-shaped morphology when seeded onto MBA-P10 (Figure 4.5 K). However, at 5 div SC slightly survived on MBA-P10, maybe due to the rapid degradation rate of the hydrogel matrix, that did not match the proliferation doubling of SC, so that the substrate for the cell growing disappeared. At 3 div, SC also showed a normal spindle-shaped morphology when seeded onto MBA-P15 (Figure 4.5 K), although the hydrogel swelling biased to some extent the optical field making difficult to obtain good pictures of the cells.

[31] V. Magnaghi, M. Ballabio, I.T.C. Cavarretta, W. Froestl, J. J. Lambert, I. Zucchi, R. C. Melcangi, Eur. J. Neurosci. 2004, 19, 2641.

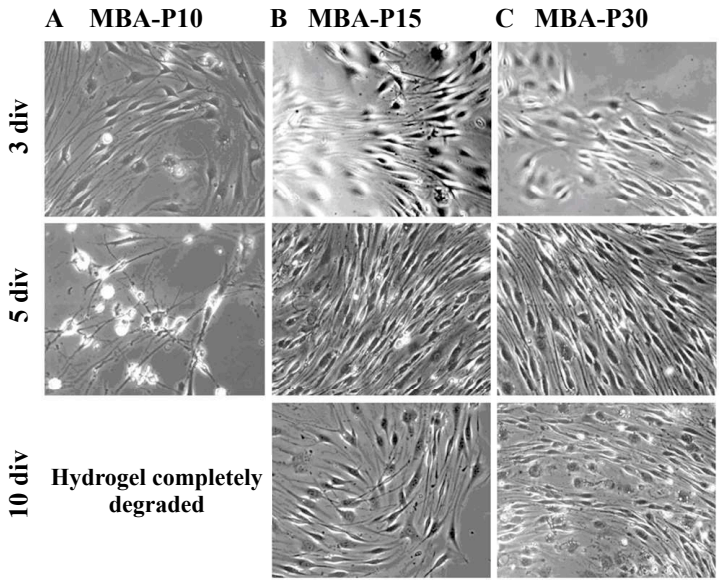

Figure 4.5 K. Cytocompatibility and proliferation of SC grown onto hydrogels of MBA-P10 (Panel A), MBA-P15 (Panel B) and MBA-P30 (Panel C), at 3, 5 and 10 div. Scale bar 20 μm.

At 5 div, SC seeded onto MBA-P15 displayed a good proliferation, which apparently increased at 10 div. Moreover, when the SC were seeded on MBA-P30 they presented good morphology at 3 and 5 div (Figure 4.5 K), similar to that of TCPS PLL-coated control cultures **(**Figure 4.5 I**)** although SC morphology looked better onto MBA-P30 at 10 div (Figure 4.5 K). Altogether the morphological results indicated that among all hydrogels tested, the MBA-P30 apparently showed the best cytocompatibility for SC. Given that BP-P exhibited better physico-chemical properties, also the BP-P25, 30 and 40% hydrogels were evaluated as scaffold for SC culturing. The cytocompatibility and its correlation with the degradation rate of hydrogels was evaluated at 3, 5 and 10 div. As shown in Figure 4.5 L, the SC seeded onto all substrates BP-P25, 30, 40 presented the typical spindle-shaped morphology at 3 div, even though the cell growth appeared slightly delayed, particularly on BP-P30, 40 (Figure 4.5 L). Then, the doubling of SC was apparently normal, compared to SC seeded onto TCPS PLL-coated dishes (Figure 4.5 I), evidencing a general good proliferation rate at 5 and 10 div (Figure 4.5 L). In order to support this finding the SC proliferation were quantitatively evaluated at 1, 3, 5, 7 and 10 div. (Figure 4.5 M). Quantitative data were compared to SC plated on TCPS PLL-coated dishes, used as control (TCPS).

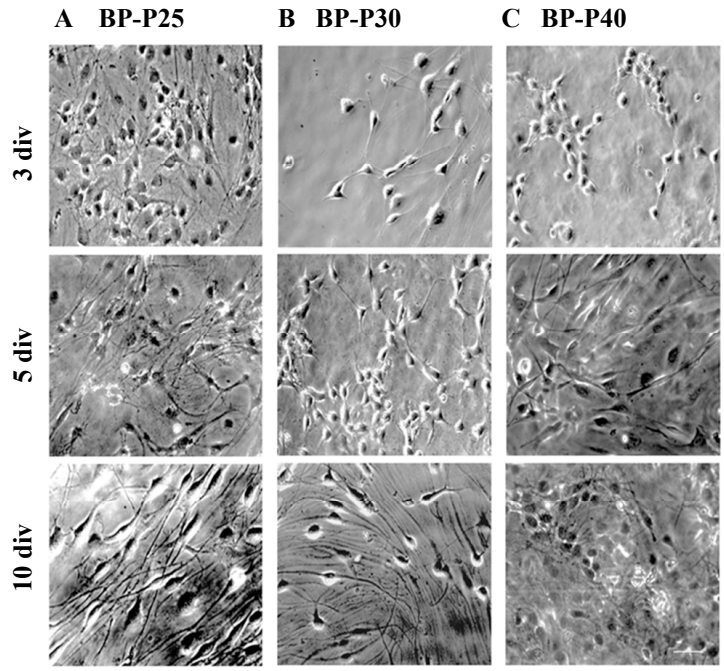

Figure 4.5 L. Cytocompatibility and proliferation of SC grown onto hydrogels of BP-P25 (Panel A), BP-P30 (Panel B) and BP-P40 (Panel C), at 3, 5 and 10 div. Scale bar 20 μm.

After an initial growing phase, the SC plated on MBA-P10 and MBA-P15 showed a strong decrease in proliferation, at 5 and 7 div respectively (Figure 4.5 M, Panel A), in agreement with morphological data.

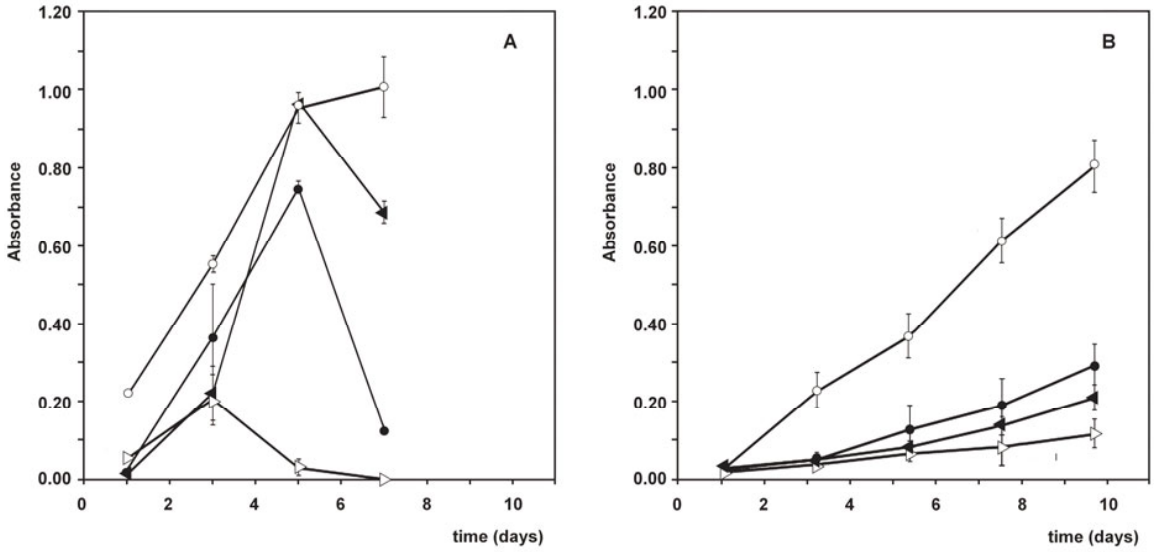

Figure 4.5 M. Quantitative proliferation rate by MTS analysis of SC grown onto MBA-P10, MBA-P15, MBA-P30 (Panel A), BP-P25, BP-P30 and BP-P40 (Panel B). Date are compared to SC grown onto TCPS PLL-coated dishes used as positive control. Data analyzed at 1, 3, 5, 7, 10 div were the mean SEM of experiments in triplicate. Panel A: TCPS (○), MBA-P10 (▷), MBA-P15 (●), MBA-P30 (◀). Panel B: TCPS (○), BP-P25 (▷), BP-P30 (●) and BP-P40 (◀).

Surprisingly, MBA-P30, which proved to be the best scaffold considering cell morphology, showed a decrease in cell proliferation at 7 div (Figure 4.5 M, Panel A). As regards the BP-P series, all samples showed an initial 5-6 div delay in growing, but later proved to be good supports for SC proliferation. Among them, BP-P30 turned out to be the best scaffold with proliferation doubling of SC in 10 div (Figure 4.5 M, Panel B).

DRG neurons cytocompatibility and proliferation on hydrogels. The sensitive neurons having their soma in the DRG represent another main cell population in the peripheral nervous system. [33] Notwithstanding these neurons are generally used as reliable tool for in vitro studies of peripheral nerves, their preparation is rather complicated and their fairy survival very brittle. In this context, the ability of the most promising hydrogels, that is those of the BP-P series, to support adhesion of DRG neurons and extension of neurite was investigated to evaluate whether they could promote nerve regeneration. The cytocompatibility and its correlation with the hydrogel degradation rate was assessed at 3, 5 and 7 div (Figure 4.5 N).

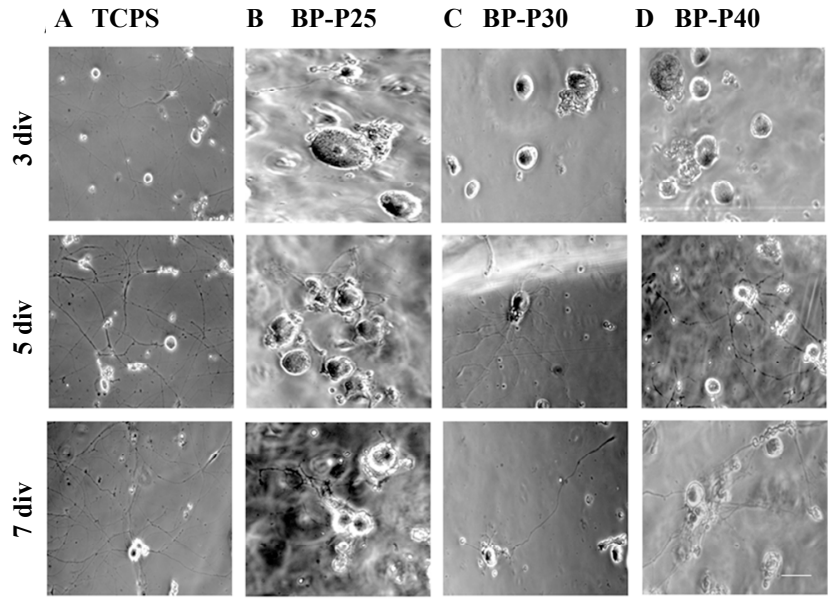

Figure 4.5 N. Cytocompatibility and proliferation of DRG neurons grown onto BP-P25 (Panel B), BP-P30 (Panel C) and BP-P40 (Panel D) at 3, 5 and 7 div. DRG neurite growth was compared to cells grown onto TCPS lamini-coated dishes and used as positive control (Panel A). Scale bar 20 μm.

Primary DRG neuron cultures grown on TCPS laminin-coated dishes, showing the typical morphology with rounded cell bodies, and a network of long axonal processes, were used as control. Neurite outgrowth was assessed using a contrast-phase microscope and evaluating parameters like process-bearing neurons and length of neurites. Morphological analysis showed the extent of neurite outgrowth for DRG neurons in all the three types of hydrogels at 3, 5 and 7 div (Figure 4.5 N).

The neurite outgrowth was visibly enhanced on day 5 and 7 on BP-P30 hydrogel. These results were confirmed by immunofluorescence for βIII-tubulin, which showed an increase in the neuron sprouting and neurite length when the DRG neurons were cultured on BP-P30 (Figure 4.5 O). Summing up, the evidence collected on SC and DRG neuron cytocompatibility and proliferation indicated that among all hydrogels tested, those of the BP-P series, and in particular BP-P30, proved suitable substrates and definitely warrant potential as culturing scaffolds for the main cells forming the peripheral nerves *in vivo*.

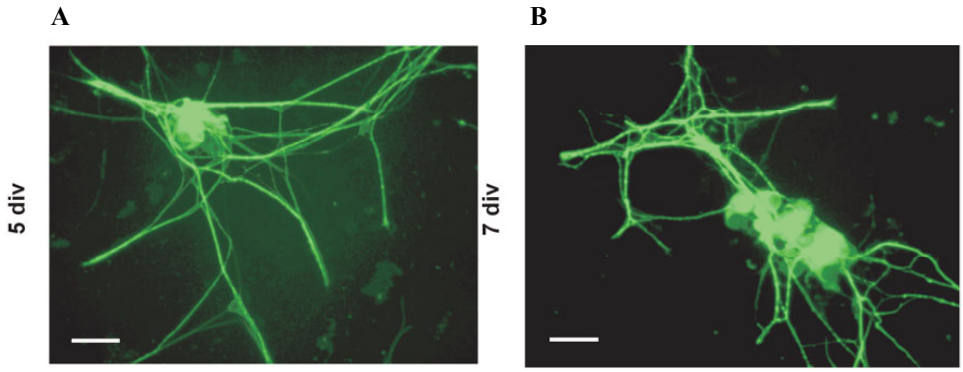

Figure 4.5 O. Immunofluorescence of DRG neurons in culture on BP-P30 at 5 and 7 div. The use of an anti-βIIItubulin antibody revealed a typical morphology with strong neurite sprouting and intact soma neurons. Scale bar 20 μm.

CHAPTER 5

CONCLUSIONS

5.1 HETERO-DIFUNCTIONAL DIMERS AS BUILDING BLOCKS FOR THE SYNTHESIS OF POLYAMIDOAMINES WITH HETERO-DIFUNCTIONAL CHAIN TERMINALS

There was no simple method hitherto to easily prepare PAAs with differently functionalized chain termini, that is, PAAs solely containing molecules of a—·····—b type. The devised strategy to overcome this problem was to prepare hetero-difunctional dimers (HDDs) of "a—a—b—b" type, that is, the mono-addition products of a bis-sec-amine to a bisacrylamide, which as strong acid salts could be indefinitely kept dormant in the dry state at 0-5 °C, but polymerized in aqueous media at pH>7.5. In this work, we report on the preparation of a selected number of HDDs and provide evidence of their synthetic potential by performing several model reactions. In particular, PAAs of controlled average molecular weight and mono-functionalized with an acrylamide- or a sec-amine group at one end, PAAs with a star-like molecular architecture, graft-PAA-protein conjugates, "tadpole-like" PAA conjugates with hydrophobic moieties able to self-assemble into nanoparticles in aqueous media were successfully synthesized. It should be noticed that the specificity of the Michael addition of amines to bisacrylamides in aqueous media, shared only by thiols under the PAA preparation conditions, allowed preparing most of the above derivatives by simply performing the polymerization of HDDs in the presence of the substrates of interest with no need of pre-synthesizing PAAs mono-functionalized at one end with an activated double bond. This greatly simplified the synthetic processes negligibly affecting the products' characteristics. Taking everything into account, it can be concluded that the aim of this research has been adequately fulfilled, thus demonstrating the wide synthetic potential of HDDs.

5.2 HYPERBRANCHED POLYAMIDOAMINES FOR THE SYNTHESIS OF HIGH-PERFORMANCE BIOMATERIALS

The critical ratio, below which the reaction leads to hyperbranched PAAs, for two systems involving different multifunctional monomers, namely cyclam (System A) and ethylenediamine (System B), has been established. The polyaddition reaction for these systems followed the Flory-Stockmayer theory. In particular, cyclam has been found to react as tetrafunctional monomer both with excess of amine hydrogens and with excess of double bonds. As for the ethylenediamine, it has proved capable to react as trifunctional monomer when reactions contained excess of amine hydrogens. In contrast, with excess of double bonds all hydrogens were able to react, and as a result it behaves like a tetrafunctional monomer. On the whole, a synthetic protocol to prepare hyperbranched PAAs with proper molecular weight and polydispersity was defined. Using these assumptions hyperbranched PAAs with multiple chain ends carrying only one type of reactive functions, that is to say aminic or acrylic one, have been easily prepared by modulating the stoichiometric balance of all monomers. They had a reasonable molecular weight, over the range $2.200 < M_n < 5.800$, with moderate polydispersity.

In view of biomedical applications, these multifunctional hyperbranched PAAs might be used for further specific functionalizations in order to tune their physico-chemical characteristics and biological performance. Overall, these findings provides the thrust to develop many purpose tailoring biomaterials with dendrimer-like characteristics, such as for instance: self assembling systems, surface-targeted nanoparticles and macromolecular pro-drugs with well-defined architectures.

5.3 POLYAMIDOAMINE-BASED MULTILAYER NANOPARTICLES AS POTENTIAL GENE AND PROTEIN DELIVERY SYSTEMS

A series of nanoparticles with low IC_{50} values suitable for the delivery of proteins and genes have been prepared from oppositely charged polymers using a layer-by-layer approach. Their physical size, charge and internal mobility have been characterized as a function of polymer type, composition and number of layers. This study demonstrates that the preparation of stable dispersions of such particles is feasible, and from a small number of building blocks, a wide range of particles is accessible. Hence, the insight derived from these results will have a wider implication for the rational design of such particles in the future.

This work clearly shows the preparation of a novel type of particle, with a modular design, formed from biocompatible polymers. One can easily anticipate that this approach will allow a variety of actives to be solubilized into the particles, protected and delivered by control of the structure of the polymer used to define the outer most layer. The design will also enable spatial separation of different actives, where each particular active can be solubilized into a discrete layer.

5.4 ISA23-BSA CONJUGATE AS ANTIMALARIAL DELIVERY SYSTEM

A BSA-PAA conjugate with high molecular weight have been obtained by simply self polymerizing an hetero-difunctional dimer, used as precursor of a well-characterized PAA named ISA23. It was non-cytotoxic and non-hemolytic neither *in vitro* on HUVETEC and RBC cells nor *in vivo* (mouse model) after intraperitoneal administration at 100 and 200 mg/Kg doses. This has bee studied as macromolecular carries for *in vivo* administration of two antimalarial drugs, namely primaquine (PQ) and chloroquine (CQ). The copolymer first proved able to efficiently bind both drugs forming stable complexes at equilibrium with the free drug. In particular, the binding experiments in PBS showed significant differences between the two drugs, PQ being more highly bound than CQ (about 78% *vs* 59%). Immunofluorescence assay clearly demonstrates that it was also able to colocalize with the parasite into parasite-infected RBC (pRBC). Isotonic formulations of this copolymer with 5.5% (w/w) PQ or CQ, named ISA23-BSA/PQ and ISA-BSA/CQ respectively, were prepared in PBS to perform biological experiments to establish their antimalarial activity. Among the formulations only ISA23-BSA/PQ was found to be able to enhance the *in vitro* PQ antimalarial activity. Hence it was selected to perform *in vivo* experiments in mouse model, in which it proved to cure mice after repeated intraperitoneal administrations. Whereas the mice treated with the same amount of plane PQ died within four days from the inoculation of parasites. These results outwardly support the mode of action of this copolymer, that is to say, the targeting of bound PQ into pRBC and the increase in bioavailability.

5.5 POLYAMIDOAMINE HYDROGELS AS SCAFFOLDS FOR IN VITRO CULTURING OF PERIPHERAL NERVOUS SYSTEM CELLS

The results of this research point to the conclusion that PAA hydrogels based on piperazine and *N*,*N*'-methylenebisacrylamide or 1,4-bisacryloylpiperazine with 1,2-diaminoethane as cross-linking agent combined cytocompatibility and ability to promote SC adhesion and proliferation with a set of tunable physico-chemical and mechanical properties, degradability and ease of fabrication, imparting them potential for applications as scaffolds for SC culturing and as guides for peripheral nerve regeneration. In particular, rheological measurements showed the formation of well-developed cross-linked networks. The mechanical strength, always inversely related to the swelling degree, was found to depend on subtle details of the macromolecular structure. In particular, the hydrogels of the BP-P series with moderate cross-linking degrees (BP-P25 and BP-P30) were remarkably robust in the swollen state owing to the presence of ordered domains acting as reinforcing agents. As regards biological properties, BP-P30 and MBA-P30 hydrogels were able to promote SC proliferation for a long time, albeit following different trends. Whereas SC rapidly grew on MBA-P30, they followed a slow but constant in vitro growing on BP-P30, that proceeded even after 10 days. The hydrogels of the BP-P series proved good culturing scaffolds also for DRG neurons, well-known for their fragility. The peculiar combination of favorable properties exhibited by the PAA hydrogels reported in this paper is seldom encountered in synthetic polymer scaffolds for peripheral nerve cells culturing.

This research work was made in cooperation with others research groups, in a multi-skilled environments. I gratefully acknowledge the research group of Prof. Michele Laus (Department of Science and Technological Innovation, Università del Piemonte orientale " A. Avogadro) for performing all rheological experiments here reported and discussed and for sharing their knowledge of physical chemistry of macromolecules; Dr. Patricia Urbàn (CRESIB, University of Barcelona) for providing biological characterizations of ISA23-BSA conjugates and their complexes with primaquine and chloroquine; Prof. Peter Griffiths (Cardiff University, School of Chemistry) for giving me the opportunity to study the self-assembling of polyamidoamines at his laboratory and for teaching me the EPR technique, and Prof. Simon Richardson (School of Science, University of Greenwich) for providing biological characterization of PAA-based nanoparticles on B16-F10 and in VERO cells.

A mio figlio Gabriele e a mia moglie Tiziana, che con i loro sorrisi radiosi hanno illuminato il mio cammino nei momenti più bui.